DIRECTIONAL STABILITY OF CRACKS UNDER BIAXIAL STRESSES

by

Guillermo Urriolagoitia Calderon, B.Sc.(Eng),M.Sc.

A Thesis submitted for the Degree of Doctor of Philosophy of the Faculty of Engineering, University of London and the Diploma of Imperial College

Department of Mechanical Engineering,
Imperial College of Science and Technology,
University of London.

March 1976

Con amor y agradecimiento a mi esposa

TERESA

que con su cariño y dedicación
ha sido la base fundamental
para el desarrollo de este
trabajo

A mis hijos

GUILLERMO

BEATRIZ

FRANCISCO

CARLOS

RICARDO

EDUARDO

que son la fuerza que me impulsa.

A la memoria de mi madre

MA. DEL SOCORRO

de quien recibí todo y a cambio
solo pidio mi superación personal.

ABSTRACT

The present work is aimed at the investigation of the development of cracks under biaxial loading conditions, and two co-related problems are approached.

In the first one, a purely theoretical study of a practical problem is carried out. The finite element method, the J contour integral method, Bueckner's method and stress field analysis, are combined in order to study the influence, that the point of crack initiation and the direction of crack propagation, have on the stress intensity factor.

The second problem tackled here is that concerning the determination of parameters that control direction of crack propagation. A combined computational-experimental approach is developed, and contributions are made in three areas.

(i) Development and testing of a computer approach to obtain characterising parameters which reflect fracture behaviour.

(ii) Design of an experimental method to control direction of crack propagation, and its implementation by means of a rig with which a biaxial stress field is applied on cracked specimens.

(iii) The directional stability parameter is identified as the second coefficient in the Williams' series (A_2) and it is shown how loading and geometry influence its value. It is demonstrated that three different physical conditions affect the A_2 value, i.e. geometry, opening load, and transverse load. The experimental crack path is followed and at different points of the path, a propagation angle (α) is measured, and it is shown a direct co-relation between A_2 and α.

ACKNOWLEDGEMENTS

The author wishes to express his gratitude to the following people:

Professor C.E. Turner for his guidance, advice and assistance during the progress and preparation of this study.

Professor J.L. Swedlow whose work on mathematical analysis, and computer programs as well as advice and assistance have been fundamental for this work.

Mr. G. Williamson technician of the Fracture Mechanics group, who built up the experimental rig.

Mr. C.J. Urriolagoitia, my father, whose help for sorting out administrative difficulties has been invaluable.

Mrs. E.M. Noel for her kindness and patience in the typing of this thesis.

The writer also wishes to thank the authorities of the "Instituto Politécnico Nacional", "Escuela Superior de Ingeniería Mecánica y Eléctrica", "Banco de México", and Conacyt, whose economic support at different times made possible the development of this work.

CONTENTS

SYMBOLS AND NOTATION

ρ	notch root radius
σ_m	maximum stress at notch root
k	stress concentration factor (SCF)
K	stress intensity factor (SIF)
K_b	stress intensity factor for bending configuration
K_c	stress intensity factor caused by a directive compressive stress
σ_1	maximum principal stress
σ_2	third - principal stress
σ_3	minimum principal stress
(r,ψ)	polar coordinator with the crack tip as origin
a	crack length
σ	applied stress to a plate or specimen
T	surface tension
E	Young's modulus
σ_x	normal stress along x
σ_y	normal stress along y
σ_{xy}	shear stress on the plane xy
K_C	critical value of the stress intensity factor
t	thickness of plate or specimen
K_{IC}	critical stress intensity factor under plane-strain conditions, with limited crack tip plasticity
K_I	stress intensity factor in mode I
K_{II}	stress intensity factor in mode II
K_{III}	stress intensity factor in mode III
G	energy release rate
P	load
λ	compliance

B	thickness
α	proportionality parameter for obtaining the value of K (depends on specimen and crack geometry)
SEN	single edge notch
R	fracture toughness as defined by Gurney and Hunt
ν	Poisson's ratio
W/A	specific fracture energy
η	function of test geometry (Turner's (1972) Chapter 3
COD	crack opening displacement
J	contour integral as defined by Rice
Γ	curve surrounding the crack tip
W	strain energy
ds	element of arc length along Γ
$\bar{T}$	traction vector
$\bar{u}$	displacement vector
p	pressure applied on a crack face (as given by Hutchinson and Turner (1975))
$X(r,\psi)$	Williams' stress function
A_i	coefficients in the Williams' series for the symmetric case
B_i	coefficients in the Williams' series for the antisymmetric case
u	crack face displacement along the x axis
v	crack face displacement along the y axis
n	number of terms being considered in the expansion of the Williams' series
k	$\frac{3-\nu}{1+\nu}$ for plane stress } as considered in the
k	$3-4\nu$ for plane strain } Williams' series
ϵ_x	strain along the x axis
ϵ_y	strain along the y axis

γ_{xy}	shear strain
μ	shear modulus
ζ	angle of crack propagation when the coefficient B_1, from the Williams' stress series, becomes apparent. Energy function of A_i, B_i
$\chi_e(r,\psi)$	even terms for the Williams' stress function
$\chi_o(r,\psi)$	odd terms for the Williams' stress function
ζ	energy function in terms of A_i, B_i
$\{\}$	column vector
$[]$	two dimensional matrix
$\{\}^T$	transpose of a column vector = row vector
$[]^T$	transpose of a matrix
$\{\sigma\}$	stress vector
$\{A\}$	coefficients vector
$[\phi(r,\psi] = [\varphi]$	a function of (r,ψ)
W	strain energy
$\{\epsilon\}$	strain vector
$[c]$	constitutive elasticity matrix (strain-stress)
$[B] = [\varphi]^T[c][\varphi]rdrd\psi$	= BVEC as specified within program ANGCRK
$\{u\}$	displacement vector = D as specified within program ANGCRK
$\{t\}$	traction vector - BDYLD as specified within program ANGCRK
Δ	space interval
ℓ	length of crack extension (Cotterell)
P_c	critical value for the directional stability parameter (σ_ψ on S), evaluated at a radius r_o, from the crack tip, characteristic of the material
r_o	core radius as defined by Sih

S	strain energy density
σ_{sc}	characteristic stress value of the material, for direction of crack extension (Williams and Ewing)
S_c	strain energy density value characteristic of the material (Sih)
S_x	uniform stress applied on the specimen along the x axis (lb/in)
S_y	uniform stress applied on the specimen along the y axis (lb/in)
$\sigma_{(S_y)}, \sigma_{(S_x)}$	stress at the crack tip, due to S_x, S_y
α_a	apparent initial angle of crack extension
α_F	final angle of crack extension
P_r	point at which α_F is measured
P_y	opening load applied to specimens.

CHAPTER 1

GENERAL PROBLEM AND INTRODUCTION

1.1 General Problem

Aspects of initiation, propagation, and re-initiation of cracks have been the main concern in the study of Fracture Mechanics. A further aspect that has recently started to develop is that of directional stability of crack propagation. In problems of practical interest, such as the one of a gear wheel in which if a crack develops, it would be preferable for the crack to run in a direction that cuts off a tooth and not towards the centre of the wheel. Another instance in which directional stability is of interest is that of turbine blades and also pressurised containers. Welded joints are also of interest concerning direction of crack propagation, here the main point is that when joining two different pieces, for example pressure vessel nozzles or reinforced components such as pipes, the material becomes heterogeneous in the welded zone, and imperfections and flaws that are crack starters appear. It is there when it becomes necessary to identify direction of crack propagation so that proper reinforcement is given.

In the first part of this study, the determination of stress fields and crack parameters takes an alternative philosophy to this problem - try to stop a crack starting on macroscale by rejecting gear blanks with defects near critical size, whilst in the second part, the problem is tackled directly by trying to identify crack parameters which define direction of crack propagation.

1.2 Introduction

The purpose of this work is to study the propagation of a crack when the conditions of rectilinear extension are disturbed. Once this happens, there arises a problem of determining not only the dimensions of the crack, but also the path of the crack propagation under such conditions of loading that a slow, quasi-static crack development is possible. This problem can actually be subdivided into two parts:

(1) obtaining the criteria for the determination of the dimensions and paths of the crack extension;

(2) determination of the expressions for the characteristics of the stress-strain state which are constituent of these criteria, through the geometry of the cracked solid with the loads applied.

The present work is devoted to the investigation of the development of cracks under biaxial loading conditions and two different but related problems have been approached. In the first one, a purely practical problem was tackled by using a well known finite element method, with the objective of obtaining the stress intensity factor for a cracked gear subject to operative conditions, and an analysis is made of the effect of a crack interfering with the stress field produced in a gear tooth in:-

(a) working loading conditions,

(b) residual stresses of the gear tooth.

The most probable position for crack initiation is deduced, crack propagation is permitted, and stress intensity factors are calculated. The second and main problem tackled here is that concerning the determination of parameters that control direction

of crack propagation. While in the former problem only analytical aspects are covered, in the second instance a hybrid experimental-computational system is devised to test the predictions of fracture mechanics, attention being focussed in mode I crack behaviour.

As a background to the determination of stress intensity factors for the gear case, a brief survey of general work developed in the field is made in Chapter 2. The whole of Chapter 3 is devoted to the description of work done in this study towards the determination of stress intensity factors, pointing out details and parts that presented difficulties and how they were overcome. Chapter 4 presents the background to the problem of directional stability of crack propagation, in order to set the foundation to back the analytical work described in Chapter 5, in which an account is made of the mathematical method used to model crack behaviour, and its computational implementation as well as a summary of the work done to test it. It was also necessary to produce experimental data to complement the computer procedure and in Chapter 6 a description is made of the development of the experimental rig to implement physically the computer work. A brief discussion is also made of special points which were a source of trouble and the way they were overcome. Experiments performed are described, and results are given as well as a discussion of the implications they have in relation to the parameters being sought. In Chapter 7 further work, both experimental and computational, is described and conclusions are reached. Finally in Chapter 8 the scope for future work is given, two main sections can be noticed. (a) Fundamental points that were originally included in a first list to be studied under the

present work - but time did not permit. (b) Further work that now seems to be desirable in the light of this work.

1.3 Brittle and Ductile Fracture

When a geometrical discontinuity occurs in a stressed material a stress concentration is likely to arise. When this geometrical discontinuity takes the form of a notch and its position and dimensions are such that they interfere dangerously with the behaviour of the material, then conditions are set for catastrophic failure that is breaking of the material, if the tip radius of a notch and the included flank angles tend to zero then the notch becomes a crack. There is a notable difference between a geometric discontinuity and a crack. In a typical machined geometrical discontinuity the stress level at the notch root could be raised in the order of 10 or 20 times if the root radius "ρ" is small, as if the crack is thought of as an elliptical void. Mathematical analysis shows that the stress level is raised to

$$\sigma_m = \sigma \left(1 + 2\sqrt{a/\rho}\right)$$

whilst in the case of the crack the stress concentration is such that the state of stress at the tip could be raised conceptually to infinity. The stress concentration originated in geometric discontinuities is known as stress concentration factor SCF and denoted by "k", while that originated in a crack is called stress intensity factor SIF and denoted by K and can be demonstrated that

$$k = \lim_{\rho \to 0} \tfrac{1}{2} \sigma_m (\pi\rho)^{\frac{1}{2}}$$

K has dimensions [stress $\sqrt{\text{length}}$]. σ_m = maximum stress at notch root, ρ = notch root radius.

The study of the stress conditions arising from situations like the one just depicted must tackle and overcome the very special characteristics of the singularity at the crack tip. The application of linear elasticity to the complicated situations around cracks has been called Fracture Mechanics.

Generally speaking one may classify the fracture of solids into two broad categories, namely Brittle Fracture and Ductile Fracture. By definition, all materials "in the ductile state" will undergo yielding before they ultimately fracture. Materials will be said to be in a "brittle state" if fracture takes place before any appreciable plastic flow occurs. Ductile fracture is usually associated with large deformations, very high rates of energy dissipation, and slow fracture velocities. Brittle fracture is a low-energy failure which, because of unstable loading conditions, takes place in a catastrophic manner, meaning that the fracture velocities are usually high.

McClintock and Irwin (1964) suggested that the fracture problem could be studied at nine distinct levels of size i.e. ions and electron cloud (10^{-7} cm), dislocations (10^{-6}cm), subgrain boundary precipitates (10^{-5}cm), subgrain slip band (10^{-4}cm), grain inclusions voids (10^{-3}cm),large plastic strains (10^{-2}cm), elastic plastic fields (10^{-1}cm), elastic singularity (1cm) and specimen or component (10cm). These could as well be grouped in three levels, i.e. atomistic (10^{-7}cm), microscopic (about 10^{-3}cm), and macroscopic (10^{-1}cm and greater). In the first case fracture occurs when bonds between atoms are broken and a new surface is created, in the last two cases fracture results from the passage of a crack through a region of material. Sometimes it is a repetitive cycling of loading

which starts up the mechanism of fracture, while another way to fracture a material is to raise the load to such a level that the material fails locally around discontinuities, and cracks or tears then spread. The growth of cracks prior to catastrophic fracture is conveniently divided into processes of initiation as microcracks, and propagation as macrocracks. The macroscopic theories of fracture assume the existence of cracks, voids, or other imperfections which may readily act as fracture nuclei, the size of these imperfections is assumed to be sufficiently large, compared to the characteristic dimensions of the microstructure, to justify the use of the tools of continuum mechanics.

Under such conditions it can be shown that a concept of crack growth during test is that the crack extension force (called G in the literature) is raised to a value corresponding to the point of instability, and Fig.1.1(a) and 1.1(b) show the response of brittle and ductile materials to the conditions described. An infinite set of variations could occur which could be placed between these two stages of brittle and ductile fracture, and which depend on many different physical parameters such as dimensions, structure, state of strain, strain rate, temperature, etc. but these are phenomenological aspects that will not be the concern of the present work.

Fracture behaviour is called brittle if the local ductility is too low to relieve the peak stresses and fracture propagates rapidly with little or no deformation of the material adjacent to the crack surface. A brittle material is one for which the strain at fracture is less than a given value, usually less than 5%. The conditions under which brittle materials fracture depend

very much on statistically variable local effects such as inclusions, grain boundaries, minute imperfections, etc. and usually test procedures are designed around a rigorous mathematical analysis involving specimen dimensions, loading conditions, and their relationship with the stresses introduced at the crack. The study of fracture initiation must be accomplished at the microscopic or atomistic level, whereas the events preceding and following fracture initiation are often controlled by the above influencing factors, and research related to these factors is normally accomplished on a macroscale level using continuum mechanics.

This study will be concerned with "Brittle Fracture" and by that it is intended to mean "a complete absence of irreversible effects measurable on the macroscopic scale". Some other conditions which will be considered as operating are, perfect isotropy, constant temperature and no influence of time effects such as creep, relaxation, etc.

1.4 Failure Criteria

Different theories have been proposed in trying to explain the fracture process, the ones described below are well known and depending on general conditions, are usually used to develop fracture criteria for crack propagation. They are distinctly applied to brittle fracture (no plastic flow) or onset of yielding, by defining a local stress value to start the instability mechanism.

(a) Maximum tensile stress theory

This is a very simple approach for the failure of brittle materials without initially considering cracks at all. It is considered that fracture can be intiated by many mechanisms,

but in order to propagate a fracture surface across the section of a component and to cause separation, it is necessary to have a tensile stress normal to the fracture surface. The maximum tensile stress theory postulates that fracture is determined by the maximum principal tensile stress σ_1, regardless of the magnitude of the other principal stresses, where $\sigma_1 > \sigma_2 > \sigma_3$.

When applied to the case of an already existing crack, it has already been shown that $\sigma_1 \rightarrow \infty$ when $r \rightarrow 0$ and there is not a general agreement on how the failure criterion could be applied although an idea of using a core region in conjunction with this criterion, has been put forward by Williams (1973) and Ewing (1972).

(b) Maximum strain theory

The maximum strain theory assumes that, under a given state of stress, there is a limiting strain of depletion of ductility which governs fracture. One popular form of limiting strain is the maximum elastic strain at the ultimate of the uniaxial tensile test for applying this criterion it is necessary to define the point in the material, in which this strain is taking place.

(c) Maximum shear stress theory

This is usually used for onset of plastic flow, i.e. yielding so it is not applicable to brittle materials and here it is only mentioned as additional information, the maximum shear stress theory states that fracture will occur when the maximum shear stress reaches a limiting value.

(d) Octahedral shear stress theory

This criterion is used to define onset of yielding, The octahedral shear stress is related to the strain energy of

distortion which is the total elastic energy stored in a unit volume, minus the elastic energy of volume dilatation. The maximum octahedral shear stress theory is widely accepted for the initiation of plastic flow and has been applied for those materials which exhibit large amounts of flow before fracture. The criterion of failure can be described as a limiting shear stress on the octahedral plane which has a normal stress equal to the mean stress. This is also called the distortion energy or Von Mises theory.

(e) Mohr theory

The Mohr theory is a more general theory than the maximum shear stress theory, in that flow or failure is initiated either (a) when the shearing stress reaches a critical value which depends on the normal stress acting on the same slip plane, or (b) when the maximum principal stress reaches a limiting value.

It has been mentioned that the conditions under which brittle materials fracture depend very much on statistically variable local effects such as inclusions, grain boundaries, minute imperfections, etc. At first thought it might seem rather hopeless to expect that any macroscopic criterion could predict fractures which originate at highly localised random imperfections at an atomic level (or, more likely, at the level of individual grains). However, Griffith (1924) showed that fractures originating near the tips of randomly oriented elliptical cracks lead to a macroscopical stress criterion failure.

CHAPTER 2

A SURVEY ON THE DEVELOPMENT OF FRACTURE MECHANICS AND BRIEF DISCUSSION ON DIFFERENT METHODS TO DETERMINE STRESS INTENSITY FACTORS

Chapter 2 is directed to two main aspects; one concerns theoretical and experimental work done in the field, and the second is centred on the use of the finite element method in relation to Fracture Mechanics. Within the review described here, care has been taken to select work that from this author's point of view is highly relevant to either the field in general, or the particular objectives of this work, specifically, initiation and propagation of Brittle Fracture, although some work related to non-linear material behaviour is discussed when necessary.

2.1 Review of Work Done on Fracture Mechanics

Griffith's (1920,1924) approach to the problem of fracture marked the beginning of the development of fracture studies; from then on investigators in the fracture field have shared in the general growth of applied mechanics.

Inglis (1913) made one of the earliest contributions to the field, he studied the behaviour of the stress field around elliptical holes in a flat sheet, and showed that the stress concentration at a crack point is infinite. Griffith and Taylor (1917) using soap films for torsion problems determined contour lines for shearing stress. Griffith (1920,1924) established the concept of crack propagation, he calculated the stresses and strains due to typical scratches with the help of mathematical work conducted by Inglis (1913) and the soap film method of stress estimation already mentioned, and

concluded that the scratches ordinarily met with could increase the maximum stresses from two to six times, according to their shape, and that this increase of the stresses was not enough to make the material fail. In view of the inadequacy of the ordinary hypothesis he attacked the problem of rupture of elastic solids by using the "theorem of minimum energy", according to this theorem the equilibrium state of an elastic solid, deformed by specified surface forces, is such that the potential energy of the whole system is a minimum, and the criterion of rupture was obtained by adding to this theorem the statement that the equilibrium position, if equilibrium is possible, must be one in which rupture of the solid has occurred, if the system can pass from the unbroken condition by a process involving a continuous decrease in potential energy.

In order, however, to apply the extended theorem to the problem of finding the breaking loads of real solids, Griffith found it necessary to take account of the increase in potential energy which occurs in the formation of new surfaces in the interior of such solids. He reasoned that, in the formation of a crack in a body composed of molecules which attract one another, work must be done against the cohesive forces of the molecules on either side of the crack. This work appears as potential surface energy, and if the width of the crack is greater than the very small distance called the "radius of molecular action", the energy per unit area is a constant of the material, namely, its surface tension.

A general theorem was stated as "in an elastic solid body deformed by specified forces applied at its surface, the sum of

the potential energy of the applied forces and the strain energy of the body is unaltered by the introduction of a crack whose surfaces are traction free", and offered proof of it. The concept of crack propagation he arrived at was:- "An existing crack will propagate if thereby the total energy of the system is lowered". Another statement in Griffith's paper is that:- "The general conclusion may be drawn that the weakness of isotropic solids, as ordinarily met with, is due to the presence of discontinuities, or flaws, whose ruling dimensions are large compared with molecular distances. The effective strength of technical materials might increase to ten or twenty times at least if these flaws can be eliminated". Griffith's theory is regarded as describing situations of pure brittle fracture.

In 1934 the advent of the dislocation theory, and in 1939 Weibull's statistical theory, both helped to explain phenomenological material behaviour.

Zener and Holloman (1944) related the Griffith crack propagation concept to the brittle fracture of metallic materials. Orowan (1945) presented an interesting discussion on X-ray work which showed extensive plastic deformation on the fracture surfaces of materials which had failed in brittle fashion. Irwin (1948) pointed out that the Griffith-type balance must be between the strain energy stored in the specimen, and the surface energy plus the work done in plastic deformation. He was the first to appreciate the importance of the fact that the local stress near a flaw depends on the product of the nominal stress σ and the square root of the flaw depth 2a, and coined the term "stress intensity factor" to emphasise this

fundamental relationship. This stress intensity factor may be physically interpreted as a parameter which reflects the re-distribution of stresses in a body, due to the introduction of a crack. In particular, these stresses indicate the type (mode) and magnitude of force transmission through the crack tip region.

Mott (1948) formulated the conditions for the dynamics of crack propagation and proposed that the velocity of crack extension is governed by the supply of kinetic energy to the crack field. This provided further evidence for Griffith's proposition for static, or slowly applied loads, that the energy necessary to support a brittle fracture must be provided from the available part, at the instant preceding fracture, of the elastic energy stored within the body which is being cracked.

Orowan (1955) demonstrated that the modified Griffith condition for brittle fracture is not only a necessary, but also a sufficient condition for crack propagation.

Irwin (1957) showed that the energy approach is equivalent to a stress-intensity approach, according to which, fracture occurs when a critical stress distribution, characteristic of the material, is reached.

Further work done by other investigators is to be discussed later on, as it is relevant to particular aspects of the fracture process that will be covered.

2.2 General Background

Briefly, Griffith's approach can be explained by stating that crack growth under plane stress conditions will occur if

$$\frac{d}{da}\left(-\frac{\sigma^2 \pi a^2}{E} + 4\,Ta\right) = 0 \qquad 2.1$$

where it can be shown that

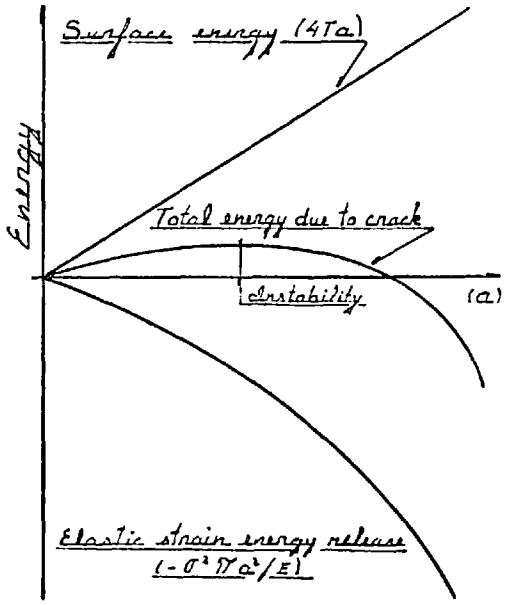

$[-\frac{\sigma^2 \pi a^2}{E}]$ represents the elastic energy loss of a plate of unit thickness, under a stress, σ, measured far away from the crack, if a crack of length 2a was suddenly cut into the plate at right angles to the direction of σ.

[4aT] represents the energy gain of the plate due to the creation of the new surface with a surface tension T.

When the elastic energy release due to an increment of crack growth, da, outweighs the demand for surface energy for the same crack growth, the crack will become unstable, and it is under this condition that a gross critical fracture stress can be defined as

$$\sigma = (2\ ET/\pi a)^{\frac{1}{2}} \qquad 2.2$$

which has, in the form of $\sigma \sqrt{a}$ = constant, been shown to hold quite well for brittle and semibrittle materials, but for semi-brittle materials T being effective surface energy, not just surface tension.

The linear theory of elasticity provides unique and single relationships among stress, strain, and energy. Therefore, a fracture criterion expressed in terms of an energy concept has its equivalent stress and strain criterion. The statement that "fracture occurs when the stress condition in a sufficiently large volume exceeds a critical value" may become a mathematical model by the use of Westergaard's (1939) stress field equations for cracks.

$$\sigma_x = \frac{K}{(2\pi r)^{\frac{1}{2}}} \cos\frac{\psi}{2}\left(1 - \sin\frac{\psi}{2}\sin\frac{3\psi}{2}\right)$$

$$\sigma_y = \frac{K}{(2\pi r)^{\frac{1}{2}}} \cos\frac{\psi}{2}\left(1 + \sin\frac{\psi}{2}\sin\frac{3\psi}{2}\right) \qquad 2.3$$

$$\sigma_{xy} = \frac{K}{(2\pi r)^{\frac{1}{2}}} \cos\frac{\psi}{2}\sin\frac{\psi}{2}\cos\frac{3\psi}{2}$$

in which, K the stress intensity factor, is a function of applied stress and crack geometry and, for a crack of length 2a in an infinite plate, is given by $K = \sigma(\pi a)^{\frac{1}{2}}$. If the critical stress system under which failure occurs is characterised by a critical value of the stress intensity factor, K_c, then a Griffith-type relationship results, without consideration of any energy-dissipation process involved. This energy-dissipation process is related to the problem of plasticity, but it will not be considered as this study is concerned with Brittle Fracture and as such, plasticity effects are considered to be negligible and there is no other effect than a local addition to the surface energy. This is based on the fact that, for brittle materials, where yielding in the region of the crack tip is very restricted, linear stress analysis implies that the local stresses and deflections depend on the stress intensity factor, K, and a criterion for brittle fracture in the presence of a crack, is that crack instability occurs when K attains a critical value.

According to the modes of separation that can occur at the crack tip the material behaviour can be described as

Mode I. The tensile component of stress is applied in the y direction, normal to the faces of the crack, either under plane-strain (thick plate, t large) or plane stress (thin plate, t small) conditions.

Mode II. The shear component of stress is applied normal to the leading edge of the crack either under plane-strain or plane-stress condition.

Mode III. The shear component of stress is applied parallel to the leading edge of the crack (antiplane strain).

And for each different mode a corresponding K_I, K_{II} or K_{III} value can be calculated.

In a section thick enough to encourage plane strain, mode I is found for this opening mode of crack deformation, load displacements are such that the crack surfaces move directly apart. Under plane-strain conditions, with limited crack tip plasticity, the critical stress intensity factor is designated K_{IC}. The value of K_{IC} can be considered as a material property which represents the material's fracture toughness, or resistance to fracture by mode I separation in the presence of a crack, this appears to be the lowest value of toughness found and hence, its practical significance. (K_{II} and K_{III} have hardly ever been found as pure cases but as value $K_{IC} < K_c$, where K_c is some mixed mode partly I and III.) Any combination of applied loads, structural configuration and crack geometry and size, which gives a stress intensity factor K_I, equal or greater than the value of K_{IC} for the material will result in failure of the structure.

As already described, there are two approaches to the study of Fracture Mechanics; the energetic treatment and the stress parameter approach. It has been mentioned that in the Griffith theory (1920,1924) the crack system is treated as a whole, assuming that cracks will propagate if the elastic energy released by their growth is greater than the energy required to

create new fracture surfaces. Alternatively, Irwin (1960) emphasised the stress conditions in the vicinity of the crack tip and used the critical intensity of the local stress field as a material constant commonly referred to as K_{IC}. It can be shown that there is a correspondence between Griffith's and Irwin's approaches to the crack problem. Under Irwin's approach the main crack parameter is defined as the energy-release rate, G. The stress intensity factor, K, is directly related to the energy-release rate in the fully linear leastic situation by:

$$K^2 = E'G$$

$$E' = \text{Young's modulus (plane stress)} \qquad (2.4)$$

$$E' = \text{Young's modulus}/1 - \nu^2 \text{ (plane strain)}$$

Irwin (1960) has noted that

$$K = \lim_{\rho \to o} \tfrac{1}{2} \sigma_m (\pi\rho)^{\frac{1}{2}} \qquad (2.5)$$

where σ_m = maximum stress at notch root; ρ = notch root radius. In this relationship, K will become insensitive to root radius whenever σ_m is inversely proportional to $\rho^{\frac{1}{2}}$. This is the case when the root radii are small compared to the notch depth or the slit length. Experimental data show that, in a finite radius specimen, it is possible to reach and exceed a value of strain energy release rate that is sufficient to satisfy the conditions for unstable fracture, and yet not have fracture ensue, making it evident that more than just the attainment of a critical value of G (or K) is involved in unstable fracture. (This point will be discussed further in Chapter 7.) It is thought that two conditions are needed to characterise fully the unstable fracturing of materials. One of these pertains to the conditions in a very small localised region near the

crack tip which are necessary to initiate unstable fracturing. The so-called failure criteria described in Section 1.3 are among others, the theoretical models developed to describe conditions more remote from the crack tip which are necessary to sustain unstable crack motion once the initiation condition has been fulfilled. Some work related to these will be discussed in Section 2.3.

The compliance calibration is an experimental method for making a stress intensity calibration for tension-loaded plate test specimens containing through-the-thickness cracks. Calibration curves are obtained by machining a progressively longer slot (simulating the crack) into a calibration test specimen and determining the compliance at each known slot size for conditions of elastic loading. A graph of compliance versus crack length is constructed and the slope of the graph may be substituted into the known equation

$$G = \frac{P^2}{2B} \frac{\partial \lambda}{\partial a} \tag{2.6}$$

and K can be calculated through equation (2.4). In all cases the stress intensity factor has the form

$$K = \sigma \sqrt{\alpha \pi a} \tag{2.7}$$

its units being [stress x length$^{\frac{1}{2}}$], α is a parameter depending on specimen and crack geometry, and one main objective of fracture mechanics is to determine the stress intensity factor.

In general most of the research done in fracture is directed to two aspects, (a) crack initiation, (b) crack propagation.

Under point (a) attention is focussed on the conditions that are conducive to initial separation of the material. It is an observed fact that regions of higher stress are more

conducive to fracture initiation, and that, in relation to point (b), once a crack has started to develop it is most likely to extend along the axis of symmetry of the stress field (if there is one), and follow a path dictated by the releasing of the stresses in the material. For this propagation to be kept going, energy considerations are of overriding importance. The criterion for extension (Griffith's) is that the energy required for separating the surfaces was just less than the decrease in elastic energy when the crack propagated. This approach has been proved to be right for brittle materials, such as glass in which there is no evidence of a dissipative flow process taking place (although even for glass, surface energy $\neq$ T, as there are effects such as moisture in atmosphere, and local plastic flow, that increase T to some "effective value"), and so the experimental and calculated values of the energy criterion are in good agreement. The extension of the Griffith theory to real materials which are not fully brittle in which dissipative processes, such as plasticity, take place, makes it necessary to take into account the work done by deforming a localised region of material as the crack progresses. If sufficient energy cannot be supplied for this process, then crack propagation will be inhibited; so the work necessary for plastic deformation is a great deterrent to crack propagation and plays a vital part in its study. There are still other factors such as temperature, environment, strain rate, geometry, etc., that affect the fracture process. For example, the first three factors affect K_{IC} (a material property), by altering the stress flow and/or micromechanism

of separation, while the geometry affects K. This leads to the conclusion that care should be exercised in order to prevent these effects from interfering in experimental work.

It has been mentioned in Section 2.1 that the work of Mott (1948) took into consideration the dynamics of crack propagation. Before this, some experiments involving stable fractures (by stable it is meant to have certain external control on crack propagation) in mica were made by Obreimoff (1930); later on, Wells (1954) concluded that a moving crack must also be associated with movement of the material near the crack, and so with exchanges in kinetic energy. Naturally, if there is insufficient energy, available to supply the requirement for creating fresh surface there can be no propagation, excess energy beyond that necessary to create surface is converted into kinetic energy of the separating parts, and the crack velocity is maintained or increased.

Roesler (1956) showed under which conditions fracture can be stable (i.e. it can be propagated at an arbitrarily slow speed) showing as well that even in brittle materials such as glass the fracture process involves energy dissipation.

The development of stable fractures in more practically important materials, such as plastics, was described by Benbow and Roesler (1957). They showed how by introducing an auxiliary compressive stress parallel to the crack, its direction and speed can be controlled. Using this technique it is possible to produce stable fractures in sheets, or strips of plastic.

Berry (1960) derived the equations of motion of cracks in tensile and cleavage (the cleavage specimen is designated single edge notch (SEN) specimen somewhere else) specimens, and showed that the behaviour of cracks in tensile samples depends on their initial size, and that large cracks are, in one sense, more stable than small cracks. He also showed that the behaviour of cracks of all sizes in cleavage samples resembles that of large cracks in tensile samples.

Svensson (1961) studied the variation of fracture energy with temperature. He found that the energy associated with a cleavage failure (micromode) decreases with increase in temperature, due to the greater thermal energy of the molecules, on the other hand, the strain energy absorbed in shear deformation preceding the growth of the crack is increased to a maximum and then falls. The increase is due to an increase in ductility at a substantially constant shear stress, at moderate temperatures. As the temperature is increased the ductility still increases, but the shear stress drops considerably until it is very low, when the material softens. Thus, the fracture energy should first fall with increase in temperature, rise to a maximum, and then fall to a low value at the softening temperature.

Gurney and Hunt (1967) called all the work that was necessary for cracking, above that required for elastic deformation, the local work to spread the crack. They conducted experiments in which cracks were spread quasi-statically, deformation modes other than fracture were suppressed so that all the work done = the fracture work, and by recording both load and corresponding displacement of load, the local specific

work of crack spreading, or fracture toughness (R) was deduced without calculating the elastic stress distribution or even measuring the shape of the test piece. The work done during cracking divided by the increase in crack area was termed R-value of the material, and is synonymous with fracture energy and fracture toughness. This term (R) includes surface energy together with non linear elastic work due to large strain at the crack front, and delayed reversible and irreversible effects associated with atomic configurational changes, as well as plastic and viscous deformation at the crack surface. Barr (1968) worked on the same lines obtaining similar conclusions.

Turner (1972) took the specific fracture energy (W/A), considered it as an approximation to G_{IC}, the fracture toughness of a brittle material, and derived an exact relationship between these two terms from linear fracture mechanics, to give the compliance and hence the work done. He showed that $G = W/\eta A$ where η is a function of the test geometry, and compared against experimental data finding good agreement with fracture toughness derived conventionally from the fracture load, provided that the fracture is completely brittle.

Mai et al (1975) working with tapered single edge notch (SEN) specimens found that they exhibited less stability than parallel SEN test pieces cracking under stiff testing conditions. He also conducted tests with load and crack applied at the thick base, instead of near the apex finding that regarding path direction, experiments agree with theory. This type of loading provides better cracking directional stability and thus easier control of the crack path together with a wider range of crack velocities in one test.

2.3 Computational Methods to Determine Stress Intensity Factors

There are a great number of numerical methods to deal with the determination of stress intensity factors. The most successful one, because of general applicability, seems to be that which makes use of a finite element method. Much literature has been devoted to the subject per se. Briefly the finite element method furnishes one with estimates of the displacement vector and stress tensor components at a limited (but more or less evenly distributed) number of points throughout a loaded structure. Although generally very good these are not exact but are approximations to the true solution.

In order to implement the method to achieve the solution of a problem by means of a finite element method (for cracked bodies) the points described hereafter have to be considered.

(a) Modelling geometry. Both, overall and localized, the mesh arrays have to be designed keeping in mind crack position so that the process of crack propagation is facilitated.

(b) Material properties. Elastic, (Young's modulus, Poisson's ratio) criterion of yielding post-elastic (stress-strain curve and laws of plastic flow), etc.

(c) Loading. Tractions, displacements, plane-stress, plane strain.

(d) Numerical evaluation of parameters and how to compare them with physical response in experimental work.

(e) Inherent limitations. Stiffness method, linear elasticity, material non-linearities, geometric non-linearities, limit loads, COD.

(f) Other aspects. Singularity representation, ordinary analysis, special elements.

(g) Beyond planar analysis. Axisymmetry, bending, three dimensions.

And for deciding on these aspects there is no substitute for experience. A number of investigators have used the finite element method in relation with elastic stress intensity factors, and a review of articles on the subject include those by Rice and Tracey (1973), Oglesby and Lomacky (1971), and Jerram and Hellem (1972).

Two basic approaches have evolved. When conventional finite elements, with polynomial interpolation functions, are used in the crack tip region, the characteristic elastic square root singularity necessitates the use of an indirect procedure, such as extrapolation of a field parameter to the crack tip or an energy method, to determine the stress intensity factor. In the first one, by choosing a value of Ψ, the value of a particular stress component (or displacement component) may be plotted as a function of r, from the results of a finite element analysis and by fitting a polynomial in $r^{-\frac{1}{2}}$ and higher powers of r to these results, the value of K_I may be estimated, although it seems that an accuracy no better than 5% can be expected. The finite element analysis method will never, of course, register an infinite stress, however, if there are points at which a continuum analysis would give a singular result, a finite element analysis will indicate a high degree of stress concentration.

Watwood (1969) made use of a finite element method to obtain stress intensity factors and reported poor accuracy from this method unless extremely small elements are used near the crack tip, and abandoned it in favour of a direct computation

of the strain energy release rate which is equivalent to K. This procedure consists of computing the strain energy for two slightly different crack lengths and employing numerical differentiation to determine the strain energy release rate. A method similar to this one is used and described in Chapter 3.

Chan et al (1970) discussed the extrapolation procedure in conjunction with constant strain triangular elements. They plotted the product of $r^{\frac{1}{2}}$ with a stress component as a function of distance, r, along a ray emanating from the tip, and performed a tangent extrapolation of this quantity to the crack tip, r = 0. Alternatively, the extrapolation may be based on the product $r^{-\frac{1}{2}}$ with a displacement.

Mowbray (1970) used an energy method very similar to experimental compliance methods to compute the energy release rate. He solved the same specimen geometry for several cracks of slightly varying length, and was able to obtain the compliance as a function of crack length. Numerical differentation of this relationship with respect to crack length enables determination of G and hence K.

Hayes (1972) made some applications of the finite element method in conjunction with two well known approaches; the J contour integral (this will be described in Chapter 3) and Bueckner's formulation (1958), and developed an efficient and accurate method that overcomes some of the usual difficulties encountered when using the finite element method approach, and originated in the singularity inherent to the stress field. A brief description of Bueckner's formulation (1958) follows. If sufficient care is taken in producing geometrical data, the strain energy U_d may automatically be evaluated for increasing

(or decreasing) crack length. One simply determines the point loads for each node and computes the crack face displacement. The next crack length is then analysed by simply relaxing the boundary conditions at the crack tip node and introducing new nodal point forces. This means that the total stiffness matrix of the finite element representation once produced, is simply adjusted for each crack length, by altering the appropriate terms (a maximum of four per nodal point), for each change in crack length. If the crack length is increased by small increments each displacement field will be very similar to that obtained previously. Thus the number of iterations required to determine the new displacements (by the finite element method) will be very small. Having, usually automatically, determined U_d for the range of crack lengths of interest, it is then simply a matter of determining its derivative with respect to crack length. Once again this procedure may be fully automated so that the net result of a single computer run is the desired relationship between crack extension force, or stress intensity factor, and crack length.

An alternative to these indirect procedures involves direct embedding of the elastic singularity in the displacement function for the near tip elements. Tracey (1972) used a mesh of isosceles trapezoidal elements focussed into the crack tip. The ring of elements nearest to the crack tip had a $r^{\frac{1}{2}}$ displacement variation specified, while the adjacent elements were ordinary isoparametric elements. He obtained 5% accuracy for the plane strain double edge notched, and notched round tensile bars using 248 degrees of freedom.

Parks (1974) presented a method based on the energy release rate which requires no special crack tip elements. Further, the solution for only a single crack is required, and the crack is "advanced" by moving nodal points rather than removing nodal tractions at the crack tip and performing a second analysis.

There are a great many works in the field that have not been mentioned because either they deal with non-linear material behaviour or simply because the time is limited and does not permit a rather extensive review of the literature in this part of the field. However, it is thought that the material selected describes quite well the general trend followed in the finite element method as applied to fracture mechanics.

2.4 General Approach to the Problem under the Present Work

A further point concerns Hayes' work (1970), he described a general procedure for designing against fracture (when the K_{IC} concept is valid), it is as follows:

(i) Carry out overall stress analysis of the structure to determine positions where cracking would be dangerous;

(ii) Carry out detailed analysis of these regions;

(iii) From the results of (ii) and using any of the approaches already described, evaluate stress intensity factors for the worst crack (generally oriented normal to the plane of maximum direct stress) for a series of crack length;

(iv) Using available test data for K_{IC} for the material to be used, determine the maximum size of flaw that is tolerable;

(v) In view of the results of (iv) accept or alter the design and/or material.

Within this work, use will be made of methods developed by Hayes, as the facilities are available; the approach used and described in Chapter 3 is very similar to the general procedure proposed by Hayes.

The problem to be tackled is a very particular one, so it is necessary to develop special subroutines to furnish the required data. Actually a whole computer program was built up in which the next steps were executed.

Subroutine 1. Mesh generation and boundary conditions.

Subroutine 2. Crack development.

Subroutine 3. Load application.

Subroutine 4. Stress computation.

Subroutine 5. K calculation.

Whereas subroutines 1, 2, and 3, were specially developed for this work, subroutine 4 is a standard finite element program, and subroutine 5 which calculates K through a J contour integral approach, was available from former work carried out by Sumpter (1973).

For the work described in the next chapter, elastic calculations were made with finite element computer programs devised at Imperial College. The finite element method is now well documented in numerous papers and in the book by Zienkiewicz (1971) and here it is necessary to give only a brief description of the program used. It employs elements of triangular shape, the apices of which will be referred to as nodes. The deformation characteristics of the elements are such that the displacement varies linearly over the element. The computer

program, calculates the deformation of each element composing the body in such a way that under the applied forces and displacements, there is equilibrium and displacement compatibility at the nodes. Stress components are calculated from the nodal displacements, and finally stresses are constant in any one element and taken to act at the centroid.

CHAPTER 3

FRACTURE MECHANICS APPROACH TO A PRACTICAL PROBLEM

In this chapter the solution of two practical problems are described. For each one a different technique for determining the stress intensity factors, for a cracked body was used. The first one applies the J contour integral method mentioned in Section 2.3, and described in Section 3.4. In the second problem use is made of the method developed by Bueckner and described in Section 2.3. In doing this study computer programs which are commonly utilised at Imperial College were used although modifications were needed to suit the special requirements of these cases. A program to generate a gear profile and a finite element mesh within it was developed as well as additional subroutines to build up the whole computational approach and obtain a solution.

The stress intensity factor determination itself, is not a new contribution, originality here rests in the fact that the problem tackled is purely practical and there are a number of details which have to be considered to achieve a solution. A detailed discussion, of some of the most interesting aspects of this problem, is presented.

3.1 Problem Definition

The failure of gear teeth from small surface or subsurface defects can be posed as an example of the type of design problem to which fracture mechanics might contribute an understanding. It has been found that in gear manufacturing, a certain quantity of gears have reached a final stage of fabrication and are then rejected because of defects in the blanks. It is intended to include Fracture Mechanics Analysis as part

of the research work to find out what are the maximum defects permissible in such blanks (type of defect, dimension, position, quantity, interelation, etc.) with the purpose of developing an acceptance criterion which could be applied in the early stages of fabrication, some of the work done towards this aim is described hereafter.

On information provided by industry it was decided to use a gear wheel typical of current design practice whose particulars are given in Appendix 3a. Two main problems are to be tackled*.

(a) Cracking of the gear under working conditions.

(b) Cracking of the gear originated on Residual Stresses.

3.2 Approach and Numerical Results

The general approach to the solution of these problems is given below:

Because of the finite element computer programs available (time and core) it was necessary to cut out a local region from the whole shape, former studies on the subject, Urriolagoitia (1970), set the basis to establish the general dimensions, and Figs.3.1a to 3.1e show the section to be used in a Finite Element Analysis.

The form of the tooth shown in Fig.3.1 represents the normal cross section of the helical gear with a normal pitch of 0.8.

A preliminary finite element analysis was made for this section; a program to generate the external contour, as well as a rough mesh within, was prepared. The boundary conditions

*The problem is a single one but here it is presented as two different cases because of the approach needed to tackle it, as there are two calculations, each one with a different method, which will have to be added together to give the effective value of K in service for a given tooth load plus residual stress.

imposed on the portion of the gear are shown in Fig.3.2; a load of 100lb. is applied at the pitch circle, in the computation plane strain is assumed and unit thickness taken. This implies the loading is per unit slant length along the helical face rather than per unit thickness of gear although the computational model is a two dimensional representation.

From the preliminary finite element analysis contours of principal stress near point A (Fig.3.1d) at the tooth root are shown in Fig.3.3 as a function of depth below the surface in the uncracked body. These stresses are taken to relate to the centroids of the elements, at the surface element the stress value is 768 lb/in^2 whereas the extrapolated value (Fig.3.4) is 804 lb/in^2.

Based on simple beam theory, using the circumferential component of force only, the nominal bending stress in the tooth root at A is 398 lb/in^2 giving a stress concentration factor of approximately 2.2. If the radial component of force is allowed for, there is a direct stress of 53 lb/in^2 and a further bending stress of 58 lb/in^2 (both compressive at the root of the loaded flank) giving a final nominal stress of 287 lb/in^2 and a stress concentration factor of 2.8 as detailed in Appendix 3b.

Point A was chosen as the point of maximum stress from the initial calculations. Subsequently in a more detailed analysis, a stress 2% higher was noted at an adjacent point B, one element removed from A, towards the root. Such discrepancies are within the limits of accuracy of the Finite Element Method.

K Calculations

A crack was introduced from point A, nominally normal to the surface. The crack direction is along a line of elements radial to a nominal circular arc connecting the flank and root circle. The true profile at the root is not this circular arc and this true profile is approximated to by the outer edge of the element (Fig.3.1d). The crack is thus not normal, by a few degrees, to the true local curvature. Since the precise direction of cracking is unknown this nominal radial direction was thought to be good enough. It arose in the first instance by reason of simplicity of mesh generation and as load is applied far away from the crack, the response obtained is thought to be a good one. However, for the case in which residual stresses are to be considered it is absolutely necessary to obtain a true normal direction to the surface and in that special case a modification is made.

Six crack length cases were computed, crack lengths of 0.24, 0.35, 0.5, 0.68, 0.83 and 1.03 mm were simulated, later on a 3mm crack was also tried. The smallest element size thus varied from approximately a/2 for the shortest crack to a/10 for the longest one. Even though Aida et al (1973) give a rough idea of the crack profile, there is not enough accurate data available, so a close representation of the crack profile was not attempted and the direction of crack propagation was assumed to be as shown in Fig.3.5 by line P-T. This first approximation was the result of an early attempt to analyse the shape with a very rough finite element mesh. The stress field though well defined, is not accurate enough to give reliable data concerning future fracture. Further analysis of the stress

field obtained with better meshes and described in Section 3.3 seems to indicate that the crack profile should be slightly different from the one studied, but by now it is considered that for the objectives of this study it is adequate to consider the crack paths as they stand.

K was calculated from the J contour integral method described in Section 3.4 using $J \equiv G$ for elastic behaviour and $K^2 = EG/1 - \nu^2$ for plane strain. J is averaged over 10 contours which give values constant to within $\pm$ 3%. This variation is within the variation hitherto found for such contour evaluations.

Contours of maximum principal stress are shown in Fig.3.7 for the cracks up to 1mm. It is thought that study of stress trajectories combined with other calculations on energy release rate for selected crack orientations might reveal the direction in which a crack would propagate under a given applied load, and further analysis on this is described in Section 3.3.

Discussion and Conclusions

Values of K for particular cracks in the root of one tooth form are given in Table 3.1. The computed values are appreciably less than a simple approximation sometimes used for cracks in regions of stress concentration, $K = k\ \sigma \sqrt{\pi a}$ where $k\sigma$ is the true local stress. The computed values are only some 10% or so more than a very simple approximation $K = \sigma \sqrt{\pi a'}$ where σ is the actual stress in the uncracked body at the point where the tip of the crack is subsequently located. These uncracked body stresses are appreciably under estimated by simple bending theory for combined loading (Appendix 3) so that a good estimate of the uncracked body stresses would be required in order to

apply this approximation for K. It cannot be said how widely or narrowly applicable such an approximation might be since only the one geometry is here considered.

The accuracy of the very short crack results might also be in question owing to the small number of elements along the crack, further discussion on this topic is given in Section 3.4.

In connection with the longest crack (3mm) the computed K value is 172 psi $\sqrt{in}$. A simple estimate of it could have been made by using the stress values given in Appendix 3, which are

Major Bending Stress	+	398 lb/in^2
Eccentric Bending Stress	-	58 lb/in^2
Direct Stress	-	53 lb/in^2

Combining the first two into an effective bending stress of 340 lb/in^2 this may be taken together with a calibration factor Y from the well known solutions for bending configurations. The span/width ratio is here small since the tooth height to the load point is less than the root width. With a/W = 0.16 is extrapolated from the span width ratio s/W = 4 to give Y = 1.65 for this a/W

$$K_b = (1.65)(340)\sqrt{0.118} = 193 \text{ (lb in units)}$$

The directive compressive stress is taken to cause a K value as for a single edge notch (SEN) piece, to be subtracted from the effective bending value.

$$K_c = 2.3 \times 53\sqrt{0.118} = 42$$

Thus the estimated value of K is

$$K = 151 \text{ psi } \sqrt{in}$$

in fair agreement with the computed value.

3.3 Stress Field Analysis and Determination of Most Probable Crack Place

For arbitrary crack paths some form of criterion is required to assess direction of propagation from any instantaneous tip position of the growing crack. Here an attempt is made to predict crack behaviour by analysis of the stress field around the crack tip. Results from different work done by other researchers is useful for this purpose. It has been found that in brittle coatings, when the strain transmitted from the surface of the specimen to the lacquer reaches a critical value in tension, the lacquer will crack perpendicular to the direction of maximum tension. The first crack will initiate at the point in the specimen developing the highest strain and, as loading is continued will grow. Here it is important to note that a stress field is developed in the specimen and any change that occurs in this field would be in magnitude but not in distribution and the crack follows that magnitude change. On analysis of the growth of a crack in the specimen, it can be seen that the stress field will change in shape and magnitude as the crack advances (this can be observed in Fig.3.7). It is the view of this author that the stress field in the neighbourhood of the crack (immediately before crack expansion) could help to establish the direction of crack propagation; D. Post (1954) observed that "The eccentricity of load, or degree of non uniformity of the tensile field, appeared to have no effect on the orientation and shape of the inner loops of the isochromatic patterns, however, the outer loops showed a tendency to tip forward with increased eccentricity (see Fig.3.6a,b). Thus, close to the crack the stress pattern

is primarily a function of the sharp stress concentration, and a little further away the influence of the non-uniform tensile field becomes perceptible". Experiments using photo-elastic techniques are reported by R.P. Hubbard (1969), among the results presented two photographs of the isochromatic field are of interest, in them it can be clearly distinguished a small deviation of the crack from the horizontal plane, and as a result, the photoelastic pattern becomes asymmetrical about the crack plane. M.L. Williams (1957) working through a mathematical series showed that the isochromatic fringe pattern for a symmetric case should be as shown in Fig.3.6c with loops emanating from the crack and perpendicular to the line of cracking (symmetry about the crack plane). While in the anti-symmetric case, that is mode II crack behaviour, the loops are parallel to the crack surfaces (Fig.3.6d) (loading parallel to crack surface on top and bottom but different values), so:-

If the crack is only mode I, the loops should be perpendicular.

If the crack is only mode II, the loops should be parallel.

A combination of mode I, mode II would show loops with an inclination either backward or forward, but there still would be symmetry of the loops around the crack plane provided there is symmetry in both the loading and the specimen geometry. When this is not the case and one has an odd geometry as well as/or load asymmetry, the stress field will be peculiar, but by considering the already mentioned points it should be possible to identify and roughly separate effects and predict possible crack behaviour.

In relation to the present work, the preliminary analysis established within which zone the mesh had to be refined. From here a new finite element analysis was performed and the pattern of lines of maximum principal stress shown in Fig.3.7a was obtained. Being lines parallel to the gear surface there was no clear indication of the point in which the crack would initiate. On the other hand, in the neighbourhood of the tooth root the differences in the individual values of the stresses, either for the elements or for the nodes, are so small that they could be attributed to intrinsic errors contained in the finite element mesh. On this basis it was concluded that in the tooth root there is a zone about 1mm wide within which the highest possibility of crack initiation is present, so it was decided to consider five different points of crack initiation within this zone. The refinement of the finite element mesh was such that it allows the introduction of a crack in any one of these five points, and the elements were fairly small (i.e. a/10) so crack growth could be followed in adequate increments. Because of the stress field pattern present in the uncracked body, it was thought that any crack developing in the proposed zone would have a high probability of increasing in a direction normal to the boundary of the specimen, so the refined mesh had been designed contemplating this possibility. Table 3.2 gives the mean characteristics of these cracks.

The results from the finite element analysis in these five cases were used to trace and analyse.

(a) Isochromatics field.

(b) Isostatics field.

(c) Isoentatics field.

In Fig.3.8 the isochromatic field for each one of the five cases is given. It can be noticed that for case 5 (Fig.3.8e) the loops are totally asymmetrical (here it is not intended to imply absolute symmetry but roughly separate the stress field in two zones above and below the crack surface) and as the crack position is changed the stress field tends to become a symmetric one until finally in case one (Fig.3.8a) these loops are normal to the crack faces. Even though there is still asymmetry in the dimension of the loops it was thought that this could be taken as indicative that provided the crack initiates at this point it will propagate along the line given. The asymmetry observed in the other cases could mean that the crack should have deviated before reaching those lengths. In addition, the isostatic field for case 1 and case 3 are shown (Figs.3.9a and 3.9b respectively). Arad (1972) reported that in tests on direction of crack propagation, it was found that the crack turned to grow along the minimum principal stress trajectory passing through its tip. So the criterion for extension was taken to be that the crack propagates along lines of minimum principal stress. It can be seen that in case 3 the highest line of minimum principal stress makes an angle with the crack surface, and the loops with high values are away from the extension of the crack line, whilst in case 1, these loops envelop this line and there is some kind of symmetry,(here one also has to consider the fact that there is no symmetry of the centroids of the elements

around the crack tip). This should make the stress on the element whose centroid is the nearest below the tip to be the highest, while the nearest element above the tip has the next highest stress. This suggests that if symmetry of the centroids of the elements around the crack tip is present it would produce a better symmetry of the stress field in the very near neighbourhood of the crack tip, which could partially take account of the fact observed, in the stress field, that the lines of stress seem to point towards a zone on top of the tip, while it was expected that these lines would be directed towards some point ahead of and on the line of the fracture. But still, for the nearest elements to the crack tip in case 3, the stress values are 636 lb/in^2 above the crack tip, and 422 lb/in^2 below, that is, even though the centroid of the element below the crack tip is closer the stress is lower, so there is a strong natural asymmetry in the stress field. On the other hand in analysing case 1, it can be seen that the stress values are 535 lb/in^2 and 572 lb/in^2 for the same elements as above, which suggests that allowing for asymmetry of the mesh, there is a strong possibility of the stress field being totally symmetric.

In Fig.3.7 the isochromatic fields for different lengths of the same crack are reproduced and it is important to point out that

Fig.3.7a Body uncracked (crack length equal zero), the isochromatics are practically parallel to the boundary (within the highest stressed zone).

Fig.3.7b Commencement of cracking (crack length = 0.0116mm). There is still a certain degree os symmetry for the stress field, the zone above the crack is stressed the most.

Fig.3.7c Crack extension (length = 0.0238mm). An isochromatic loop pattern has formed, and the axes of symmetry for the different loops, above and below the crack, follow directions approximately parallel to the gear surface.

Fig.3.7d, 3.7e Further crack extension (lengths = 0.036mm, 0.0521mm) the axis of the loop above the crack has only a slight variation in direction while the one below moves gradually to approach the direction of the axis above.

Fig.3.7f, 3.7g Full crack (lengths = 0.068mm, 1.03 mm) the axes convergence reached for case of Fig."e" is kept.

A further point is that once the notch is introduced the correlation between stress values above and below the crack tip is roughly the same, the value above being always higher.

The final conclusion from the analysis of the stress field above was that the crack should initiate at the point for which the coordinates are x = - 8.914mm, y = 416.977mm (with reference to the gear centre) and continue to extend along a line with an angle of 0.80078 radians in relation to the horizontal axis, this seems to be confirmed by results and analysis of the K values, given in the next section.

3.4 J Values and Determination of Most Probable Crack

Using the method described by Hayes (1970) and by Sumpter (1973) (actually as a subroutine of the finite element program) the values of J for the different cracks (lengths and positions) were calculated, these are given in Table 3.3 and depicted in Fig.3.10a. In relation to this set of results it is important to point out that in this Fig.3.10a there are two zones of special interest. In zone 1, crack length range 0.0 to 0.5 there is no clear definition of the different K curves, it is thought this is due to the natural limitations of the finite element method as the relationships between element size and crack length are 1, $\frac{1}{2}$, 1/3 and 1/4, so rather poor results can be expected within this zone. If it was decided that values in this region were needed, it would be a matter of refining the finite element mesh. However, for the present case, where a crack 1mm long is being analysed, it is thought the present mesh is small enough.

The fact of having both the highest K value (here again it has to be pointed out that it cannot be firmly established which one of them is a better one, the one for 0.80078 or that for 0.82747) for an angle between 0.80078 and 0.82747, and that the curves are almost coincident, seems to indicate that the critical crack position is somewhere within these limits. It could be possible to define a narrower zone than this one by adjusting the finite element mesh and running cracks within that zone but this would not improve the analysis already done so it was decided that the point is adequately substantiated and no further extension of the work (unless experimental) in relation with this topic seems to be necessary.

3.5 Alternatives to Approach the Residual Stress Problem and Discussion

The aim of this part of the work is to obtain the K value for a cracked tooth under residual stress. Two sets of information are available:-

1. Stress pattern depicted in Fig.3.11
2. Results and work done in the former cracked gear and described in the first part of this chapter.

To solve this case, the first step concerns the method to be used.

Because of the conditions given as well as availability of programs and computer facilities, two methods could be considered as a possibility, these are the J contour integral and Bueckners Method.

On revising work published, Rice (1968), it was noticed Rice's statement that when the crack faces are not stress free his method is not applicable; a plausible reason for this is described below.

As it is well known, the J contour integral is defined as

$$J = \int_{\Gamma} (W dy - \bar{T} \cdot \frac{\partial u}{\partial x} ds)$$

J being an average measure of the strain on the crack tip, Γ is a curve surrounding the crack tip, the integral being evaluated in a contraclockwise sense starting from the lower crack surface and continuing along the path Γ to the upper crack surface. $\bar{T}$ is the traction vector defined according to the outward normal along Γ, $T_i = \sigma_{ij} n_j$, u is the displacement vector, and ds is an element of arc length along Γ. The analysis by Rice was as follows. "Consider any two paths (Fig.3.12a) Γ_1 and Γ_2 surrounding the crack tip; traverse Γ_1 in the contraclockwise sense,

continue along the upper flat notch surface to where Γ_2 intersects the crack, traverse Γ_2 in the clockwise sense, and then continue along the lower flat notch surface to the starting point where Γ_1 intersects the crack. This describes a closed contour so that the integral of $Wdy - T(\partial u/\partial x)ds$ vanishes. But $\bar{T} = 0$ and $dy = 0$ on the portions of the path along the crack surfaces. Thus the integral along Γ_1 contraclockwise and the integral along Γ_2 clockwise sum to zero. J has the same value when computed by integrating along either Γ_1 or Γ_2, and path independent is proven".

In examining the case under study one is interested in the term

$$\bar{T} \cdot \frac{\partial u}{\partial x} ds$$

where , in relation with the present case we have

The traction $\bar{T}$	On the path from Γ_1 to Γ_2 at the upper crack face, this traction is negative (as it is directed going in to the body).
The element of arc length ds	Is positive (it is measured from Γ_1 to Γ_2) the integration is being performed along the positive x direction.
The traction $\bar{T}$	On the path from Γ_2 to Γ_1 at the lower crack face is negative (same reason).

The element of arc length ds	Is negative (integration being carried out from Γ_2 to Γ_1 in the negative x direction).
The partial differential $\frac{\partial u}{\partial x}$	Is the strain on the path followed.

It is quite clear that provided $\partial u/\partial x$ is the same both in the upper and lower face the integration over these parts of the path would be zero, for this to be true it is necessary to have symmetry in loading and in geometry. For this case, symmetry in loading exists but not in geometry, so the quantities $\bar{T} \frac{\partial u}{\partial x} ds$, corresponding to the upper and lower crack faces, do not cancel out and the J contour integral becomes different for different points on the crack face, so the conclusion is that loads applied (tractions) on the crack faces do make a difference on the J contour integral and so it is not possible to use this method in the present case.

Further comments on this topic were made by Hutchinson and Turner (1975) who gave a formula to obtain J for cracks loaded on the face by say pressure p

$$\int_{\Gamma_2} = \int_{\Gamma_1} + 2 \int_{-r_2}^{-r_1} p \frac{\partial v}{\partial x} dx$$

where r_1 and r_2 are the distances from the crack tip over which p is applied, v is crack face displacement, $J = \int_{\Gamma_1}$, as $r_1 \to 0$, so

$$J = \int_{\Gamma_2} + 2 \int_0^{r_2} p \frac{\partial v}{\partial x} dx$$

If p is constant from the tip to same radius r_2, then

$$J = \int_{\Gamma_2} + 2\ p\ v\ (r_2)$$

If this is to be path independent then $\int_\Gamma$ must itself vary with r_2 to compensate for the variation of p v (r_2), and this formulation could be used for residual stress problems by Bueckner's method, which is the next possible choice as most of the computer material developed for the former case could be used although some additions are necessary.

Bueckner's (1958) method for evaluation of K is well known and a generalised description is presented to approach the problem, two situations are considered.

1. A body with prescribed boundary conditions on which certain tractions on surface S_1 and boundary displacements on surface S_2 are given. A crack is presumed to exist in the body with upper and lower faces C_1 and C_2 (Fig.12a).
2. Consideration of the same body, subject to the same loading, after a virtual crack extension resulting in new surfaces C_1' and C_2' (Fig.3.12b).

The combination of these two situations towards a sum state (Fig.3.12c) and a difference state (Fig.3.12d) allows the evaluation of tractions on the crack face which can be regarded as those tractive components of stress which act on the notional surfaces C_1' and C_2' prior to virtual crack extension. With these tractive components and the displacements obtained on applying them to the body it is possible to obtain the potential energy "u_d" and by allowing the crack to go progressively from zero to full length it is possible to obtain $\partial u_d/\partial a$, that is obtain G.

Boundary Conditions and Loading

The dimensions are those already given. A finite element analysis is to be used, for plane strain and unit thickness, with the same boundary conditions as in the former case but with no load at the pitch circle.

From analysis of the data given it is concluded that

(a) the stress distribution on points under the surface of the body is compressive and parallel to the body's surface;

(b) the crack will be perpendicular to the body surface, being the stress pattern imposed normal to the crack surfaces;

(c) there is no shear stress accompanying this normal stress;

(d) it was concluded that an opening effect takes place at some stage of the process in which the residual stresses are set up into the body, so the effect of the normal stress is to open up the crack.

The mesh used in the former case should be slightly modified so that the crack length is 3mm and normal to the true local surface of the tooth root.

The loading for this case is introduced as concentrated forces (tractions) applied to the nodes on the crack face, the value of each individual load as calculated from the stress pattern is given in Table 3.4 A preliminary analysis done in order to find out how well this loading would reproduce the stress pattern given, was carried out and the results of this are shown in Fig.3.13, (further discussion is given in Section 3.6).

3.6 Analysis of the Stress Field

In the computer simulation of this problem there are some characteristics of the stress field which must be preserved, and provided this is done in the computer analysis, the simulation will be a reliable one. In this case the data given establishes certain known values for the stresses on the crack faces, i.e. normal stress is as the pattern given in Fig.3.11(a) and shear stress equal to zero along the crack faces. Relevant results from the finite element analysis when the loading method described is applied, are given in Fig.3.13b. From this figure it could be wrongly concluded that the necessary conditions are not preserved as differences are encountered on the stress pattern produced in the body, but it is the singularity introduced by the crack in the stress field, and its influence in the neighbourhood of the tip that projects a deceptive pattern. Proper analysis of the stress field proves the correctness of the loading method. In order to illustrate this point use is made of Fig.3.14 which shows the neighbourhood of the crack as well as the respective positions of lines to which reference is to be made in the analysis below.

In Table 3.5 and 3.6 values of normal and shear stresses along lines perpendicular and parallel to the crack face are given. Plots of normal and shear stresses along those lines are given in Figs.3.15 (a to j).

In analysing Figs.3.15 (a,b,c) it can be seen that: the shear stress on elements which are the nearest to the crack face are -951 lb/in^2 and 693', 1982' and 798', 2635' and -2828' (by definition negative shear on the upper crack face and positive shear on the lower one mean positive traction, and the

other way around), for lines 1, 3 and 5 respectively; from these figures one can conclude that it is not the particular value of the stress in an element which should be looked at, but the whole stress field. If these values were considered either each one by itself or the six, without relating them to the whole of the stress field, the conclusion would undoubtedly be that the shear stress at the crack surfaces is different from zero (even though it is known that the shear boundary forces fed to the finite element programme are zero). Proper analysis of the whole zone shows the fact that the stress field in the neighbourhood of the crack faces tends to zero and it is this tendency which shows that all these values are a computer approximation to zero. This is very clear in Figs.3.15a, 3.15b and 3.15c although in the latter one it is not as clear as in the former two cases. Obviously, the singularity introduced by the crack becomes apparent at the neighbourhood of the tip. A finer mesh in this zone would show that the already described tendency of the shear values towards zero for the former two cases, applies to the third one as well. Another point to consider is that the straight lines drawn on Fig.3.14 do not always cross the elements through the centroids. As the line is nearer or farther away from a centroid the stress value for the element is respectively more or less representative of the true stress on that segment of the line. Because of this, some of the values are not really representative of the true stress in certain zones, and this is obvious for those zones in which the line (along which the stress is being evaluated) crosses the element far away from its centroid.

The argument already used for shear, applies to normal stresses and with relation to Figs.3.15d to 3.15j the points described below are relevant.

Fig.3.15d. Plot of normal stress values along line "1" (the farthest away from the crack tip). The stress value on the nearest element to the crack face is -14206 lb/in^2 but the tendency of the stress curve is towards a smaller value, the expected value (from Fig.3.13) is around -11500 lb/in^2. The conclusion is that the stress pattern is the correct one in that zone. The same analysis applies to Fig.3.15a with reference to line "2".

Fig.3.15f. Here, it can be seen that the influence of the x coordinate starts to show up and in order to perform a better analysis one has to split the stress values of at least the first 8 elements along this line. Obviously the true stress value for points on the line would be somewhere in between these values. It is thought that it is relevant to find out the tendency of the stress curve, and the two plots on this figure are good enough for this purpose showing similar tendencies in the neighbourhood of the crack surface. This tendency is clearly towards the value given in Fig.3.13. The same analysis is applicable to Figs.3.15g and 3.15h although for these it could seem that the stress values are different from the ones expected. However, it is thought that in this neighbourhood the influence of the stress field singularity is such that any small change of the coordinates greatly affects the stress value obtained (it has to be kept in mind that the stress values are for the centroids of the elements and these centroids are away from the crack face), but this stress field, on approaching the

crack face, has a tendency towards the expected value. A finer mesh would show this point. However, in solving the present problem this finer mesh is not necessary and so far, the analysis of results has shown that the stress values on the crack faces are as expected so it is thought that the whole stress pattern is correct.

3.7 Elastic Potential Energy and K Values

Results from the finite element calculations were used to obtain the values of the elastic potential energy for different crack lengths and these are given in Table 3.7 By differentiating these values with respect to crack length and later on fitting a polynomial, the curve of K_I values given in Fig.3.16 was obtained.

In relation to this stress intensity factor curve, it is fundamental to point out that for the present case there is a combined mode I mode II behaviour. This is because even though there is symmetry in the loading, the geometry of the specimen is asymmetrical, but the mode II effect is a negligible one. This statement rests in the fact that there is no shear stress on the crack surface so there is not a singularity on the mode II crack behaviour, that is, in considering the mathematical representation of the stress field around the crack, the first coefficient corresponding to the antisymmetric representation (directly proportional to K_{II}) equals zero. Only higher order terms are considered and these approach zero when the crack tip is approached. For the case treated in the first part of this chapter this is not so (there is a singularity in mode II) as the loading is not symmetric, and it has to be pointed out that the K values given there include mode I and mode II crack behaviour.

CHAPTER 4

FRACTURE UNDER COMPLEX STRESSES AND DIRECTION OF CRACK PROPAGATION

4.1 Instances in which it is Desirable to Control Direction of Crack Propagation

A case has already been discussed in which it was necessary to have a criteria for directional stability of crack propagation. The case of the gear tooth presented in Chapter 3 is only one among many in which it is desirable to control direction of crack propagation so that failure, if it occurs, is by loss of a tooth rather than complete severence of the gear. Another instance similar to the gear case in which this approach might apply, concerns turbine blades. Most of the research being conducted in laboratories uses test specimens which deal only with cracks loaded symmetrically (mode I behaviour), however, it will be shown (Section 4.5) that even when loading and geometry are symmetric, there may be a natural tendency for the crack to run away from the axis of symmetry. This tendency immediately introduces mode II behaviour and it has been shown (Section 2.2) that this makes slight changes in parameters such as fracture toughness that are considered to be dependent on only mode I behaviour. The nature of this change is negligible for the purposes of fracture toughness determination, but it surely has a strong influence (i.e. this influence is not negligible) in two other aspects, (i) fracture initiation mechanism, (ii) direction of crack propagation. It is well known that the stress intensity factor K_{II} designates the amplitude of the crack-tip stress owing to skew-symmetric loading, so it will only operate when asymmetry, either in loading or geometry, is present. In experimental work

this asymmetry is always present, sometimes coming from non-alignments in the experimental rig (this effect could be a very strong one), or from inhomogeneities in the material (which set up local stress concentrations). These effects have always shown up in the laboratory, the very fact that strong differences in crack path have been obtained in experiments which are supposed to be repetitive in their operative conditions, show the differences that a minor defect in material homogeneity could make.

In practice, problems of this type arise in multi-phased materials such as composites, bridge and aircraft structures, welded materials reinforced components, etc. in which inhomogeneities and flaws already exist and/or develop because of natural working circumstances. If conditions to control crack path can be known, then it should be possible, when a crack exists and propagates into a body, to drive its tip towards a zone in which arresting conditions exist.

The onset of rapid crack extension (and any other experimental behaviour) is not always sharply defined, but the load at which it occurs (for brittle materials) is very little different from the maximum load recorded. It is not clear how, for a practical case, one would calculate a representative value of say K_{1c}, or any other parameter which would agree with those obtained from a different specimen design, and because of this it can be said that some degree of uncertainty always exists, and that some specimens are conservative (standard K_{1c} method with its limitations on thickness, linearity, etc. seems to have overcome this difficulty). Since it is not known how conservative they are, a penalty may be imposed on the material that is being evaluated if a wrong

specimen type is used to evaluate the necessary parameters, so special care must be exercised when deciding upon specimen type. If this is so for the case of such a parameter as K_{1c}, which has been so extensively studied, then it can be seen how difficult the task of obtaining parameters to define directional stability of cracking could be. Surely there are a lot of questions which have to be answered before having a solution to this problem, they concern the effect of local inhomogeneities, anisotropies, residual stress, biaxiality, rate effect, is only a rapid crack unstable in direction or would a slow crack also be unstable? does scatter in K_{1c} values really matter? eg do high values of scattered K_{1c} data correspond to cracks wandering off direction?

The conclusion is that when performing experimental work, intended to define directional stability of crack propagation, it is necessary to select one of these aspects as variable and try to keep the others as constant as possible. For the purpose of the present study, mainly the effect of loading biaxiality will be looked at, but it is necessary to keep an open mind and try to identify possible co-relations between experimental results and any of the topics already mentioned.

4.2 Review of Work Done on Directional Stability of Crack Propagation

A great deal of valuable work has already been conducted regarding directional stability of crack propagation, a short summary of some of the most important is given hereafter. It is felt by this author that the review presented is brief but this is because only work highly relevant to the specific objective of the present study was selected and presented here with the purpose of using it as an additional tool to expand the understanding of the phenomena that is being dealt with.

One of the very first comments on direction of cracking is found in Griffith (1920) who stated that, "it is necessary in the present application, however, for the resulting stress system to be symmetrical about the crack, as otherwise it is not obvious that the latter will remain straight as it spreads. The only stress distribution which will be considered, therefore, is that in which the principal stresses in the plane of the plate, at points far from the crack, are respectively parallel and perpendicular to the crack, and are the same at all such points. This is equivalent to saying that, in the absence of the crack, the plate would have been subjected to uniform principal stresses in and perpendicular to its plane. It is also necessary, on physical grounds, for the stress perpendicular to the crack and in the plane of the plate to be a tension, otherwise the surfaces of the crack are forced together instead of separated, and they cannot remain free from traction".

Obreimoff (1930) was the first one to study stable crack spreading. By wedging open a crack in mica and finding the length of crack in equilibrium with a given displacement normal to the crack surface, he also estimated the local work of crack spreading from simple beam theory.

Irwin (1957). In a discussion of the stress field parameters which significantly influence the fracture process, proposed that cracks will grow in a direction controlled by the orientation of the maximum stress direction at the crack tip.

Benbow and Roesler (1957). The aim of their work was the determination of a specific fracture energy which is shown to govern crack propagation. They used a wedge as the instrument for opening the crack on a flat strip specimen, and showed that transverse compression inhibits the crack growth normal to the plane

of symmetry and so it must, to some extent, provide directional stability of crack propagation.

Forsyth (1961). Proposed that the fatigue fracture process occurs in metals through two steps, phase I. Flaw growth takes place in a direction parallel to the crystallographic plane of maximum shear stress. Phase II - macroscopic fracture propagates in a direction perpendicular to that of the maximum stress.

Guernsey and Gilmain (1961). Reported photoelastic work made on the stress distribution in the vicinity of the root of the crack in a SEN specimen. This work indicated the nature of the deformation sustained by the uncracked region but did not explore the stress distribution over the complete sample as a function of crack length. They showed that the gradient of the maximum tensile stress in the vicinity of the crack tip is such that the crack tends to deviate from its median position and turn towards the edge of the sample, a tendency which increases with increasing deviation, so it is necessary to apply constraints to the sample to so change the stress distribution that the crack remains in the median plane. In relation to this topic, in Section 3.3 a similar analysis is made for a cracked gear, here the stress field was obtained numerically, but there is ample evidence that these field values are as good as the experimental ones, and it leads to the conclusion that the crack should propagate along a line of minimum principal stresses emanating from the crack tip, i.e. perpendicular to maximum principal stress.

Erdogan and Sih (1963) carried out a study of the initial direction of crack growth in a biaxial stress field and re-examined the original hypothesis of Griffith that the crack extends in a direction perpendicular to the local maximum tensile

stress. A series of fracture experiments on plexiglass sheets with an inclined crack was performed and the results checked reasonably well with the criterion of maximum stress. They stated two hypotheses for the extension of cracks in brittle materials under slowly applied loads:-

(a) the crack grows in a direction normal to the maximum local stress at the tip of the crack;

(b) the crack growth in this direction releases the maximum energy.

They also showed the first hypothesis to be true for the initial stages of propagation.

Schijve (1964). Studied the effect of the fracture angle on the shear stress distribution in the neighbourhood of the crack, describing the nucleation and the growth of a fatigue crack as being geometrical consequences of dislocation movements at the surface and in the crack tip region respectively. In his report he mentions some work carried out at NLR (Nationeal Luct-en Ruimtevaantlaboratorium, Amsterdam) in which a fatigue machine combined with a microscope and stroboscopic light was developed to follow crack propagation. Fatigue experiments were carried out and the results showed a constant rate of crack propagation while the crack was running straight. When a change of orientation in the crack occurred it was preceded by a slowing down of the growth (at the surface). Then no crack growth was observed for some time after which growing continued in another direction. The first part of this new crack extension sometimes occurred quite rapidly. Schijve argued that it is possible that the direction of growth before the change of orientation could not be maintained, because it was not compatible with the path of the crack below the surface. This restraint released the shear stress on the slip system being active at the surface, and the crack growth slowed down. Crack growth along another slip plane required an increase of shear stress

on that plane, which was effected after the crack below the surface had gone through some further growth, such a process leads to unbalanced crack extension at the surface and probably it will occur at the interior of the material as well, which implies that crack extension does not simultaneously occur along the entire crack front.

Valluri (1965). Made a study of the biaxial failure of metals and polymers, developing failure envelop concepts in which, failure planes described by the principal stress components, were used as loci of points of limiting stability for fracture under multiaxial loading conditions.

Cotterell (1965). Defined two classes of fracture: 1. fracture path completely predictable, and 2 fracture path predictable only after initial random propagation. Class I fracture occurs when there is a line of principal stress passing through the tip of the initiating notch or slit, across which the stress is a maximum away from the tip. (Cotterell did not establish a dimension for the distance "away from the tip", what his analysis states is not that σ_n is an absolute maximum but that the direction of maximum release of energy and of propagation in a perfect solid, is along a line of local symmetry.) All Class II fractures eventually become Class I. He also showed that although the probability for incremental growth in any one direction is low, the line of local symmetry is a highly probable path for macroscopic growth, and concluded that concerning crack behaviour, after a possible initiation of random Class II fracture, the macroscopic fracture path becomes very predictable. Fracture growth will be along the line of local symmetry across which the principal stress is a maximum, confirming the hypothesis that cracks will extend in a radial direction from the tip normal to the direction of maximum tangential stress. Later on Cotterell (1966), from consideration of the second term in the power series solution of the stress field in a

cracked body, reached the same conclusion, i.e. that a crack will propagate along the principal stress plane passing through its tip. Cotterell considered that there is only one line of principal stress passing through the tip of the crack - the line of local symmetry. In general two lines of principal stress normal to each other would be expected, but it must be remembered that the crack is considered to be the limit of an ellipse and in the limit the second line of principal stress becomes the line of the crack in the negative direction.

Gurney and Hunt (1967). The main topic of this work has already been presented in Chapter 2, i.e. determination of the local specific work of crack spreading or fracture toughness (R). Under this same work a principle controlling the path of a quasi-static crack is proposed that is, crack paths should be those directions into which strain energy is released at the maximum rate of entropy production for a cracking process, and offers some experimental confirmation.

Barr (1968). Found that the direction of rolling of the material during manufacturing, has an influence on the crack path. He also tried different geometries in trying to obtain directional stability of crack propagation, this involved linear variations of the I value (second moment of inertia of the section), sudden change of cross section, gradual change of cross section, special loading conditions, etc, but only partial success was obtained. Barr discussed as well, the effect that bending stresses have on the path of the crack in a test specimen.

Arad (1972). Some of the experiments he carried out were on grooved specimens and concluded that a general feature of the outcome of the series of tests was that irrespective of the groove orientation angle, the crack did not extend along the plane of the groove. However, the specific characteristics of the crack

propagation process could be influenced by the depth of the surface grooves. Up to a groove with about 60% reduction in specimen thickness, the initial crack turned immediately to form along a minimum principal stress trajectory.

Aida and Kobayashi (1969). Results obtained in their work suggest that a fatigue fracture that is initially under biaxial load will propagate initially in the direction of maximum value of K_I, and at the same time the K_{II} value tends to decrease until it reaches its minimum value. In Section 5.3 of the present study, some work which is relevant to this topic, is discussed.

Tuba and Wilson (1970). Proposed the use of a criticality plane described in terms of the three stress intensity factor components K_I, K_{II} and K_{III}.

Cotterell (1970). Reported tests on the criterion developed in relation with the sign of the second coefficient of the Williams series, and suggested a simpler criterion based on the engineer's theory, for the determination of the stability of fracture path in the compact tension test. This will be discussed in some detail in Chapter 7.

Roberts and Kibler (1971). Found that under conditions of application of a combined static and reversed bending type of loading, the direction of fatigue crack growth on a macroscopic scale, was in the plane of the initial crack. Consideration of crack growth at a relatively lower scale, proved the growth mechanism to be as that described by Irwin (1957) and others, i.e. small extension in the direction perpendicular to that of maximum principal stress. However, due to the reversing nature of the load cycle, in each full cycle two principal stress directions, distributed symmetrically about the crack plane, are obtained and thus the crack tends to propagate in a saw-pattern.

Williams and Ewing (1972). Applied a uniaxial stress to thin plates of polymethylmethacrylate (PMMA) containing a crack angled to the stress field, and showed that inclusion of the stress component parallel to the crack can improve the correlation between linear theory and experiment, using a critical stress at a critical distance for interpretation of the stress intensity factor. This inclusion of the stress component parallel to the crack means that the second term in the series expansion for the stress distribution in the neighbourhood of the crack tip is considered.

Finnie and Saith (1973). Discussed Williams and Ewing's work, and pointed out an error in the mathematical development carried out. Finnie and Saith's correction gave an improved correlation between theory and experimental results for centre notched sheets in tension.

Sih (1973). Proposed a new concept for fracture path prediction. For elastic materials the new criterion is expressed in terms of the strain energy density factor S. The application of the S-factor to fracture prediction is based on two hypotheses: (a) crack initiation occurs when the strain energy density factor reaches a critical value, (b) the initial crack growth takes place in the direction along which the strain energy density factor possesses a stationary maximum value. Since strain energy is considered, the prediction is a function of Poisson's ratio and will also differ for plane stress and plane strain conditions.

Finnie and Weiss (1974). Performed two experiments with beryllium sheet in order to compare the new Sih theory with the original Erdogan and Sih approach. Beryllium was used for these tests as its Poisson's ratio in the plane of the sheet is almost

zero and the experiments were simplified by making β = 45 deg. (being β the angle between loading direction and crack). They state that their experimental results strongly support the original Erdogan and Sih analysis rather than Sih's new theory.

Coughlan and Barr (1974). Carried out a finite element analysis for a square plate, with an angled crack, under biaxial loading conditions, as well as experimental work using PMMA (ν = 0.3) and good agreement was obtained between the numerical and experimental results, and these results compare favourably with the results of Sih.

Mai et al (1975). Carried out tests on tapered SEN specimens, suggesting a modified test with loading applied at the thick base instead of near the apex, showing that experiments agree with theory, providing a better control of the crack path, concluding that backface loading may be chosen as an optimum alternative means for the determination of valid fracture toughness of materials, especially when good stability of cracking is desired for experimental applications such as in environmental testing. They also concluded that the simple criterion $\sigma_y/\sigma_x > 1.0$, coupled with elementary beam theory for the determination of a straight propagating crack along the mid plane of the specimen, is adequate for their analysis.

4.3 Mathematical Description of the Stress Field in the Neighbourhood of a Crack

Many investigators have studied the elastic stress distributions around cracks, with some of the earliest contributions from Inglis (1913) who studied an external crack using elliptical bounding surfaces, Westergaard (1934) who initially treated the crack problem as a series of expansions and later on (1939) by

the complex variable technique. Williams (1952) investigated the plane-stress distribution near the vertex of an infinite sector of included angle α for various boundary conditions and in (1957) considered the case where two radial edges of the plate are unloaded and the included angle approaches 2π, which corresponds to the case of a crack with flank angle $\omega = \alpha - 2\pi = 0$. He showed that the function

$$\begin{aligned}\chi(r,\psi) = \sum_{n=1}^{\infty} \{ &(-1)^{n-1} A_{2n-1} r^{n+\frac{1}{2}} [-\mathrm{Cos}(n-3/2)\psi + \left(\frac{2n-3}{2n+1}\right)\mathrm{Cos}(n+\tfrac{1}{2})\psi] \\ &+ (-1)^{n} A_{2n} r^{n+1} [-\mathrm{Cos}(n-1)\psi + \mathrm{Cos}(n+1)\psi]\} \\ + \sum_{n=1}^{\infty} \{ &(-1)^{n-1} B_{2n-1} r^{n+\frac{1}{2}} [\mathrm{Sin}(n-3/2)\psi - \mathrm{Sin}(n+\tfrac{1}{2})\psi] \\ &+ (-1)^{n} B_{2n} r^{n+1} [-\mathrm{Sin}(n-3/2)\psi + \left(\frac{n-1}{n+1}\right)\mathrm{Sin}(n+1)\psi]\}\end{aligned} \tag{4.3.1}$$

describes the stress field in the neighbourhood of the notch with zero angle, pointing out that even though the field equation and the boundary conditions along the radial edges are satisfied, the constants A_i and B_i are undetermined. Their values depend upon the loading conditions, more specifically, either upon the boundary conditions at infinity in the case of an infinite sector, or upon those at some fixed radius when the plate has finite dimensions. For the latter practical case, all the Eigen functions in general will be present in order to determine a solution in the large.

From the general definition of the stress function it is known that

$$\begin{aligned}\sigma_r &= \frac{1}{r^2}\frac{\partial^2 \chi}{\partial \psi^2} \\ \sigma_\psi &= \frac{\partial^2 \chi}{\partial r^2} \\ \sigma_{r\psi} &= \frac{1}{r}\frac{\partial^2 \chi}{\partial r \partial \psi} + \frac{1}{r^2}\frac{\partial \chi}{\partial \psi}\end{aligned} \tag{4.3.2}$$

the mathematical development of these partial derivatives is shown in Appendix for Chapter 5 and the equations for the stress fields are obtained as

$$\sigma_r = \sum_{n=1}^{\infty} \{(-1)^{n-1} r^{n-3/2} A_{2n-1} (n-\tfrac{1}{2})[(n-7/2)\cos(n-3/2)\psi - (n-3/2)\cos(n+\tfrac{1}{2})\psi] + (-1)^n r^{n-1} A_{2n}\, n\,[(n-3)\cos(n-1)\psi - (n+1)\cos(n+1)\psi]$$

$$+(-1)^{n-1} r^{n-3/2} B_{2n-1} (n-\tfrac{1}{2})[(n-7/2)\sin(n-3/2)\psi - (n+\tfrac{1}{2})\sin(n+\tfrac{1}{2})\psi]$$

$$+(-1)^n r^{n-1} B_{2n}\, n[(n-3)\sin(n-1)\psi - (n-1)\sin(n+1)\psi]\} \frac{1}{1+\nu} \qquad (4.3.3)$$

$$\sigma_\psi = \sum_{n=1}^{\infty} \{(-1)^{n-1} r^{n-3/2} A_{2n-1} (n-\tfrac{1}{2})[(n+\tfrac{1}{2})\cos(n-3/2)\psi - (n-3/2)\cos(n+\tfrac{1}{2})\psi] + (-1)^n r^{n-1} A_{2n}\, n[(n+1)\cos(n-1)\psi - (n+1)\cos(n+1)\psi]$$

$$+ (-1)^{n-1} r^{n-3/2} B_{2n-1} (n-\tfrac{1}{2})[(n+\tfrac{1}{2})\sin(n-3/2)\psi - (n+\tfrac{1}{2})\sin(n+\tfrac{1}{2})\psi]$$

$$+ (-1)^n r^{n-1} B_{2n-1}\, n[(n+1)\sin(n-1)\psi - (n-1)\sin(n+1)\psi]\} \frac{E}{1+\nu} \qquad (4.3.4)$$

$$\sigma_{r\psi} = \sum_{n=1}^{\infty} \{(-1)^{n-1} r^{n-3/2} A_{2n-1} (n-\tfrac{1}{2})[(n-3/2)\sin(n-3/2)\psi - (n-3/2)\sin(n+\tfrac{1}{2})\psi]$$

$$+ (-1)^n r^{n-1} A_{2n}\, n[(n-1)\sin(n-1)\psi - (n+1)\sin(n+1)\psi]$$

$$+ (-1)^{n-1} r^{n-3/2} B_{2n-1} (n-3/2)[(n-3/2)\psi - (n+\tfrac{1}{2})\cos(n+\tfrac{1}{2})\psi]$$

$$+ (-1)^n r^{n-1} B_{2n}\, n[(n-1)\cos(n-1)\psi - (n-1)\cos(n+1)\psi]\} \frac{E}{1+\nu} \qquad (4.3.5)$$

These equations fully describe the stress field in the neighbourhood of a crack and will be fundamental in the present study.

4.4 The Stress Field and Directional Stability of Crack Propagation

Regarding the stress field, when a crack propagates there must be a gradual change in it, this has been shown in Section 3.3. When a material is stressed, and the condition is reached that the strength in the material is equal to its toughness, the material separates, resulting in a longer crack, Clausing (1969) has presented a good discussion on this point. The new crack dimension depends on conditions existing just before extension occurs. To illustrate this point, let us take as an example a blunt crack (meaning by this, that its tip is slightly rounded, with a ρ radius) and apply an energy criterion for extension. As load is applied to the specimen, energy is being stored and of course, a stress field characteristic of the geometry, develops. When a critical energy level (which is a characteristic of the material and a function of ρ) is reached, the crack extends by a jump of the crack tip, the tip of the crack becoming sharp. It is fairly easy to understand this jump, as when the crack extension starts the change in geometry at the tip is a sudden one and there is an excess of energy available (as the energy necessary to propagate a blunt crack is higher than that necessary to propagate a sharp crack), this energy is partially transformed into kinetic energy and partially into surface energy (brittle fracture). This jump has an effect on the stress field because new geometric conditions are settled, and this effect is basically that the principal stresses at the crack tip (σ_1 and σ_2) change but the tangential stress remains zero, this is provided that the loading and geometry before and after crack propagation are symmetric. These changes could set up conditions conducive to directional instability of crack propagation, regardless of symmetry in geometry and loading.

It has been shown, Benbow and Roesler (1957), Cotterell (1966,1970), Mai et al (1975) that directional stability is achieved if, at the crack tip, the principal stress (σ_x) along the crack surface (as calculated theoretically) is equal to or lower than the stress perpendicular to the crack surface (σ_y). This effect is shown by the isochromatic field ($\sigma_y - \sigma_x/2$), as was shown in Section 3.1. Cotterell (1966) argued that as the crack length is increased, for certain loading conditions, the fringes (isochromatic lines) at the crack tip neighbourhood, become more upright and finally, for cracks longer than certain finite length, lean backwards. He also pointed out that for a SEN specimen only those fractures initiated from initial notches short enough to cause the isochromatic fringes to lean forward, run straight for any appreciable distance before deviating to one side or another. The work described in Section 3.3 of this study, leads to the same conclusions.

The isochromatics behaviour already described, only shows the changes that are occurring in σ_1 and σ_2. With this as background, it can be stated that the conditions that govern directional stability change as the crack extends, and this is whether or not the specimen and loading conditions remain symmetric. This aspect will be discussed further in Chapter 7.

A further point can be made by means of the following discussion, supposing that a SEN specimen is being analysed, and that in order to determine the stresses, the Williams' series is to be used. To start with, only transverse load is applied i.e. load parallel to the crack, and it is perfectly symmetrical so, under this loading, there will not be any stress singularities, i.e. $A_1 = B_1 = 0$ (A_i and B_i are symmetrical and antisymmetrical coefficients in the Williams' series), the A_2 coefficient will

have a value which when multiplied by $F(\theta)$ should describe the transverse stress, and higher order terms have zero value coefficients. The next step is to introduce mode I and/or mode II behaviour. This will introduce a singularity and also the A_2 coefficient will be modified, its full value being the addition of the effects of each load, but it will still determine the value of σ_x and so could define (through $\sigma_y/\sigma_x > 1$ Cotterell, 1970) directional stability. So it can be said that the second coefficient in the series is very important because its value is directly related with σ_x at the crack tip, and the already discussed changes in the stress field, are depicted by any change in this second coefficient.

4.5 Directional Stability of Crack Propagation and Proposed Criteria

It is thought that a factor of considerable importance in the process of fracture under arbitrary loading conditions, is the determination of the path of crack extension. The aim of this part of the work is to investigate proposed criteria for directional stability of crack propagation, mainly under mode I although some aspects of mode II will be tackled as well.

The bibliographical material which has been reviewed, as well as personal work, has led this author to think that the direction of crack propagation aspect of the fracture process, could be depicted as follows.

There are two types of conditions that influence the fracture process. (a) Global conditions - such as geometry, loading, material, environment, etc. and (b) local conditions - such as flaws and material imperfections encountered in the neighbourhood of the fracture path. The former can be modelled mathematically

and the crack behaviour is predictable, the latter cannot be predicted (unless by statistical analysis), as they could be thought of as accidental elements in a material's structure and as such they are unpredictable. Taking this into consideration, the process of propagation of the crack could be described as:

(1) Geometry, loading, material, environment, etc., establish global conditions which in the first instance determine, in a general way, where the crack will go.

(2) As the loading process takes place (either displacement or load), local conditions become apparent. These are a consequence of imperfections, and modify the stress field in the neighbourhood of the crack tip.

(3) When the condition in which the stress in the material is equal to the critical fracture stress (material's toughness), the material separates and the fracture advances until its tip reaches a point in which arresting conditions exist, i.e. the stress level in the material is lower than the material's toughness, so crack propagation stops.

(4) If, under (3), global conditions dominate, the crack will extend in a prescribed way, a predictable path, according to Cotterell (1966) class I fracture and stop. If the local conditions are the ones that dominate, the crack will propagate in a random direction (most probably towards the imperfection), in a class II fracture and stop.

(5) Once it has stopped, global conditions for the new general geometry are settled and a new process for further crack propagation starts.

Regarding global and local conditions, there are some factors that are known to influence this global condition, i.e. specimen dimensions (for SEN specimens, the square ones have a better directional stability than the long ones), grooving is another geometrical influence, and stressing (compression) the specimen longitudinally to the crack surface has a stabilising effect as well. Up to now, the quantification of this directional stability has not been fully achieved, however, it is perfectly clear that there are experimental conditions which can set up a greater degree of directional stability i.e. in reference to a σ_x stress (by this it is meant the magnitude of the transverse stress set up within the specimen because of the application of a compressive load parallel to the crack) the higher it is, the longer the crack runs straight, so even if limits are not numerically quantified, it can certainly be established that a specimen is highly stable (concerning direction of crack propagation) under certain experimental conditions.

According to this and in relation with directional stability of the extension process, in point (1) above, the global condition at the start of an experiment could be

(a) highly stable

(b) stable

(c) unstable.

For case (a), when (2) operates, two different situations could develope:-

(i) the local condition could not be such as to overcome the global one, so the crack runs straight;

(ii) the local condition is such that it overcomes the global one, so the crack extends in a random direction and stops.

Once it has stopped, new global conditions become apparent and, as the initial global conditions were highly stable, most probably the new ones are still highly stable and the crack will tend to come back to the original path.

For case (b), when (2) operates, two different situations could develop:-

(i) The crack runs straight unless a local condition becomes apparent.

(ii) Any small local condition overcomes the global one and the crack runs away from the straight path. As the crack was just stable, any change in direction will make it more unstable and it will keep changing for the worse.

For case (c), when (2) operates, the crack will only become more and more unstable.

It has been pointed out that it is extremely difficult to predict local conditions, however this is not especially relevant as this author's view is that, regardless of what the local conditions are, global conditions are the main factors that control crack path and if these conditions can be kept highly stable, the crack will continue its extension in the original direction. So, the first step under this part of the work should be to establish roughly which are the parameters that govern global conditions, so that in a second step they can be quantified.

In the past, different criteria for directional stability have been put forward, here it is intended to do some work on two of these approaches, although only the first step already mentioned will be covered.

It is proposed:-

1. To investigate the roll of the second coefficient of the William's series, as a parameter defining directional stability.

2. To use the values determined for the coefficients in the Williams' series, and apply to the SEN specimen the criteria proposed by (a) Williams and Ewing (1972) i.e. determination of a critical stress at a core radius, (b) Sih (1973) i.e. determination of the critical Strain Energy Density Factor S.

Further discussion on this topic is to be done in Section 6.5.

CHAPTER 5

THE WILLIAMS' STRESS FUNCTION AND ITS APPLICATION TO THE SINGLE EDGE PLATE SPECIMEN

In this chapter the basic problem of analysis of a crack tip stress field is being examined by means of the Williams stress series. The main steps to develop a computer program for obtaining the values of higher order coefficients are discussed, and work on the testing of this program is done by comparing results with former work carried out by other researchers.

5.1 The Coefficients of the Williams' Stress Series as Parameters Characterising the Behaviour of Cracked Specimens

Williams (1957) obtained the function

$$\begin{aligned}\chi(r,\psi) = \sum_{n=1}^{\infty} \{ & (-1)^{n-1} A_{2n-1} r^{n+\frac{1}{2}} \\ & \left[-\cos(n-3/2)\psi + \frac{2n-3}{2n+1}\cos(n+\tfrac{1}{2})\psi\right] \\ & + (-1)^{n} A_{2n} r^{n+1} \left[-\cos(n-1)\psi + \cos(n+1)\psi\right] \} \\ + \sum_{n=1}^{\infty} \{ & (-1)^{n-1} B_{2n-1} r^{n+\frac{1}{2}} \\ & \left[\sin(n-3/2)\psi - \sin(n+\tfrac{1}{2})\psi\right] \\ & + (-1)^{n} B_{2n} r^{n+1} \left[-\sin(n-1)\psi + \frac{n-1}{n+1}\sin(n+1)\psi\right] \}\end{aligned} \qquad (5.1.1)$$

from which a complete stress field description in a crack tip neighbourhood can be obtained; in Section 5.2 it will be shown how the expressions for σ_r, σ_θ and $\sigma_{r\theta}$ are arrived at from the expression given. Other researchers working in this field have obtained conclusions presented hereafter.

Cotterell (1965) in analysing the symmetric terms of the stress field (mode I only) defined two classes of fracture, this was done by taking into consideration the way a crack behaves.

Class I. Fractures that, when they deviate from the ideal path, straight ahead of the crack (for mode I) have a tendency to return to the original path.

Class II. Fractures that have the tendency to continue to deviate from the ideal path.

Later on, Cotterell (1966) showed that the first term of this series determines the stress intensity factor generally accepted to control the initiation of fracture in a brittle material and the second controls stability of the crack direction; stability of crack propagation is controlled by the third term, and the fourth term determines whether the maximum shear stress on the prolongation of the crack increases or decreases with distance from the crack tip. In his study he considers a distance "ℓ" from the original crack tip to a point in which the extended crack is to have its new crack tip, and through a mathematical analysis obtains the expression

$$d\theta = \left[1 - \frac{4}{\pi}\left(\frac{A_2}{A_1}\right)\left(\frac{S}{\ell}\right)^{\frac{1}{2}}\right]d\phi \qquad (5.1.2)$$

which relates the original angle of crack propagation $d\theta$ and the angle of further extension $d\phi$, establishing that if A_2 is negative then $d\phi > d\theta$ (see Fig.5.1) and the fracture has the tendency to return to its original path, however, it seems some cases could not be fully accounted for with this criterion. According to Cotterell the fact of A_2 being negative means that the crack goes back to its original direction, if the case of a straight notch is analysed, it is supposed that crack extension

has taken place from say point "a" to point "b", and the A_2 value obtained here is to be applied to equation 5.1.2, so if A_2 is positive, then $d\theta > d\emptyset$ and the crack is unstable and runs away from the original direction.

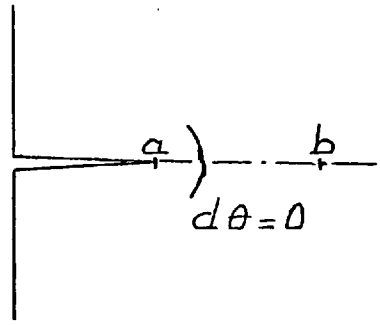

If A_2 is negative, then $d\emptyset$ is different from $d\theta$ so that the crack should also run away, and finally when $A_2 = 0$, $d\emptyset = d\theta = 0$ and the crack continues running straight, this discrepancy could be viewed as an exception. It will be shown that the A_2 value for specimens with very small straight cracks, in a symmetric stress field, is very near zero, but as the crack advances a situation develops in which the A_2 value becomes positive, even though the crack keeps going straight, i.e. the crack becomes unstable. The fact that the specimen and loading are still symmetric, should be the only factor that makes the crack keep to the original path, and theoretically there is no other influence affecting this behaviour so there should not be any change in crack direction. Experimentally, the picture is quite different, any material has flaws and imperfections which are physical factors that affect the local stress field at the crack tip neighbourhood, and as directional stability is very weak, any small change of the stress field could drive the crack tip away from the original path and the crack obtained is depicted below.

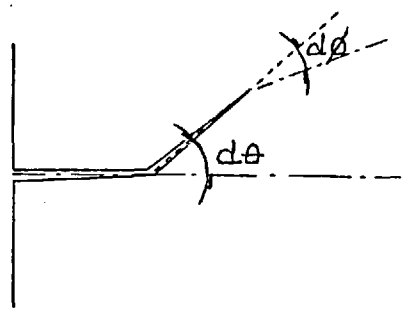

The analysis for this configuration will be that given by Cotterell i.e. if $A_2 = 0$, $d\emptyset = d\theta$ and the crack in the next extension will follow a path parallel to the original one, if A_2 = negative, $d\emptyset > d\theta$ and the next increment in crack extension is going back to the original direction, and finally if A_2 = positive, $d\emptyset < d\theta$ and on further increments of crack extension the crack goes further away from the original crack.

Results from further work made by Cotterell (1970) on specimens that exhibited directionally stable crack paths, made him conclude that equation (5.1.2) seems to fail to give a reasonable prediction of the stability of the path. However, this author in trying to reproduce Cotterell's work noticed a small error in his approach, this is reported in Section 5.6.

Examination of the expressions for stresses shows that the sign of the coefficient A_2 is directly related to the transverse stress (parallel to the initial crack) applied to the specimen, being negative whenever a compressive transverse stress is present at the crack tip. Other workers, Benbow and Roesler (1957), Guernsey and Gilmain (1961), Larsson and Carlsson (1973), have shown experimentally this relationship.

In relation to the antisymmetric terms, the first term is also directly related to the stress intensity factor but in mode II, while the coefficient B_2 turns out to be of no great

interest here in that it represents a rigid rotation term in the series for displacements and does not appear in the expressions for stress.

The present chapter will be focussed on the determination of the second and higher order coefficients of the series expansion as applied to practical cases so that a relation between experimental work and the value of the coefficients can be established or otherwise. A secondary objective to keep under consideration is to study the influence of higher order terms on crack behaviour.

5.2 Definition of the Stress Field from the Williams Series

In order to define the equations expressing the stress field, it was necessary, under the approach being described here, to obtain expressions for the displacements "u" and "v", the mathematical development shown in Appendix 5a was done by Professor J.L. Swedlow (1974); it was obtained

$$2\mu\, u = \int_0^a \{ (-1)^{n-1} A_{2n-1} r^{n-\frac{1}{2}} [-(k+n-3/2)\cos(n-\tfrac{1}{2})\psi + (n-\tfrac{1}{2})\cos(n-5/2)\psi]$$
$$+ (-1)^n A_{2n} r^n [-(k+n+1)\cos n\psi + n\cos(n-2)\psi]$$
$$+ (-1)^{n-1} B_{2n-1} r^{n-\frac{1}{2}} [(k+n+\tfrac{1}{2})\sin(n-\tfrac{1}{2})\psi - (n-\tfrac{1}{2})\sin(n-5/2)\psi]$$
$$+ (-1)^n B_{2n} r^n [-(k+n-1)\sin n\psi + n\sin(n-2)\psi] \} \sin\psi \qquad (5.2.1)$$

$$2\mu\, v = \int_0^a \{ (-1)^{n-1} A_{2n-1} r^{n-\frac{1}{2}} [-(k+3/2-n)\sin(n-\tfrac{1}{2})\psi - (n-\tfrac{1}{2})\sin(n-5/2)\psi]$$
$$+ (-1)^n A_{2n} r^n [-(k-1-n)\sin n\psi - n\sin(n-2)\psi]$$
$$+ (-1)^{n-1} B_{2n-1} r^{n-\frac{1}{2}} [-(k-n-\tfrac{1}{2})\cos(n-\tfrac{1}{2})\psi - (n-\tfrac{1}{2})\cos(n-5/2)\psi]$$
$$+ (-1)^n B_{2n} r^n [(k-n+1)\cos n\psi + n\cos(n-2)\psi] \} \cos\psi \qquad (5.2.2)$$

where $k = \frac{3-\nu}{1+\nu}$ for plane stress, and $k = 3-4\nu$ for plane strain, ν is Poisson's ratio, and n is the number of terms being

considered in the expansion of the Williams' function. The procedure to obtain $\{\sigma\}$ is to find

$$\epsilon_x = \partial u/\partial x$$
$$\epsilon_y = \partial v/\partial Y \qquad (5.2.3)$$
$$\gamma_{xy} = \partial u/\partial Y + \partial v/\partial x$$

from these

$$\sigma_x = \alpha\, \epsilon_x + \beta\, \epsilon_y$$
$$\sigma_y = \beta\, \epsilon_x + \alpha\, \epsilon_y \qquad (5.2.4)$$
$$\sigma_{xy} = \mu\, \gamma_{xy}$$

and finally

$$\sigma_r = \frac{\sigma_x+\sigma_y}{2} + \frac{\sigma_x-\sigma_y}{2} \text{Cos } 2\psi + \sigma_{xy} \text{ Sin } 2\psi$$
$$\sigma_\psi = \frac{\sigma_x+\sigma_y}{2} + \frac{\sigma_x-\sigma_y}{2} \text{Cos } 2\psi - \sigma_{xy} \text{Sin } 2\psi$$
$$\sigma_{x\psi} = \frac{\sigma_y}{2} \text{Sin } 2\psi - \frac{\sigma_x}{2} \text{ Sin } 2\psi + \sigma_{xy} \text{Cos } 2\psi$$

This was done as shown in Appendix 5b, where only the derivation of σ_r is shown; the whole expressions for the values of σ_r, σ_θ and $\sigma_{r\theta}$ arrived at by the procedure described, are given in Section 4.3, Equations 4.3.3, 4.3.4 and 4.3.5. Having obtained these relationships, it is possible to develop an approach for the determination of the coefficient values as described in Section 5.4.

5.3 Value of the Coefficients and their Influence on the Stress Field

In order to examine the influence of the different coefficients on the stress field, it was decided to start with a symmetric specimen. Many different researchers have reported the fact that when a SEN specimen is cracked, directional instability becomes apparent even though loading and geometric conditions are perfectly symmetrical. It can be shown experimentally, that the application

of symmetric opening loads on the cleavage specimen produces patterns that although symmetrical, present local maxima ahead of the tip, which are away from the crack plane, and these local maxima are the ones which are responsible for direction of crack extension. A brief mathematical description of the behaviour of the specimen, once this local maximum becomes apparent, is given hereafter.

Consider σ as given by the first three terms of the stress series, i.e.

$$\sigma = \frac{C_1}{4r^{\frac{1}{2}}}(f_1 + f_2) + Cf_3 \qquad (5.3.1)$$

where for σ_r

$$f_1 = [-5\,\mathrm{Cos}\,\frac{\psi}{2} + \mathrm{Cos}\,\frac{3\psi}{2}]A_1 \qquad (5.3.2)$$

$$f_2 = [-5\,\mathrm{Sin}\,\frac{\psi}{2} + 3\,\mathrm{Sin}\,\frac{3\psi}{2}]B_1 \qquad (5.3.3)$$

$$f_3 = 2(1+\mathrm{Cos}\,2\psi)A_2 \qquad (5.3.4$$

and for σ_θ

$$f_1 = [-3\mathrm{Cos}\,\frac{\psi}{2} - \mathrm{Cos}\,\frac{3\psi}{2}]A_1 \qquad (5.3.5)$$

$$f_2 = [3\,\mathrm{Sin}\,\frac{\psi}{2} - 3\mathrm{Sin}\,\frac{3\psi}{2}]B_1 \qquad (5.3.6)$$

$$f_3 = 2(1 - \mathrm{Cos}\,2\psi)A_2 \qquad (5.3.7)$$

The coefficient B_1 has been included here. This term is an antisymmetric one, that is, its value is zero if symmetry in loading and geometry exists, but it has to be pointed out that the criteria being discussed here, establish that the stress conditions in the neighbourhood of the crack tip are the ones that determine the direction of crack propagation (experimentally it is possible that local anisotropies exist) and if there is a local anistropy away from the axis of symmetry, the crack would initially propagate towards this anisotropy as it is a stress concentrator. This fact makes the value of B_1, for the new

condition, become different from zero as the specimen is not a symmetric one any more, and it is then that the value of the A_2 coefficient would determine if the crack goes back to the initial path or otherwise.

A further point to be made (and it will be proved later) is that as both opening load and specimen geometry establish the values for all the coefficients of the stress series, for most cases (with no transverse load) the coefficient A_2 is positive, (this is because it is proportional to the transverse stress at the crack tip. Whenever this stress is a tension, A_2 is positive and otherwise). This means local instability, that is, there is a high possibility that if the crack deviates, it will not go back to its initial path. Furthermore, to start with, the coefficients being calculated are for the straight crack; once it propagates the crack tip has got a new position and the value of A_2 has to change. The view is taken that if initial propagation is along the ideal path, the value of the coefficient would be that one which is the least unstable for the conditions given. But as loading and geometry establish the initial value for the coefficient, if this value means instability to start with, then any propagation away from the axis of symmetry will make it more unstable and even if this initial value is just above the one for stability, the new conditions could bring it to instability. So if directional stability is desired, an initial condition in which a high directional stability exists is sought in order that, when crack extension puts the crack tip away from the ideal path, there is still directional stability and the crack tends to go back to the initial path.

In looking at numerical values for the stresses, Fig.5.2 (a,b,c) show plots of the functions f_1, f_2, f_3 and in Fig.5.2(d,e,f) is depicted another function resulting from the addition of the former three under different conditions. For selecting these conditions certain fixed values of coefficients A_1, B_1 and A_2 have been chosen in order to substantiate the point; of course for real cases the relationship among them will depend on factors such as geometry, loading conditions, boundaries, etc.

Fig.5.2(d,e,f) show the influence A_2 and B_1 have on the stress field and the position of its maximum. Different combinations of coefficients are shown for $\sigma\psi$. To start with, a hypothetical case in which only $(f_1 + f_2)$ Fig.5.2(d) is considered; a fixed curve which will be called initial condition is then obtained. When during an experiment, natural conditions arise that change crack path, its influence is shown by a change on the coefficient value, so that one of the functions becomes dominant; supposing that:

(a) Coefficient A_1 is dominant. Then the maximum on the curve approximates to $\psi = 0$.

(b) Coefficient B_1 is dominant. The maximum on the curve moves towards $\psi = \emptyset_1$.

(c) When initial conditions are set under A_1, B_1 a local maximum exists and if the third function is considered, its effect is to move this local maximum either away from $\psi = 0$ if A_2 is positive or towards $\psi = 0$ when its value is negative. This is shown in Fig.5.2e for A_2 positive and Fig. 5.2(f) for A_2 negative.

This brief discussion has been restricted to some of the first terms but of course each term makes its contribution and

will in turn have an effect on this maximum and its position; how significant this effect is, will depend mainly on the values of "r" and the coefficients.

5.4 General Problem, Its Solution and Programming

It has been shown that it is required to identify higher terms in the series representation of stresses at the crack tip. The aim of this section is to describe the work done in order to obtain these coefficients, so that

(a) Former work on the significance of the second coefficient is confirmed or otherwise.

(b) Further research on the implications of the second and higher order terms can be made.

(c) Numerical analysis on different specimen configurations can be done, as it is expected to determine optimum specimen dimensions and conditions to carry on experimental work on direction of crack propagation.

The information in hand is

$$\chi(r,\psi) = \chi_e(r,\psi) + \chi_o(r,\psi) \qquad (5.4.1)$$

in which the even and odd terms of this series can be represented by

$$\chi_e(r,\psi) = \sum_{n=1,2,3..} \{(-1)^{n-1} A_{2n-1} r^{n+\frac{1}{2}} [-\cos(n-3/2)\psi + \frac{2n-3}{2n+1}\cos(n+\tfrac{1}{2})\psi]$$
$$+ [(-1)^n A_{2n} r^{n+1} [-\cos(n-1)\psi + \cos(n+1)\psi] \} \qquad (5.4.2)$$

and

$$\chi_o(r,\psi) = \sum_{n=1,2,3..} \{(-1)^{n-1} B_{2n-1} r^{n+\frac{1}{2}} [\sin(n-3/2)\psi - \sin(n+\tfrac{1}{2})\psi]$$
$$+ (-1)^n B_{2n} r^{n+1} [-\sin(n-3/2)\psi + \frac{n-1}{n+1}\sin(n+1)\psi] \} \qquad (5.4.3)$$

It is sought to find a function

$$\zeta = \iint_A W r dr d\psi - \int_{s_\sigma} t_i u_i \, ds \qquad (5.4.4)$$

in terms of the coefficients "A_i" and "B_i", and it is required that ζ

is stationary (a minimum) with respect to the coefficients. For doing this it is necessary, at any point, to define the stress $\{\sigma\}$, this can be done as described in Section 4.3 where

$$\{\sigma\} = \begin{Bmatrix} \sigma_r \\ \sigma_\psi \\ \sigma_{r\psi} \end{Bmatrix} \quad \text{so} \quad \{\sigma\}^T = [\sigma_r \ \sigma_\psi \ \sigma_{r\psi}] \tag{5.4.5}$$

the coefficients for the series can be represented as

$$\{A\} = \begin{Bmatrix} A_1 \\ B_1 \\ A_2 \\ B_2 \\ \vdots \end{Bmatrix} \tag{5.4.6}$$

and it is known as well that

$$\{\sigma\} = [\emptyset(r,\psi)]\{A\} \tag{5.4.7}$$

or

$$\{\sigma\} = [\varphi]\{A\} \tag{5.4.7a}$$

and

$$W = \tfrac{1}{2}\{\sigma\}^T\{\epsilon\} \tag{5.4.8}$$

where

$$\{\epsilon\} = [C]\{\sigma\} \ ; \text{ being } [C] = \text{cte} \tag{5.4.9}$$

or

$$W = \tfrac{1}{2}\{A\}^T[\varphi]^T[C][\varphi]\{A\} \tag{5.4.9a}$$

it is also known that

$$\begin{aligned} u &= \iint W r dr d\psi \\ &= \tfrac{1}{2}\{A\}^T \iint_A [\varphi]^T[C][\varphi] r dr d\psi \{A\} \\ &= \tfrac{1}{2}\{A\}^T[B]\{A\} \end{aligned} \tag{5.4.10}$$

and it has been shown (Appendix 5a)

$$\begin{aligned} u = \frac{1}{2\mu}\sum_{n=1}^{\infty} \{ & (-1)^{n-1}A_{2n-1}r^{n-\frac{1}{2}}[-(k+n-3/2)\cos(n-\tfrac{1}{2})\psi + (n-\tfrac{1}{2})\cos(n-5/3)\psi] \\ & + (-1)^{n-1}B_{2n-1}r^{n-\frac{1}{2}}[(k+n+\tfrac{1}{2})\sin(n-\tfrac{1}{2})\psi - (n-\tfrac{1}{2})\sin(n-5/2)\psi] \\ & + (-1)^{n}A_{2n}r^{n}[-(k+n+1)\cos n\psi + n\cos(n-2)\psi] \\ & + (-1)^{n}B_{2n}r^{n}[-(k+n-1)\sin n\psi + n\sin(n-2)\psi]\} \end{aligned} \tag{5.4.11}$$

$$v = \frac{1}{2\mu}\sum_{n=1}^{\infty}\{(-1)^{n-1}A_{2n-1}r^{n-\frac{1}{2}}[-(k-n+3/2)\mathrm{Sin}(n-\tfrac{1}{2})\psi - (n-\tfrac{1}{2})\mathrm{Sin}(n-5/2)\psi]$$

$$+ (-1)^{n-1}B_{2n-1}r^{n-\frac{1}{2}}[-(k-n-\tfrac{1}{2})\mathrm{Cos}(n-\tfrac{1}{2})\psi - (n-\tfrac{1}{2})\mathrm{Cos}(n-5/2)\psi]$$

$$+ (-1)^{n}A_{2n}r^{n}[-(k-1-n)\mathrm{Sin}\ n\psi - n\ \mathrm{Sin}(n-2)\psi]$$

$$+ (-1)^{n}B_{2n}r^{n}[(k-n+1)\mathrm{Cos}\ n\psi + n\ \mathrm{Cos}(n-2)\psi]\ \} \qquad (5.4.11a)$$

or $$\{u\} = \begin{Bmatrix} u \\ v \end{Bmatrix} = [\theta(r,\psi)]\ \{A\} \qquad (5.4.11b)$$

and specifying stresses on the specimen surface as tractions

$$\{t\} = \begin{Bmatrix} t_x \\ t_y \end{Bmatrix} \qquad (5.4.12)$$

$$\int_{s_\sigma} t_i u_i ds = \int_{s_\sigma} \{t\}^T[\theta]\ \{A\}ds$$

$$= \int_{s_\sigma} \{t\}^T[\theta]ds\{A\} = \{R'\}^T\{A\} \qquad (5.4.12a)$$

so

$$\zeta = \tfrac{1}{2}\{A\}^T[B]\ \{A\} - \{R\}^T\{A\} \qquad (5.4.$$

and by differentiating with respect to $\{A\}$ in order to minimise, it is obtained

$$[B]\ \{A\} - \{R\} = 0 \qquad (5.4.13)$$

The computer implementation of the program shown in Appendix 5c, used to obtain the solution to Equation (5.4.13), was developed using a finite difference method applied to the Taylor series.

In this program, subroutine SET UP obtains BVEC as

$$\mathrm{BVEC} = \int \mathrm{D.BDYLD.ds} \qquad (5.4.14)$$

where BVEC = [B]

D = displacements of boundary points of the specimen

BDYLD = Tractions applied to the specimen boundary points

The numerical calculations within the program are actually done as

$$BVEC[NTRM] = \Sigma D[NBPT,NTRM].BDYLD[I,NBPT]$$

Where NTRM is the number of terms being considered in the expansion of the Williams' series

NBPT is the number of boundary stations along the edges of the specimen. (Fig.5.3)

I is equal to 1 or 2, depending on the applied specimen traction being considers [1 for x, and 2 for ẏ traction].

The matrix D (displacements) is obtained as described in Appendix 5a and is given as

$$\begin{aligned}
D(I,N-3) &= (-1)^{n-1} r^{n-\frac{1}{2}}\{[(n-3/2-k)\mathrm{Sin}(n-\tfrac{1}{2})\psi - (n-\tfrac{1}{2})\mathrm{Sin}(n-5/2)\psi]\mathrm{Cos}\psi \\
&\quad + [(n-3/2+k)\mathrm{Cos}(n-\tfrac{1}{2})\psi - (n-\tfrac{1}{2})\mathrm{Cos}(n-5/2)\psi]\mathrm{Sin}\psi\}BDYLD(M,N) \\
D(I,N-2) &= (-1)^{n-1} r^{n-\frac{1}{2}}\{[(n+\tfrac{1}{2}-k)\mathrm{Cos}(n-\tfrac{1}{2})\psi - (n-\tfrac{1}{2})\mathrm{Cos}(n-5/2)\psi]\mathrm{Cos}\psi \\
&\quad - [(n+\tfrac{1}{2}+k)\mathrm{Sin}(n-\tfrac{1}{2})\psi - (n-\tfrac{1}{2})\mathrm{Sin}(n-5/2)\psi]\mathrm{Sin}\psi\}BDYLD(M,N) \\
D(I,N-1) &= (-1)^{n} r^{n}\{[(n+1-k)\mathrm{Sin}\psi - \mathrm{Sin}(n-2)\psi]\mathrm{Cos}\psi \\
&\quad + [(n+1+k)\mathrm{Cos}\psi - \mathrm{Cos}(n-2)\psi]\mathrm{Sin}\psi\}BDYLD(M,N) \\
D(I,N) &= (-1)^{n} r^{n}\{[(n-1-k)\mathrm{Cos}\psi - \mathrm{Cos}(n-2)\psi]\mathrm{Cos}\psi \\
&\quad - [(n-1+k)\mathrm{Sin}\psi - \mathrm{Sin}(n-2)\psi]\mathrm{Sin}\psi\}BDYLD(M,N) \qquad (5.4.15)
\end{aligned}$$

and

$$BDYLD(I,N) = t(I,N)/E' \qquad (5.4.16)$$

where N = number of the boundary station

n = number of coefficients being considered

$E' = E(1 + \nu)$

(r, ψ) = Polar coordinates at which stresses are evaluated.

With relation to the actual application of the finite difference method to this problem, the main points are described below.

To start with, a certain number of boundary points are chosen along the stressed boundaries, representing this boundary by the straight line shown below:

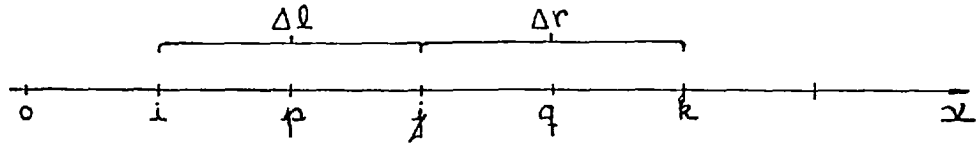

Let $x_k - x_j = \Delta r$ $\qquad$ $\Delta r + \Delta \ell = x_k - x_i$

$x_j - x_i = \Delta \ell$ $\qquad$ $\Delta r - \Delta \ell = x_k - 2x_j + x_i$

The Taylor's series are given as

$$f(x) = f(x_j) + \Delta x f'(x_j) + \tfrac{1}{2}\Delta x^2 f''(x_j) + \tfrac{1}{6}\Delta x^3 f'''(x_j) t... \quad (5.4.17)$$

from which, for consecutive points i,j,k

$$f_k = f_j + \Delta r f'_j + \tfrac{1}{2}\Delta r^2 f''_j + \tfrac{1}{6}\Delta r^3 f'''_j + ...$$

$$f_j = f_j \quad (5.4.18)$$

$$f_i = f_j - \Delta \ell f'_j + \tfrac{1}{2}\Delta \ell^2 f''_j - \tfrac{1}{6}\Delta \ell^3 f'''_j ...$$

considering these functions up to the second term only,

(1) $$a f_k + b f_j + c f_i = f'_j \quad (5.4.19)$$

is obtained where

$$a = \frac{\Delta \ell}{\Delta r(\Delta r + \Delta \ell)}$$

$$b = -\frac{\Delta r}{\Delta \ell(\Delta r + \Delta \ell)} \quad (5.4.20)$$

$$c = \frac{\Delta r - \Delta \ell}{\Delta r \Delta \ell}$$

and $\quad a + b + c = 0;\ \Delta r a - \Delta \ell c = 1;\ \Delta r^2 a + \Delta \ell^2 c = 0$

(2) $$a f_k + b f_j + c f_i = f''_j \quad (5.4.21)$$

where

$$a = \frac{1}{\Delta r(\Delta r + \Delta \ell)}$$

$$b = -\frac{1}{\Delta r \Delta \ell} \quad (5.4.22)$$

$$c = \frac{1}{\Delta \ell(\Delta r + \Delta \ell)}$$

In cutting the Taylor series to the second derivative, it can be demonstrated that the error obtained in evaluating the function, is proportional to Δ^4.

The former equations have slightly different applications along the specimen boundary, i.e.

(a) First station.

(b) Intermediate stations.

(c) Last station.

For first station the analysis is applied to

(a)

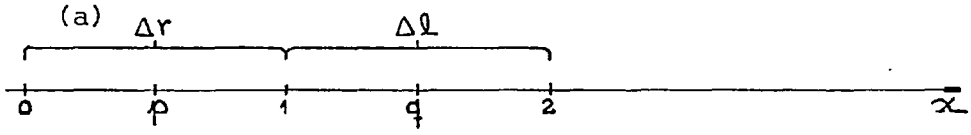

$$F_q - F_o = f_1(\Delta\ell - \frac{3\Delta r}{8} + \frac{4\Delta x^2}{8\Delta r}) + f_2(\frac{\Delta r}{8} - \frac{\Delta\ell^2}{2\Delta r}) \qquad (5.4.23)$$

and the correspondance between the former work on D and this is

$$f_1 = D(1,j); \qquad f_2 = D(2,j)$$

For intermediate stations

(b)

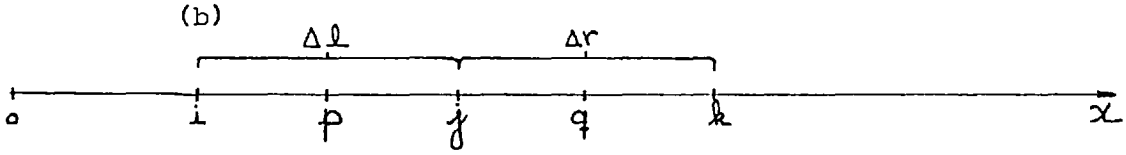

$$F_q - F_p = f_i(1/48\Delta\ell)(-5\Delta\ell^2 + 5\Delta r\Delta\ell + \Delta\ell^2)$$
$$+ f_k(1/48\Delta r)(\Delta r^2 + 5\Delta r\Delta\ell - 5\Delta\ell^2) \qquad (5.4.24)$$
$$+ f_j(1/48\Delta r\Delta\ell)(5\Delta r^3 + 18\Delta r^2\Delta\ell + 18\Delta r\Delta\ell^2 + 5\Delta\ell^3)$$

where

$$f_i = D(N-1,j); \quad f_j = D(N,j); \quad f_k = D(N+1,j)$$

and finally for the last station

(c)

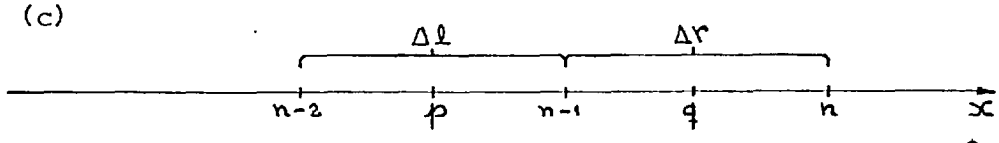

$$F_n - F_p = f_{(n-1)}(\Delta r + \frac{3}{8}\Delta\ell + \frac{\Delta r^2}{2\Delta\ell}) + f_{(n-2)}(\frac{\Delta\ell}{8} - \frac{\Delta r^2}{\Delta\ell}) \qquad (5.4.25)$$

where $f_{(n-1)} = D(M-1,j)$ and $f_{(n-2)} = D(M-2,j)$

and M = total number of boundary stations.

So expression (5.4.15) is implemented and solved by means of subroutine SOLVER, and applied to obtain values of the coefficients A_n, B_n.

5.5 Test Cases, Results and Comparison against Methods Already in Use

Convergence test for program ANGCRK.

In applied mathematics, it is quite common to initialise the process of obtaining the solution to a problem, by starting with an approximate solution which does not quite satisfy the boundary conditions and then adjusting it until it does. In the science of Fracture Mechanics, this process has been called "boundary collocation", and the solution already described in Section 5.4 is a kind of boundary collocation technique in the sense that the data that are being considered for the solution of the problem are the applied loads on points at the boundaries of the specimen.

For the boundary collocation methods, there is no general proof for their convergence, thus it does not necessarily follow that the terms in the series expansion stabilise as the number of terms increase, so the accuracy of solution to a given problem can only be estimated by repeating the analysis for an increasing number of boundary points until the change in value of the terms become insignificant. Convergence within the present work was tested as follows:-

(a) convergence with respect to the number of terms in the series;

(b) convergence against the number of boundary stations.

The actual value of the coefficients A_n for the stress series, depends on the number of coefficients considered in solving the system of equations. As the number of terms is increased the real value of the coefficient is approached. To find out which value is the correct one, the curve (A_n vs n) should be plotted and stabilisation looked for. Another way to approximate the real value is by fixing a ΔA_n for successive values of

the number of terms. This was done and 20 terms proved to be an acceptable value.

Fig. 5.4 shows the convergence curve for A_1 and $K_1/P\sqrt{\pi a}$ obtained for two different specimens, i.e. 2.2 x 1.0 x 0.3ℓ as in Gross (1964), and 12.0 x 1.0 x 0.3ℓ as in Benbow (1957). It can immediately be seen that for a relationship ℓ/W small, the value of the coefficient A_1 stabilises quite well for a small number of boundary stations. This is not so for the specimen 12.0 x 1.0 x 0.3ℓ, which requires approximately 200 boundary points to stabilise.

A whole range of crack lengths, to simulate Gross' work (1966) was run and results are reported in Table 5.1. The values obtained with the present method agree completely with those by Gross.

Finally on the same topic, specimens with dimensions 12.0 x 1.0, 8.0 x 1.0, 6.0 x 1.0, 4.0 x 1.0, 2.2 x 1.0, and crack lengths 0.3ℓ were simulated for 198 NBPT (NBPT = number of boundary points), the value of the parameter $K_I/P\sqrt{\pi a}$ was calculated as described later on within this Section 5.5, and results are shown in Table 5.2. For all cases, the results from the present method are between those obtained by Gross (1964) and the ones obtained by Hayes (1970).

Test cases, results and comparison against other methods already in use. Once a test for convergence was made, different cases were chosen to test the program developed. Work done by Wilson (1965), Gross et al (1964) and Hayes (1970) was taken as a reference.

W.K. Wilson (1965) used a collocation method and the Muskhelishvilli complex variable method to determine the stress intensity factor for the standard Manjoine specimen, and compared his results against those obtained from an experimental compliance method.

The dimensions of the specimen he simulated are given below,

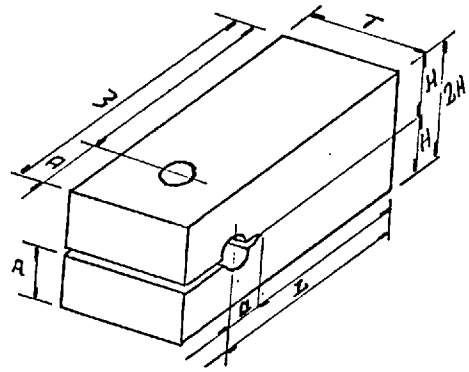

L = 9/8in a = $\frac{1}{2}$in

H = $\frac{1}{2}$in T = 1in

W = $1\frac{7}{16}$in D = $\frac{5}{16}$in

A = $\frac{7}{16}$ in B = $\frac{1}{2}$in

and three different cases were considered, i.e.

Case 1. H/L = 0.444 and ∂/L = 0.347

2. H/L = 0.444 and ∂/L = 0.444

3. H/L = 0.444 and ∂/L = 0.587

The shape for a bidimensional computer simulation becomes

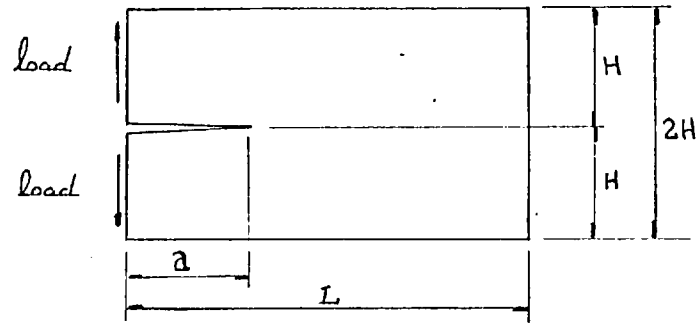

With a constant unit width and either plane stress or plane strain defining the state of stress, only dimension "∂" is to be altered for each case simulated. The values of "∂"are

∂_1 = 0.39, ∂_2 = 0.5, ∂_3 = 0.661

The three cases were set on program ANGCRK and the values of the first coefficient of the Williams series, stress intensity factor ($K_I = -A_1\sqrt{2}$), and dimensionless parameter ($K_I\sqrt{\partial}/P$) obtained were,

	Case 1	Case 2	Case 3
A_1	- 12.261	- 14.883	- 21.615
K_I	17.33	21.05	30.55
$K_I \sqrt{c/P}$	10.82	14.89	24.80

The load used for the simulation carried out under the present work was 100lb. As this value (P) appears as an inverse factor on the values given in Wilson's paper, it is necessary to consider the relationship between any of the above values and the corresponding one in Wilson's paper, say the second case; so

$$6.305/14.89 = 0.424$$

Using this factor for the three cases:-

Case 1 = 10.82 x 0.424 = 4.59; Case 2 14.89 x 0.424 = 6.305; Case 3 24.8 x 0.424 = 10.52 which can be compared with Wilson's values as shown in Table 5.3 where D_{IF_1} is the difference encountered between the complex method and the collocation method, while DIF_2 is the difference of the complex method against results obtained with program ANGCRK. As can be seen the differences are within the same limits and so it can be concluded that the present computational approach is an acceptable one. It has to be pointed out, as well, that Wilson's results are backed by experimental work which is reported in ASTM 410.

Hayes (1970) using a finite element technique obtained the stress intensity factors for a series of plate length to width ratios of 2.0, 4.0 and 6.0. It was decided to simulate this work and the results obtained are shown in Fig. 5.5. A dimensionless parameter (K^2W/P^2) is applied to the results for the present work. Gross et al (1964) mention that for their work, "P" is the load per unit thickness, this point is not very clear as the approach is bidimensional and

supposes a unit thickness. In analysing results, it was concluded that this load P, for the program ANGCRK, is the value of the transverse load applied on each one of the boundary points, i.e. per unit width so for specimen 12 x 1, the values of the dimensionless parameter $K_I/\sigma\sqrt{\pi a}$ (where σ = P) are as follows:

NBPT	K_I	a	P	$K_I/P_1\sqrt{\pi a}$
100	2.24	3.6	2.5	0.913
162	2.15	3.6	1.429	1.5603
200	1.94	3.6	1.25	1.604

It can be seen that the value of the dimensionless parameter converges to around 1.6; this is in agreement with Gross' values for his specimen 2.2.x 1.0 and his statement that the curve $[K^2w^2/P^2$ vs a /w] (equivalent to $[K_I/P\sqrt{\pi a}$ vs $\ell/d]$ for Haye's cases) can be applied to any ℓ/d value greater than about 0.8. The values obtained by the three different methods are

	Gross	Hayes	Present Method
$K_I/P\sqrt{\pi a}$	1.6628	1.5796	1.604

this also seems to indicate that Hayes was right in his statement that the correct value of K_I could be somewhere between the values given by Gross and those calculated by him.

5.6 Computer Simulations of Work done by Cotterell

In trying to reproduce work done by B. Cotterell (1970) differences in the results were obtained in the values of the terms corresponding to the coefficients of the power series. In Cotterell's paper the following values are given.

---

*Table 5.4 gives the whole set of results for different crack lengths.

ℓ/W	$A_1/(P/D)$	$A_2/(P/D)$	$A_3/(P/D)$	$A_4/(P/D)$
0.2	2.543	0.728	- 1.704	0.156
0.3	2.554	1.444	- 2.826	0.186
0.4	2.775	2.093	- 4.340	0.182
0.5	3.260	2.774	- 6.851	0.180
0.6	4.210	3.564	-12.150	0.448
0.7	6.167	5.296	-26.860	2.250

while the values obtained for computations made with program ANGCRK are

ℓ/W	$A_1/(P/D)$	$A_2/(P/D)$	$A_3/(P/D)$	$A_4/(P/D)$
0.2	2.190	0.241	- 0.693	0.187
0.3	3.295	0.579	- 1.191	0.210
0.4	4.780	0.885	- 1.870	0.194
0.5	7.000	1.187	- 2.950	0.208
0.6	10.800	2.52	-11.580	0.358
0.7	18.230	2.52	-11.580	0.358

Having found this difference in the results, it was noticed that the series presented in Cotterell's paper and that on which program ANGCRK is based, are slightly different, that is:-

σ_θ values - the series used within program ANGCRK is given as

$$r^{n-3/2}(n-\tfrac{1}{2})[(n+\tfrac{1}{2})\mathrm{Cos}(n-3/2)\psi - (n-3/2)\mathrm{Cos}(n+\tfrac{1}{2})\psi] \qquad (5.6.1)$$

$$r^{n-3/2}(n-\tfrac{1}{2})[(n+\tfrac{1}{2})\mathrm{Sin}(n-3/2)\psi - (n+\tfrac{1}{2})\mathrm{Sin}(n+\tfrac{1}{2})\psi] \qquad (5.6.2)$$

$$r^{n-1}n[(n+1)\mathrm{Cos}(n-1)\psi - (n+1)\mathrm{Cos}(n+1)\psi] \qquad (5.6.3)$$

$$r^{n-1}n[(n+1)\mathrm{Sin}(n-1)\psi - (n-1)\mathrm{Sin}(n+1)\psi] \qquad (5.6.4)$$

where (5.6.1) and (5.6.3) are the terms corresponding to the symmetric case, i.e. coefficients $A_{1,3,5..}$ and $A_{2,4,6..}$, while (5.6.2) and (5.6.4) are those for the antisymmetric case (coefficients B_1, B_2).

Taking the symmetric case and substituting values of n = 1,2, the following results are obtained.

Coefficient	Function ψ	
A_1	$\frac{1}{4\sqrt{r}}\left[3\,\mathrm{Cos}\,\frac{\psi}{2} + \mathrm{Cos}\,\frac{3\psi}{2}\right]$	(5.6.5)
A_2	$2\,\sin^2\psi = 2(1-\mathrm{Cos}\,2\psi)$	(5.6.6)
A_3	$\frac{3r^{\frac{1}{2}}}{4}\left[3\,\mathrm{Cos}\,\frac{\psi}{2} + \mathrm{Cos}\,\frac{5\psi}{2}\right]$	(5.6.7)
A_4	$6r\,[\mathrm{Cos}\,\psi - \mathrm{Cos}\,3\,\psi]$	(5.6.8)

As shown below all these terms, except the one for A_3, are equal to those given by Cotterell. For A_3 the terms are:-

$\left[5\,\mathrm{Cos}\,\psi + \mathrm{Cos}\,\frac{5\psi}{2}\right]$ Cotterell's

$\left[3\,\mathrm{Cos}\,\frac{\psi}{2} + \mathrm{Cos}\,\frac{5\psi}{2}\right]$ Program ANGCRK

This difference also exists for σ_r and $\sigma_{r\theta}$.

It is thought that as results obtained with the present method are in full agreement with those obtained by Wilson (1965), Hayes (1970), Gross (1964), it can be concluded that the series being used here is correct.

A further point to be made here concerns the correspondence between the coefficients used within this work (A_{ns}) and those in Cotterell's (A_{nc}), i.e.

$$-\sqrt{\ell}\,A_{1s} = A_{1c} \qquad (5.6.9)$$

where "ℓ" is the length of crack extension.

$$4\,A_{2s} = A_{2c} \qquad (5.6.10)$$

$$3\sqrt{\ell}\,A_{3s} = A_{3c} \qquad (5.6.11)$$

$$-4\ell A_{4s} = A_{4c} \qquad (5.6.12)$$

The approach is as follows

$-A_1$ proportional to K_I

$$K_I = \lim_{r \to o} \sigma_{\psi} \sqrt{2\pi r} \qquad (5.6.13)$$

$$K_I = \lim_{r \to o} \sqrt{2\pi r} \left\{ \frac{A_1}{4\sqrt{r}} \left[-3\cos\frac{\psi}{2} - \cos\frac{3\psi}{2} \right] + 0[r^o] \right\}$$

$$= \lim_{r \to o} \sqrt{2\pi} \left\{ \frac{A_1}{4} [-3(1)-1] + 0(r^o) \right\}$$

$$= \lim_{r \to o} \sqrt{2\pi} \{ - A_1 + 0(r^o) \}$$

$$K_I = - A_1 \sqrt{2\pi} \qquad (5.6.14)$$

$$\frac{K_I}{\sigma\sqrt{\pi a}} = \frac{- A_1 \sqrt{2\pi}}{\sigma \sqrt{\pi}\sqrt{a}} = - \frac{A_1}{\sigma} \sqrt{\frac{2}{a}}$$

CHAPTER 6

EXPERIMENTAL WORK AND COMPUTATIONAL SIMULATION ON DIRECTIONAL STABILITY OF CRACK PROPAGATION

6.1 General Characteristics and Specimen

The present section aims to describe the design of experiment, rig, and computer simulation. Under the study being carried out one is concerned with establishing the conditions that improve directional stability of crack propagation and implement them practically; a second objective is the simulation of the experiments by means of a computer.

Gurney and Hunt (1967) have discussed the main factors to bear in mind when selecting the test specimen, most of them are concerned with the recording of the load-displacement history in order to evaluate the energy put into the process. Even though the objective of the present work is basically different, it is interesting to note that most of those conditions are satisfied by choosing rectangular test specimens with either edge cracks or central cracks. It is recognised, Barr (1968), that uniform rectangular specimens with central cracks give better results than specimens with edge cracks. He found that there is a tendency for the crack to run out uncontrollably when it starts off as an edge crack. This had already been reported by Benbow and Roesler (1957); Berry (1960) and others, who proposed different ways to avoid this problem such as applying transverse load to the specimen, Benbow and Roesler (1957), Svensson(1966); groove the specimens in the direction the crack is required to propagate and/or change the specimen geometry, Barr (1968). The work done under the present study, and described in the previous sections, has led to choosing a specimen

with a single edge notch, so for the experimental work it is necessary to overcome this tendency to run out and it is obvious that the application of transverse load is the most suitable method to control cracking under the present work.

It was decided that Perspex (PMMA) is a good material for the study of crack propagation. Some of the reasons for selecting it are: the material is brittle; easy to obtain and fairly cheap; easy to machine especially the initial slot from where the crack starts; it has photoelastic properties that could facilitate, if desired, a wider study of the stress field; as the material is transparent it is very easy to follow the crack path.

6.2 Experiment Design and Rig Design

In order to assess the correspondence between experimental and theoretical work it is absolutely necessary to establish which is the best set of circumstances that will produce the expected material behaviour and how this behaviour matches the theoretical approach. The selection of this set of circumstances concerns the experiment design, while for the rig design, one is concerned with the physical implementation of the conditions depicted by the above set of circumstances, by means of mechanical devices.

The objectives of the experimental work to be performed can be described as:-

(a) reproduce work done by Benbow and Roesler (1957),

(b) measurement of the loads applied to the specimen,

(c) assessment of the direction of crack propagation for different loading conditions,

(d) contemplate the possibility of analysing the specimens photoelastically,

(e) test, in conjunction with computer work, the possible correspondence between the second coefficient of the Williams' stress series and directional stability of crack propagation.

Work done by other researchers, as well as that described in Chapters 4 and 5 of this study have already shown that the cleavage specimen is the one to be considered, the relevant information about it is given hereafter.

Specimen:	Cleavage specimen (single cracked edge plate)
Dimensions:	Maximum 12 x 4 x $^1/_4$ (in) see Fig. 6.1
	Minimum 4 x 1 x $^1/_4$ (in)
	It should be possible to cover the whole range of dimensions between these limit values.
Loading:	(a) Transverse load: Maximum 500 lb/in^2 (Compressive)
	(b) Opening load: Maximum 600 lb
	Minimum 0 lb
	(c) Load to be applied independently.
Other Limitations:	Constraint against buckling for narrow specimens, rigidity of the rig is essential, availability of accessory equipment and apparatus to calibrate and operate the rig has to be considered.

Very many problems were encountered during the design stage and most of them were solved satisfactorily. The rigid straining frame shown in Fig.6.2 was developed. By means of this frame, load is applied to an initially rectangular specimen which has a slot cut into it along the centre line parallel to the longer edges. The end of this slot is cut into a swallow-tail shape with a sharp blade. This system was devised in order

to achieve control of the cracking process, provision was made to apply compressive transverse load so that direction of crack propagation could be controlled. The splitting force is transmitted to the specimen through a set of pins passing through four specimen-holding blocks (two of them instrumented with strain gauges). These blocks are forced apart by a calibrated screw with right and left hand threads which in rotating induces the separation of the blocks. The load is measured by means of the strain gauges on the blocks. The compression force required to control the crack path is applied by means of eight individual fingers, at the far end of the plate, which are driven by horizontal screws. Each finger is instrumented with a couple of strain gauges in such a way that any bending stress applied is suppressed. This feature allows a good control of the whole stress field.

In all, some 20 strain gauges are used for measuring the magnitude of opening load and eight pairs for the transverse loads. As the measuring equipment provides half a wheatstone bridge, it was necessary to provide dummy gauges to build up the half bridge needed (28 half bridges). The calculations of stresses for the measuring points of the rig are given in Appendix 6.a. In brief, the most relevant parts of the rig and their function are:

Piece No.	Named	Function
3	Opening load cell	Plate that contains a set of five cantilever beams throughout which load is applied. Strain gauges are conveniently located on these beams to measure opening load.
5	Opening bolt	Double threaded screw to drive the opening movement of plates No.3.

Piece No.	Named	Function
9	Lateral blocks	Blocks to prevent buckling of the specimen.
10	Base frame	Frame to support the whole rig.
13	Transverse load cell	Elements to measure transverse load
27	Transverse bolt	Screw to apply transverse load.
1	Opening frame	Frame to hold opening load cells.
12	Transverse frame	Frame to hold transverse load cells.

6.3 Experimental Data, Description and Results

Apparatus

(a) Instron Tensile Testing Machine

Model TT-C, capacity up to 10,000 lb.

(b) Data-Log with a capacity up to 100 Wheatstone bridges, facilities to make gauge readings of up to 4 readings/sec, and accessory equipment to record either by printing or punching the readings.

Rig calibrations

Two types of loads have to be calibrated.

(a) Transverse load. The transverse frame holding the eight transverse load cells was mounted on an Instron machine, the strain gauges on the load cells were connected to a "data log" (instrument for the automatic recording of the strains developed in the load cells). Each individual element was calibrated under compressive load. The results of these calibrations are shown in Table 6.1a and Fig.6.3a. The response of the measuring elements was an excellent one and no deviations from the expected linear behaviour were detected to within 2%. Photographs (Fig. No.6.5) show the experimental calibration detail.

(b) Opening load. The same procedure was used as with the axial frame, but unexpected behaviour was detected and two kinds of problems became apparent. One was that the fit between the moving pieces was not as good as expected, and the second was that it was extremely difficult to simulate accurately the combined opening-transverse load needed to calibrate the beams, and extraneous effects were recorded. Problem one was easily overcome but it was not possible to solve the second one totally, and a rather poor calibration was obtained.

As the calibration of the rig for the transverse load was successful it was decided to perform a whole set of experiments under these circumstances and later on use the computer to scan the zone of possible values for the opening load. Discussion of this work is given in Chapter 7.

Later on a modification to the rig was made. By then it had been found (Section 6.4) that it was not necessary to determine wholly the distribution of the opening load along the edge of the specimen but just its total magnitude, this simplified the modification needed to measure opening load. This time, the opening bolt was instrumented with four strain gauges put in such a way that two of them measure axial strain and the other two determine any torsional strain so, if required, the stress system could be theoretically analysed, this was not necessary as the calibration proved to be a successful one.* Another set of experiments was done and results and discussion are presented in Chapter 7.

Experiments and operational description

Two types of experiments were performed.

(a) Specimen under opening load plus transverse load.

*See Table 6.1b and Fig.6.3b.

(b) Specimen under opening load and no transverse load.

Under experiment (a) the procedure was as follows:

(1) Obtain an approximate value of transverse load under which one could expect straight crack propagation, this was done by means of results reported by Benbow and Roesler (1957).

(2) Under no load, all the load cells were set to zero reading (it was found that this could be done within $\pm$ 2 microstrains).

(3) Apply the transverse-load, determined in (1). Through the transverse load cells.

(4) Record the readings for transverse load.

(5) Apply opening load and print the readings. Usually readings were taken while load was being applied. This was repeated until it was noticed that the crack started to extend, then continuous readings were taken until the rate of crack extension was so small as to seem that crack propagation had stopped. (No detectable crack growth after five minutes.)

In experiment (b) the same procedure was followed but for point 3.

Specimens 12 x 4, 8 x 4, 6 x 4, 4 x 4 (in) were tried and the complete loading records are given in Tables 7.7 to 7.11 Fig. 7.17 show the loading history for specimen No.6/4 and discussion about it is made in Section 7.4.

6.4 Computer Simulation of Experimental Work and Results

In Section 5.4 the work done to develop the program to calculate the coefficients for the Williams' series has been described, in order to obtain these coefficients, the data required is; load applied on each boundary point, Young's modulus

Poisson's ratio and specimen dimensions. For the experimental work it is known that there are five precise points on which load is applied; as the coordinates of boundary points, as calculated with the computer program for the different specimens, will not always be coincident with those from the experimental work, it was necessary to test, with the computer, the effect of different loading on the values of the coefficients. This is reported hereafter.

Effects of load applied on different boundary points

Five cases were considered, Fig. 6.4 shows schematically the physical description and loading conditions are described below.

General conditions. A transverse applied stress of 400 lb/in^2. Specimen dimensions 12 x 4, crack length 3.6 in.

Particular conditions.

(a) Total opening load, 100 lb applied on the boundary point of the cracked edge, the nearest to the crack surface.

(b) Total opening load, 100 lb applied on a boundary point half way on the cracked edge.

(c) Total opening load, 100 lb applied on the boundary point of the cracked edge, farthest away from the crack surface.

(d) Four loads of 6.25 lb applied on boundary points at the neighbourhood of the crack face plus three loads of 25 lb applied on points at the edge further away; the coordinates of these seven points were approximately those of the real experimental specimen.

(e) The opening load is applied as a uniform stress on the edge; total opening load magnitude is 100 lb.

The values obtained for the first three coefficients of the Williams' series, are shown in Table 6.2. In relation to these results the first fact to be pointed out is that the computer formulation is critically sensitive to the application point only for that point the farthest away from the crack plane.

It is considered that the values obtained for case (e) are the best ones. It can also be observed that the coefficient values are directly proportional to opening load, and for the different cases being the same load applied along the same direction, all values should be equal to those of case (e) (differences for cases (a) and (b) can be considered negligible and a consequence of the behaviour described below).

Case (c) is the odd one, it is thought that the great difference encountered between the values for this case and those for the others is because the position of neighbouring points to that on which load is applied, influence the results obtained; for case (a) this is not as critical as there are no boundary stations on the crack face, but for case (c) one of the neighbouring boundary points is along the upper specimen edge and its X coordinate is an influencing factor.

In reference to case (d), the values obtained are a consequence of the point just discussed. In order to gain a better understanding about the computer program response, this case (d) was treated in two ways:

(i) as described;

(ii) as seven individual cases, four of these cases had one load of 6.25 lb applied to a different point, and the other three had a load of 25 lb applied on other points.

The superposition of effects under (ii) should reproduce case under (i), this was so, and data and results of these seven cases are given in Table 6.3.

It is immediately apparent that allowing for the already described behaviour for the extreme points, the addition of the coefficients for cases 1 to 7 is approximately equal to case (e). In relation with A_2 it has to be remembered that its value is proportional to both opening load and axial (this point will be discussed further in Chapter 7), so if it is desired to obtain the value of case (e) from these seven cases, only those parts of A_2 proportional to opening load should be considered, plus one of the parts proportional to the axial load.

Additional work was done in connection with the influence of Young's modulus on the coefficient values. Some cases were run with the same data but different values of Young's modulus. The results obtained show that Young's modulus has no influence on the value of the coefficients, (most probably this should be clear from theoretical analysis, but this author has made no attempt towards probing this point).

Finally, the conclusion from this section is that the experimental work can be correctly simulated in the computer by applying a uniform stress along the edges of the specimen, which is equal in magnitude to the total opening load.

The specimens tried experimentally were all simulated with the computer program, and a whole range of crack lengths up to 0.9ℓ with a load of 10 lb was done for specimens considered. Coefficient values for these cases are shown in Table 6.4 and depicted in Fig.7.5. Analysis of these results is done in Chapter 7.1.

6.5 Computational Determination of Parameters Defining Criteria for Direction of Crack Propagation

Up to now the work done in this study seems to indicate a straight correspondence between A_2 (second coefficient of the Williams' series) and direction of crack propagation, further discussion related to this point is given in Chapter 7. Here, the computer implementation for evaluating criteria of directional stability for crack propagation is discussed.

For Brittle Fracture in an isotropic material under combined stress, Griffith (1924) stated that the "general condition for rupture will be the attainment of a specific tensile stress at the edge of one of the cracks". This is in fact the maximum normal stress criterion of fracture, which assumes that the crack moves along a path normal to the direction of greatest tension so that the component of shear stress on the line of expected extension of the crack is zero. Erdogan and Sih (1963) obtained results that checked reasonably well with this criterion, later on Cotterell (1966) and Pook (1971) confirmed the former work. More recently, Williams and Ewing (1972) have shown that data on direction of crack propagation can vary substantially depending on a critical distance from the crack tip where measurements were made. The second criterion to be considered is that due to Sih (1973), the S criterion, even though this one is not as yet fully tested. One of the basic concepts of the S criterion is that fracture initiates from an interior element near the crack tip. According to this criterion, incipient fracture is reached when the strain energy density factor at this interior element attains a critical value, "S_c", characteristic of the material under consideration. In both

cases, Williams and Ewing with σ_ψ, and Sih with S, the approach to the problem is to obtain the maximum value of the critical parameter by differentiating the expression that defines it and equating to zero, i.e.

$$\frac{dP_c}{d\psi} = 0 \qquad (6.5.1)$$

where $P_c = \sigma_\psi$ for Williams, and S for Sih. Since $P_c = f_{(r,\psi)}$ Williams and Ewing define a critical distance, r, which should be a material characteristic. Sih chose to analyse the fracture field defining a finite core region, surrounding the notch tip, such that r is not allowed to be any smaller than r_o, which he relates to properties of the material and nature of deformation. So for both cases, it can be considered that $P_c = f_{(\psi)}$, and through Equation (6.5.1), it is straightforward to obtain the value of ψ for which P_c is stable (maximum).

In this work, obtaining the values for these criteria will follow a different approach, ie. define r_o and search for the maximum by means of a numerical method. So the function to be considered as a criterion is either

$$\begin{aligned}\sigma_\psi = \sum_{n=1} \{ & (-1)^{n-1} r^{n-3/2} A_{2n-1} (n-\tfrac{1}{2}) \\ & [(+\tfrac{1}{2})\mathrm{Cos}(n-3/2)\psi - (n-3/2)\mathrm{Cos}(n+\tfrac{1}{2})\psi] \\ & + (-1)^{n} r^{n-1} A_{2n}\, n[(n+1)\mathrm{Cos}(n-1)\psi - (n+1)\mathrm{Cos}(n+1)\psi] \\ & + (-1)^{n-1} r^{n-3/2} B_{2n-1} (n-\tfrac{1}{2})[(n+\tfrac{1}{2})\mathrm{Sin}(n-3/2)\psi - (n+\tfrac{1}{2})\mathrm{Sin}(n+\tfrac{1}{2})\psi] \\ & + (-1)^{n} r^{n-1} B_{2n} n[(n+1)\mathrm{Sin}(n-1)\psi - (n-1)\mathrm{Sin}(n+1)\psi] \} \frac{E}{1+\nu}\end{aligned} \qquad (6.5.2)$$

or, as given by Sih (1973)

$$S = \frac{1}{8\mu}[(1-2\nu)(\sigma_x+\sigma_y)^2 + (\sigma_y-\sigma_x)^2 + 4\sigma_{xy}^2] \qquad (6.5.3)$$

So in order to determine direction of crack propagation it is necessary to determine the r coordinate characteristic of the material and obtain the value of ψ for which the criterion under consideration (either σ_ψ or S) attains a maximum, and provided this maximum is equal to or higher than σ_c or S_c (depending on which criterion is being used), characteristic of the material as well, the crack will propagate in that specific direction.

It has been shown that the stress field in the crack neighbourhood is depicted by Equations 4.3.3, 4.3.4 and 4.3.5. These equations are repeated here for convenience.

$$\sigma_r = \sum_{n=1}^{\infty} \{(-1)^{n-1} r^{n-3/2} A_{2n-1} (n-\tfrac{1}{2})[(n-3/2)\cos(n-3/2)\psi$$

$$- (n-3/2)\cos(n+\tfrac{1}{2})\psi]$$

$$+ (-1)^n r^{n-1} A_{2n}\, n[(n-3)\cos(n-1)\psi - (n+1)\cos(n+1)\psi]$$

$$+ ([1)^{n-1} r^{n-3/2} b_{2n-1} (n-\tfrac{1}{2})[(n-7/2)\sin(n-3/2)\psi$$

$$- (n+\tfrac{1}{2})\sin(n+\tfrac{1}{2})\psi]$$

$$+ (-1)^n r^{n-1} b_{2n} n[(n-3)\sin(n-1)\psi - (n-1)\sin(n+1)\psi]\}$$

$$[\frac{E}{1+\nu}] \qquad (6.5.3)$$

$$\sigma_\psi = \sum_{n=1}^{\infty} \{(-1)^{n-1} r^{n-3/2} A_{2n-1} (n-\tfrac{1}{2})[(n+\tfrac{1}{2})\cos(n-3/2)\psi$$

$$- (n-3/2)\cos(n+\tfrac{1}{2})\psi]$$

$$+ (-1)^n r^{n-1} A_{2n} n[(n+1)\cos(n-1)\psi - (n+1)\cos(n+1)\psi]$$

$$+ (-1)^{n-1} r^{n-3/2} b_{2n-1} (n-\tfrac{1}{2})[(n+\tfrac{1}{2})\sin(n-3/2)\psi$$

$$- (n+\tfrac{1}{2})\sin(n+\tfrac{1}{2})\psi]$$

$$+ (-1)^n r^{n-1} b_{2n} n[(n+1)\sin(n-1)\psi - (n-1)\sin(n+1)\psi]\}$$

$$[\frac{E}{1+\nu}] \qquad (6.5.4)$$

$$\sigma_{r\psi} = \sum_{n=1}^{\infty} \{(-1)^{n-1} r^{n-3/2} A_{2n-1} (n-\tfrac{1}{2})[(n-3/2)\mathrm{Sin}(n-3/2)\psi$$

$$- (n-3/2)\mathrm{Sin}(n+\tfrac{1}{2})\psi]$$

$$+ (-1)^{n} r^{n-1} A_{2n} n[(n-1)\mathrm{Sin}(n-1)\psi - (n+1)\mathrm{Sin}(n+1)\psi]$$

$$+ (-1)^{n-1} r^{n-3/2} b_{2n-1} (n-\tfrac{1}{2})\mathrm{Cos}(n-3/2)\psi - (n+\tfrac{1}{2})\mathrm{Cos}(n+\tfrac{1}{2})\psi]$$

$$+ (-1)^{n} r^{n-1} b_{2n} n[(n-1)\mathrm{Cos}(n-1)\psi - (n-1)\mathrm{Cos}(n+1)\psi] \}$$

$$[\frac{E}{1+\nu}] \qquad (6.5.5)$$

Sih (1974), Chose to ignore the terms of higher order than one as their contribution for $r \ll$ (than a characteristic length) is negligible in comparison with the $1/\sqrt{r}$ terms; in the present work, all the calculated coefficients (about 20) for the Williams series are considered, and the directional stability criterions are evaluated from Equations 6.5.3, 6.5.4, 6.5.5.

Within the crack stress field, there are an infinite number of points in which the criterion function can be evaluated, and for localising the critical one an optimization approach should be employed. The author collaborated with Swedlow (1974) in the development of a computer program to search for the critical value of the function that defines directional stability, and a brief description of this approach is made hereafter.

Mathematically, there are two ways to achieve the desired objective;

(1) Indirect methods, in which the first and second derivation of the function are evaluated and from them the maximum is obtained.

(2) Direct methods (specifically elimination), in which the value of the function is calculated, and as information is accumulated one moves into regions where the maximum may lie and eliminates areas where it cannot be.

The elimination technique called the Golden Section, Wilde and Beightler (1967), has been employed to develop the computer program to determine the parameters desired. Some of the basic conditions needed to apply a method such as the one mentioned are:-

(a) It is desirable to have but one variable as elimination methods are extremely effective then, so it was decided to fix "r" and vary "ψ".

(b) The function should be an unimodal objective function defined in a closed region. Suppose that we wish to find the location X^* where $y(x)$ achieves its maximum value y^* in an interval $\ell < x < r$. The unimodality of $y(x)$ assures that there is only one local maximum, more precisely, $y(x)$ is assumed to increase monotonically up to the maximum, after which it decreases monotonically (unimodal here does not require smoothness or even continuity). Strict unimodality makes it possible to say, after examining the results of any pair of evaluations of the objective function, that the maximum lies in some interval shorter than the original one.

Having examined the function and decided that it can be treated by an elimination method, one has to establish the initial interval to evaluate and from there start searching for a maximum. Of course it is not known in advance how many evaluations to use and the procedure is usually to change the variable and keep experimenting until the change in value of the criterion of interest is negligible. A procedure like this would produce the desired result but would not be an efficient one. It is necessary to use a search plan so that the solution will close on the maximum as quickly as possible in the search,

and the already mentioned Golden Section search is such a technique that, being completely independent of the number of evaluations, is highly efficient. In it, if one represents by "j" the number of experiments already run, it can be demonstrated that the experimental plan should place successive experiments in such a way that the interval "I" between successive experiments is given by

$$I_1^{n-j} = I_1^{n-(j-1)} + I_1^{n-(j-2)} \qquad (6.4.1)$$

Actually, what is done by this technique is to hold the ratio of successive intervals constant; calling this ratio τ,

$$\frac{I_1^{n-j}}{I_1^{n-(j-1)}} = \tau = \frac{I_1^{n-(j-1)}}{I_1^{n-j}} \qquad (6.4.2)$$

by dividing equation 6.4.1 throughout by $I_1^{n-(j-1)}$ and noting that

$$\frac{I_1^{n-(j+1)}}{I_1^{n-(j-1)}} = \tau^2$$

it is found $\tau^2 = \tau + 1$ as shown in the diagram below

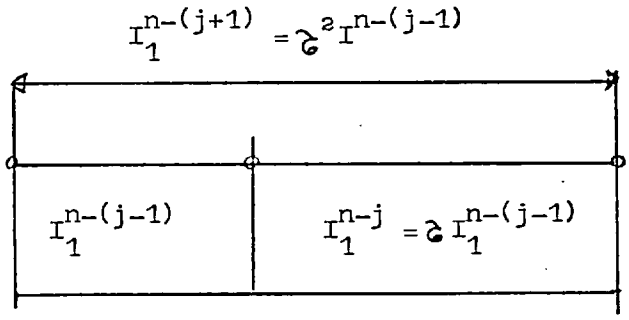

Only one root of this equation is positive, and so it is seen that

$$\tau = \frac{1 + \sqrt{5}}{2}$$

The results of two experiments determine which segment is explored further, and the remaining segment will contain one of the previous trials and to continue the search it is only a matter of placing

the next experiments symmetrically in the interval. After n experiments, the interval remaining is given by

$$I^n = \frac{1}{\partial^{n-1}}$$

so it is a matter of deciding which is a satisfactory minimum interval and performing a series of calculations on the criterion proposed until the maximum value of the function is obtained. Program Hunter (Appendix 6) was developed as described; data for it are specimen dimensions, coefficient values, stress state, and material constants.

The values of the critical parameter and the crack extension angle for specific values of the radius were obtained for some of the specimens and are given in Table 6.3. Further discussion on these results is given in Section 7.7.

CHAPTER 7

COMPUTER AND EXPERIMENTAL WORK ON DIRECTIONAL STABILITY OF CRACK PROPAGATION

In this chapter a summary of computer and experimental work on Directional Stability of crack propagation is presented, and the relationship between the two sets of results are discussed.

Computer study is made of cases that can be checked experimentally, the results obtained are interesting and the correlation between experiments and computation seems to be a good one. There is, as well, some computer work that cannot be verified experimentally with the rig in its present state. However, provided the co-relation of the former work is a good one, tentative conclusions can be drawn purely on the basis of the computer work.

Independent analysis either from the computer simulation on the experimental work is made and discussions are presented on directional stability of crack propagation and other parameters already put forward by previous researchers which help to explain the phenomena that seem to be taking place.

7.1 Analysis of Simple Approaches to Define Directional Stability of Crack Propagation

Some of the earliest work done with the program ANGCRK was directed at obtaining the first coefficient values (specifically A_1, A_2, A_3) for a pair of specimens geometrically similar, i.e. dimensions 12 x 2, and 6 x 1 (Fig.7.1c), with the crack running up to 5/6 of the full length. The results are depicted in Figs.7.1a,b. The values for the coefficients, as well as cracking conditions, are given in Table 7.1.

Cotterell's (1966) original approach was that only negative values of A_2 would mean that the crack is directionally stable, so according to the values obtained, both cracks are unstable. However, a conclusion here could be that there is a higher instability for specimen 12 x 2 than for specimen 6 x 1. (Some work carried out at Imperial College on steel, for specimens which are geometrically similar, i.e. dimensions are 2:1, have given results showing that smaller specimens are more stable, that is, proportionally the crack runs straight farther. This seems to agree with the computational work on A_2.)

A simple approach to this work, to try to explain the difference in A_2 values, was made. By using beam theory, the stress values at the crack tip, in the longitudinal direction (along X), are

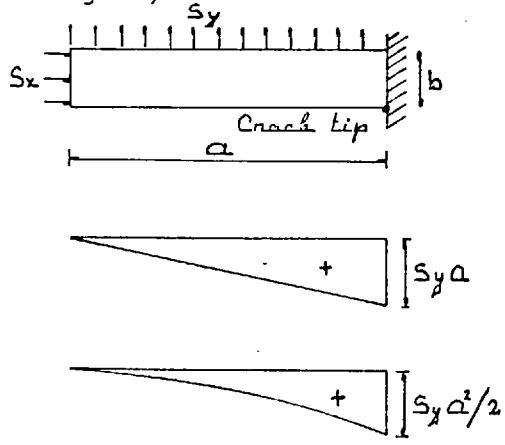

$$\sigma_x = \sigma_{(S_y)} + \sigma_{(S_x)}$$

$$\sigma_{(S_y)} = \frac{My}{I} \; ; \; M = S_y a^2/2; \; y = 6$$

$$I = b^3/12$$

$$\sigma_{S_x} = -S_x \; ; \; \sigma_{S_y} = 3 S_y a^2/b^2$$

$$\sigma_x = 3 S_y a^2/b^2 - S_x$$

and for the different crack lengths, the stress values are identical, as for both the relationship between a and b is kept constant. This approach through σ_x was tried because it was thought that the difference between values of A_2 for similar specimens was due to a possible difference in the stress value along the X axis, however, it seems that consideration of only σ_x through beam theory cannot account for the differences in A_2 values, so some other condition has to be considered.

Cotterell (1970) suggested a similar approach to define directional stability, i.e. "if $\sigma_y/\sigma_x > 1$, the crack is directionally stable". In order to test this, it was decided to apply the loading conditions, described by Cotterell (1970), i.e. the opening load is applied at the edge of the specimen as a concentrated load, see Fig.7.3, a feature not included in Cotterell's work, was the application of transverse load, and this has to be considered. The values of the transverse stress (σ_x) at the crack tip are calculated as shown in Appendix 7, given in Table 7.2, and depicted in Fig.7.2. On account of these results, it could be said that for this case, σ_y/σ_x values being between zero and one, the specimen is in a zone nearly stable, but the values obtained would mean that as the crack advances, the specimen goes from an unstable condition for short cracks to a stable condition for longer ones, a fact which does not seem to agree with experimental work.

A further point must be raised, the effect of the transverse load S_x, is to reduce the tension, along the x axis, introduced by the opening load at the crack tip. If there was a case in which a sufficiently high compressive stress was applied, say -1392 lb/in^2, σ_y/σ_x would become negative, as shown in Table 7.3. Clearly, for this case, as there is such high transverse stress applied, the crack will run straight, but $\sigma_y/\sigma_x < 1$. So it seems that this is not in agreement with Cotterell's argument. However, it could be that Cotterell's criterion was meant to be applied to the case of the SEN speciment with only opening load applied. In Section 7.2 a discussion is made of specimen geometry and its stabilising effect, it is possible that it is this effect which could be accounted for with Cotterell's argument.

7.2 Second Coefficient of the Williams' Series and its Dependence on Physical Parameters

It will be shown that the value of the A_2 coefficient depends on load and geometry, and that:-

(a) The dependence on load can be split into that caused by the σ_y stress (mainly opening load) and that caused by the σ_x stress (transverse load and opening load).

(b) The dependence on geometry is centred on the dimensions length, width and crack length. In considering changes of geometry, two divisions will be made. (i) Dimensions "length and width", which have an influence on the proportionality between the A_2 value and transverse stress, and (ii) the dimension crack length, which has an influence on the proportionality between A_2 and the opening load.

Work on the determination of the values of A_2 for the specimen depicted in Fig.7.1(c) of dimensions 6 x 1, 6 x 4 and 6 x 6 from 0.2ℓ crack length was carried out. The values obtained are shown in Table 7.4. In this table the A_2 values have been split so that there are two parts which, when added become A_2 for the composite load system. One part is proportional to the load along the "y" axis, and the other to the load along the x axis.

It is noticed that for the same geometry but different crack length, that part of A_2 which is proportional to the transverse load , remains constant i.e. the crack length does not affect this value, however, that part of A_2 which is proportional to opening load changes when the crack length is increased, and this change could be a notable one (see values for specimen 6 x 1). This could be explained by arguing that the normal stress, at the crack tip along the x axis (σ_x),

depends mainly on crack length. When the crack grows this stress is increased and as A_2 mainly shows this effect, its value changes as well (positive for a tension stress and negative for compression). In order to reverse this effect (for stabilising direction of crack propagation), a higher compressive x stress is needed so that the tension stress from the opening load is nullified.

There is another factor to be considered when determining proportional parts for A_2. As can be noted in Table 7.4, the proportional part of A_2 dependent on the transverse load, is a function of specimen dimensions, i.e. a, b, ℓ, and directly proportional to σ_x, this proportionality factor being equal to -0.31456 for the specimen 6 x 1 i.e. each compressive longitudinal load of 10lb changes the A_2 value in -0.31456. For specimen 6 x 4 the proportionality factor is -0.5 and finally for specimen 6 x 6 it is -0.62476. So, for specimen 6 x 1 $\times 0.3\ell$ if it is necessary to neutralise the effect of an opening load of 10lb, the transverse load to be applied on the lateral boundaries of the specimen would be 31\ lb, while for specimen $6x4x0.5\ell$ it would be 34.5, and finally for specimen $6\times6\times0.5\ell$, A_2 would become zero by applying a transverse load of only 6.2lb. This is a point which could partially explain the observed fact of square specimens being more stable than rectangular ones (longer in the x direction).

The specimen shown in Fig.7.3 was considered as well for calculation of A_2. The values obtained are shown in Table 7.5. Conclusions similar to those reached for the former specimens can be drawn from these figures. Further work on this topic and experimental application is discussed in the following section.

7.3 Influence of the Applied Loads on the First Coefficients of the Williams' Series, and Link to Experimental Work

In the test specimen in Fig.7.3, the factors affecting the values of coefficient A_2 (a, ℓ, b, S_x, P_y) are shown, and this dependence has already been demonstrated. Further work on the influence of S_x and P_y over A_2 is to be discussed within this section. This time, the stress conditions chosen are S_x = 0.0, 10.0, 20.0, 30.0, 40.0, 50.0 combined in each case with P_y = 10.0. This loading was applied to specimens 6.0 x 6.0, 6.0 x 4.0 and 6.0 x 1.0. Under these conditions program ANGCRK was run and the set of values obtained for coefficient A_2 is shown in Table 7.6, and depicted in Figs.7.4. The following points are relevant:

(a) the rate of change for A_2 is higher for longer specimens (x direction);

(b) even though different transverse loads are applied the pattern of the curve (A_2 vs a) Fig.7.4a,b,c, is kept. The way the transversal load affects this curve is by shifting it along the A_2 axis;

(c) for no transverse stress, there is a definite crack length for which A_2 = 0 (about 2.2in for specimen 6.0 x 6.0, 1.3in for specimen 6.0 x 4.0, and 0.35 for specimen 6.0 x 1.0);

(d) the shifting of the (A_2 vs a) curve changes the crack length for which A_2 = 0;

(e) the shape of the curve (A_2 vs a) is similar to the curve (σ_y/σ_x vs a).

The A_2 behaviour shown is significant. In the past it has been put forward by Cotterell (1965) that this is the parameter defining directional crack instability and that the condition

$A_2 = 0$, marks the critical point above which the crack is unstable (A_2 positive), becoming stable below the critical point (A_2 negative), and this seems to reflect quite well experimental behaviour, where it has been shown, that cracks are made stable by applying transverse stresses.

Computer work which is to be linked with experimental work, was conducted on specimens 12.0 x 4.0, 8.0 x 4.0, 6.0 x 4.0 and 4.0 x 4.0. In Figs.7.5 curves (A_1 vs a/ℓ), (A_2 vs a/ℓ), and (A_3 vs a/ℓ) are depicted, while the actual coefficient values are given in Tables 7.5. Initially only opening load was considered. The same specimen behaviour already noted in the former work was obtained, but for these a different combined loading was applied, i.e.

(a) Transverse load = 0.10 lb/in (S_x)
Opening load = 10, 20, 40 lb (P_y)

(b) Transverse load = 0, 20, 30 lb/in (S_x)
Opening load = 20 lb (P_y)

Coefficient values were obtained and plotted for each specimen. The following points are relevant.

(i) As in former work, specimen dimensions define a characteristic slope for the curve (A_2 vs transverse load). This is shown in Fig.7.7. Loading conditions used for these cases were those from "b".

(ii) The values for coefficients A_1, A_2, A_3, for these cases, are given in Tables 7.5, it is possible from these data to find out which is the main influence on the behaviour of these first three coefficients, opening load being responsible for the changes experienced by the three of them, while transverse load affects solely the coefficient A_2 and this effect (for A_2) is not proportional to crack length.

(iii) If Fig.7.6 is considered, by using the slope value characteristic of the specimen, Section 7.2, and knowing the loading conditions, it is straightforward to define a transverse load value that makes A_2 become zero or negative.

Based on these facts, an experimental approach can be proposed as follows.

Once the desired experimental conditions are defined, through them the behaviour of the coefficients of the Williams' series is set up as well. This is done as follows. For experimental work, a factor which is necessary to consider is the material, as material properties will determine the opening load that is needed to extend the crack, i.e. K_{IC} or G_{IC}. When in loading the specimen, the value of K_I (which is proportional to A_1 and so to opening load) becomes equal to K_{IC}, the crack extends. The opening load level fixes specific values for all the coefficients in the Williams series, and it has been shown that for no transverse load, these coefficients are negative for A_1 and A_3, and positive for A_2, so A_2 being positive, the crack is directionally unstable. In order to stabilise the crack A_2 should become zero or negative and for obtaining this condition it is necessary to proceed as follows:-

(a) Define the opening load value necessary to reach K_{IC}.

(b) Obtain A_2 value induced by the opening load defined from "a".

(c) Know the proportionality factor between A_2 and transverse load (S_x) characteristic of the specimen.

(d) From "c", calculate S_x necessary to overcome the A_2 value obtained from "b", and apply it to the specimen so that the experiment is carried out under directionally stable conditions.

7.4 Load Application, Rig Response and Physical Interpretation of Gauge Readings

It has been shown in the computer analysis that the effects of the opening and axial load can be separated, this is a feature that if it could be applied to experimental results would be a great help to the analyst. In the sections to follow, it is shown that this is so, and the different characteristic behaviour is analysed as a consequence of geometry, transverse load, or opening load.

In order to calibrate the rig, it was necessary to have a device to apply, upon the load cells, the combined transverse and opening load. It was found that this device should be a very special one because of the fact that the transverse and opening load had to be applied simultaneously. Practically this introduced a high uncertainty in load determination, as when opening load is applied, there is a displacement of the loading point, and under the calibration conditions the response from the gauges was not repeatable, and it was not possible to properly calibrate the rig for the opening load. However, as a high number of attempts to calibrate in this initial state were made, it was possible to define a wide zone, within which the actual opening load value is located. Attempts were made to combine the results from calibration (regarding that opening load zone) with theoretical analysis of the configuration, but this implied assumptions and guesswork about the physical behaviour of the rig and specimen, which in brief would mean unreliable results, so two courses of action were plausible.

(1) Design of an additional load cell (as described in Section 6.3).

(2) Carry out experimental work with the rig in its initial state (i.e. study of stress field and effect of transverse load).

The work under (2), was carried out while the elements needed for the rig modification were being made available, and is described hereafter.

(i) Load application and rig response

In Fig.7.16, the gauges position within the rig is shown. In trying to get a better understanding of the phenomena taking place while the crack propagates, the loading records were plotted. Figs.7.17(a to h) depict the whole loading record given in Table 7.7(f) (specimen No.6/4). Five loading zones (although only four seem to be defined) are of interest here.

Zone 1. Transverse load application. This is done through the transverse load cells at the far end of the specimen. As can be seen in Table 7.7(f), a balance of gauge readings, 60 μs, for gauges 21 to 27 was obtained (the small differences are because the calibration constants for each cell are slightly different).

Zone 2. Opening load application. This is the actual process which leads to the crack extension. Some differences that show the physical behaviour of the specimen, can be noticed, i.e. in gauges 23,24 (nearest to the crack tip) the opening load effect at the crack tip zone is clearly noticeable. An initial higher normal stress (here, because of the way in which the gauges were connected to the bridge, compression is read as positive) originated on the transverse load, diminishing when the opening load has a small releasing effect on this compressive stress. In the main, this compressive stress remains so that at the breaking point there is still compression parallel to the

crack tip. This should mean stable directional behaviour (actually the angle of crack extension was ≈ 2 deg). The gauges 22 and 25 show almost the same pattern as the former ones. For gauges 21,26 the opening load has a different effect, increasing the value of gauge readings. This means that compression is being put on. Finally, gauges 20,27 show a similar behaviour to 21,26. It is interesting to notice that in the first stages of opening load application, some irregularity in the expected trend of the curve is detected, however, it rapidly corrects itself and then the curve follows what is thought to be the correct pattern. This most probably shows the kind of behaviour obtained during calibration. The rest of the gauges show reliable responses as they follow similar trends. The main fact to point out is that all the gauges show a load peak at the point of fracture.

Zone 3. Crack extension. Within this zone different behaviours are obtained for the strain gauges, i.e. for those gauges farther away from the crack tip, 20 to 27, the stress is released at a uniform rate, and for those nearer to the crack tip, 0 to 19, the stress is released at a higher rate immediately after crack extension and then stabilises to a fairly constant decreasing rate.

Zone 4. Removal of opening load. The remaining strain values, shown by strain gauges 20 to 27, after removal of opening load, are slightly lower than the original ones. The strains for gauges 0 to 19 show similar tendencies but this is not a uniform pattern.

Zone 5. Removal of transverse load. Gauges at the far end (20 to 27) show zero readings but the other ones (0 to 19) still show strain, this is a point that is not clear. Zero values were

expected. It is thought this behaviour is because once displacements have taken place, on removal of the loading the relative position of pieces in the rig and those in connexion with the specimen, do not go back to their relative original position, and keep the specimen slightly strained.

A further attempt was made to obtain some kind of calibration by measuring the distances involved in the position of the gauges on the rig, and through beam theory and the relative electrical constants of interest, work out the theoretical stress values, but it was not possible to obtain any sensible result.

The type of analysis using the loading measured at different boundaries, as depicted in Fig.7.17(a to h), seems to the writer to be a valuable one, because as the rig response is monitored at the boundaries on which load is being applied, it is possible to understand very well the way in which the stress field varied. But it is necessary to solve the technical difficulties encountered so that proper calibration of each gauge is achieved. Once this is sorted out, a more refined experimental method should be planned. This point will be put forward in Chapter 8.

(ii) Physical interpretation of gauge readings

When the crack propagates, for most cases there is a sudden initial crack extension after which a slow continuous propagation takes place, the readings from the gauges show this by means of a high change in the reading immediately after the peak value, and then keeping a slow rate of change of the magnitude of the readings. The fact that during the second stage of crack propagation the velocity of crack extension is low, suggests that the readings are values slightly above the critical ones necessary

for the crack to stop (arrest). The observed effects of raising the load once the crack is propagating in this second stage or has stopped, are:- (a) it raises the rate of crack extension, (b) it originates a noticeable directional change. Roughly, it is possible to imagine how the crack developed by just having a look at the loading record after initial crack extension. As can be seen in the different tables, when the crack continues to propagate by itself, i.e. without load increments, the direction of crack propagation changes but in a stable manner, whilst in changing loading conditions the change in direction is a sudden one. It could even be possible to form a rough idea of the way a crack has run by just having the loading record of the specimen, when in the loading history a sudden rate of change is observed between two subsequent readings (readings taken at constant rate), it can be assumed that load was applied at that instant, it could not be thought that the mentioned reading change was because of change in the direction of crack extension, as it would not take place unless an inhomogeneity was encountered, and this, for a slowly propagating crack, most probably would stop crack propagation. Another possibility would be that the small quantity of potential energy (which is being transformed into kinetic energy for the running crack) that the test piece still possesses, could be used to overcome the energy level necessary to surpass the inhomogeneity by separating the material, in which case, most probably a change in direction would take place as well as a reduction in the velocity of crack propagation, although the behaviour just described has not been observed in the experiments performed.

(iii) Effect of crack tip radius

Two experimental cases are considered in relation to this topic, those of specimen 8 x 4 (case 1 and 5), for which the characteristics are

Crack Tip	Sharp	Blunt
Load value to start crack extension	325 lb	412 lb
Length of crack extension	0.375in	0.75 in

The same experimental conditions applied to both. Photographs in Fig.7.11 (a and e) show the crack path obtained.

When examining the case of the blunt crack, it can be seen that the crack tip radius only affects the opening load necessary to extend the crack, this radius has the effect of reducing the stress concentration at the crack tip neighbourhood, so in order to raise the stress level to that corresponding to the fracture toughness, it is necessary to apply a higher opening load. When the material finally separates, there is in the body a certain state of strain. The separation of the material means a transition from a tip with a finite radius to a tip with a sharp radius characteristic of the moving crack. This geometrical condition has the effect of producing a stress concentration in the neighbourhood of the crack tip, higher than in the former case so that within the new conditions of the system, there is no equilibrium. This stress level developed at the crack tip means in fact that there is an excess of strain energy within the body, which has to be spent. Berry (1961) has shown that this energy is split between surface energy and kinetic energy, so the crack experiences a sudden jump.

The same can be argued for the case of a sharp crack, with a small difference. The sharp crack is made by means of fine tools, and it was found that at the best the tip radius approximates the natural characteristic one of a moving crack and so the obtained value of load (represented by the reading of 342lb) approximates the true fracture toughness of the material. This is easy to understand: the tip radius being smaller, a proportionally higher stress concentration is produced(compared with the case of the blunt crack) and a lower opening load is needed to reach the fracture toughness. This in turn means less strain energy available and so a shorter length of jump for crack extension. Some researchers have obtained a practical sharp tip by pre-fatiguing their specimens, this could be done under the present approach for future work.

Something else that must be pointed out is that regardless of crack tip geometry, the crack paths were identical, which again seems to show the influence of the transverse load as the factor controlling crack path. Further discussion on this topic is made in Section 7.6.

7.5 Analysis of Experimental Crack Path under Biaxial Loading and Co-relation to Theoretical Predictions

In the present section use is made of shadow photographs taken of the cracked specimens, in order to illustrate relevant points and how it is thought that through them, a link between theoretical results, obtained from the computer program, and experimental ones, could be established.

Figs.7.8 to 7.12 show a visual record of the paths the cracks followed, when the loads of which details are given in Tables 7.7 to 7.11, were applied on the specimens.

In all some 40 specimens were tested in two different experimental stages. For the first experimental stage, as it had not been possible to achieve a proper calibration for the opening load see Section 7.4 an attempt was made to apply different levels of transverse stress and see what effect it had on the crack path. Results were very promising as with no transverse load the crack path always went away from the original one, while on introducing a low transverse load, the deviation of the crack path was reduced, transverse load was subsequently increased until for a level high enough, the crack path became straight. For the second stage, a new load cell for the opening load had been introduced and proper calibration achieved so a whole analysis could be made quantifying all the parameters that have an influence in crack propagation. Within the different discussions to follow, use will be made of results from these two experimental stages and any relevant experimental detail will be given whenever it is necessary.

In order to facilitate discussions on the crack propagation phenomena, it is necessary to define, for the present analysis, some terms to be used (see Fig.7.13).

(i) In the experimental work, the actual crack propagation developed as follows:-

(a) An initial slow crack propagation following the same direction as the original crack, under this "phase I" (see Fig. 7.14) crack extension the surface of the crack appears as slightly rough areas with a fan shaped marking of lines .

(b) A very fast crack propagation following a natural direction established by the different specimen parameters. For this "phase II" (Fig.7.14) crack extension the crack surface is very clean and smooth, like a mirror surface.

(c) A slow decreasing crack propagation, following the same trend of path initiated under phase II. The surface of the crack under this "phase III" (Fig.7.14) crack extension is very similar to that under phase I.

(ii) For most cases, especially when there is a well defined radius at the crack tip or a blunt crack, there is a very short straight extension (phase I). Immediately after this the crack propagates (phase II) and deviates towards a direction with an "apparent initial angle" (α_a), and as propagation continues there is a continuous change of this angle until at point P_r, whose coordinates will be identified, the crack has a final angle (α_F). Point P_r could be either in the zone of phase II or of phase III. This is not highly relevant for the time being.

For each specimen of interest, the already defined angles and lengths were measured and are given in Tables 7.12 to 7.15, in which is also included

(i) the opening load (three quantities are given I = initial reading from the gauge, A = reading just after crack extension (for most of the cases under phase II) B = peak reading for opening load (has taken place).

(ii) SC - this is the maximum load (lb) applied to the specimen by the opening load, it equals B-I, and should be equivalent to the fracture toughness;

(iii) Sload. It is the quantity (B-A) and it was expected (according to Section 7.4) that some kind of proportionality should exist between the phase II crack propagation length and this quantity;

(iv) A_2 coefficient value as calculated from Tables 7.5.

Tables 7.12 to 7.15 are self-conclusive, however, the following points are of interest:-

(a) for most cases the fracture has a very small starting zone in which the crack runs straight. This is thought to originate in the fact that the crack tip did have a finite radius which creates a local stress field and establishes a local direction of propagation, but once the crack surpasses the local condition, the crack tip becomes sharp and the extension follows the natural path dictated by the specimen boundary conditions;

(b) in Fig.7.8(a to d), a series of photographs of the different cracked specimens is shown, it can be clearly seen that for specimens 4, 6, 8, the apparent initial angle (αa) experiences a gradual change, running away from the original straight path, and the change is a low one for the smallest specimen, becoming higher for specimen 6, and reaching its maximum for 8. It was expected that specimen 12 should have an even higher α_a, but this was not so, and on repetition of the experiments on specimen 12, the same result was achieved;

(c) regarding the value of the transverse load required to stabilise the crack path, it is shown that the value required to stabilise the smaller specimens is lower than that for the longer ones. Besides, it can be said that for the small specimens (square), under biaxial loading, the condition is achieved in which the crack really follows a straight path, while for the rectangular ones (larger in the transverse sense), one has to resort to a definition of straight path, i.e. like the one mentioned by Benbow and Roesler (1959), and accept as straight paths, those

which are slightly away from the axis of symmetry. The point which has to be kept in mind is that provided the apparent initial angle (αa) changes subsequently towards the initial crack direction, the crack is directionally stable (class I fracture according to Cotterell (1965) definition), and this is a fact shown by all the crack paths, that is, whenever a transverse load is applied, the crack tends to come back to the straight path and the higher the transverse load, the smaller the initial deviation;

(d) the subsequent point has already been mentioned in the last paragraph, but here it concerns specimen geometry. It is clearly shown by experimental results that the larger (in the transverse sense) the specimen, the higher is the transverse load necessary to stabilise crack path (for a specimen 12 x 4, it is clearly seen that a higher load is necessary to reduce the apparent initial angle;

(e) for all the different specimens, no transverse load, produces a directionally unstable crack extension. When transverse load is considered instability is reduced, and as transverse load increases the instability diminishes until eventually, the condition of straight crack propogation is reached;

(f) regarding the actual opening load value at which the crack extends, only for those cases of specimens 12 x 4 and 4 x 4, could it be said that a positive conclusion has been obtained, as for the first case (12 x 4) there are 5 cases in which the opening load values repeats, while for specimen 4 x 4 this is so for four specimens. There is not enough information for specimens 8 x 4 and 6 x 4. Furthermore, it has to

be pointed out that from the opening load values, about 30% seem to be completely out of range, two causes may be relevant:- (1) the specimens were cut from different sheets of material, some of them were tested after about three months had elapsed since they were cut, and others within a week, (2) the whole experimental method is still in a state of development, and even though great care was taken in trying to set experimental repeatable conditions, the method still needs to be refined.

A further point to be discussed is that for most of the experimental cases tried, a tendency to directionally stable conditions was obtained (this is a characteristic of the rig) and this was so in spite of the fact that there was directional instability for the initial conditions. (This point will be discussed further in Section 7.6.) When initial conditions are unstable and at the same time an imperfection either from the material or from the rig configuration becomes apparent, then the crack runs away. It is thought that there is still a small defect coming from the rig (introducing mode II crack behaviour) which is slightly interfering with the stress field. However, these are practical difficulties that can be overcome, the main point is to show that the directional crack response can be characterised by the coefficient A_2, and it seems, according to the combined computer and experimental results that this is so. It can be seen (Tables 7.5) that the value of the coefficient A_2 is negative for specimens with a transverse load high enough (for each geometry, depending on the opening load value, it is necessary to have a minimum transverse load), and experimentally these specimens showed directional stability. On the other hand A_2 is always positive for cases in which no transverse load was applied and these experimentally, showed directional instability.

7.6 Directional Stability Level, Transverse Load Influence, and Possible Co-relation with Energy Input to the System

(a) Experimental directional stability, rig response and crack path. Some of the earliest experimental work (specimen No.1) showed that under combined biaxial loading, the crack initially extended showing it to be a class II fracture (Cotterell, 1965) tending to go back to the initial path. Once the crack extension had naturally stopped, the opening load was increased and the crack path changed direction still towards the original path. Within this section an attempt is made to co-relate this behaviour with the A_2 coefficient. Actually, the loading record of the already mentioned specimen No.1 was not taken. However in the following discussion, use will be made of load values obtained from specimen 3/12, in order to illustrate the different points under consideration.

The experimental work on crack extension under combined transverse and opening load for this specimen showed that:- when the crack is about to extend there is a peak opening load the value of which was 340lb, and the transverse load 360 lb/in. This opening load in turn sets the A_2 coefficient value (originated in the combined loading) at +36.626. Once the crack had extended and deviated away from the transverse axis, further opening load was applied and the crack deviated towards the initial path. It had been initially expected that it should be the other way around, i.e. increase in opening load means increase in directional instability and the crack should turn away from the original path, but this was not so.

In examining the opening load values (for specimen 3/12) it was found that in crack extension from a = 3.35 in to a = 4.51 in, the opening load values went down from 340lb to

140lb, whilst the transverse load remained at 360lb/in. That is, the cracked situation could be viewed as a completely new case with: (a) opening load = 140lb, (b) transverse load = 360lb/in, (c) crack length = 4.51 in and so, the A_2 coefficient value for this condition is set to 14.40 . Which means that the directional stability level is higher now than it initially was, and the crack should tend to go back to the original path, which explains satisfactorily the observed crack behaviour.

(b) Transverse load and its influence on crack path. The data shown in Tables 7.15 as well as the photographs of the crack path in Fig.7.12, show different specimens (same dimensions), under the same loading conditions i.e. 2/12, 3/12, 4/12. It is shown as well, that for specimen 6/12 a high transverse load made the system partially overcome a tendency to behave asymmetrically. When the case with a lower transverse load is considered, this asymmetric tendency is more apparent, and its effect can be clearly noticed on the initial apparent angle and the crack extension path of the already mentioned specimens. While in specimen 6/12 the crack path tends to go back to the centre, this tendency is not as marked for specimen 2/12. Another experiment in which loading conditions were the same, was that for specimen 3/12 in which the crack followed the same path as it did for specimen 2/12.

Having analysed the results, it was concluded that this tendency was because the blocks to apply the opening load (pieces No.3, opening load cells) were slightly out of centre with respect to the transverse load cells and on operation this introduced an unbalancing effect (mode II). The rig was dismantled and corrected, and specimen 4/12 was tested with the same loading conditions as for specimens 2/12 and 3/12. This

time a better experimental result was obtained as the difference in crack path can show (Fig.7.12), as well as load values in Table 7.15, which are similar to those from specimen 6/12. This time the crack path is closer to the axis of symmetry of the specimen, than those of specimens 2/12 and 3/12, and the difference it shows when compared with specimen 6/12 is thought to be only because of differences in the transverse load magnitude.

(c) Observed behaviour of crack propagation and possible co-relation with energy input. In general, for a cracked body under a rising load, it is an observed fact that, as the load increases, any crack existing in the body does not initially expand. When the load reaches a certain value the crack begins to spread, with the extension behaviour for a given material depending on the manner in which the load is applied. In some cases, the crack extends rapidly up to complete rupture of the body, in other cases it extends slowly, eventually stopping. Barenblatt (1961) in his approach to the theory of cracks, by an equilibrium model stated the hypothesis:

(i) the tensile stress at the contours of the crack is finite;

(ii) the opposite faces of a crack close smoothly at its contour;

and from them the formulation of the problem of equilibrium cracks is possible. In the case of stable equilibrium, the slow quasistatic transition of cracks from one equilibrium to another takes place when the load is increased gradually. But, if the equilibrium is unstable, the slightest excess over the equilibrium load is followed by a rapid crack extension. In some cases, when there exists no neighbouring stable states of

equilibrium, this could lead to complete rupture of the body.

Practically, the statements above can be illustrated by results from specimens 1/8 and 4/8, for which the loading records are given in Table 7.14. The only difference between the conditions under which these specimens were tested, is the geometry of the crack tip (a geometric factor that obviously influences position of neighbouring stable states). In the first case, when the load level was raised to 325lb the crack showed the already mentioned slow quasistatic transition natural of a stable state. In the second case the behaviour of the unstable equilibrium state is obtained at a load level of 412lb, here, because of physical conditions (specifically crack tip radius) the crack is prevented from extending slowly so that the only way for the crack to spread, is by a sudden jump from a_1 to a_2. That is, because of crack tip conditions, when the material finally separates to make the crack grow, there has been put into the body a considerable amount of energy, which is in excess of that in the former case, so at the point of crack propagation there is energy available to create new surface and supply kinetic energy.

7.7 Transverse Load, Mode II Influence, and Crack Path

Photographs in Fig.7.15 show the crack paths for different 12 x 4 specimens, the loading records for these specimens are shown in Tables 7.11.* The first point to be made concerns the values of the recorded transverse loads in gauges 20 to 27, it can be seen that for these tests the unbalance between gauges (20 to 23) and (24 to 27) is almost zero, which means that this time the alignment of the system is very good and the mode II influence for crack propagation is very small. This is shown as well in the magnitude of the transverse load necessary to make the crack run straight, it is noticed that with as little as 280 lb/in, the crack is already running straight, while in the former cases (Section 7.6), in which it was concluded that mode II was operating, it was necessary to go up to 700 lb/in to obtain a path that could be considered straight. The photographs of Fig.7.15 are in a sequence starting with the one with the least transverse load (160 lb/in) and up to 440 lb/in. It is clear that the transverse load has a strong influence in the direction of crack propagation and these figures show it quite well. However, when a more detailed analysis is made, i.e. measurement of the initial apparent angle (α_a) and final angle (α_F) already defined, the results shown in Table 7.16 are obtained, and here the co-relation does not seem to be as straightforward. Clearly there is still another factor that is showing up in these results, i.e. the crack tip shape. In relation to this, two of the specimens had a tip completely blunt and they show the two highest initial apparent angles. This state of the crack tip is a local condition that dominates the initial stage of crack

*Only three records are shown.

propagation and directs the path at random, but once this initial stage takes place, the local condition disappears and global conditions take over (in this case dominance of transverse load) and re-direct the crack towards a path which is natural for the whole system, the straight path.

The results from the two sets of experiments, i.e. those with a mode II effect (Section 7.6(b)) and those with no mode II effect (or at least a negligible one), seem to show that it is the influence of mode II behaviour (because of the bi-axial stress field introduced by anisotropies, inhomogeneties, etc, that could appear at each stage of crack propagation) which is being controlled by the transverse load, and that the value of A_2, which effectively has a relation to direction of crack propagation, shows a level of directional stability. That is, for a symmetric specimen, if it is highly stable (a high negative A_2 value), a strong local condition would be necessary to make the crack run away from the straight path, but once the local condition is overcome, the crack returns. If there is a weak stability (A_2 very near zero), it is very probable that the crack will deviate, but with the possibility of the crack returning. Finally, if this A_2 coefficient is positive, any local condition, perhaps at microscopic level, will make the crack turn away from the former path and it will never come back. However, when mode II behaviour starts to operate, the whole stress field in the neighbourhood of the crack is modified, i.e. global conditions are modified, and in order to overcome this situation, a strong transverse load is necessary. The function of this transverse load is to correct these global conditions so that the tendency of the crack path is again towards the original direction.

The writer's opinion is that stable and unstable directional behaviour develops as the crack propagates, this is reflected in A_2 and when it decreases with crack extension (tending to a negative value), the crack can be considered directionally stable. This is a point which seems to be substantiated by results shown in Tables 7.12 to 7.15 in which positive values for A_2 are obtained, but as the crack extends, the coefficient value diminishes.

7.8 Angle of Crack Extension as obtained Computationally from the Criteria Considered

A full discussion of the results obtained from computation for the expected angles of crack extension cannot be made because only a very limited number of cases were tried, and in addition experimental results would have to be found very carefully if comparison is to be meaningful. Some work was done with the specimens 12 x 4, 8 x 4, 6 x 4, 4 x 4, and others* These have been the first attempts to use this computational approach (regarding determination of the angle of crack extension) and there is still some uncertainty on the whole approximation as it is necessary to fully co-relate the mathematical numerical approach, the behaviour of the criteria, zones of relevance, etc. Experience will show which is the best criterion to apply and this experience will be gained by means of a combined computational-experimental approach. The first step has been the development of the computational method (i.e. Williams and Ewing criterion of a maximum circumferential stress σ_ψ at a core radius, and Sih's criterion of minimum strain energy density, (S) and the testing of this computational approach has only been initiated by the cases and discussion given within this section. It has already been shown, Section 6.5, how the stress field in

*Results obtained are shown in Table 7.17.

the crack neighbourhood is scanned and the critical value of the criterion function is obtained, fixing the angle at which the crack is expected to grow. As expected, it was found that the value of the criterion function varies with the core radius. The conclusions that can be arrived at from the few cases run are very limited.

(a) There are zones of disagreement between the two tested criteria.

(b) Williams and Ewing's criterion seems to show results that are consistent and well behaved. The values obtained show a well defined trend.

(c) The trend of values obtained from Williams and Ewing's criterion show a certain degree of similarity with experimental results (see Fig. 7.18) in which the apparent initial angle for the same specimens are shown).

(d) For all the cases in which transverse load of the specimen was considered, the expected angle of crack extension is very near zero.

(e) Another fact to point out concerns the dimension of the radius at which the criterion function should be evaluated. Both William and Ewing, and Sih point out that it is a material characteristic, and Williams and Ewing have given it to be 0.002in for PMMA. Probably this is the sort of dimension that would be involved for most of the materials and it can be seen that for a zone with that dimension, both criteria give very similar (equal) results.

An attempt was made to obtain some sort of description of the curve of maximum values of the criterion function, and for this the values from the Williams and Ewing criterion were

considered. Fig. 7.18 depicts this curve for specimen 12 x 4 and conditions given in Table 7.17(a).

Extensive work needs to be done using this approach. Experimental work linked with the computational method should be carefully planned so that a better understanding of the phenomena can be achieved and if need be, the necessary modifications to the numerical approach can be made.

7.9 Initial and Final Directional Stability Level

In Section 7.6(a) a particular case, in which the directional stability level for two stages of crack extension in a specimen, was discussed. As this point is considered to be of the greatest importance, the same approach was applied to all the remaining specimens for which experimental data was available. Table 7.18 shows results obtained by a combination of the experimental and computational work for this, the two stages of crack extension considered were:-

(i) Initial conditions.

a_i = Initial crack length.

$O.P._i$ = Opening load value, as measured from the experimental rig, when initial crack extension took place.

T.L. = Transverse load.

(ii) Final conditions.

a_F = Final length of crack (considering that this final length is defined by the change in fracture surface i.e. phase II and Phase III).

$O.P._F$ = Opening load value measured just after extension under phase II has taken place.

T.L. = Transverse load (same as for initial conditions).

For final conditions in most of these cases there was a small deviation of the crack path from the original direction. Neglecting mode II effects and considering the final crack length as a completely straight one, the first three coefficient values given in Table 7.18 were obtained.

These results clearly show that the value of A_2 is positive to start with (directional instability and moves towards a negative A_2 value gradually approaching a stable state). That is, the fact that A_2 diminishes with crack extension means higher directional stability.

In Table 7.18, a set of data which firmly establishes a relationship between the A_2 value and the experimental angle of crack extension is given. All the values considered, except A_2, were taken from the experimental work, and from these, the A_2 coefficients were calculated as described in Section 7.2. (The program ANGCRK was used as well as a final check and the same values were obtained.)

It has been considered, for the present discussion, that the mode II effect introduced by the crack running asymmetrically, is supposed to be negligible.

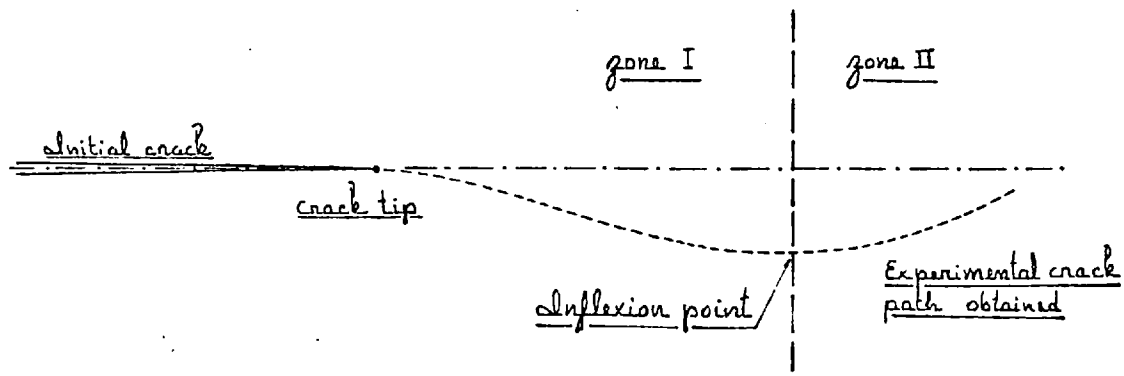

The figure above shows the typical observed crack path. For all cases, except those with no transverse load, whenever the angle of crack extension diminishes, the A_2 value decreases as well. As this analysis was the latest development of this study, it was made with the experimental data already available and so, only cracks that were within zone one were considered. However, specimen 5/8 (8 x 4) is the closest to the inflexion point, with a final angle very near zero, and the corresponding A_2 value being already negative, i.e. negative A_2 value means that the crack goes back towards the straight extension. Speciment 4/4 (4 x 4) also shows a negative A_2 final value, although the final angle of crack extension is not still zero.

Even though only one case is presented in which there is true straight propagation and a corresponding negative A_2 value, the tendency shown is quite clear and further work using this approach will prove this point.

CHAPTER 8

CONTRIBUTIONS OF THE PRESENT WORK, CONCLUSIONS AND SCOPE FOR FUTURE WORK.

8.1 Contributions of the Present Work

The test procedure was designed around a rigorous mathematical analysis involving specimen dimensions, loading conditions, material properties, and their relationships with the stresses introduced at the crack. The experimental rig presented many problems. Most of them were satisfactorily overcome, and results were obtained so that correspondence between computational and experimental method was demonstrated.

The discussion presented in Chapters 6 and 7 indicates that much valuable work can be carried out based on the solutions now available so that rational inclusion of this work can be accomplished within the already broad Fracture Mechanics fields. However, there is a need to refine these solutions in order to tackle most of the work proposed as scope for future work.

In the first part of this study, an approach to a practical problem was presented. Use was made of the stress field in the neighbourhood of the crack and a correlation between this and crack behaviour was looked for. It was shown how valuable the finite element method is as a tool for Fracture Mechanics, when used in conjunction with the J contour integral and with Bueckner's method. Analysis of the stress field, prior to crack extension, was made and an attempt was made to co-relate it with future path, some conclusions were reached but experimental verification is required.

Under the second part of this work, a combined computational experimental method to obtain parameters of interest to Fracture Mechanics, was developed and proved to work properly. The method was applied to obtain a parameter defining directional stability and partial success was achieved. It is also possible, working through the first coefficients of the Williams' series, to obtain the values of K_I and K_{II} for complex loading situations, further work is required in this particular matter. There are some other aspects of Fracture Mechanics that could very well be tackled by using the present method but require further special work and/or modifications either to the method or to the computer approach or experimental rig, and because of this they are presented in Section 8.3 as scope for future work, where two parts are listed, under "1" there is a brief description of work that was originally intended to be done under the present study but time did not permit. In "2" some work is described that has become apparent in the light of the present study.

8.2 Conclusions

The computer program developed for determining the coefficients for the Williams series expansion has been fully tested, both by comparing results with those from other researchers and by experimental work done under the present study. The results are satisfactory and the scope for future work using the method developed is wide.

The main objectives of the project have been partially achieved. Correspondence between the second coefficient of the Williams series and the direction of crack propagation has been shown, it has been demonstrated as well that the geometry of the specimen has an influence on this second coefficient, i.e. a

co-relation exists between specimen dimensions, loading, and directional stability of crack propagation.

It has also been established that for all cases of the rectangular or near square DCB type geometries (except for a few with extremely small crack lengths) the application of opening load, but no transverse load, produces positive A_2 coefficient values, which imply directional instability, and experimentally the crack behaviour is like this.

There is evidence which indicates that the change in value of A_2 is of the greatest importance for directional stability, it was pointed out in Section 7.9 that most of the specimens tested experimentally had conditions which according to A_2 had certain initial level of directional instability and that on crack extension, neglecting deviations, the new directional stability level was higher (i.e. smaller A_2 values), which agrees completely with the observed experimental behaviour.

A final approach to fully substantiate the point that a negative A_2 value means directional stability was made by applying the computer program ANGCRK to two specimens that are commonly known to be directionally stable, i.e. single edge crack bend (three point crack bending, a specimen with dimension 8 x 2in was considered), and single edge crack tension (a specimen with dimensions 15 x 1.5in was considered). The values of the first three coefficients of the Williams series are shown in Tables 8.1. As expected the values of A_2 are negative (up to a $\approx$ 0.8in for the single edge crack bend and up to a $\approx$ 0.6in for the single edge crack tension specimen), which again seems to demonstrate a co-relation between A_2 and directional stability.

8.3 Scope for Future Work

(1) Two aspects originally intended to be developed within this work were not fully tested.

(i) Definition of a critical value of A_2 as a parameter defining a point of directional stability.

One of the initial objectives of this work was to obtain a qualitative relationship between the second coefficient of the Williams series and the direction of crack propagation. It has been demonstrated that whenever a sufficiently large transverse compressive load is applied to the specimen, the crack path follows the original path. However a critical point separating stable and unstable directional paths has not been identified, within the scope for future work and by refining the present method this could be done.

(ii) Other criteria for directional stability.

Some work on different criteria for directional stability of crack propagation had been planned and a computer program for evaluating these criteria was developed (Section 6.5). However, shortage of time rendered it impossible to fully test this program. Some of the results obtained were given in Section 7.7 with a very brief discussion, but it is thought that a great deal of work is necessary in relation to this program and possible co-relation with experimental implementation of it.

(iii) Although it was not fully planned, during the design stage of the experimental rig it was found that provision could be made for making photoelastic studies at the crack neighbourhood, so this facility was incorporated. Work in this field should prove to be interesting, especially under complex loading, either by introducing an angled crack (which introduces mode II loading)

or by applying a fixed relationship between opening and transverse load to study biaxial effects.

(2) In the light of the present work, some ideas for future work have evolved. They concern different topics most of which the writer knows only superficially and so only time would have permitted the development of the necessary method to obtain reliable information. However, a very brief attempt has been made to illustrate some of the points, and a description of these follows. The first point concerns:

(i) Conditions of crack arrest - Fig. 8.1 shows the specimen crack surface obtained on crack extension, and Table 8.2 gives relevant data about the conditions in which extension took place. The first point to be made here concerns the magnitude of the opening load. As could be expected it is practically the same for all the specimens. The small changes noticed can be easily explained by one of two facts:-

(a) possible differences in tip radius;

(b) as crack extension occurred during load application and there is no clear assessment of the rate with which load was applied it is quite possible that the point of maximum applied load occurs nearer or farther away in time from the last reading taken by the opening load cell.

The second point concerns crack arrest. In Figs.8.1 (a to e) the difference in length of phase II crack surfaces can be clearly seen, so the initial crack extension can be measured. Even though this was not an objective of these experiments, it turned out that crack extension in specimen no. 6/12, Fig.8.1(a), was completely phase III (no sudden crack extension), while on specimens 4/12, 2/12, 3/12 the initial length of crack extension is

progressively higher and there is a direct correspondence between these lengths and the opening load value at which crack arrest (here crack arrest is taken as the change from a high velocity spreading to a low velocity) was obtained. This measurement of the value of load for crack arrest was obtained in all cases, so it is thought that within future work, the experimental rig could be used to study conditions for crack arrest.

(ii) Studies on the fracture toughness value - The work done shows the fact, already known that the fracture toughness of the material is independent of the transverse load. It has also been shown that straight cracks can be obtained by applying transverse load, so it should be possible to obtain multiple determinations of toughness for the same specimen at different crack lengths. Work can be done on the fracture toughness (R) as defined by Gurney. It has to be kept in mind that in the present method, load is applied through displacement of the specimen arms, so by measuring both, load and displacement, it should be possible to plot the curve (x - u) as Gurney did and compare results. The evidence obtained from the different specimens suggests that the actual opening load values for increasing crack lengths are as depicted in Fig.8.2. It should be pointed out that for the opening load, because of the way in which load is applied (a displacement of the specimen's arms), there is a reduction of the load value as the crack advances. As the objective of the experiment was not to co-relate opening load with crack lengths, no complete records of crack lengths were taken, the only true load values in the curve depicted (Op.load vs a), are those shown. Anyway, on the basis of the observed behaviour

an experiment can be devised in order to obtain the true experimental curve (Op.load vs a). It has also been shown that an opening load value for a given crack length, induces a particular positive A_2 value, the curve (Op.load vs a) would be used to determine through A_2, the transverse load necessary for straight crack propagation and from it the previously mentioned multiple determination of toughness can be made.

(iii) In order to be able to apply the approach developed in this work, to more complex situations, say determination of critical parameters for complicated structures, a fully computed approach is proposed in which for application to real problems, the finite element method is combined with program ANGCRK. The approach would be to obtain the stress field developed within a cracked body, isolate a zone (with the form required for program ANGCRK, see Fig.8.3 and use the stress field to calculate normal and tangential tractions along the isolated zone boundaries. From these tractions the coefficients for the Williams series can be computed parameters of interest thus obtained.

TABLE 3.1

STRESS INTENSITY FACTORS

Crack Length mm	K psi $\sqrt{in}$ computed	$k_t \sigma \sqrt{\pi a}$	$\sigma \sqrt{\pi a}$
1.03	147	281	116
0.87	144	236	115
0.67	139	230	115
0.51	133	198	113
0.35	122	198	108
0.24	108	166	103

TABLE 3.2

CHARACTERISTICS OF THE DIFFERENT CRACK LENGTHS CONSIDERED ON THE GEAR

Crack	Initiating Point		Angle (Rad	Length (mm)
	in.x	in.y		
1	-.35095	16.41645	0.80078	1.03
2	-.35095	16.41645	0.82647	1.03
3	-.35872	16.4043	1.10256	1.03
4	-.36165	16.4043	1.10256	1.03
5	-.36480	16.40175	1.13479	1.03

TABLE 3.3

J VALUES FOR DIFFERENT CRACKS

Crack Length \ Angle Rad	0.80078	0.82747	0.97397	1.09140	1.10256	1.13479
0.11	85.797	85.7	80.798	94.9	91.101	88.639
0.22	107.88	108.00	110.54	116.4	110.68	107.20
0.35	121.95	121.00	123.34	123.04	119.89	116.27
0.52	133.00	131.37	131.11	128.07	125.48	121.13
0.68	140.35	139.28	135.86	131.74	129.27	126.00
0.83	144.00	143.00	138.11	134.04	131.58	128.40
1.03	146.11	146.97	140.7	136.05	133.94	131.26

TABLE 3.4

LOAD VALUES TO BE APPLIED AT THE NODES

ON THE CRACK SURFACES

Nodes on the Lower Face	Load(lb)	Nodes on the Upper Face	Load(lb)
328	- 36.487	5	36.487
329	- 95.352	254	95.352
330	-172.14	255	172.14
331	-205.77	256	205.77
332	-179.18	257	179.18
333	-174.36	258	174.36
334	-170.70	259	170.70
335	-147.49	260	147.49
336	-112.07	261	112.07
337	- 78.72	262	78.72
338	- 49.16	263	49.16
339	- 11.59	264	11.59
340	- 2.00	45	2.00

TABLE 3.5

VALUES OF NORMAL STRESS ALONG THE DIFFERENT LINES

SHOWN IN FIG. 3.14(lb/in^2)

Line 1		Line 2		Line 3		Line 4	
Elem.	Stress	Elem.	Stress	Elem.	Stress	Elem.	Stress
467	-14206	472	-25823	476	-6776	477	-1581
455	-10500	448	-24443	464	-10642	465	-6171
443	-16076	424	-22718	452	-7100	453	-2581
431	-12920	400	-21241	440	-11159	441	-6635
419	-17467	339	-18641	428	-7308	429	-3000
407	-15753	24	-16192	416	-11731	417	-7425
395	-17995	30	-16308	392	-11734	393	-7813
383	-16257	3	-14478	345	-8290	346	-8181
				33	-7343	347	-5000
				5	-7530	39	-6504
				74	-6617	40	-3971
				83	13645	41	-5142
				82	-7105	74	-6617
						83	13645
						82	-7105

TABLE 3.5 (cont.)

Line 5		Line 6		Line 7		Line 8	
Elem	Stress	Elem	Stress	Elem	Stress	Elem	Stress
478	2016	356	21390	467	-14206	479	-107444
466	-1330	355	1047	468	-24306	480	-15157
454	535	354	1500	469	-29988	481	-25745
442	2314	353	13281	470	-28115	482	-31076
430	2035	352	1057	471	-27068	483	-29138
418	-3356	351	2525	472	-25823	484	-27840
406	- 280	350	2642	473	-22492	485	-26192
394	-3906	349	-1124	474	-17397	486	-22645
348	-2941	40	-3971	475	-11994	487	-17329
349	-1124	41	-5142	476	- 6776	488	-11612
40	-3971	48	-2112	477	- 1581	489	- 6121
41	-5142	42	1235	478	2016	490	- 16
74	-6617	83	13645	356	21390	586	17264
83	13645	82	-7105			587	15939

TABLE 3.6

SHEAR STRESS VALUES ALONG THE DIFFERENT LINES SHOWN IN FIG.3.14(lb/in^2)

Line 1		Line 1		Line 3		Line 3		Line 5		Line 5	
Elem	Stress	Elem	Stress	Elem	Stress	Elem	Stress	Elem	Stress	Elem	Stress
467	693	479	- 951	484	1982	472	768	490	2635	478	-2828
455	414	491	- 671	496	-1217	460	-1261	502	4093	466	-6306
443	2684	503	-3401	520	58	448	- 420	514	4852	454	-3611
431	1696	515	-3764	532	2460	436	-1368	526	4654	442	-2656
419	4062	527	-5364	544	919	424	-1221	538	6838	430	-7074
407	3275	539	-5931	556	2278	412	-1231	550	6914	418	-4889
395	5227	551	-6720	374	2339	400	-1617	562	7723	406	-6735
383	4504	563	-7496	373	3834	388	- 900	574	7789	394	-5527
331	5763	382	-7608	372	2410	338	99	365	8746	348	-7746
332	5937	381	-8265	79	3604	23	- 625	363	7065	349	-4484
14	7103	330	-8083	67	1864	24	- 828	364	4471	40	-5202
15	6022	329	-7562	6	1288	3	-2490	77	5799	41	-4113
Upper Crack Side		Lower Crack Side									

TABLE 3.6 (cont.)

Line 1		Line 1		Line 3		Line 3		Line 5		Line 5	
Elem	Stress	Elem	Stress	Elem	Stress	Elem	Stress	Elem	Stress	Elem	Stress
11	4627	16	-4543	12	1596	4	-2610	71	4551	74	-5423
20	3929	25	-2627	61	1022	64	-4075	78	5902	83	-7991
28	2124	34	-1124	62	1194	73	-3581	87	2959	82	-4580
37	1993	26	-1185	80	2254			80	2254		
		35	- 615	81	- 76			88	2818		
		44	- 297								
		53	- 266								
		45	403								
		54	- 725								
		13	- 86								
		70	- 356								
Upper Crack Side		Lower Crack Side									

TABLE 3.7

ELASTIC ENERGY VALUES FOR DIFFERENT CRACK LENGTHS

Crack Length (in)	Energy Value (lb/in)
0.10503	19.088
0.087261	18.818
0.077362	17.656
0.068877	16.007
0.061894	14.090
0.055089	11.806
0.048370	9.2845
0.041476	6.7247
0.03467	4.4084
0.027951	2.5285
0.021235	1.1282
0.014165	0.32527

TABLE 5.1

COMPARISON OF VALUES OF $2\pi A_1/P^2$ AS OBTAINED BY THE METHOD DEVELOPED IN THIS WORK, AND GROSS' RESULTS

a/ℓ	A_1	$2\pi A_1/P^2$	
		Present Method	Gross
0.1	-0.09561	0.482	0.445
0.2	-0.1503	1.191	1.180
0.3	-0.2224	2.600	2.603
0.5	-0.48534	12.410	12.399
0.7	-1.2425	81.400	-

For the present method, NBPT = 182;

P = 0.345

TABLE 5.2

NBPT			
ANGCRK	198	12.0 x 1.0 x 0.3ℓ	1.604
	198	8.0 x 1.0 x 0.3ℓ	1.631
	198	6.0 x 1.0 x 0.3ℓ	1.652
	198	4.0 x 1.0 x 0.3ℓ	1.654
	198	2.2 x .0 x 0.3ℓ	1.6599
	Gross		1.5796
	Hayes		1.6628

TABLE 5.3

VALUES OF $K_I \sqrt{a/P}$ AS GIVEN BY DIFFERENT METHODS

Loading Condition	H/L	C/L	$K_I \sqrt{a/P}$			Dif_1*	Dif_2*
			Complex Method	Collocation Method	Program ANGCRK		
Shear Stress	0.444	0.347	4.737	4.599	4.590	2.8 %	2.8 %
Shear Stress	0.444	0.444	6.305	6.332	6.305	0.43%	-
Shear Stress	0.444	0.587	10.670	10.600	10.520	0.63%	1.5 %

Dif_1 is the difference between complex method and collocation method

Dif_2 is the difference between complex method and Program ANGCRK

TABLE 5.4

STRESS INTENSITY FACTORS FOR UNIFORMLY LOADED SINGLE EDGE CRACKED SPECIMENS (EFFECTIVELY INFINITE IN LENGTH)

$K_I/\sigma\sqrt{\pi a}$			
a/d	Gross et al (1964)	Hayes (1970)	Present Method
0.1	1.1864	1.1062	
0.2	1.3734	1.2961	
0.3	1.6628	1.5796	1.604
0.4	2.1066	2.0079	
0.5	2.8298	2.6798	

TABLE 6.1(a)

LOAD CALIBRATION FOR TRANSVERSE CELLS

Load (lb)	Load Cell Reading (μv)							
	20	21	22	23	24	25	26	27
20	112	122	105	114	106	103	117	108
40	220	249	218	228	221	208	235	217
60	335	375	330	347	338	315	347	327
80	448	498	444	463	457	425	462	435
100	563	622	555	577	575	537	576	547
120	677	745	668	698	696	650	690	660
140	790	874	782	814	815	763	810	775
160	909	995	893	935	935	878	930	890
180	1020	1120	1008	1051	1053	993	1050	1002
200	1135	1248	1124	1173	1175	1108	1168	1115
μv/Load	5.68	6.22	5.75	5.83	5.83	5.48	5.81	5.54

TABLE 6.1(b)

LOAD CALIBRATION FOR OPENING LOAD

Opening Load (lb)	First Assemblage			Second Assemblage		
	μv			μv		
	1 *	2 *	3 *	1 *	2 *	3 *
0	-46	40	52	0	-29	45
100	26	102	120	46	16	95
200	91	171	190	92	61	140
300	166	242	261	138	109	187
400	238	312	330	184	154	235
500	308	380	400	229	203	278
$\frac{\text{Load}}{\mu v}$	1.413	1.470	1.438	2.182	2.16	2.15
Average	1.44			2.164		

* for each particular calibration (1, 2, 3) different values of transverse load were applied in conjunction with the opening load.

TABLE 6.2

RESULTS

Case	A_1	A_2	A_3	A_4
a	-40.3226	-0.4078	-21.2494	0.320
b	-39.3164	-0.8442	-20.6243	0.415
c	-64.057	9.3999	-33.241	1.291
d	-45.460	1.7205	-23.7423	0.661
e	-40.405	-0.349	-21.148	0.517

TABLE 6.3

	Case	Load	A_1	A_2	A_3	A_4
1-198	1	6.25	- 2.52492	-15.60978	-1.37875	0.013097
2-197	2	6.25	- 2.42185	-15.65214	-1.32460	0.012180
3-196	3	6.25	- 2.47243	-15.63257	-1.35082	0.01292
4-195	4	6.25	- 2.47043	-15.63385	-1.34870	0.01401
6-193	5	25.00	- 9.83291	-12.67850	-5.19663	0.09838
9-190	6	25.00	- 0.75057	-12.69464	-5.11628	0.14883
12-187	7	25.00	-16.01811	-10.11745	-8.35084	0.31725

TABLE 6.4

COEFFICIENT VALUES FOR SPECIMEN 4 x 4

	A_1	A_2	A_3
0.1ℓ	- 0.68086	-0.012870	-00.17578
0.2	- 0.85622	0.10595	- 0.30783
0.3	- 1.04127	0.19862	- 0.41413
0.4	- 1.27620	0.28472	- 0.53307
0.5	- 1.62405	0.36351	- 0.69659
0.6	- 2.22784	0.44140	- 1.01109
0.7	- 3.44878	0.57641	- 1.87494
0.8	- 6.41977	1.13795	- 5.23577
0.9	-15.85566	5.78747	-27.06240

COEFFICIENT VALUES FOR SPECIMEN 6 x 4

	A_1	A_2	A_3
0.1ℓ	- 0.95084	0.057679	- 0.30236
0.2	- 1.24700	0.25484	- 0.51259
0.3	- 1.53919	0.44354	- 0.70979
0.4	- 1.84374	0.62667	- 0.90316
0.5	- 2.19409	0.80258	- 1.10287
0.6	- 2.71039	0.95420	- 1.33785
0.7	- 3.77872	1.07542	- 1.82175
0.8	- 6.69945	1.35074	- 3.84640
0.9	-17.86976	4.67371	-20.43743

COEFFICIENT VALUES FOR SPECIMEN 12 x 4

	A_1	A_2	A_3
0.2ℓ	- 1.80256	0.47063	- 0.80076
	- 3.0 282	1.02170	- 1.46217
0.3	- 4.04007	1.62739	- 2.10940
0.4	- 5.00505	2.21707	- 2.71333
0.5	- 6.02231	2.83414	- 3.38994
0.6	- 6.97822	3.45972	- 4.03048
0.7	- 8.03905	4.07437	- 4.70821
0.8	-10.11481	4.54930	- 5.57145
0.9	-22.82669	5.43279	-13.67574

COEFFICIENT VALUES FOR SPECIMEN 8 x 4

	A_1	A_2	A_3
0.2ℓ	- 1.31190	0.15279	- 0.46465
	- 1.80256	0.47063	- 0.80076
0.3	- 2.28660	0.78602	- 1.12740
0.4	- 2.77604	1.09078	- 1.44532
0.5	- 3.27723	1.40243	- 1.77803
0.6	- 3.83434	1.69837	- 2.10147
0.7	- 4.78749	1.93386	- 2.51018
0.8	- 7.57352	2.13052	- 3.86985
0.9	-20.14883	4.52048	-17.30471

Loading conditions for all cases

Opening load 10 lb (P_y)

Transverse load 0 (S_x)

(Tables 7.5 are a complement for covering different S_x/P_y relationships)

TABLE 7.1

COEFFICIENT VALUES

(i) $\ell = 6$ (ii) $\ell = 12$ $\sigma_x = 10$ lb/ins

$b = 1$ $b = 2$ $\sigma_y = 10$ lb/ins

a		$\ell/6$	$\ell/3$	$\ell/2$	$2\ell/3$	$5\ell/6$
A_1	i	-9.025	-29.999	-62.464	-105.885	-160.087
	ii	-3.191	-10.606	-22.084	- 37.436	- 56.599
A_2	i	2.49625	13.5517	32.78309	63.15581	109.33239
	ii	1.248	6.775	+16.391	31.577	54.666
A_3	i	-6.369	-26.097	-58.630	-107.607	-179.529
	ii	-4.503	-18.453	-41.450	. 76.089	-126.946

TABLE 7.2

NORMAL STRESS VALUES AT THE CRACK TIP FOR

$S_x = 10$ lb/in $P_y = 10$ lb

a	σ_y	σ_x	σ_y/σ_x
0.2	5.975	28	0.214
0.5	6.936	100	0.069
1.0	7.8	220	0.0355
2.0	15.94	460	0.0347
3.0	31.66	700	0.0453
4.0	78.75	940	0.0838
5.0	345	1180	0.292
5.5	1440	1300	1.109
5.8	9225	1372	6.22

TABLE 7.3

NORMAL STRESS VALUES AT THE CRACK TIP FOR

$S_x = 1392$ and $P_y = 10$

a	σ_y	σ_x	σ_y/σ_x
0.2	36.5	-1344	-0.0267
0.5	41.0	-1272	-0.0322
1.0	48.9	-1142	-0.0428
2.0	80.4	- 912	-0.0728
3.0	146.0	- 672	-0.217
4.0	336.0	- 432	-0.776
5.0	1376	- 192	-7.16
5.5	5556	- 72	-77.2
5.8	55000	0	-

TABLE 7.4

PROPORTIONAL PARTS OF A_2 VALUES FOR SPECIMENS

6 x 6, 6 x 4, 6 x 1,

LOADING CONDITIONS S_x = 10 lb/in, P_y = 10 lb/in

ℓx2b / a	Prop.	6.0 x 1.0	6.0 x 4.0	6.0 x 6.0
0.2	i	-0.51950	-0.54224	-1.08600
	ii	-0.20494	-0.34201	-0.46149
	iii	-0.31456	-0.50023	-0.62451
	iv	Stable	Stable	Stable
0.5	i	-0.0981	-0.81937	-1.0509
	ii	0.21470	-0.31912	-0.42305
	iii	-0.31280	-0.50025	-0.62785
	iv	Stable	Stable	Stable
1.0	i	1.77758	-0.71591	-0.98316
	ii	2.08718	-0.21616	-0.35840
	iii	-0.31018	-0.49975	-0.62476
	iv	Unstable	Stable	Stable
2.0	i	9.479	-0.04802	-0.73216
	ii	9.79450	0.45208	-0.10737
	iii	-0.31550	-0.50010	-0.62479
	iv	Unstable	Stable	Stable
3.0	i	23.20145	1.22262	-0.23829
	ii	23.51677	1.72227	0.38541
	iii	-0.31532	-0.49965	-0.62370
	iv	Unstable	Unstable	Stable
4.0	i	44.39859	2.79720	0.58688
	ii	44.71380	3.29766	1.21127
	iii	-0.31521	-0.50037	-0.62439
	iv	Unstable	Unstable	Unstable

i - Total value of A_2

ii - Value of A_2 proportional to P_y

iii - Value of A_2 proportional to S_x

iv - Stability condition according to sign of A_2

TABLE 7.5(a)

COEFFICIENT VALUES FOR SPECIMEN 4.0 x 4.0

WITH DIFFERENT LOADING CONDITIONS

a	S_x/P_y	0/10	0/20	10/10	10/40	10/20	20/20	30/20
0.4	A_1 A_2 A_3	- 0.680 - 0.012 - 0.175						
0.8	A_1 A_2 A_3	- 0.856 0.105 - 0.307						
1.2	A_1 A_2 A_3	- 1.041 0.198 - 0.414	-2.082 0.397 -0.828	-1.041 -0.001 -0.414	-4.165 0.594 -1.656	-2.082 0.197 -0.828	-2.082 -0.002 -0.828	-2.082 -0.202 -0.828
1.6	A_1 A_2 A_3	- 1.276 0.284 - 0.533						
2.0	A_1 A_2 A_3	- 1.624 0.363 - 0.696						
2.4	A_1 A_2 A_3	- 2.227 0.441 - 1.011						
2.8	A_1 A_2 A_3	- 3.448 0.576 - 1.874						
3.2	A_1 A_2 A_3	- 6.419 1.137 - 5.235						
3.6	A_1 A_2 A_3	-15.855 5.787 -27.062						

For a = 1.2; S_x = 10lb/in -> A_{2A} = - 0.19996 (constant for any crack length)
P_y = 10lb -> A_{20} = 0.19862
$A_2 = A_{2A} + A_{20}$

(Table 6.4 gives a complete record for S_x/P_y = 0/10 and a = 0.1ℓ to 0.9ℓ)

TABLE 7.5(b)

COEFFICIENT VALUES FOR SPECIMEN 6.0 x 4.0

WITH DIFFERENT LOADING CONDITIONS

a	S_x/P_y	0/10	0/20	10/10	10/40	10/20	20/20	30/20
0.6	A_1	- 0.950						
	A_2	0.057						
	A_3	- 0.302						
1.2	A_1	- 1.247						
	A_2	00.254						
	A_3	- 0.512						
1.8	A_1	- 1.539	-3.078	-1.539	-6.156	-3.078	-3.078	-3.078
	A_2	0.443	0.887	1.524	1.524	0.637	0.387	0.137
	A_3	- 0.709	-1.419	-0.709	-2.839	-1.419	-1.419	-1.415
2.4	A_1	- 1.843						
	A_2	0.626						
	A_3	- 0.903						
3.0	A_1	- 2.194						
	A_2	0.802						
	A_3	- 1.102						
3.6	A_1	- 2.719						
	A_2	0.954						
	A_3	- 1.337						
4.2	A_1	- 3.778						
	A_2	1.075						
	A_3	- 1.821						
4.8	A_1	- 6.699						
	A_2	1.350						
	A_3	- 3.846						
5.4	A_1	-17.869						
	A_2	4.673						
	A_3	-20.437						

For a = 1.8; $S_x = 10 \rightarrow A_{2A} = -0.24995$ (constant for any crack length)

$P_y = 10 \rightarrow A_{20} = 0.44354$

and as these loads change, there is a proportional change in A_{2A}

$$A_2 = A_{2A} + A_{20}$$

(Table 6.4 gives a complete record for $S_x/P_y = 0/10$ and $a = 0.1\ell$ to 0.9ℓ)

TABLE 7.5(c)

COEFFICIENT VALUES FOR SPECIMEN 8.0 x 4.0

WITH DIFFERENT LOADING CONDITIONS

a	S_x/P_y	0/10	0/20	10/10	10/40	10/20	20/20	30/20
0.8	A_1 A_2 A_3	- 1.311 0.152 - 0.464						
1.6	A_1 A_2 A_3	- 1.802 0.470 - 0.800						
2.4	A_1 A_2 A_3	- 2.286 0.786 - 1.127	-4.573 1.572 -2.254	-2.286 0.473 -1.127	-9.146 2.831 -4.509	-4.573 1.259 -2.255	-4.573 0.947 -2.255	-4.574 0.634 -2.255
3.2	A_1 A_2 A_3	- 2.776 1.090 - 1.445						
4.0	A_1 A_2 A_3	- 3.277 1.402 - 1.778						
4.8	A_1 A_2 A_3	- 3.834 1.698 - 2.101						
5.6	A_1 A_2 A_3	- 4.787 1.933 - 2.510						
6.4	A_1 A_2 A_3	- 7.573 2.130 - 3.869						
7.2	A_1 A_2 A_3	-20.148 4.520 -17.304						

For a = 2.4 in; S_x = 10 lb/in -> A_{2A} = - 0.31250 (constant for any crack length)

P_y = 10 lb -> A_{20} = 0.78602

$A_2 = A_{2A} + A_{20}$

(Table 6.4 gives a complete record for S_x/P_y = 0/10 and a = 0.1ℓ to 0.9ℓ)

TABLE 7.5(d)

COEFFICIENT VALUES FOR SPECIMEN 12.0 x 4.0

WITH DIFFERENT LOADING CONDITIONS

a	S_x/P_y	0/10	0/20	10/10	10/40	10/20	20/20	30/20
1.2	A_1	- 1.802						
	A_2^1	0.470						
	A_3^2	0.800						
2.4	A_1	- 3.042						
	A_2^1	1.021						
	A_3^2	- 1.462						
3.6	A_1	- 4.040	-8.081	-4.040	-16.160	-8.080	-8.080	-8.080
	A_2^1	1.626	3.254	1.211	6.094	2.839	2.423	2.008
	A_3^2	- 2.109	-4.218	-2.110	- 8.438	-4.220	-4.221	-4.222
4.8	A_1	5.005						
	A_2^1	2.217						
	A_3^2	- 2.713						
6.0	A_1	- 6.022						
	A_2^1	2.834						
	A_3^2	- 3.389						
7.2	A1	- 6.978						
	A_2	3.459						
	A_3^2	- 4.034						
8.4	A_1	- 8.039						
	A_2^1	4.074						
	A_3^2	- 4.708						
9.6	A_1	-10.114						
	A_2^1	4.549						
	A_3^2	- 5.571						
10.8	A_1	-22.826						
	A_2^1	5.432						
	A_3^2	-13.675						

For a = 3.6 in; S_x = 10 lb/in -> A_{2A} = - 0.41558 (constant for any crack length)

P_y = 10 lb -> A_{20} = 1.62639

$A_2 = A_{2A} + A_{20}$

(Table 6.4 gives a complete record for S_x/P_y = 0/10 and a = 0.1ℓ to 0.9ℓ)

TABLE 7.6

A_2 COEFFICIENT VALUES FOR DIFFERENT LOADING CONDITIONS AND DIRECTIONAL STABILITY OF PROPAGATION

Values depicted in Fig.7.4

Specimen 6 x 6

a	S_x/P_y 0/10	10/10	20/10	30/10	40/10	50/10	
0.2	-0.44885	-1.086	-1.7232	-2.3604	-2.9976	-3.6348	Stable
0.5	-0.41377	-1.0509	-1.6881	-2.2253	-2.8625	-3.4997	
1.0	-0.35840	-0.9831	-1.60785	-2.2326	-2.8573	-3.4821	
2.0	-0.10737	-0.7316	-1.3556	-1.9802	-2.6047	-3.2288	
3.0	0.38541	-0.23829	-0.8619	-1.4856	-2.1093	-2.7331	
4.0	1.2240	0.5868	-0.0370	-0.661	-1.3849	-1.9106	
5.0	7.57679	6.9539	6.3311	5.7083	5.0855	4.4627	Instable
5.5	45.86069	45.2343	44.6080	43.9817	43.3554	42.729	
5.8	150.79623	150.1412	149.4862	148.8311	148.1761	147.5211	

TABLE 7.6 (cont)

	a	S_x/P_y 0/10	10/10	20/10	30/10	40/10	50/10	
Specimen 6 x 4	1.0	-0.215	-0.715	-1.215	-1.715	-2.215	-2.714	Stable
	2.0	0.452	-0.048	-0.548	-1.048	-1.548	-2.048	
	3.0	1.722	1.22	0.7229	0.223	-0.276	-0.776	
	4.0	3.2972	2.7972	2.2969	1.796	1.296	0.7958	Unstable
	5.0	7.2769	6.7769	6.278	5.779	5.281	4.782	
	5.5	36.8899	36.3899	35.8957	35.4051	34.9072	34.4130	
	5.8	170.3402	169.8402	169.341	168.857	168.3654	167.8738	
Specimen 6 x 1	0.2	-0.20501	-0.5195	-0.8341	-1.1486	-1.4632	-1.777	Stable
	0.5	0.21462	-0.0981	-0.4109	-0.7237	-1.036	-1.349	
	1.0	2.08776	1.777	1.4674	1.1572	0.847	0.5368	
	2.0	9.7945	9.479	9.163	8.848	8.533	8.218	
	3.0	23.20145	22.890	22.580	22.2696	21.959	21.648	
	4.0	44.39859	44.083	43.769	43.455	43.139	42.8249	Unstable
	5.0	76.61821	76.307	75.996	75.686	75.375	75.064	
	5.5	89.71938	89.4063	89.0932	88.7802	88.4672	88.1541	
	5.8	189.10466	188.7919	188.4791	188.12	187.8536	187.5409	

SPECIMEN Nº 1/4 4×4

AXIAL LOAD NO AXIAL LOAD (2 LOADING CYCLES)

Table 7.7(a) Loading record

Reading Nº	UPPER FORWARD GAUGES										LOWER FORWARD GAUGES										BACKWARD GAUGES								
	0	1	2	3	4	5	6	7	8	9	10	11	12	13	14	15	16	17	18	19	20	21	22	23	24	25	26	27	
	-134	147	-30	0	3	-14	-28	43	61	–	66	-159	17	-14	1	-7	96	-83	-5	0	-4	1	-0	4	-3	-1	3	2	NO LOADING
	-129	176	-13	43	-45	35	-221	154	-4	–	108	-283	84	-95	59	-35	97	-98	160	-64									
	-129	184	-15	48	-53	42	-240	166	0	–	123	-301	101	-114	72	-44	97	-101	172	-71									
	-131	181	-12	49	-49	39	-231	154	0	–	117	-294	95	-107	64	-39	97	-99	161	-62									
	-133	178	-12	46	-46	38	-225	145	-1	–	117	-230	91	-100	59	-37	99	-99	155	-58									
	-132	176	-11	46	-45	36	-221	141	-1	–	115	-283	90	-97	56	-35	99	-98	152	-55									
	-133	176	-11	45	-43	36	-219	139	0	–	116	-281	88	-96	53	-35	98	-98	150	-53									
	-133	177	-10	45	-43	35	-217	135	-1	–	115	-280	87	-94	53	-34	98	-98	149	-52									
	-134	175	-10	44	-42	32	-215	133	-5	–	115	-277	86	-91	51	-33	98	-98	146	-50									
	-135	174	-11	43	-41	32	-212	131	0	–	114	-275	86	-90	48	-33	99	-98	144	-50									
	-135	173	-10	43	-40	33	-211	130	0	–	114	-274	84	-89	49	-33	99	-98	142	-48									
	-136	188	-16	49	-50	37	-226	142	-5	–	132	-279	100	-98	63	-35	100	-99	152	-54									OPENING LOAD
	-141	174	-15	39	-38	31	204	121	-4	–	125	-261	86	-81	47	-29	100	-97	136	-44									
	-143	168	-15	35	-34	29	-193	111	0	–	121	-252	80	-71	42	-25	101	-95	127	-38									
	-142	167	-16	33	-31	28	-186	106	0	–	117	-246	76	-66	39	-22	101	-95	124	-35									
	-144	165	-15	32	-30	28	-181	103	3	–	116	-243	72	-62	37	-22	100	-95	120	-32									
	[illegible]	159	-17	28	-24	24	-168	93	6	–	112	-233	65	-54	29	-19	100	-93	111	-26									Reading After ½ Rev.
	-151	146	-39	3	-34	-134	-159	41	-137	–	65	-218	33	-55	-123	-37	82	-98	68	-14									Read After 12 Rev.
	-143	157	-45	1	-32	-155	-38	-9	-121	–	19	-176	-2	-38	-124	-32	83	-86	-38	5									

SPECIMEN Nº 4/4 4×4

AXIAL LOAD 100 lb/in²

Table 7.7(d) Loading record

Reading Nº	UPPER FORWARD GAUGES										LOWER FORWARD GAUGES										BACKWARD GAUGES								O.L	
	0	1	2	3	4	5	6	7	8	9	10	11	12	13	14	15	16	17	18	19	20	21	22	23	24	25	26	27	32	
	112	-58	-89	24	38	222	23	-93	8	-	-89	293	250	0	106	28	-26	71	120	-32	125	125	119	120	118	100	93	78	-8	TRANS. LOAD
	-40	-53	-88	21	-63	334	8	-71	9	-	-34	256	375	-85	184	9	0	25	154	-99	161	141	120	100	95	83	88	84	34	OP. LOAD
		-60	-129	39	-110	388	-10	-31	32	-	24	232	459	-149	239	-13	1	27	170	-154	178	152	125	100	93	84	96	98	58	
	5	-54	-174	64	-149	438	-37	7	50	-	89	201	544	-216	299	-46	-1	26	194	-207	197	164	132	95	88	84	106	110	85	
	5	-52	-185	72	-160	458	-46	21	55	-	112	189	532	-239	323	-60	2	25	205	-227	204	171	134	98	87	85	111	116	96	
	46	-62	-112	21	-62	345	-14	-46	147	-	15	235	458	-148	219	0	2	27	143	-143	207	162	125	84	57	72	149	182	31	
	45	-67	-97	19	-47	341	-9	-57	151	-	4	241	445	-137	209	-5	-4	27	139	-136	210	163	122	81	53	71	150	188	31	
	52	-67	-94	21	-44	339	-8	-58	153	-	3	242	441	-134	207	-2	-5	28	139	-134	211	162	120	80	52	71	151	190	30	
	50	-67	-84	23	-26	338	-2	-67	158	-	-5	247	424	-121	198	1	-4	27	132	-120	216	160	114	70	43	65	154	202	25	
	111	-74	-87	25	68	273	26	-89	-19	-	-107	281	221	-3	109	29	-17	90	112	-22	110	119	106	114	119	101	86	50	-22	OP. LOAD REMOVED
	53	-73	-88	16	0	175	47	-101	-12	-	-142	173	120	-47	109	23	20	44	75	-58	-8	-5	0	0	-3	-2	5	2	-14	

SPECIMEN Nº 2/4 4×4

AXIAL LOAD No axial load

Table 7.7(b) Loading record

Reading Nº	UPPER FORWARD GAUGES										LOWER FORWARD GAUGES										BACKWARD GAUGES								O.L	
	0	1	2	3	4	5	6	7	8	9	10	11	12	13	14	15	16	17	18	19	20	21	22	23	24	25	26	27	32	
	29	-17	-14	7	3	10	5	-21	4	-	2	-2	15	12	22	0	-2	0	2	-1	-4	3	2	-3	-2	-1	2	3	-5	NO LOAD
	1	31	-70	26	-1	14	-42	27	-18	-	6	-47	25	-5	135	-45	21	-36	7	-4	-1	2	1	-3	-5	-2	3	3	33	
	-12	71	-80	35	-9	18	-84	38	-30	-	55	-71	25	-6	211	-73	34	-72	6	-4	-2	2	1	-3	-2	-1	3	3	54	
	-37	124	-92	57	-25	25	-151	57	-49	-	139	-102	26	-9	307	-119	63	-131	6	-7	-2	3	1	4	-2	-2	4	2	89	
	-41	134	-93	58	-26		-158	57	-48	-	150	-94	25	-7	258	-85	40		3	-4	-2									
		89	-91	28	-13	20	-113	17	-21	-	107	-44	25	-7	229	-73	33	-74	3	-4	-3	2	2	-3	-1	-2	3	3	58	
	-15	77	-93	21	-9	19	-106	12	-17	-	102	-38	24	-6	221	-69	31	-69	3	-3	-4	1	1	-3	-1	-1	3	2	56	
	-13	72	-93	19	-7	21	-102	9	-14	-	98	-34	24	-7	213	-65	29	-66	3	-2	-2	2	1	-2	-1	-2	3	3	53	
	-11	69	-93	18	-7		-98	7	-12	-	96	-31	24	-8	208	-63	28													
			-93	17	-6	17	-98	5	-10	-	94	-28	23	-8	203	-60	27	-60	5	-2	-3	1	2	-4	-2	-2	4	2	50	
			-94	14	-5	21	-95	1	-8	-	91	-25	23	-8	199	-58	25	-56	5	-4	-3	1	1	-3	-2	-2	4	1	49	
	-6	60	-94	13	-4	20	-91	3	-5	-	88	-23	23	-7	195	-55	24	-54	3	-5	-3	1	1	-3	-2	-1	4	2	48	
	-4	57	-94	12	-3	19	-90	2	-4	-	86	-21	22	-7	190	-54	22	-50	4	-2	-3	5	4	0	-2	-2	3	2	46	
		50	-93	9	-4	20	-83	-3	3	-	79	-15	22	-8	178	-49	20	-45	6	-4	-4	5	5	-1	-3	-1	4	2	42	

SPECIMEN Nº 3/4 4×4 Table 7.7(c) Loading record

AXIAL LOAD 80 lb/in²

Reading Nº	UPPER FORWARD GAUGES										LOWER FORWARD GAUGES										BACKWARD GAUGES								O.L.	
	0	1	2	3	4	5	6	7	8	9	10	11	12	13	14	15	16	17	18	19	20	21	22	23	24	25	26	27	32	
	157	-24	-76	33	0	102	21	-69	22	-	62	75	-5	-5	80	38	5	21	1	3	126	142	120	122	117	105	86	78	-14	TRANS. LOAD
	85	13	-86	34	-12	147	-56	-64	-47	-	113	-74	15	-15	213	-4	2	24	0	-3	132	139	103	98	89	83	78	92	29	OPENING LOAD
	60	24	-86	58	-21	254	-149	-67	-52	-	189	-207	19	-16	335	-77	2	25	24	-16	145	157	106	94	82	83	97	134	66	
	59	24	-88	62	-24	298	-166	-63	-53	-	202	-221	22	-20	352	-89	5	22	42	-29	149	163	105	92	77	82	95	144	88	
	50	25	-90	71	-31	299	-186	-62	-52	-	201	-180	14	-14	309	-51	2	26	22	-23	150	159	92	83	64	80	121	189	50	
	58	-17	-81	42	8	297	-124	-73	-31	-	194	-167	15	-14	259	-44	2	26	18	-22	150	160	50	81	60	80	122	193	48	
	58	-19	-81	40	11	294	-118	-74	-30	-	190	-161	16	-14	294	-40	2	26	15	-21	150	158	89	80	59	79	124	157	46	
	58	-21	-81	39	13	292	-114	-75	-28	-	188	-157	16	-14	288	-37	3	25	13	-20	150	159	87	79	58	80	125	200	45	
	59	-23	-82	38	16	292	-112	-74	-25	-	185	-153	15	-14	284	-34	2	26	12	-18	151	158	86	78	57	79	125	202	44	
	55	-25	-81	38	17	292	-109	-75	-24	-	184	-151	15	-13	282	-32	2	26	10	-18	151	157	85	78	56	80	127	205	44	
	57	-29	-81	35	23	285	-98	-75	-16	-	177	-141	16	-14	272	-26	2	26	8	-17	154	157	83	74	53	79	129	211	42	
	109	-77	-77	31	23	160	25	-67	11	-	41	52	-2	-5	76	38	6	24	1	1	109	120	103	116	109	101	86	61	-17	OP. LOAD REHOUED
	54	66	-84	130	2	130	3	-89	4	-	-40	-23	8	-4	55	28	4	24	-4	-2	-5	3	-4	1	-4	0	6	-7	-12	TRANS. LOAD REHOUED.

SPECIMEN Nº 5/4 4×4

AXIAL LOAD 100 lb/in²

Table 7.7(a) Loading record.

Reading Nº	UPPER FORWARD GAUGES										LOWER FORWARD GAUGES										BACKWARD GAUGES								O.P. Load	
	0	1	2	3	4	5	6	7	8	9	10	11	12	13	14	15	16	17	18	19	20	21	22	23	24	25	26	27	32	
	62	-64	-58	33	23	12	-83	79	198	-	-23	-33	11	81	49	32	-1	37	13	-4	69	77	68	70	70	66	77	68	-10	TRANS. LOAD
	56	-39	-83	+43	14	22	-231	233	65	-	-6	-86	23	11	177	-12	13		38	-2	78	81	59	66	61	63	118	104	31	O.P. LOAD
	42	-15	-94	69	4	27	-326	315	-5	-	25	-133	37	-11	256	-49	14	30	93	-30	93	92	58	68	56	66	135	125	61	
	40	-1	-104	100	-4	37	-382	352	-19	-	51	-160	54	-25	307	-80	16	26	137	-69	105	102	57	67	49	62	144	137	92	
	35	8	-113	122	-10		-424	366	-18	-	66	-173	62	-29	326	-88	17		147											
		8	-111	118	-9	38	-422	359	-16	-	50	-110	51	13	247	-35	13	28	98	-57	113	105	46	60	35	55	160	171	53	
	40	-37	-86	62	9	36	-340	282	19	-	43	-94	50	19	232	-27	11	28	90	-54	115	106	44	57	32	54	141	176	51	
	41	-41	-85	59	5	36	-335	276	21	-	42	-92	50	21	226	-25	11	28	87	-51	115	106	45	57	32	55	161	177	49	
	40	-42	-84	59	9	35	-330	273	24	-	41	-89	50	23	224	-22	10	28	85	-51	116	107	44	56	32	54	162	179	49	
	40	-44	-83	57	8	34	-327	270	26	-	40	-88	49	23	222	-21	10	28	84	-50	116	105	43	56	30	53	162	180	48	
	41	-45	-83	56	8	33	-325	269	25	-	39	-86	49	24	219	-20	11	28	83	-49	117	107	43	55	29	53	163	182	47	
	41	-55	-81	48	9	30	-294	243	47	-	32	-69	47	33	195	-8	+9	27	71	-41	120	107	36	49	23	49	161	168	37	
	50	-73	-70	29	22	13	-101	46	140	-	-30	-37	36	110	53	25	0	30	15	-2	44	54	64	74	70	72	78	69	-23	O.P. LOAD REMOVED
	51	-72	-79	36	20	11	-114	23	146	-	-37	-37	35	65	28	30	5	35	15	-4	2	23	0	-5	-4	-1	6	36	-21	TRANS. LOAD REMOVED

SPECIMEN Nº 6/4 4×4

AXIAL LOAD 760 lb/in²

Table 7.7(f) Loading record

Reading Nº	UPPER FORWARD GAUGES										LOWER FORWARD GAUGES										BACKWARD GAUGES								Loading Conditions and Crack Development
	0	1	2	3	4	5	6	7	8	9	10	11	12	13	14	15	16	17	18	19	20	21	22	23	24	25	26	27	
1	43	36	0	10	22	29	-3	1	15	-	70	78	16	11	15	0	6	46	26	4	55	62	56	58	56	52	59	57	Transverse load
2	-29	62	-23	20	11	19	-5	8	72	-	119	66	19	-15	49	-4	50	-34	25	-13	57	66	47	47	42	39	53	61	opening load
	-155	80	-79	63	-65	213	-24	41	37	-	332	15	152	-63	181	-86	91	-72	62	-128	86	108	56	45	35	32	69	116	— —
	-158	83	-100	70	-83	236	-37	61	32	-	380	5	240	-76	212	-107	93	-76	65	-158	94	120	55	45	35	32	75	128	— —
	-160	83	-116	83	-103	250	-52	82	32	-	427	-4	275	-91	235	-117	97	-85	64	-187	102	131	61	45	33	30	79	145	
	158	82	-120	76	-95	240	-48	82	45	-	420	5	271	-83	226	-121	91	-83	62	-180	103	132	61	43	33	28	80	148	
3	-152	83	-112	68	-86	226	-41	74	49	-	404	8	258	-72	212	-106	87	-79	62	-165	104	136	60	40	27	27	80	154	Signs Crack Propagation Initiation of new crack tip
	-145	81	-106	58	-75	219	-34	67	65	-	382	7	245	-64	198	-96	88	-76	61	-154	107	138	58	37	24	25	80	158	
	-143	82	-101	53	-71	215	-35	62	70	-	372	10	239	-60	191	-71	88	-76	58	-150	107	140	57	38	22	25	79	160	
	-140	83	-99	49	-68	210	-32	60	74	-	367	12	235	-58	187	-88	88	-74	58	-147	108	141	57	36	20	24	80	161	
	-140	83	-98	48	-65	208	-32	58	78	-	362	14	231	-56	183	-85	88	-73	56	-144	109	142	56	35	21	24	79	163	
	-138	81	-96	45	-64	204	-31	56	80	-	359	15	228	-54	180	-84	88	-74	56	-142	110	142	56	35	19	23	80	163	
	-136	82	-94	44	-62	201	-30	54	83	-	353	17	233	-52	174	-80	90	-73	54	-135	112	143	54	34	18	22	79	165	
	-135	82	-96	42	-60	199	-31	53	84	-	350	18	222	-51	172	-80	89	-73	54	-137	111	143	54	34	17	22	80	166	
	-135	82	-93	41	-60	198	-29	52	86	-	345	19	221	-51	171	-78	90	-73	53	-135	112	144	54	33	17	22	80	168	
4	-126	84	-83	28	-46	177	-24	42	102	-	317	30	193	-39	146	-62	93	-70	45	-118	117	147	49	28	8	15	77	178	Final Reading
5	-41	100	-22	20	5	70	-4	6	64	-	100	23	21	-15	58	-3	93	-44	51	-3	48	56	37	50	41	35	54	60	Opening Load Removed
6	-67	87	-30	23	-5	34	-4	4	-1	-	47	-63	16	-16	6	-14	89	-69	20	-6	1	5	-1	7	0	0	5	-2	Trans. Load Removed

SPECIMEN Nº 1/6 6×4 — Table 7.8(a) Loading record

AXIAL LOAD : NO

Reading Nº	UPPER FORWARD GAUGES										LOWER FORWARD GAUGES										BACKWARD GAUGES								
	0	1	2	3	4	5	6	7	8	9	10	11	12	13	14	15	16	17	18	19	20	21	22	23	24	25	26	27	
	-34	96	-15	-13	-27	29	-26	-3	-81	-	0	-85	5	-33	-34	-22	52	-83	-21	5	6	10	3	12	4	0	-11	5	NO LOAD
	-102	205																											
	-76	103	-20	0	-34	58	-29	1	-90	-	59	-100	135	-41	-12	-35	61	-93	-24	-43	6	5	3	11	4	-2	-12	3	
	-102	105	-32	3	-50	84	-35	-1	-109	-	134	-74	144	-62	16	-46	56	-100	-56	-121	6	9	2	11	4	-1	-10	2	
	-130	115	-56	23	-84	150	-55	16	-134	-	306	-68	284	-96	76	-121	97	-116	-92	-258	5	9	2	11	4	2	11	2	
	-132	117	-61	28	-91		-60	20	-136	-	342	-71	305	-105	88	-129	97		-81	-278	6	9	3	11					
	-137		-61	27	-90	162	-59	19	-135	-	338	-71	301	-102	87	-129	96	-121	-82	-276									
	-135	117	-55	27	-90	168	-60	20	-135	-	332	-70	302	-101	88	-128	96	-125	-81	-275									
	-141	115	-62	30	-94	167	-65	22	-137	-	354	-73	311	-106	94	-131	97	-125	-77	-285									
	-135	115	-62	30	-94	166	-63	21	737	-	353	-73	310	-106	93	-131	96	-123	-80	-283									
→	-138	120	-62	30	-93	167	-63	22	-138	-	351	-73	308	-105	92	-130	97	-122	-77	-282									
	-137	-119	-61	29	-93	165	-63	21	-158	-	349	-73	308	-105	92	-128	96	-122	-78	-279									
	-137	119	-61	29	-93	165	-62	19	-135	-	342	-72	307	-103	91	-128	97	-121	-79	-277									
	-136	119	-61	27	-91	158	-60	18	-137	-	345	-68	302	-101	87	-125	96	-118	-81	-274									
	-135	116	-60	23	-90	156	-57	16	-132	-	340	-62	278	-96	83	-124	95	-118	-82	-267									
	-134	115	-59	23	-88	155	-56	15	-131	-	338	-61	277	-95	81	-122	96	-116	-83	-268									
	-133	114	-59	22	-87	155	-55	14	-131	-	336	-59	276	-93	80	-122	95	-117	-83	-266									
	-133	114	-60	21	-87	153	-55	14	-130	-	335	-58	274	-92	80	-121	95	-116	-83	-264									
	-132	114	-59	21	-85	153	-55	14	-129	-	334	-57	274	-91	79	-121	95	-116	-83	-265									
	-132	114	-59	21	-85	152	-54	13	-129	-	333	-56	272	-91	79	-121	96	-115	-84	-264									
	-132	113	-58	20	-86	153	-54	13	-129	-	331	-57	272	-90	78	-120	95	-115	-83	-263									
	.	.	.	.	.	.	.	.	.	.	.	.	.	.	.	.	.	.	.	.									
	-120	111	-56	9	-69	150	-39	11	-83	-	295	-49	254	-65	89	-98	50	-107	-83	-219									
		110	-50	9	-70	168	-35	13	-82	-	376	-35	314	-72	133	-122	96	-118	-65	-228									LOAD II
	-137	103	-63	5	-79	160	-46	16	-68	-	331	-5	291	86	58	-104	97	-113	-72	-251									
	-130	102	-65	5	-76	156	-43	13	-67	-	378	-2	280	-62	52	-101	97	-111	-73	-243									
	-128	102	-63	5	-73	152	-40	12	-68	-	371	1	275	-60	82	-95	98	-111	-73	-237									
	-126	102	-62	3	-73	150	-40	12	-67	-	366	1	271	-60	86	-98	98	-109	-74	-235									
	-124	101	-63	2	-72	149	-39	11	-66	-	364	3	269	-59	84	-97	98	-108	-75	-232									
	-123	101	-61	2	-72	146	-38	11	-66	-	360	5	265	-58	83	-96	98	-107	-76	-230									
	-124	100	-61	0	-70	146	-37	10	-67	-	356	4	265	-58	82	-95	99	-107	-76	-228									
	-122	100	-61	0	-70	145	-36	10	-66	-	353	4	261	-57	80	-95	97	-107	-77	-227									
	-122	100	-60	1	-70	144	-37	10	-66	-	352	5	259	-57	79	-95	97	-106	-76	-226									
	-121	101	-60	-1	-70	145	-36	9	-67	-	350	6	257	-57	78	-94	98	-107	-77	-229									
	-121	99	-60	4	-67	144	-35	9	-66	-	348	6	256	-56	78	-94	98	-107	-76	-222									
	-120	99	-59	4	-69	142	-35	10	-66	-	347	7	255	-56	77	-92	97	-105	-77	-221									
	-120	100	-60	4	-68	142	-35	9	-66	-	346	7	254	-55	76	-92	96	-105	-77	-220									
	-121	100	-59	3	-68	141	-35	8	-66	-	344	8	252	-55	76	-92	98	-106	-77	-220									
	-120	100	-59	3	-67	141	-35	9	-66	-	342	7	252	-55	75	-92	98	-106	-77	-220									
	-113	99	-59	3	-68	141	-34	8	-65	-	340	8	251	-54	75	-91	50	-104	-78	-219	3	7	-1	7	-0	-2	-7	1	
	-63	103	-14	-6	-21	65	-22	3	-25	-	-7	-105	9	-28	13	-20	76	-63	-20	7	2	7	-2	7	0	-3	-8	1	

SPECIMEN Nº 2/6 dimensions 6 × 4 — Table 7.8(b) Loading record

AXIAL LOAD 160 lb/in²

Reading Nº	UPPER FORWARD GAUGES										LOWER FORWARD GAUGES										BACKWARD GAUGES								O.L.	
	0	1	2	3	4	5	6	7	8	9	10	11	12	13	14	15	16	17	18	19	20	21	22	23	24	25	26	27	32	
	-3	4	4	-3	-5	4	-3	-9	12	-	-3	-3	5	0	12	0	-1	1	-4	-3	-3	-2	2	-2	0	2	1	3	-2	NO LOAD
	77	67	0	-5	-3	27	25	15	43	-	29	24	36	27	145	73	-1	4	-3	4	121	126	118	115	119	112	118	114	-9	TRANS. LOAD
	-3	57	-2	32	-4	107	-50	55	-8	-	110	-13	120	-36	262	3	3	-3	1	-3	149	142	132	119	126	114	116	108	41	OP. LOAD
																													≈80	
	-4	4	4	15	11	137	[illegible]	101	62	-	137	-9	125	-35	233	2	-5	-5	-3	-5	109	146	106	116	125	153	191	227	29	
	-3	2	6	10	16	136	8	96	67	-	130	-3	119	-29	226	8	-5	-5	-3	-6	109	144	101	112	120	151	192	229	26	
	-5	2	6	10	17	135	10	94	68	-	128	-2	116	-28	223	10	-1	-6	-4	-7	108	143	98	110	118	149	192	231	25	
	-5	1	5	9	17	134	10	93	70	-	125	-4	115	-26	221	11	0	-5	-4	-6	108	143	58	110	116	148	192	231	25	
	-4	1	6	8	17	132	12	90	71	-	124	-3	113	-25	219	12	-1	-5	-5	-7	108	143	97	108	114	148	191	231	24	
	-5	0	6	7	17	132	11	91	71	-	124	-2	112	-24	218	13	-4	-5	-4	-7	108	142	55	107	113	148	191	232	24	
	-5	1	5	4	22	126	18	81	81	-	116	6	102	-16	207	21	-1	-5	-7	-8	107	138	87	58	102	142	192	235	20	
	-6	-1	8	4	23	125	19	74	50	-	112	9	54	-16	207	25	-3	-6	-6	-9	97	128	80	90	73	135	187	227	18	Final Reading
	-11	4	1	12	-4	48	36	67	19	-	-9	-36	14	-15	133	-19	4	3	5	-9	-1	13	10	-12	2	0	13	26	10	TRANS. LOAD REMOVED
	-6	-1	8	-3	4	28	34	-3	58	-	-10	-8	-6	-1	16	2	-7	-9	3	0	-5	-4	10	-9	0	3	13	-4	-17	

SPECIMEN Nº 3/6 6×4. Table 7.8(c) Loading record

AXIAL LOAD 160 lb/in²

Reading Nº	UPPER FORWARD GAUGES										LOWER FORWARD GAUGES										BACKWARD GAUGES								O.L.	
	0	1	2	3	4	5	6	7	8	9	10	11	12	13	14	15	16	17	18	19	20	21	22	23	24	25	26	27	32	
	16	75	35	-24	-2	-5	11	8	114	-	52	8	82	172	75	28	-11	2	-8	11	115	121	114	113	111	115	120	116	-3	TRANS. Ladd
	-35	116	-3	-2	-27	-10	-8	52	28	-	173	-30	151	85	138	-27	-5	1	5	-1	95	109	109	112	119	135	146	148	50	
	-39	115	-2	-2	-29	14	-15	63	27	-	184	-40	159	74	148	-35	-4	0	9	-2	95	111	109	115	121	137	148	151	63	
	-42	122	-2	-2	-32	14	-17	65	27	-	187	-43	159	71	151	-36	-4	1	8	-3	97	111	111	113	121	136	149	149	61	
	-51	138	-2	-2	-43	22	-35	88	24	-	211	-59	174	51	169	-48	-4	0	17	-8	97	113	112	115	124	140	150	152	76	
	-58	154	-1	-3	-51	28	-48	107	22	-	229	-71	184	34	183	-61	-2	-1	26	-14	98	115	112	115	123	140	153	154	87	
	-72	184	-1	-3	-70	47	-76	151	16	-	267	-96	207	4	216	-83	5	-10	46	-30	99	117	112	116	125	142	155	158	120	
						64	-88	169	5	-	282	-107	207	-12	224	-93	9	-19	54	-35	96	115	109	114	124	141	154	159	143	
	-98	227	-3	-4	-93	25	-120	211	3	-	328	-133	242	-45	268	-121	30	-13	76	-67	100	119	111	117	128	157	207	253	78	
	-38	111	-4	-4	-36	22	-18	148	80	-	252	-63	174	32	163	-54	-7	-11	32	-37	83	80	72	117	100	152	209	263		
	-35	84	-4	-2	-25	18	0	113	80	-	231	-46	160	50	146	-42	-14	-9	20	-31	97	75	62	106	82	141	212	279	63	
	-85	91	5	-15	-21	16	-30	65	58	-	131	-58	85	23	85	-35	-4	-10	3	-51	1	1	1	-1	2	2	2	0	54	TRANS. LOAD REMOVED
	-15	19	5	-18	-8	-4	-4	0	46	-	20	-12	23	43	19	-5	-33		-16	-12	1	2	2	1	2	2	1	0	-31	

SPECIMEN Nº 4/6 6x4

AXIAL LOAD 130 lb/in

Table 7.8(d) Loading record

Reading Nº	UPPER FORWARD GAUGES										LOWER FORWARD GAUGES										BACKWARD GAUGES								
	0	1	2	3	4	5	6	7	8	9	10	11	12	13	14	15	16	17	18	19	20	21	22	23	24	25	26	27	
	46	20	12	2	32	131	-16	27	167	-	57	89	94	-2	99	-1	0	-5	-1	49	112	123	116	113	112	111	116	107	T. LOAD
	c	5	-64	75	2	179	-37	55	121	-	143	96	214	-134	110	0	38	-77	71	-45	121	137	125	115	113	110	117	107	
	3	5	-78	86	0	190	-37	55	111	-	152	97	236	-151	113	0	39	-85	85	-62	121	140	127	116	115	112	120	112	
	2	5	-76	84	0	190	-38	59	112	-	151	98	235	-149	114	0	37	-84	84	-62	120	139	127	117	114	112	119	111	
	3	3	-79	86	1	189	-37	60	111	-	140	110	250	-149	117	0	33	-85	86	-74	122	146	130	120	115	114	124	118	
	3	3	-67	75	-4	185	-36	57	117	-	153	117	243	-135	117	1	29	-82	75	-66	121	146	128	118	113	113	123	117	I
	4	3	-88	93	-3	191	-42	72	121	-	182	120	279	-152	121	0	36	-86	91	-98	123	160	135	123	115	116	133	131	
	3	4	-78	82	0	187	-39	66	125	-	176	128	273	-144	121	0	33	-83	84	-92	124	160	135	122	114	115	131	132	
	3	3	-63	66	-4	179	-36	61	130	-	165	137	261	-126	120	1	30	-79	72	-80	125	160	134	117	108	112	131	134	
	2	3	-60	64	-3	178	-35	61	132	-	163	139	260	-124	129	2	28	-78	70	-78	125	160	135	117	108	111	131	133	II
	2	4	-56	57	-3	168	-35	62	154	-	174	160	273	-107	121	1	24	-72	63	-94	147	190	134	104	81	100	138	168	LOAD
		6	-32	40	2	163	-30	57	162	-	155	165	253	-85	115	-3	20	-65	48	-75	159	196	127	89	60	90	136	181	
	49	14	14	4	47	144	-12	34	125	-	51	76	102	23	110	3	-16	-6	-12	36	94	113	108	113	112	114	114	100	OP. LOAD REMOVED
	14	9	11	0	2	110	2	19	92	-	24	6	19	8	109	0	-4	-19	-42	0	2	-1	4	-6	4	-2	5	20	T. LOAD. REMOVED

SPECIMEN Nº 5/6 6x4 Sharp Crack

AXIAL LOAD 360 lb/in²

Table 7.8(e) Loading record

Reading Nº	UPPER FORWARD GAUGES										LOWER FORWARD GAUGES										BACKWARD GAUGES								O.L.
	0	1	2	3	4	5	6	7	8	9	10	11	12	13	14	15	16	17	18	19	20	21	22	23	24	25	26	27	32
	162	61	16	37	74	332	-43	18	78	-	34	35	142	52	81	27	65	-110	12	40	256	281	250	259	254	247	254	242	7
	129	57	15	36	59	373	-59	33	85	-	47	45	177	32	57	18	82	-152	19	14	267	287	253	256	248	238	242	221	30
	45	49	21	33	38	430	-94	43	96	-	76	48	223	11	117	15	93	-180	23	-11	268	289	253	256	249	239	241	222	46
	-64	4	-30	49	-29	571	-122	96	114	-	189	55	345	-53	184	-4	129	-268	48	-101	284	308	262	263	252	242	244	221	113
	-64	4	-28	49	-28	594	-122	94	113	-	187	55	351	-58	192	-7	131	-282	53	-116	283	310	263	265	253	244	247	225	136
	-66	2	-52	55	-47	532	-120	108	119	-	224	52	380	-73	206	-12	136	-238	58	-129	286	313	265	266	255	245	259	252	86
	-53	3	-7	23	14	520	-89	54	127	-	160	70	319	-27	157	13	111	-228	26	-77	271	308	258	256	246	247	263	256	83
	-51	4	-3	21	21	515	-86	48	127	-	153	70	313	-23	152	14	109	-226	25	-72	271	309	257	255	245	246	263	259	82
	-47	6	9	20	38	495	-79	35	124	-	138	74	298	-12	142	17	104	-214	19	-61	270	307	252	250	238	244	265	267	75
		8	14	22	44	485	-77	27	124	-	130	75	285	-7	138	19	102	-206	16	-54	272	307	250	247	235	243	266	271	70
	-47	-41	-75	-8	7	355	-119	50	84	-	60	12	140	-26	58	-8	88	-204	2	-90	4	12	3	0	-4	1	7	14	63	TRANS. LOAD REMOVED
	-5	-13	20	11	38	242	-59	-34	47	-	-6	-29	-31	-9	64	10	73	-120	-34	10	3	4	5	2	5	0	7	1	-6	OPENING LOAD REMOVED

SPECIMEN Nº 1/8 8×4

AXIAL LOAD No axial load.

Table 7.9(a) Loading record

Reading Nº	UPPER FORWARD GAUGES										LOWER FORWARD GAUGES										BACKWARD GAUGES.								O.L.	
	0	1	2	3	4	5	6	7	8	9	10	11	12	13	14	15	16	17	18	19	20	21	22	23	24	25	26	27		
	13	8	-18	18	-9	-669	-135	257	440	–	260	-155	20	-6	409	141	-127	-160	1	-2	28	38	14	36	42	-26	-25	27	8	NO LOAD
	6	5	-29	60	-36	-669	-179	299	328	–	317	-203	30	-31	446	99	-101	-172	4	1									43	
	4	0	-38	88	-43																									
	6	-1	-49	127	-52	-645	-233	342	219	–	386	-249	61	-64	503	64	-80	-195	5	-12									78	
		-5	-76	213	-74	-630	-326	387	187	–	486	-271	113	-95	582	36	-65	-224	35	-52									119	
	4	-4	-79	222	-76	-623	-338	395	183	–	501	-273	123	-102	596	30	-61	-232	44	-64									148	
		3	-90	240	-81	-621	-365	406	177	–	530	-277	136	-110	617	26	-56	-237	56	-72									157	
	-15	5	-93	249	-84	-628	-372	416	182	–	546	-277	145	-115	632	20	-53	-241	64	-83									112	
	-28	-30	-35	189	-42	-654	-304	338	342	–	371	-289	65	-56	493	64	-88	-200	8	-28	26	36	14	33	39	26	22	25	84	
	-5	1	-2	15	1	-682	-98	239	337	–	200	-176	18	-5	361	155	-120	-138	5	-4	26	34	13	33	35	-26	-23	25	-9	OP. LOAD REMOVED.

SPECIMEN Nº 3/8 8×4

AXIAL LOAD 0.0

Table 7.9(c) Loading record

Reading Nº	UPPER FORWARD GAUGES										LOWER FORWARD GAUGES										BACKWARD GAUGES.								
	0	1	2	3	4	5	6	7	8	9	10	11	12	13	14	15	16	17	18	19	20	21	22	23	24	25	26	27	
	30	49	-2	-221	1	217	-64	62	135	–	98	-71	27	47	261	71	4	-37	-172	30	-16	-17	0	-4	2	-3	6	2	No Load
	-2	16	-4	-180	-2	262	-80	61	114	–	140	-113	51	34	289	41	21	-48	-172	27	-16	-17	-2	-6	0	-1	7	1	
	-5	51	-19	-165	-36	306	-90	69	137	–	197	-147	88	31	333	21	43	-63	-151	9	-16	-17	-2	-6	1	-1	6	1	
	-36	86	-48	-156	-70	365	-109	94	149	–	270	-170	125	19	376	0	65	-81	-115	-14	-16	-17	-1	-7	1	-2	7	1	
	-32	80	-38	-159	-64	351	-105	90	154	–	260	-165	113	26	366	0	60	-76	-126	-8	-16	-17	-1	-6	1	-2	7	0	
	-27	73	-33	-161	-38	347	-102	86	159	–	252	-162	105	30	360	3	57	-73	-129	-5	-16	-16	-2	-6	1	-2	6	1	
	-24	69	-29	-166	-51	340	-98	84	166	–	242	-160	96	34	352	7	54	-69	-153	0	-17	-17	-1	-6	0	-1	6	0	
	-24	68	-29	-166	-50	339	-98	84	167	–	239	-160	92	34	350	8	53	-68	-133	0	-17	-17	-1	-7	0	-2	5	1	
	-23	67	-28	-165	-49	338	-97	87	168	–	238	-160	90	35	349	8	53	-69	-133	2	-17	-17	-2	-6	0	-2	7	0	
	-22	66	-27	-167	-48	339	-97	83	169	–	236	-157	89	35	349	10	53	-68	-133	2	-16	-18	-1	-6	0	-2	7	0	
	-21	65	-26	-168	-46	336	-96	83	172	–	231	-158	83	36	345	11	52	-67	-135	4	-17	-17	-2	-7	0	-1	6	1	
	-20	63	-26	-169	-44	333	-94	84	173	–	228	-158	78	36	344	12	51	-65	-136	4	-16	-18	-2	-6	1	-2	6	1	
	-29	47	-52	-187	-64	87	-104	58	1	–	152	-155	11	21	103	-5	32	-69	-163	-3	0	-1	-3	4	5	-12	-7	0	AFTER 48 HOURS.
	-1	17	-1	-186	-29	14	-85	36	-55	–	54	-92	-41	24	51	21	9	-49	-199	18	-1	-1	-2	4	5	-10	-6	-1	OP. LOAD. REMOVED

SPECIMEN Nº 2/8 8×4 Table 7.9(b) Loading second

AXIAL LOAD No axial load

Reading Nº	UPPER FORWARD GAUGES										LOWER FORWARD GAUGES										BACKWARD GAUGES								
	0	1	2	3	4	5	6	7	8	9	10	11	12	13	14	15	16	17	18	19	20	21	22	23	24	25	26	27	
	-6	4	0	1	-1	2	3	-1	0	-	4	0	-3	-3	-2	-2	0	0	-4	0	-5	-4	-2	-3	-4	-5	2	-3	No load
	-58	5	3	1	-2	9	-10	8	-18	-	42	-8	4	-10	10	-9	10	5	6	-9	-2	-1	1	2	0	-1	5	-2	
	-75	3	2	12	-18	24	-50	35	-17	-	84	-28	0	-24	30	-24	20	8	32	-34	-1	0	1	2	1	0	1	-3	
		3	-2	24	-29	28	-80	54	-22	-	121	-39	1	-30	49	-32	30	10	50	-51	-1	1	1	1	0	0	2	-1	
		21	-10	47	-51	25	-125	95	-31	-	182	-58	5	-35	84	-52	48	6	78	-87	0	0	2	2	0	0	1	-3	
	-71	7	-5	36	-42	15	-109	78	-13	-	156	-48	6	-27	65	-40	36	10	65	-75	0	1	2	1	1	1	1	-2	
	-71	5	-5	35	-41	18	-108	77	-11	-	152	-49	5	-26	65	-40	36	12	64	-73	0	0	1	2	0	0	1	-3	
	-76	2	-12	14	-54	-146	-107	48	-131	-	108	-52	4	-36	-54	-44	21	3	37	-64	-2	-1	-4	2	-1	3	4	-4	TIME
	-76	3	-11	14	-55	-136	-106	48	-128	-	110	-52	0	-41	-27	-57	41	1	70	-115	-1	0	-4	3	-2	2	3	-3	
	-81	0	-25	20	-65	-136	-137	101	-65	-	141	-57	-1	-37	-39	-49	28	1	51	-98	-1	0	-4	3	-1	3	4	-4	
	-81	0	-25	20	-65	-136	-137	101	-65	—	141	-57	-1	-37	-39	-49	28	4	51	-98	-1	0	-4	3	-1	3	4	-4	
	-78	-4	-25	16	-63	-134	-133	97	-61	-	132	-56	-3	-36	-41	-47	26	6	47	-95	-1	0	-4	2	-1	3	3	-3	
	-77	-5	-24	16	-62	-132	-130	94	-58	-	126	-56	-2	-36	-45	-47	26	6	46	-92	-2	0	-4	2	-2	2	4	-4	
	-76	-7	-23	15	-60	-130	-128	93	-56	-	121	-56	-3	-36	-45	-45	23	6	45	-92	-1	0	-5	3	-1	3	5	-4	
	-76	-7	-22	13	-61	-130	-126	92	-53	-	118	-56	-3	-35	-47	-45	23	5	44	-90	-2	0	-4	2	0	3	5	-3	
		-11	-20	12	-57	-117	-121	89	-42	-	104	-56	-3	-35	-48	-42	20	7	40	-85	-2	0	-3	2	-2	4	5	-4	TIME
	-72	-13	-19	11	-57	-106	-117	86	-33	-	97	-56	-4	-35	-45	-41	21	8	39	-82	-2	0	-4	3	-2	2	4	-3	
	-53	-23	-0	0	-16	-122	4	-14	-95	-	-60	-7	0	0	-110	-14	4	-2	-15	-2	-2	0	-3	2	-1	3	3	-5	OP. LOAD. REMOVED

SPECIMEN Nº 4/8 8×4

AXIAL LOAD 240 lb/in.

Table 7.9(d) Loading record

Reading Nº	UPPER FORWARD GAUGES										LOWER FORWARD GAUGES										BACKWARD GAUGES								
	0	1	2	3	4	5	6	7	8	9	10	11	12	13	14	15	16	17	18	19	20	21	22	23	24	25	26	27	
	-3	3	+1	3	1	1	-1	10	1	–	2	-4	-3	3	-1	-1	3	0	-1	-1	1	-2	0	-1	0	1	0	0	
	87	-10	26	37	16	82	-4	80	81	–	33	19	39	7	145	1	36	48	19	29	169	185	172	175	174	177	175	168	
	-30	12	-15	56	1	98	10	111	96	–	71	39	155	44	203	-17	111	22	-2	-20	206	201	185	169	173	169	165	150	
	-87	17	-30	82	-6	116	2	115	92	–	125	34	240	-93	249	-61	135	26	-21	-74	217	205	193	171	179	171	171	155	
	-119	11	-28	110	-12	126	7	126	93	–	160	31	281	-116	274	-76	155	18	-16	-103	221	214	198	174	183	181	176	161	
	-132	8	-38	134	-14	H25	-24	137	91	–	191	26	311	-135	298	-88	138	18	-6	-131	227	219	203	176	188	182	181	168	
	-125	0	-14	108	-2	123	-4	122	105	–	162	46	283	-106	264	-67	129	22	-24	-100	218	215	199	175	185	173	181	168	
	-128	-1	-6	102	0	122	0	120	107	–	154	46	276	-100	260	-63	127	24	-26	-94	218	215	197	174	184	182	181	168	
	-127	-3	-3	98	1	121	-3	118	110	–	150	49	273	-97	256	-60	127	25	-29	-90	217	213	197	176	184	188	181	169	
	-126	4	-2	94	-5	121	-2	118	110	–	148	51	270	-94	253	-59	127	26	-30	-89	215	214	197	175	185	186	181	169	
	-125	4	-1	93	-3	121	0	117	112	–	146	51	268	-92	253	-57	126	27	-30	-87	215	213	197	174	184	184	182	169	
	-125	2	0	92	-3	122	1	117	113	–	143	52	266	-91	249	-56	127	27	-31	-85	214	212	197	175	184	184	181	169	
	-124	1	1	91	-4	122	2	116	113	–	142	52	264	-90	248	-55	126	28	-32	-84	214	212	196	174	183	187	181	169	
	-123	2	2	90	-2	121	3	116	113	–	140	53	262	-88	247	-54	125	28	-33	-83	214	211	196	175	183	184	181	167	
	-121	0	5	85	-1	119	5	114	115	–	135	54	257	-84	242	-51	125	29	-34	-78	211	211	196	174	183	183	182	170	
	-120	-2	-2	84	-1	122	7	114	117	–	134	55	256	-84	238	-50	125	30	-35	-77	211	212	196	174	183	185	182	170	
	-105	-18	19	70	22	107	20	120	149	–	124	58	228	-55	243	-26	127	38	-39	-51	195	200	181	165	173	186	182	174	
	+34	-57	62	68	31	92	24	108	57	–	37	9	45	20	155	33	103	107	-5	13	156	181	172	166	167	181	185	169	(A LOAD REMOVED)
	-66	-48	13	6	32	59	48	51	61	–	45	-68	-28	1	92	-3	102	51	-36	-21	-8	3	-1	-9	-5	6	9	9	

SPECIMEN Nº 5/8 8×4

AXIAL LOAD 856 lb/in²

Table 7.9(e) Loading record

Reading Nº	UPPER FORWARD GAUGES										LOWER FORWARD GAUGES										BACKWARD GAUGES								O.L.	
	0	1	2	3	4	5	6	7	8	9	10	11	12	13	14	15	16	17	18	19	20	21	22	23	24	25	26	27	32	
		124	109	9	50	-486	-100	276	155	–	398	-112	291	427	106	27	56	-234	-62	164	622	622	619	628	623	621	619	621	-10	TRANS. LOAD
	293	121	75	36	18	-421	136	369	182	–	486	-145	335	86	171	-30	55	-268	-43	79	634	621	616	619	616	610	603	594	70	
	136	92	58	87	-46	-308	-247	515	163	–	634	-202	415		263	-126	74	-312	-13	48	669	639	630	623	625	612	607	583	121	
	51	38	58	85	-25	-83	-309	585	152	–	704	-234	458	264	316	-184	83	-334	-25	37	680	646	638	626	634	621	619	592	179	
	12	11	44	65	-24	-15	-359	649	152	–	757	-253	489	231	342	-216	84	-340	-13	43	686	652	645	632	642	627	628	601	115	
	27	8	36	19	89	-125	-263	543	192	–	678	-208	419	306	245	-135	41	-291	-58	22	631	627	626	628	635	633	644	636	108	
	73	9	57	16	122	-174	-222	478	189	–	631	-184	380	343	202	-97	36	-281	-77	23	606	610	610	619	621	625	642	642	87	
	346	51	125	-10	173	-319	-157	250	77	–	415	-143	230	426	85	17	72	-222	-80	147	606	604	603	610	606	603	601	605	-40	(A LOAD REMOVED)
	6	-14	7	1	11	-733	-45	119	203	–	162	-117	14	44	-150	-63	7	-273	-96	58	3	15	-1	5	-4	3	1	36	3	TRANS. LOAD REMOVED

SPECIMEN Nº 1/12 12×4

AXIAL LOAD No axial load

Table 7.10(a) Loading record

Reading Nº	UPPER FORWARD GAUGES										LOWER FORWARD GAUGES										BACKWARD GAUGES.								O.L.
	0	1	2	3	4	5	6	7	8	9	10	11	12	13	14	15	16	17	18	19	20	21	22	23	24	25	26	27	32
	-20	21	-10	-12	-3	-8	-3	-6	1	-	11	2	6	4	-7	-8	-2	-9	5	1									0
		2	-56	-18	-46	80	-39	42	4	-	85	100	117	-31	55	-22	-43	-97	66	-78									49
	-132	-3	-73	-20	-60	108	-53	57	0	-	144	141	145	-53	74	-32	-7	-111	83	-99									62
		-20	-129	-15	-109	185	-103	106	3	-	306	194	248	-119	147	-66	25	-146	132	-175									117
	-276	-26	-165	-3	-138	230	-124	150	17	-	399	204	307	-155	193	-89	41	-164	154	-223									150
		-25	-164	-4	-137	230	-125	149	10	-	398	205	305	-152	190	-88	39	-163	151	-221									149
	-272	-27	-159	-10	-129	194	-120	134	20	-	375	216	286	-134	165	-68	28	-139	145	-190									129
	-229	-20	-133	-37	-100	171	-108	108	24	-	348	229	267	-118	146	-53	17	-127	134	-169									115
	-227	-20	-130	-39	-100		-108	106	22	-	348	230	264	-115	140	-52													
		-19	-129	-35	-98	164	-106	106	24	-	346	230	265	-115	136	-52	-124	-127	134	-165									114

SPECIMEN Nº 2/12 12×4

AXIAL LOAD 355 lb/in²

Table 7.10(b) Loading record

Reading Nº	UPPER FORWARD GAUGES										LOWER FORWARD GAUGES										BACKWARD GAUGES.								O.L.	
	0	1	2	3	4	5	6	7	8	9	10	11	12	13	14	15	16	17	18	19	20	21	22	23	24	25	26	27	32	
	134	258	-172	-518	99	5	-55	403	783	-	537	-286	421	-264	278	26	22	1	-242	305	0	-1	2	-2	-3	-2	-3	11		NO LOAD
	221	322	-160	-480	144	-54	6	468	738	-	578	-265	423	-229	275	51	67	57	-210	298	253	248	252	254	254	254	251	251	-9	TRANS. LOAD
	150	278	199	-479	119	-5	-2	572	550	-	677	-292	451	-274	348	76	77	28	-196	281	271	254	255	249	247	240	235	223	31	
	62	253	-224	-463	99	11	-21	631	434	-	754	-258	477	-294	392	64	80	-12	-187	274	273	257	259	249	249	241	233	227	54	
	44	237	-237	-455	90	+38	-29	661	413	-	789	-301	491	-305	423	58	79	-38	-180	271	273	254	258	249	250	241	234	229	83	
		206	-251	-428	77	75	-42	737	346	-	855	-307	523	-325	469	52	60	-78	-164	265	274	256	260	249	254	246	238	236	93	
	-84	94	-262	-392	53	131	-47	843	332	-	559	-316	588	-359	551	31	35	-119	-139	230	280	260	263	252	258	251	240	241	147	
	-98	91	-267	-389	46	142	-49	868	332	-	583	-318	606	-371	577	20	31	-123	-133	217	281	261	263	252	260	251	242	242		
	-104	87	-269	-387	47	144	-49	874	341	-	588	-319	605	-368	575	22	31	-123	-132	219	280	260	263	252	259	252	242	241	83	
	208	68	-215	-404	90	109	5	819	361	-	887	-305	535	-326	467	53	32	-103	-163	257	214	229	246	257	267	276	277	309	78	
	-48	60	-204	-406	98	103	12	808	363	-	873	-303	525	-319	461	54	32	-100	-166	261	209	227	245	257	268	278	280	313	76	
	-42	64	-200	-408	101	102	17	802	365	-	865	-302	522	-317	446	56	30	-100	-167	263	205	224	243	258	267	279	282	316	74	
					102	99	19	799	367	-	861	-302	520	-315	447	56	32	-99	-167	263	203	224	241	257	268	280	282	318	73	
	179	271	-109	-439	154	-72	02	466	471	-	519	-288	407	-213	248	114	48	101	-200	298	225	235	243	252	252	253	254	262	-48	OP. LOAD REMOVED.
	75	191	-139	-455	118	-123	-56	397	461	-	481	-304	401	-245	139	53	14	-2	-215	278	12	19	5	-5	5	1	4	3	-31	T. LOAD REMOVED.

SPECIMEN Nº 3/12 12×4

AXIAL LOAD 355 lb/in²

Table 7.10(c) Loading record

Reading Nº	UPPER FORWARD GAUGES										LOWER FORWARD GAUGES										BACKWARD GAUGES								O.L	
	0	1	2	3	4	5	6	7	8	9	10	11	12	13	14	15	16	17	18	19	20	21	22	23	24	25	26	27	32	
	245	-145	-28	43	-60	45	-297	162	-40	-	-60	107	67	-105	69	114	2	0	29	4	-1	1	-1	1	1	0	0	-2	-2	
		-134	-5	179	-19	-16	-125	153	-115	-	-24	60	127	-84	174	280	60	25	19	53	245	251	250	251	249	248	249	253	1	TRANS. LOAD
		-142	-47	181	-40	-16	-136	198	-153	-	35	168	365	-127	238	228	24	-17	24	-47	239	241	240	242	239	235	237	237	37	
	119	-141	-84	169	-57	-3	-163	222	-142	-	142	230	530	-164	274	150	24	-36	46	-78	262	254	253	245	239	235	230	224	63	
	83	-140	-107	165	-68	15	-186	249	-119	-	230	262	638	-195	311	98	37	-47	29	-133	271	257	257	245	241	237	231	223	110	
	35	-152	-157	188	-98	47	-241	312	-64	-	372	306	814	-249	338	19	71	-84	10	-241	290	271	269	251	244	242	229	221	157	
	23	-159	-170	196	-104	9	-258	328	-50	-	402	316	847	-260	398	5	78	-43	10	-163	205	223	238	251	257	274	275	308	65	
		-171	-56	128	-46	-5	-170	244	-20	-	212	305	651	-193	231	69	21	-37	2	-141	190	216	231	249	258	277	283	322	56	
	270	-175	10	197	-29	-70	-145	175	-119	-	-24	46	143	-67	116	267	68	34	36	60	225	241	240	250	249	247	251	259	-22	
	172	-192	-33	42	-85	-83	-207	192	-72	-	-65	57	59	-101	-39	94	12	2	7	-24	25	25	8	10	2	0	1	45	-11	

SPECIMEN Nº 4/12 12×4

AXIAL LOAD 360 lb/in²

Table 7.10(d) Loading record

Reading Nº	UPPER FORWARD GAUGES										LOWER FORWARD GAUGES										BACKWARD GAUGES								O.L.	
	0	1	2	3	4	5	6	7	8	9	10	11	12	13	14	15	16	17	18	19	20	21	22	23	24	25	26	27	32	
	529	-122	361	-97	-66	26	193	-108	-283	--	-68	346	-166	153	-78	-365	-106	60	624	-567	249	250	249	255	250	250	252	252	1	TRANS. LOAD
	204	-133	298	-32	-82	97	144	-62	-385	--	-32	266	-90	762	-15	-384	-81	-14	635	-679	245	242	243	247	245	244	241	238	36	
	129	-127	209	-88	-88	192	153	-42	-503	-	60	305	-18	748	46	-394	-53	-101	660	-766	257	246	244	248	254	245	242	237	72	
		-152	128	-161	-109	276	169	-41	-536	-	149	372	50	711	117	-408	-37	-197	694	-836	253	247	252	250	258	246	246	244	115	
	63	154	110	-63	-118	306	165	-33	-541	-	171	382	66	702	131	-412	-37	-229	706	-855	251	247	252	251	258	248	247	245	143	
		-154	104	-112	-121	313	167	-33	-532	-	183	387	72	695	143	-412	-40	-238	709	-857	255	247	253	250	259	246	247	245	130	CRACK EXT.
		-154	142	-135	-86	256	155	-62	-527	-	137	374	20	727	83	-387	-64	-185	681	-804	224	233	246	253	267	250	263	254	89	
	101	-154	154	-142	-74	251	210	-68	-520		128	370	10	734	77	-386	-68	-179	675	-735	219	229	247	254	268	250	265	280	84	
	113	-151	162	-143	-65	244	219	-74	-517	-	116	366	-3	740	63	-380	-75	-167	668	-752	215	225	244	255	268	250	268	285	78	
	313	-134	293	-174	-26	24	185	-104	-480	--	-195	250	-148	789	-82	-332	-118	66	649	-530	230	230	244	251	258	244	252	263	-37	OFF LOAD (REMOVED)
	205	-158	228	-206	-48	-53	209	-109	-465	-	-243	257	-160	165	-100	-367	-150	-20	621	-588	32	23	4.	-1	6	4	4	41	-24	TRANS. LOAD (REMOVED)

SPECIMEN Nº 5/12 12×4

AXIAL LOAD 500 lb/in.

Table 7.10(e) Loading record

Reading Nº	UPPER FORWARD GAUGES										LOWER FORWARD GAUGES										BACKWARD GAUGES								O.L.	
	0	1	2	3	4	5	6	7	8	9	10	11	12	13	14	15	16	17	18	19	20	21	22	23	24	25	26	27	32	
	-3	4	7	-4	3	240	-1	3	1	–	1	-5	4	0	-3	4	-5	191	-3	0	-9	-10	-6	-8	-12	-3	6	0	2	NO LOAD
	-95	-2	-28	19	-3	258	7	61	19	–	124	42	221	53	63	-21	5	63	-39	-47	375	367	369	373	374	370	365	363	55	
	-158	-1	-58	37	-9	279	3	64	50	–	208	99	340	94	105	-50	-9	27	-5	-125	385	371	370	372	373	371	367	362	108	
	-170	-2	-66	42	-12	292	2	64	62	–	236	110	374	89	124	-59	-12	12	4	-154	383	373	372	375	373	372	368	362	150	
	-191	-5	-77	48	-15	–	-1	67	73	–	254	116	397	84	132	-64	-14	–	5	-165	384	373	371	373	370	369	367	365		
	–	-7	-57	34	-7	271	3	63	82	–	200	112	338	108	87	-42	-20	36	-9	-116	383	370	369	370	371	371	369	365	86	
	-151	-17	-35	-22	-4	268	3	63	90	–	175	105	316	110	76	-38	-20	40	-14	-105	380	370	371	369	371	370	369	365	80	
	-143	-20	-26	16	-3	266	2	65	57	–	162	97	298	111	66	-35	-19	45	-17	-94									73	
	-16	-3	28	-4	4	243	-21	0	8		-49	-54	71	74	-12	4	5	182	22	32	-10	-10	-7	-8	-13	-4	6	0	-13	O.P. LOAD REMOVED

SPECIMEN Nº 6/12 12×4

AXIAL LOAD 710 lb/in²

Table 7.10(f) Loading record

Reading Nº	UPPER FORWARD GAUGES										LOWER FORWARD GAUGES										BACKWARD GAUGES								O.L.	
	0	1	2	3	4	5	6	7	8	9	10	11	12	13	14	15	16	17	18	19	20	21	22	23	24	25	26	27	32	
	1	337	217	-375	15	431	65	105	354	–	256	-21	493	468	417	-176	25	445	-1	347	502	500	502	502	502	508	500	512	7	TRANS. LOAD
	-27	329	209	-376	12	450	67	123	367	–	277	-22	510	460	432	-187	30	424	-5	315	501	498	499	499	498	505	494	504	71	O.P. LOAD
	-131	320	205	-378	-15	490	60	163	378	–	330	-26	567	449	481	-209	36	371	-18	237	494	495	495	496	497	502	492	504	90	
	-212	303	185	-371	-35	531	50	206	394	–	376	-35	616	435	522	-230	43	322	-34	172	492	492	493	494	493	499	491	499	135	
		303	186	-371	-35	534	51	205	393	–	376	-36	615	434	518	-229	43	319	-34	174	491	491	493	494	493	498	491	500	151	
	-218	301	183	-369	-38	539	49	210	397	–	381	-35	620	432	527	-232	44	315	-35	166	493	492	493	495	494	498	491	499	144	
	-222	300	182	-368	-39	536	49	211	396	–	381	-37	619	432	527	-231	43	318	-35	168	493	492	494	495	492	497	491	500	131	
	-193	300	158	-378	-24	521	61	197	399	–	361	-30	601	442	506	-220	36	332	-35	184	486	488	490	491	493	499	495	506	90	
		444	338	-724	303	3532	388	654	1844	–	1016	217	1250	1038	3730	-76	71	601	50	357	808	844	843	857	865	908	842	942	105	NEXT MORNING
	-129	524	390	-714	392	3433	386	538	1848	–	822	215	1052	1063	3511	21	43	793	135	655	830	856	855	856	866	915	852	937		O.P. LOAD REMOVED
	-576	321	403	-784	314	3196	283	500	1711	–	742	164	646	886	3326	-34	-22	564	-35	306	32	39	18	15	11	42	26	113	-28	TRANS. LOAD REMOVED

Specimen No 15 12×4

AXIAL LOAD 40 lb/in = 350 lb/in²

Table 7.11(a) Loading record

	UPPER FORWARD GAUGES										LOWER FORWARD GAUGES										BACKWARD GAUGES								Loading conditions and crack Development
1	0	1	2	3	4	5	6	7	8	9	10	11	12	13	14	15	16	17	18	19	20	21	22	23	24	25	26	27	
2	-3	-1	5	1	0	-3	3	-4	0	-	-3	-1	1	-3	-3	-5	-2	-2	0	0	1	-1	0	-1	1	0	0	0	NO LOAD
3	51	45	17	-1	65	124	51	23	16	-	58	-12	59	51	70	37	60	93	-28	35	232	251	233	233	232	217	234	221	AXIAL LOAD
4	40	37	4	0	57	137	48	29	33	-	78	-13	64	46	79	30	59	72	-14	20	228	248	232	232	231	218	235	225	1ST LOAD
	38	36	-2	-4	55	142	44	32	36	-	86	-13	68	44	84	29	60	66	-9	13	228	250	233	234	231	219	235	225	2ND LOAD
	36	35	-4	-4	52	144	42	33	37	-	90	-14	71	43	87	27	61	62	-5	9	227	250	233	234	231	219	236	225	3RD LOAD
	32	34	-4	2	51	146	39	35	39	-	95	-13	75	42	90	27	61	57	-2	6	228	251	234	233	231	219	236	225	4TH LOAD — OPENING
	21	34	-13	4	46	153	33	38	44	-	96	-14	75	42	91	26	61	44	-3	-3	223	251	234	235	231	219	238	226	5TH LOAD
	12	35	-19	3	43	158	29	42	47	-	123	-15	91	39	108	21	65	36	4	-8	229	251	234	235	232	220	238	227	6TH LOAD
	3	34	-28	7	38	166	20	45	51	-	138	-16	101	38	120	17	66	22	8	-19	230	251	235	236	231	220	239	230	7TH LOAD
5						170		46	52	-	138	-17	100	33	118	16	67	18	9	-18	231	250	235	236	231	220	238	228	8TH LOAD
	-4	34	-35	11	35	171	16	51	57	-	151	-16	108	36	127	14	67	14	11	-26	232	252	236	237	232	220	239	230	—
	-5	35	-32	10	35	170	16	48	55	-	149	-17	107	36	124	15	67	16	11	-25	231	251	235	238	232	221	240	230	
	-3	35	-32	9	36	169	17	48	55	-	147	-17	106	36	124	15	67	16	10	-23	231	251	235	237	231	221	238	230	
	-2	35	-30	9	37	168	17	48	54	-	146	-16	105	36	124	14	67	18	10	-21	230	251	236	237	232	220	240	230	
	1	35	-28	8	38	165	19	47	53	-	143	-16	102	38	121	17	65	21	9	-19	230	251	235	237	232	221	239	231	
	-3	34	-25	6	41	165	22	45	53	-	138	-15	100	39	117	18	64	23	7	-17	228	250	234	237	232	222	240	252	
	0	34	-23	5	42	163	23	43	52	-	137	-15	98	40	116	19	64	24	7	-15	227	251	235	236	232	222	240	234	
	1	34	-22	4	43	162	24	42	53	-	134	-15	97	40	114	19	64	27	6	-14	227	249	234	236	232	223	240	233	
	3	33	-20	3	42	161	25	42	53	-	133	-15	97	39	112	20	61	27	6	-13	227	249	233	237	231	223	240	233	
	3	33	-20	2	43	160	25	40	52	-	131	-15	95	40	111	21	62	27	6	-12	226	249	234	237	231	222	241	234	
	4	32	-19	2	45	159	26	40	52	-	130	-14	95	40	110	21	62	29	5	-11	227	249	234	236	232	222	240	235	
	5	33	-17	2	44	159	27	39	52	-	128	-14	94	41	110	21	62	29	5	-10	226	248	234	236	232	222	240	235	
	5	33	-17	2	45	158	27	38	51	-	128	-15	93	42	109	22	61	30	5	-10	225	249	233	236	231	222	240	234	
	5	32	-15	1	45	156	28	39	51	-	126	-13	94	42	107	21	62	31	4	-10	226	248	233	236	232	222	241	236	
	6	32	-15	0	46	157	27	38	50	-	127	-14	93	42	108	21	61	31	3	-9	225	247	233	237	231	223	241	236	
	7	32	-15	1	46	157	28	38	51	-	124	-14	93	42	106	22	60	32	4	-9	225	248	234	236	230	222	241	236	
	7	32	-15	0	46	157	29	38	52	-	125	-14	91	41	106	22	61	33	4	-7	225	249	234	237	230	223	241	235	
	7	32	-14	5	46	156	29	37	51	-	124	-14	91	42	107	22	60	33	3	-7	225	247	233	236	231	223	241	236	
	7	33	-14	+5	48	156	29	37	51	-	122	-14	91	41	105	23	61	33	3	-8	225	248	233	235	231	222	242	236	
	8	32	-12	5	46	155	30	37	51	-	122	-14	90	43	106	23	60	34	3	-7	224	247	233	237	231	222	242	236	
	9	33	-13	4	47	155	30	37	50	-	121	-14	90	42	104	23	60	34	3	-6	224	248	232	236	231	222	241	236	

Initiation of crack extension

When load was long applied the crack started to extend and continuous readings were taken while extension was taking place

Specimen No 15 12×4 Table 7.11(a) Loading record

Axial load 40 kN/mm² (CONT).

6	18	30	-2	-1	52	142	36	31	46	-	105	-13	81	45	89	28	57	45	-1	0	215	241	229	234	227	221	240	234	
7	1	28	-10	-4	52	145	36	32	60	-	127	-6	90	53	95	28	51	31	2	-8	204	235	226	236	229	228	249	253	LOAD
	2	28	-7	-6	54	144	38	30	60	-	124	-5	85	53	93	29	50	33	2	-5	204	234	226	236	229	228	249	250	
	4	28	-6	-7	53	143	38	29	59	-	122	-6	88	53	92	30	50	33	0	-4	204	234	226	235	229	228	248	251	
	5	28	-6	-5	54	143	39	29	58	-	121	-5	87	53	93	29	49	30	2	-10	201	232	226	235	228	228	248	252	
	1	26	-11	-7	53	145	39	30	62	-	128	-5	89	54	92	30	49	32	2	-8	202	234	226	235	229	228	249	252	
	2	26	-7	-8	54	144	39	30	61	-	125	-5	88	54	92	31	49	33	0	-5	202	234	225	235	229	227	248	252	
	0	26	-14	-7	51	142	38	35	74	-	149	-1	100	59	99	28	45	24	6	-20	154	229	224	234	229	231	254	260	
	-2	24	-11	-12	55	138	43	28	69	-	135	-4	91	62	88	34	42	31	0	-11	195	230	224	236	229	230	251	257	
	1	25	-6	-13	56	136	44	26	55	-	129	-3	88	62	85	34	41	34	-1	-5	196	230	224	234	229	230	250	256	
	4	25	-4	-14	56	135	45	25	64	-	125	-3	87	63	82	35	40	35	-1	-4	197	232	225	234	229	229	251	256	
	6	25	-3	-16	57	134	47	23	62	-	123	-4	86	62	83	35	41	38	-1	-3	197	231	225	235	230	229	252	256	
	8	25	-2	-14	57	132	47	22	62	-	121	-3	84	63	81	35	41	38	-2	-1	197	232	225	234	228	230	251	256	
	7	26	0	-15	58	132	47	22	61	-	119	-4	84	62	81	35	40		-3	-1	198	231	224	234	228	229			
	7	25	-5	-15	58	132	47	22	60	-	118	-4	83	63	78	34	40	41	-3	-4	197	232	224	234	229	229	250	254	
8	20	25	4	-17	61	121	50	16	53	-	101	-5	73	64	69	40	39	51	-2	6	199	231	222	230	228	224	246	250	FINAL REDUCTA
9	58	47	37	-15	81	101	57	9	8	-	24	-12	41	57	41	50	50	102	-32	51	204	228	216	221	222	210	229	225	OPENING LOAD RECORD
10	30	14	-12	-45	9	-18	-21	-34	0	-	-57	-4	3	10	-3	40	-7	32	-12	24	4	19	0	3	1	0	3	11	AXIAL LOAD REMOVED

Further load while crack was growing

Crack started to grow when load was applied. Continuous readings.

SPECIMEN Nº 14 12×4

AXIAL LOAD 320 lb/in²

Table 7.11(6) LOADING RECORD

Reading Nº	UPPER FORWARD GAUGES										LOWER FORWARD GAUGES										BACK(RAD) GAUGES								Loading Conditions and crack Development
	0	1	2	3	4	5	6	7	8	9	10	11	12	13	14	15	16	17	18	19	20	21	22	23	24	25	26	27	
1	-6	1	4	1	5	-	4	1	-2	-	-5	-1	-1	-2	+4	-1	+4	11	-2	-5	-1	0	0	-1	-2	1	1	0	NO LOAD
2	-2	26	39	4	57	143	6	-17	44	-	42	-3	49	40	93	71	18	25	26	41	226	249	230	233	234	220	231	218	AXIAL LOAD
3	-30	9	23	7	45	170	-4	-12	58	-	80	-1	74	32	115	54	24	8	7	12	221	247	228	233	237	224	232	222	LOAD
	-34	+7	20	8	45	175	-6	-10	58	-	86	-1	77	30	119	52	25	6	6	8	220	246	229	234	237	225	231	223	LOAD
4	-36	4	15	7	42	181	-10	-9	61	-	94	-1	83	28	124	49	26	2	4	1	220	247	229	235	238	226	231	222	Readings while equalizing cracks sides and centre
	-41	1	8	6	38	189	-14	-6	63	-	102	-1	88	26	128	46	28	-2	2	0	220	246	229	235	239	227	231	223	
	-39	1	9	5	41	189	-13	-8	61	-	102	-1	87	26	128	46	28	-2	1	0	219	246	229	235	237	226	231	222	
	-38	1	9	5	40	188	-13	-8	60	-	102	-1	88	27	128	46	28	-2	2	-5	219	245	227	235	237	226	230	222	
	-38	1	9	4	41	186	-13	-8	61	-	102	-1	88	26	128	45	28	-2	2	-1	218	246	228	234	238	227	231	222	
5	-43	0	5	4	38	196	-16	-5	64	-	113	-1	95	23	134	42	29	1	0	-8	219	246	229	236	239	229	230	224	LOAD
6			6	4	39	196	-17	-5	63	-	111	0	95	24	133	43	29	0	0	-7	218	245	229	235	239	228	231	224	Crack Extension
	-42	5	4	3	39	195	-15	-5	64	-	112	0	94	23	133	42	30	1	-1	-7	218	245	229	235	239	229	231	223	
	-41	0	5	4	39	196	-16	-6	63	-	111	-1	94	24	133	39	29	-5	0	-8	219	244	229	235	238	229	231	224	
	-42	0	5	3	39	196	-16	-6	64	-	111	0	94	23	132	45	29	-4	0	-7	219	246	228	235	239	226	230	223	
	-43	0	5	4	38	195	-17	-7	63	-	111	0	94	26	132	43	29	-5	0	-7	219	245	229	235	239	228	231	223	
	-42	-1	6	4	39	196	-17	-6	64	-	111	0	93	23	133	44	29	-5	0	-7	218	246	229	235	239	229	230	224	
	-42	-1	5	3	40	195	-15	-6	63	-	111	-1	94	25	133	42	29	-5	0	-7	217	245	229	235	239	228	231	224	
	-43	-1	6	3	38	195	-16	-7	63	-	111	0	93	24	132	43	30	-5	0	-6	218	245	228	234	239	229	230	225	
	-41	-1	5	4	39	196	-16	-6	62	-	110	0	94	24	132	44	29	-5	0	-6	218	245	230	236	239	229	230	224	
7						200	-17	-6	63	-	111	0	93	25	132	43	29	-2	0	-8	218	245	228	235	239	230	231	223	LOAD
8	-46	4	4	3	37	200	-19	-3	66	-	117	-1	98	22	135	40	30	-2	-1	-12	216	244	229	236	239	230	230	225	Next Max load was applied the crack got a flat end
	-45	4	3	3	36	200	-18	-5	65	-	117	0	97	22	134	40	29	-1	-2	-12	216	244	229	236	240	230	230	224	
	-44	-1	3	3	37	208	-19	-4	66	-	122	0	103	19	144	36	31	-6	-4	-21	218	245	229	235	242	233	230	226	
	-49	2	-1	0	34	204	-23	-1	68	-	125	1	102	21	137	39	30	-1	-4	-15	214	241	227	237	243	235	231	229	
									Crack relaxation without Readings																				
9	-32	-2	11	-2	52	193	-7	-17	70	-	95	1	83	32	121	50	24	2	-5	-4	207	237	225	236	247	240	233	235	Crack started to extend
	-32	-2	11	-2	52	193	-7	-17	70	-	95	1	83	32	121	50	24	2	-5	-4	207	237	225	236	246	241	232	235	
10	-32	-3	11	-3	54	192	-6	-18	70	-	94	1	82	32	121	52	25	2	1	3	206	237	225	238	248	242	234	235	
11	-27	-9	24	-2	-67	168	11	-21	76	-	68	0	61	36	96	56	24	15	0	23	152	227	232	236	251	246	224	230	
12	-44	-8	10	-6	43	-62	9	-40	-91	-	21	-4	37	19	-87	30	20	13	-7	27	165	205	212	228	242	205	184	209	AFTER 20 Rdgs.
13	2	25	61	-1	55	-42	31	-40	-100	-	-18	1	1	26	-82	57	15	42	7	65	167	204	209	217	225	187	176	177	opening load removed
14	-20	4	0	-4	19	-105	30	-26	-135	-	-24	13	-35	-21	-145	+5	-2	25	-30	31	3	5	0	5	5	-1	-3	-5	AXIAL LOAD Removed.

SPECIMEN № 17 12 × 4 — Table 7.11(c) LOADING RECORD

Axial Load 320 lb/in² — Blunt Crack — Sudden Crack extension.

Reading №	UPPER FORWARD GAUGES										LOWER FORWARD GAUGES										BACKWARD GAUGES								Loading Conditions and Crack Development
	0	1	2	3	4	5	6	7	8	9	10	11	12	13	14	15	16	17	18	19	20	21	22	23	24	25	26	27	
1	-1	50	74	10	72	111	-1	-19	-44	-	90	34	22	-20	52	18	53	51	-11	32	229	245	227	233	231	217	230	221	TRANS load
2	-9	33	11	25	56	178	-28	-29	-1	-	170	57	39	-51	95	3	54	0	17	1	218	241	226	236	234	224	237	234	OPENING LOAD
	-15	34	-4	28	51	195	-32	-22	9	-	192	60	42	-60	106	-2	57	-8	27	-6	217	240	227	236	235	225	240	238	
	-19	33	-6	26	48	204	-36	-17	14	-	207	61	43	-67	113	0	57	-18	34	-11	215	240	227	237	236	225	242	241	
	-23	34	-14	25	25	212	-39	-14	17	-	218	62	43	-73	119	-2	59	-24	39	-16	215	240	227	237	236	226	242	242	
	-27	36	-24	23	41	221	-41	-8	21	-	233	62	43	-80	127	-5	60	-35	46	-22	212	239	226	236	236	227	241	244	
	-28	36	-26	22	41	222	-44	-6	21	-	236	62	42	-81	130	-5	60	-35	47	-22	211	239	227	237	236	226	243	245	
	-29	37	-25	22	42	225	-43	-7	20	-	235	62	42	-83	130	-5	60	-39	47	-22	213	239	227	237	236	228	242	243	
	-33	39	-35	18	36	242	-46	-1	25	-	252	61	41	-90	141	-10	64	-56	58	-37	214	240	228	238	237	227	245	249	
	-46	40	-44	19	20	249	-53	8	38	-	285	63	43	-89	160	-17	66	-61	63	-42	215	240	228	239	238	231	245	249	
		41	-46	21	11	260	-59	18	45	-	307	64	43	-104	173	-25	74	-63	70	-52	215	240	230	239	239	229	247	250	
	-61	41	-47	22	6	267	-59	23	47	-	318	65	44	-105	180	-28	77	-66	70	-58	215	242	230	239	240	220	247	253	
		41	-48	20	0	274	-63	30	52	-	330	64	45	-106	187	-32	82	-67	72	-66	216	241	230	240	240	230	248	253	
	-80	43	-49	20	-1	284	-67	39	58	-	348	65	46	-109	200	-36	90	-69	76	-75	218	242	231	237	240	231	249	253	
	-90	44	-50	19	-9	295	-72	49	64	-	366	66	44	-113	211	-41	97	-70	78	-85	219	243	231	239	241	232	250	254	
		44	-50	19	-15	303	-76	57	68	-	381	65	45	-115	220	-45	104	-70	79	-93	221	244	232	241	242	233	250	256	Sudden Crack Extension
3		44	-50	20	-14	303	-76	56	68	-	381	66	-4	-81	83	16	61	30	26	1	181	218	219	235	237	233	256	271	
4	-4	14	-9	2	87	174	0	-8	36	-	213	85	-1	-78	79	18	64	34	23	1	184	219	219	235	237	232	256	272	Further Slow Crack Ext.
	2	16	0	-2	87	162	3	-8	28	-	202	84	-2	-74	75	20	65	41	19	5	186	221	220	234	236	232	255	270	
	3	17	1	-2	86	158	4	-8	27	-	197	84	-3	-73	73	20	65	44	17	7	186	222	220	235	235	231	254	270	
	5	18	-3	-3	87	154	5	-9	24	-	192	83	-4	-73	70	21	65	47	15	9	188	223	220	235	234	230	253	267	
5	11	55	85	-7	79	62	-19	-35	-42	-	54	26	-9	-31	22	26	100	127	-20	53	221	234	221	229	225	214	229	220	Opening load Removed
6	13	15	0	-14	20	-16	-11	-19	-17	-	-19	-15	-16	-6	-19	24	59	79	-4	26	10	7	2	-1	-2	1	9	24	Axial load Removed

TABLE 7.12(a)

RELEVANT DATA ON THE CRACK PROPAGATION OF SPECIMENS 4.0 x 4.0

a_i = initial crack length = 1.0 in a_f = final crack length to calculate A_2 values = a_i +(length under phase II)

4 x 4	Crack Tip	Crack Length under Phase I (mm)	α_a (deg)	α_F (deg)	P_r coord. (mm)	Crack Length Under		Opening Load (lb)	Trans-verse Load (lb/in^2)	Sc (lb)	$\delta\ell$ lb	A_2 Initial Load Final
						Phase II (mm)	Phase III (mm)					
1/4	Sharp	≈ 1	8 Increases	13.6	y = 7 x = 23	There is not a clear difference		-	NO			
2/4	Rounded	≈ ½	5.8 Increases	11.5	y = 5.5 x = 27	7	21	B 194 A 126	NO	205	68	
3/4	Rounded	1	Decreases 26	12.5	y = 7.1 x = 21.8	11	12	B 192 A 115	80	222	77	1.32 1.06
4/4	Rounded	½	16.5 Decreases	8	y = 7 x = 33.5	20	14	B 209 A 68	100	227	141	1.75 0.22
5/4	Rounded	1	18 Decreases	11.5	y = 6.7 x = 35.6	10	16	B 201 A 115	100	222	86	0.61 0.51
6/4	Sharp	1	9 Decreases	3	y = 1.3 x = 24	NO	24	-	160	-	-	

TABLE 7.13(a)

RELEVANT DATA ON THE CRACK PROPAGATION OF SPECIMENS 6.0 x 4.0

6 x 4	Crack Tip	Crack Length under Phase I (mm)	α_a (deg)	α_F (deg)	P_r Coord. (mm)	Crack Length Unde		Opening Load (lb)	Trans-verse Load (lb/in^2)	Sc (lb)	Load (lb)	A_2 Dimension-less Initial/ Final
						Phase II (mm)	Phase III (mm)					
1/6	Sharp	No	19 Increases	30	y = 14.5 x = 31.5	No		-	No	-	-	
2/6	Slight ly Rounded	1	23 Increases	4	y = 11.2 x = 51	23	28	-	160	-	-	
3/6		No	22 Increases	3	y = 11.0 x = 51	36	17	B 312 A 170	160	318	142	7.58 9.6
4/6	Rounded	1	14 Decreases	5	y = 4.5 x = 38	14	17	-	160	-	-	
5/6	Sharp	No	4 Decreases	<1	y = 1 x = 52	No	52	B 296 A 187	360	296	109	2.58 1.6

a_i = initial crack length = 1.574 in
a_f = final crack length to calculate A_2 values = a_i + (length under phase II)

TABLE 7.14 (a)

RELEVANT DATA ON THE CRACK PROPAGATION OF SPECIMENS 8.0 x 4.0

8 x 4	Crack Tip	Crack Length under Phase I (mm)	α_a (deg)	α_F (deg)	P_r Coord. (mm)	Crack Length Under		Opening Load (lb)	Transverse Load (lb/in^2)	Sc (lb)	δ Load (lb)	A_2 Dimensionless Initial/ Final
						Phase II (mm)	Phase III (mm)					
1/8	Sharp	1	21 Increases	46	y = 14.5 x = 20.0	9	15	I 17 B 342 A 244	No	325	98	22,03
2/8	Sharp	< ½	14 Increases	33	y = 6.5 x = 13	NO	14	-	NO	-	-	
3/8	Sharp	< ½	14 Increases	29	y = 11.7 x = 26.5	NO	29	-	NO	-	-	
4/8	Blunt	½	13.5 Decreases	6	y = 3.8 x = 20	.5	30		240			
5/8	Sharp	< ½	7 Decreases	1	y = 2.5 x = 36	19	15	I - 22 B 390 A 250	850	- 412	- 140	1.23 1.95

a_i = initial crack length = 2.125in
a_f = final crack length to calculate A_2 values = a_i + (length under phase II)

TABLE 7. 15 (a)

RELEVANT DATA ON THE CRACK PROPAGATION OF SPECIMENS 12 x 4

12 x 4	Crack Tip	Crack Length under Phase I (mm)	α_a (deg)	α_F (deg)	P_r Coord (mm)	Crack Length Under		Opening Load (lb)	Transverse Load (lb in^2)	Sc (lb)	S Load (lb) Final Load	A_2 Dimensionless Initial/ Final
						Phase II (mm)	Phase III (mm)					
1/12	Blunt	3	10 Increases	21	y = 6.3 x = 26.5	27	35 15	B 327 A 281	No	327	46	49.6 54.6
2/12	Sharp	No	18 Decreases	13	y = 7.5 x = 26.5	15	13	I 20 B 320 A 181	360	340	140 (200)	36.55 20.95
3/12	Blunt	1	17 Decreases	9.5	y = 6.8 x = 26.5	29	9	I 2.18 B 342 A 142	360	340	201 (110)	36.55 14.05
4/12	Blunt Slight Sharpness	1	13 Decreases	11	y = 5.7 x = 26.5	6	19	I 2.18 B 312 A 194	360	310	118 (152)	31.95 17.80
5/12	Blunt	-	6.5 Increases	23	y = 6.0 x = 26.5	No	30	B 327 I 4.5	No	-	-	
6/12	Blunt Slight Sharpness	1	12 Decreases	4.5	y = 3.0 x = 26.5	No	26	I 2.18 B 329 A 314	700	327	15	20.4

a_i = initial crack length 3.35 in

a_f = final crack length to calculate A_2 values = a_i + (length under phase II)

TABLE 7.12(b)

	Case 1	Case 2	Case 3	Case 4	Case 5	Case 6
Load (lb)	-	67.5	76.3	142	85	-
*Length(mm)	-	15.26	24	44	22	-
Transverse load	NO	NO	80	100	100	160
$\Delta\alpha$	5.6 Increases	5.7 Increases	13.5 Decreases	8.5 Decreases	6.5 Decreases	6 Decreases

TABLE 7.13 (b)

	Case 1	Case 2	Case 3	Case 4	Case 5
$\Delta\alpha$	+ 11	- 19	- 19	- 9	- 5
α	Increases	Decreases	Decreases	Decreases	Decreases

TABLE 7.14 (b)

	Case 1	Case 2	Case 3	Case 4	Case 5
load	98	-	-	140	-
length under phase II	20	-	-	41	-
	+ 25	+ 19	+ 15	- 7.5	- 6
α	Increases	Increases	Increases	Decreases	Decreases

TABLE 7.15 (b)

	Case 1	Case 2	Case 3	Case 4	Case 5
Load (lb)	46	140	201	118	15
Length under Phase II mm	27	15	29	6	-
α	+ 11	- 5	-7.5	- 2	-7.5
	Increases	Decreases	Decreases	Decreases	Decreases

*The length of crack extension considered here is that under phase II

There is a definite co-relation between the load value and the length of crack extension. There is a co-relation as well between the change in the angle of the crack ($\Delta\alpha$) increasing when there is no transverse load and decreasing when transverse load operates.

TABLE 7.16

VALUES OF INITIAL APPARENT ANGLE AND FINAL ANGLE FOR SPECIMENS 12 x 4 (Fig.7.15)

x_r	31 mm							
	a	b	c	d	e	f	g	h
Crack tip	Sharp	Sharp	Sharp	Blunt	Blunt	Sharp	Sharp	Sharp
Load (lb/in)	160	240	280	320	320	320	400	440
α_a	12.5	16	7	19	24	7	10	14
α_F	12.5	7	4	- 2	0	3	2.5	5

TABLE 7.17 (a)

Specimen		14.1315	- 63.98
12 x 4	0.2	0.60388E-03	0.0
a = 3.6		6.2757	- 88.07
Coefficients	0.5	0.8950E-04	94.32
A_1 -8.080		1.99681	-116.02
A_2 2.354	0.8	0.29126E-04	- 94.32
A_3 -4.218		-2.01791	0.91
Loading	1.2	0.17664E-04	-123.18
σ_x = 0.0		-2.74774	0.91
P_y = 20.0	1.6	0.4317E-04	- 43.40

TABLE 7.17 (b)

Specimen		7.62776	- 49.11
8 x 4	0.2	0.17460E-03	0.0
a = 3.6		3.16823	- 73.4
Coefficients	0.5	0.29263E-04	- 85.68
A_1-4.972		0.81072	- 74.65
A_2 1.572	0.8	0.10817E-04	- 88.07
A_3-2.254		-0.87343	0.91
Loading	1.2	0.98658E-05	- 94.32
σ_x = 0.0		-1.27531	0.91
P_y = 20.0	1.6	0.11945E-04	- 43.62

TABLE 7.17 (c)

Specimen		7.40398	- 48.58
6 x 4	0.2		
a = 2.4		0.1105E-03	0.0
Coefficients		5.91252	- 57.73
A_1-3.078	0.5	0.40276E-04	- 71.49
A_2 0.887		5.512	- 57.73
A_3-1.418	0.8	0.31101E-04	- 70.23
Loading		5.29198	- 57.73
σ_x = 0.0	1.2	0.25975E-04	- 71.14
P_y =20.0		5.4247	- 47.61
	1.6	0.23079E-04	- 77.39

TABLE 7.17 (d)

Specimen	0.2	3.57991	0.91
4 x 4		0.27715E-04	0.0
a = 1.8		1.34967	0.91
Coefficients	0.5	0.7064E-05	- 67.28
A_1-2.082		0.48006	0.91
A_2 0.397	0.8	0.26177E-05	- 72.43
A_3-0.818		0.17672E-02	- 11.59
Loading	1.2	0.18786E-05	- 19.66
σ_x = 0.0		0.11072	- 14.75
P_y =20.0	1.6	0.32395E-06	- 16.50

TABLE 7.17 (e)

Specimen 4 x 4

Loading	Coefficient		Radius	Value of the Criteria	Expected Angle of Crack Growth (deg)
$\sigma_x = 10\frac{lb}{in}$	A_1	-4.1652		$\sigma_\psi = 1.2725$	0.91
$P_y = 40lb$	A_2	0.5945	2.0		
$a = 1.2in$	A_3	-1.6565		S = 0.1945E-05	0.91
$\sigma_x = 0$	A_1	-1.04127		$\sigma_\psi = 1.78392$	0.91
$P_y = 10lb$	A_2	0.19862	0.2		
$a = 1.2in$	A_3	-0.41413		S = 0.6928E-05	0.0
$\sigma_x = 20\frac{lb}{in}$	A_1	-2.0827		$\sigma_\psi = 3.5798$	0.91
$P_y = 20lb$	A_2	-0.00268	0.2		
$a = 1.2in$	A_3	-0.8283		S = 0.17059E-04	0.91
$\sigma_x = 30\frac{lb}{in}$	A_1	-2.08283		$\sigma_\psi = 3.5788$	0.91
$P_y = 20lb$	A_2	-0.22026	0.2		
$a = 1.2in$	A_3	-0.82836		S = 1.3899E-05	0.91

TABLE 7.17 (f)

Specimen 6 x 1

Loading	Coefficient		Radius	Criterion Value	Expected Angle of Crack Growth
$\sigma_x = 400\frac{lb}{in}$ $P_y = 100lb$ $a = 0.2in$	A_1 A_2 A_3	-13.814 - 4.187 -17.880	0.002	σ_ψ = -306.462 S = 0.147	0.91 deg 0.91 deg
ditto		ditto	0.02	σ_ψ = - 90.148 S = 0.0113	0.91 deg 0.91 deg
ditto		ditto	0.2	σ_ψ = - 9.816 S = 0.000145	0.91 deg 0.91 deg
ditto		ditto	2.0	σ_ψ = - 0.736 S = 0.000328	0.91 deg -35.11deg
ditto	A_1 A_2 A_3	-13.814 + 4.187 -17.880	0.02	σ_ψ = -306.471 S = 0.13565	0.91 deg 0.91 deg
ditto	A_1 A_2 A_3	-13.814 0.0 -17.880	0.02	σ_ψ = -306.466 S = 0.1409	0.91 deg 0.91 deg
ditto	A_1 A_2 A_3	-13.814 - 4.187 -17.880	0.02	σ_ψ = -306.462 S = 0.1469	0.91 deg 0.91 deg

TABLE 7.18

VALUES OF A_2 FOR EXPERIMENTAL CASES

(a) Specimen 4 x 4

	3/4		4/4		5/4		
	Initial	Final	Initial	Final	Initial	Final	
O.L.	192	109	209	67.6	200	115	lb
T.L.	80	80	100	100	100	100	lb/in
a	1.0	1.414	1.0	1.788	1.0	1.433	in
A_2	1.32	1.06	1.75	- 0.27	0.61	0.51	
α	26	18	16.5	10	18	15.5	degree

(b) Specimen 6 x 4

	3/6		5/6	
	Initial	Final	Initial	Final
O.L.	312	170	296	187
T.L.	160	160	360	360
a	1.574	2.992	1.574	2.2
A_2	7.58	9.6	2.58	1.6
α	22	10	4	1

(c) Specimen 8 x 4

	5/8		
	Initial	Final	
O.L.	412	250	lb
T.L.	850	850	lb/in
a	2.125	2.937	in
A_2	1.231	- 1.95	
α	7	1	deg

TABLE 7.18 (cont.)

(d) Specimen 12 x 4

	1/12		2/12		3/12		4/12		6/12		
	Initial	Final	Initial	Final	Initial	Final	Initial	Final	Initial	Final	
O.L.	327	281	340	200	340	140	310	192	329		lb
T.L.	0	0	360	360	360	360	360	360	700		lb/in
a	3.38	4.44	3.38	3.97	3.38	4.52	3.38	3.616	3.38		in
A_2	49.6	54.6	36.55	20.95	36.55	14.05	31.95	17.8	20.4		
α	10		18		17		13		12		degree

TABLE 8.1

COEFFICIENT VALUES FOR SINGLE EDGE CRACK BEND SPECIMEN AND SINGLE EDGE CRACK TENSION SPECIMEN

(a)

a	0.2	0.4	0.6	0.8	1.0
A_1	-8.031	-11.059	-14.599	-19.145	-25.484
A_2	-5.116	- 3.583	- 2.181	- 0.643	1.515
A_3	1.428	- 1.908	- 5.413	-10.035	-17.420

(b)

a	0.3	0.6	0.9
A_1	-18.027	-33.835	-370.759
A_2	- 5.165	- 3.722	135.285
A_3	5.622	- 2.512	-444.330

TABLE 8.2

CRACK ARREST

Specimen	Fig.8.1	O.L.	Load	Length of Crack Ext. (Phase II)	T.L.
6/12	a	327	0	0	700
4/12	b	283	118	6	360
2/12	c	320	140	15	360
1/12	d	327	* 46	27	0
3/12	e	342	201	29	360

*The crack extension for this specimen was not totally phase II, this can be noticed on the cracked surface.

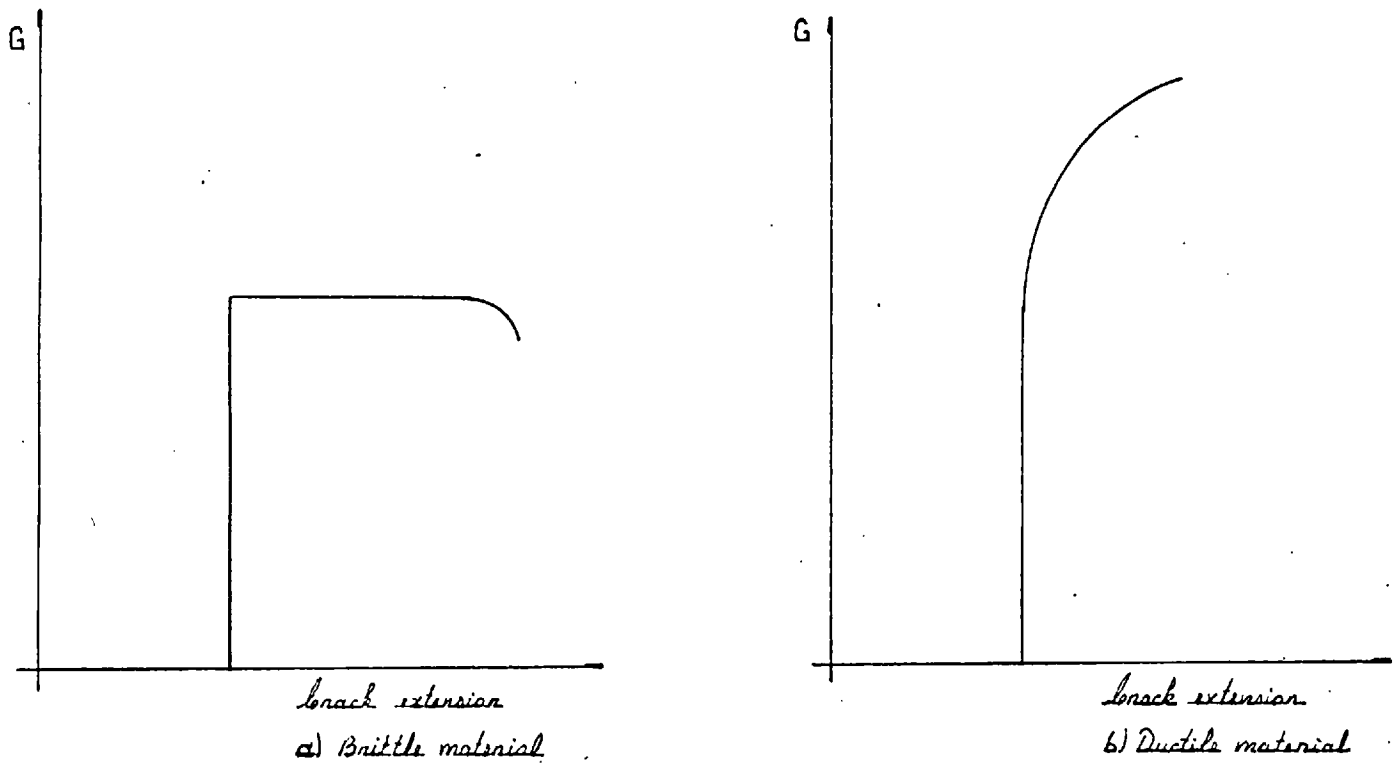

Fig. 1.1 Material behaviour

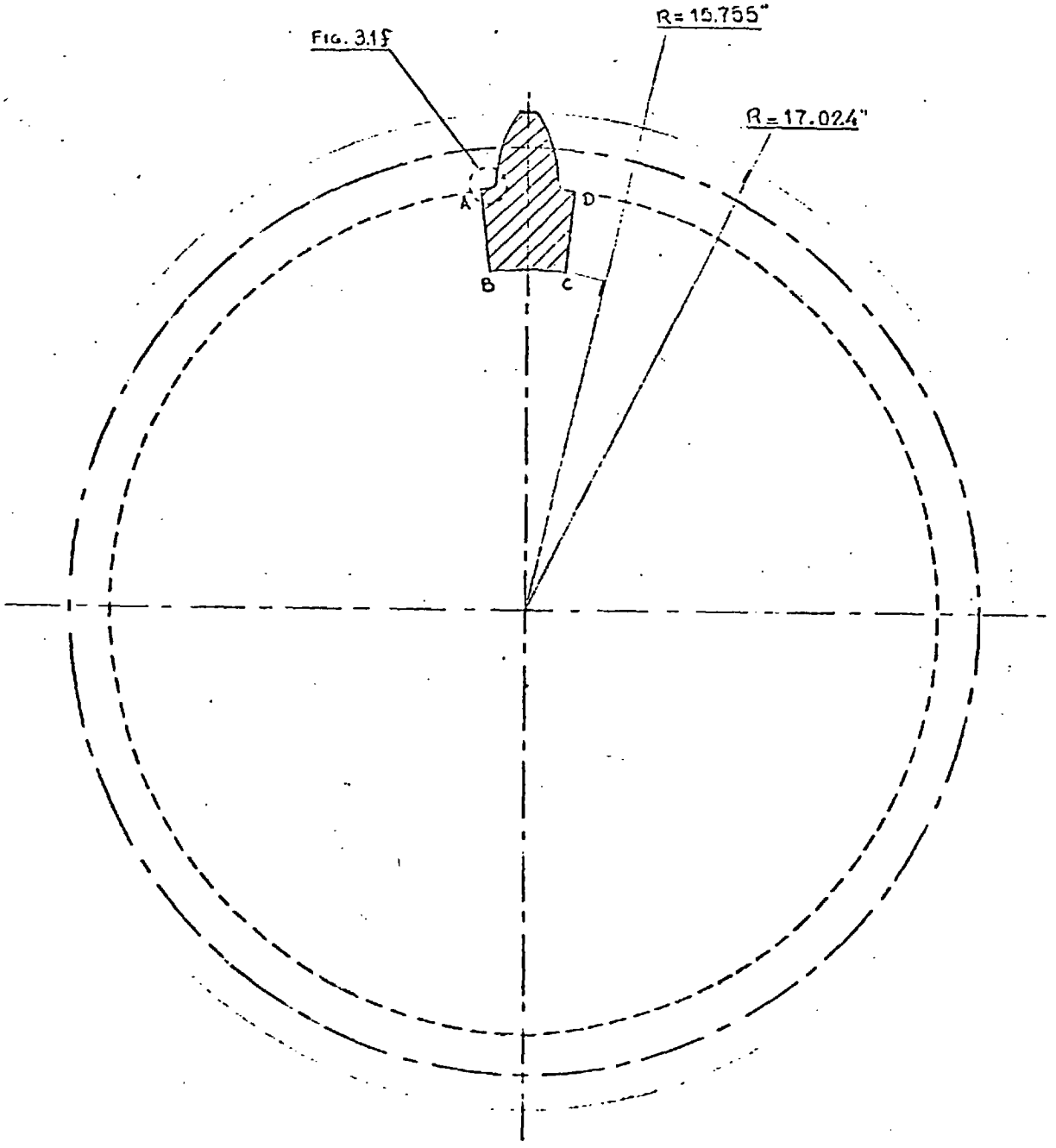

GEAR TOOTH FIG. 3.1a	Section considered for the finite element method

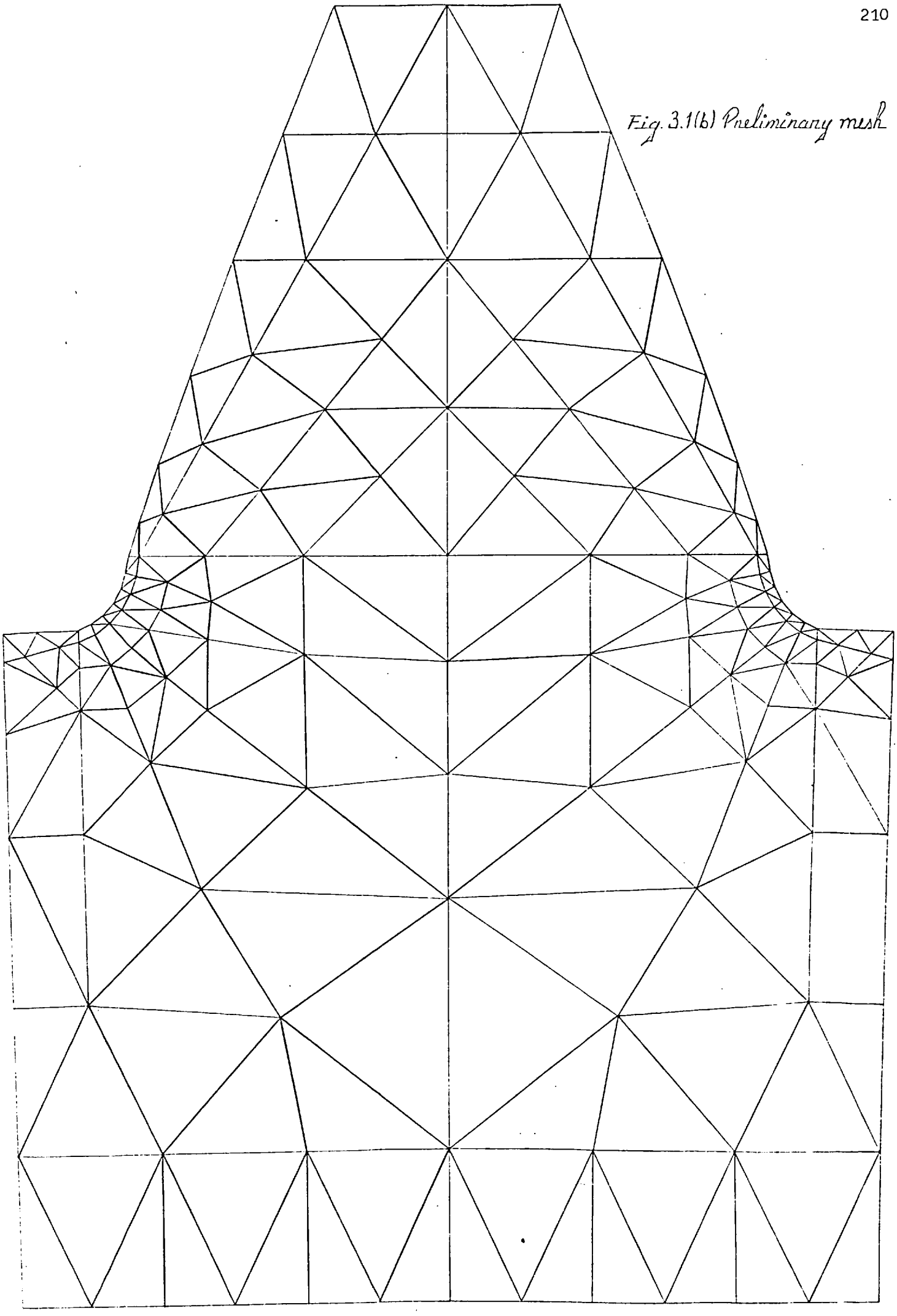

Fig. 3.1(b) Preliminary mesh

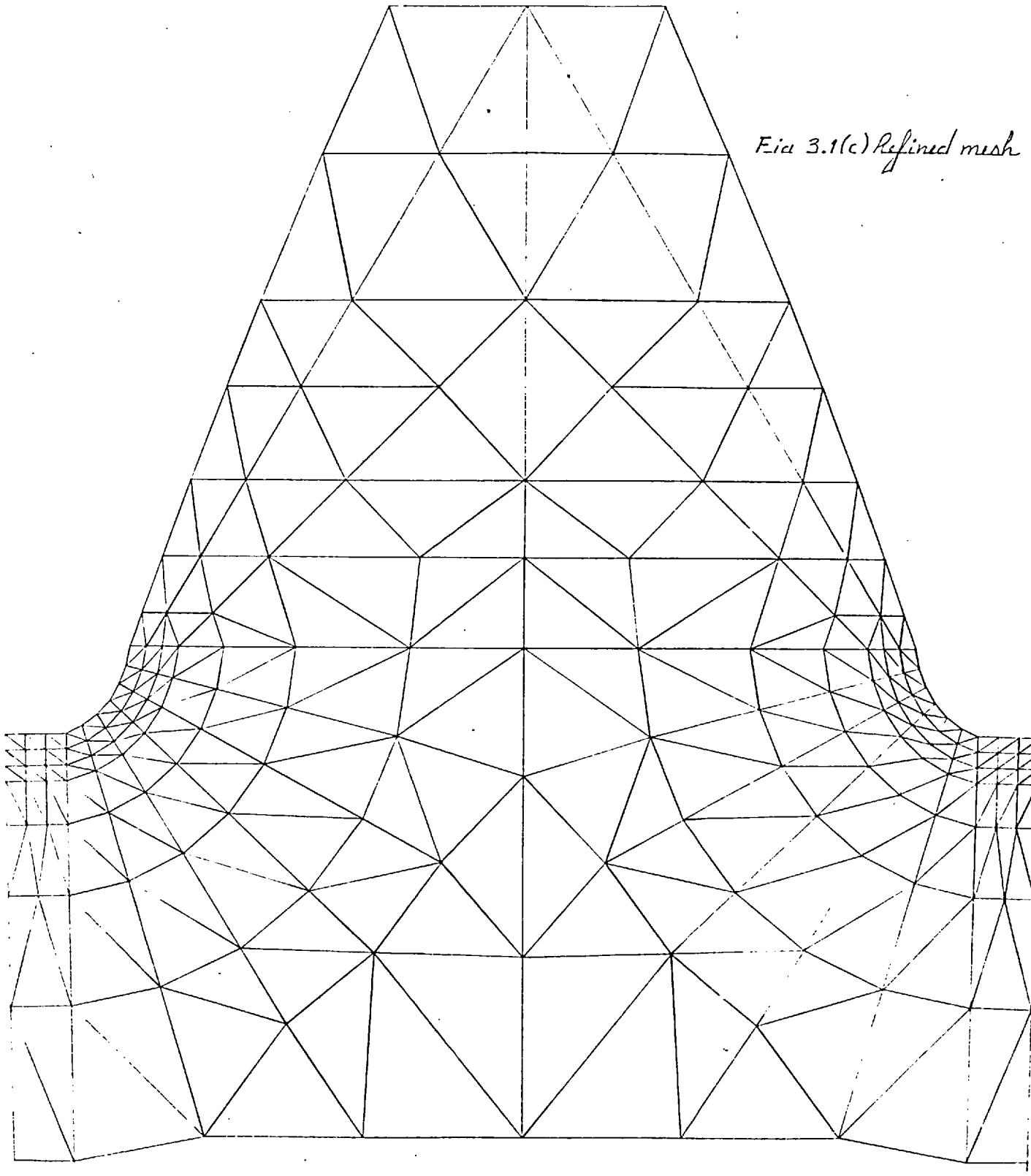

Fig 3.1(c) Refined mesh

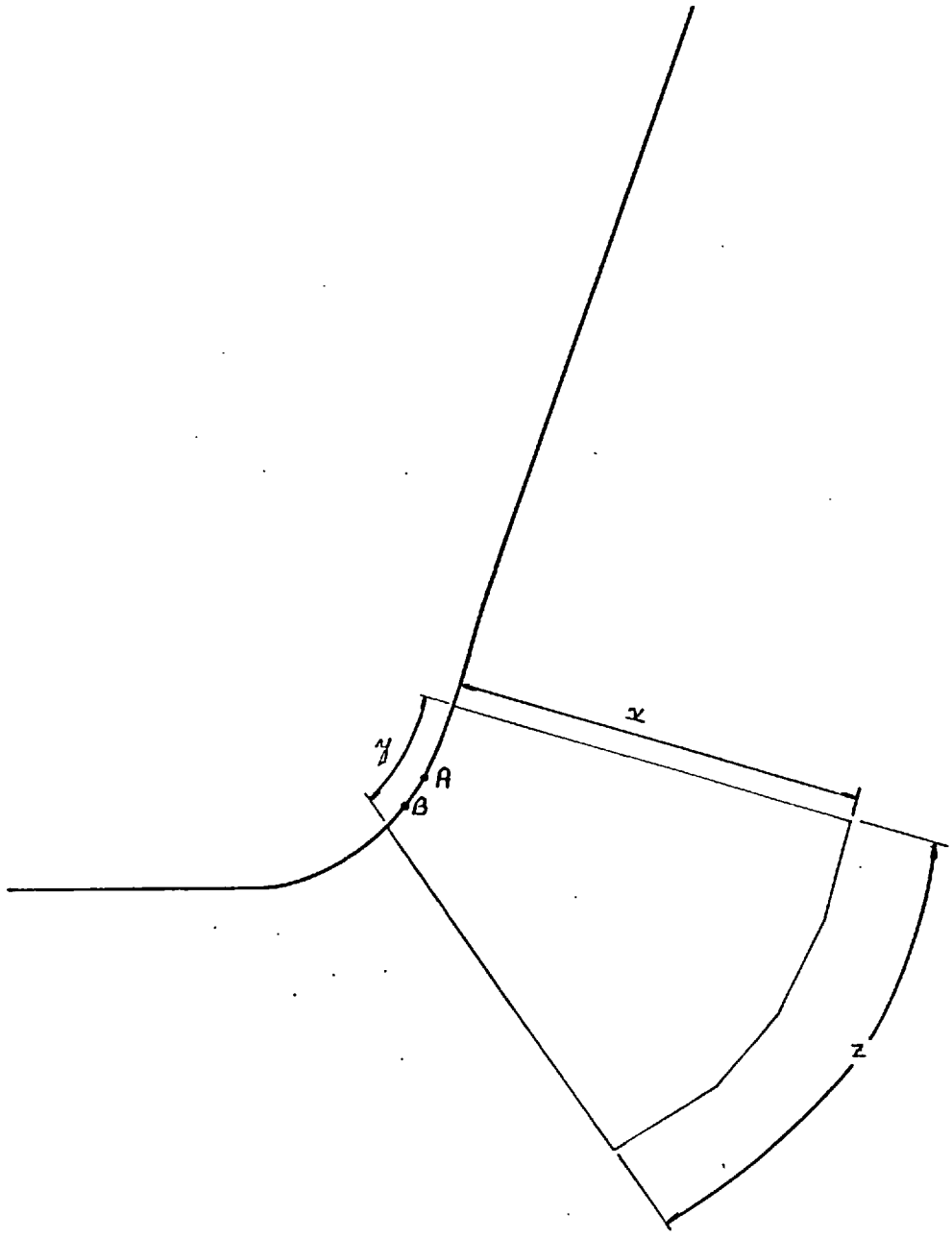

196 Triangular elements on the stress concentration region

Fig 3.1(d) Region of refined mesh at the tooth root

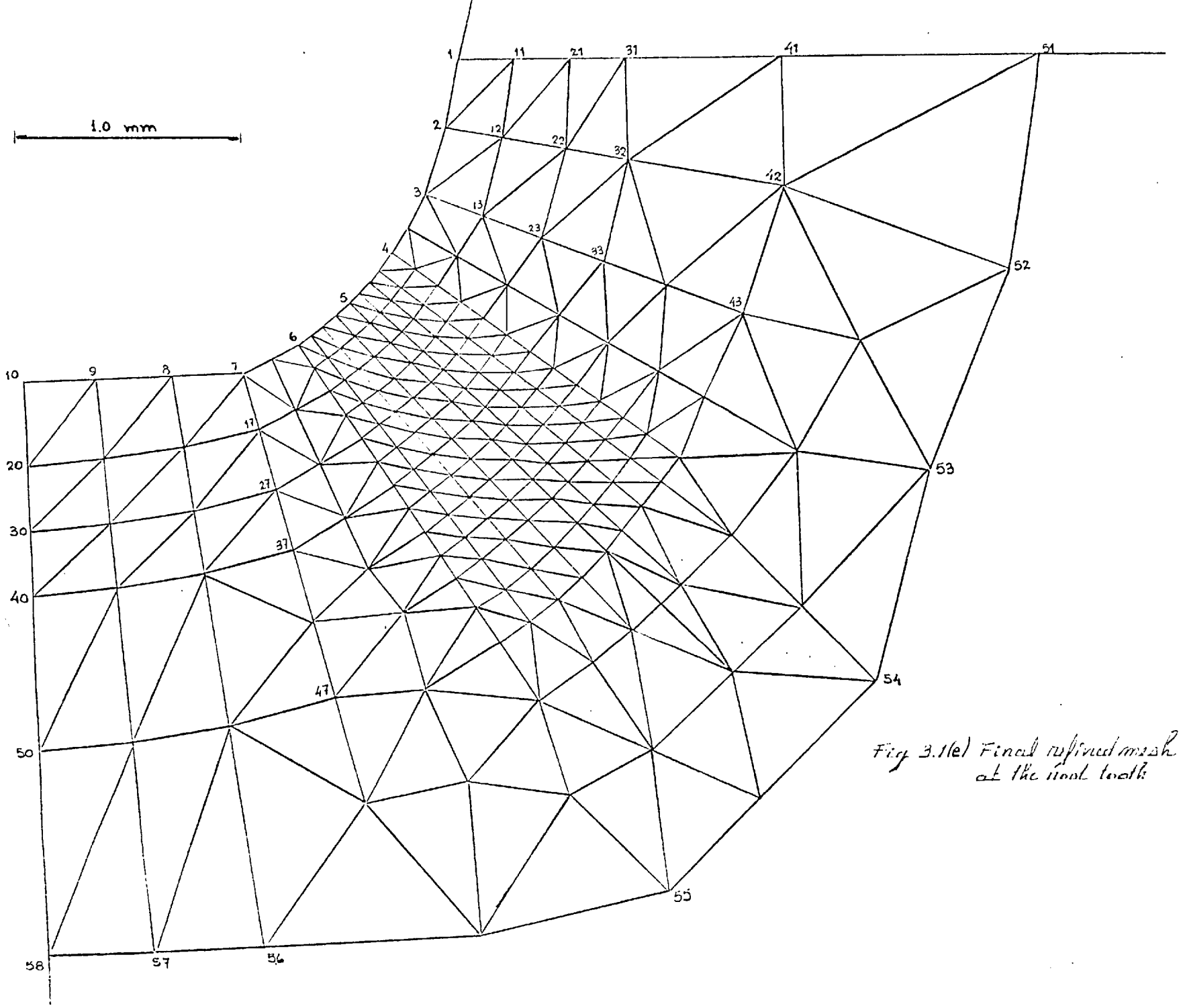

Fig 3.1(e) Final refined mesh at the root tooth

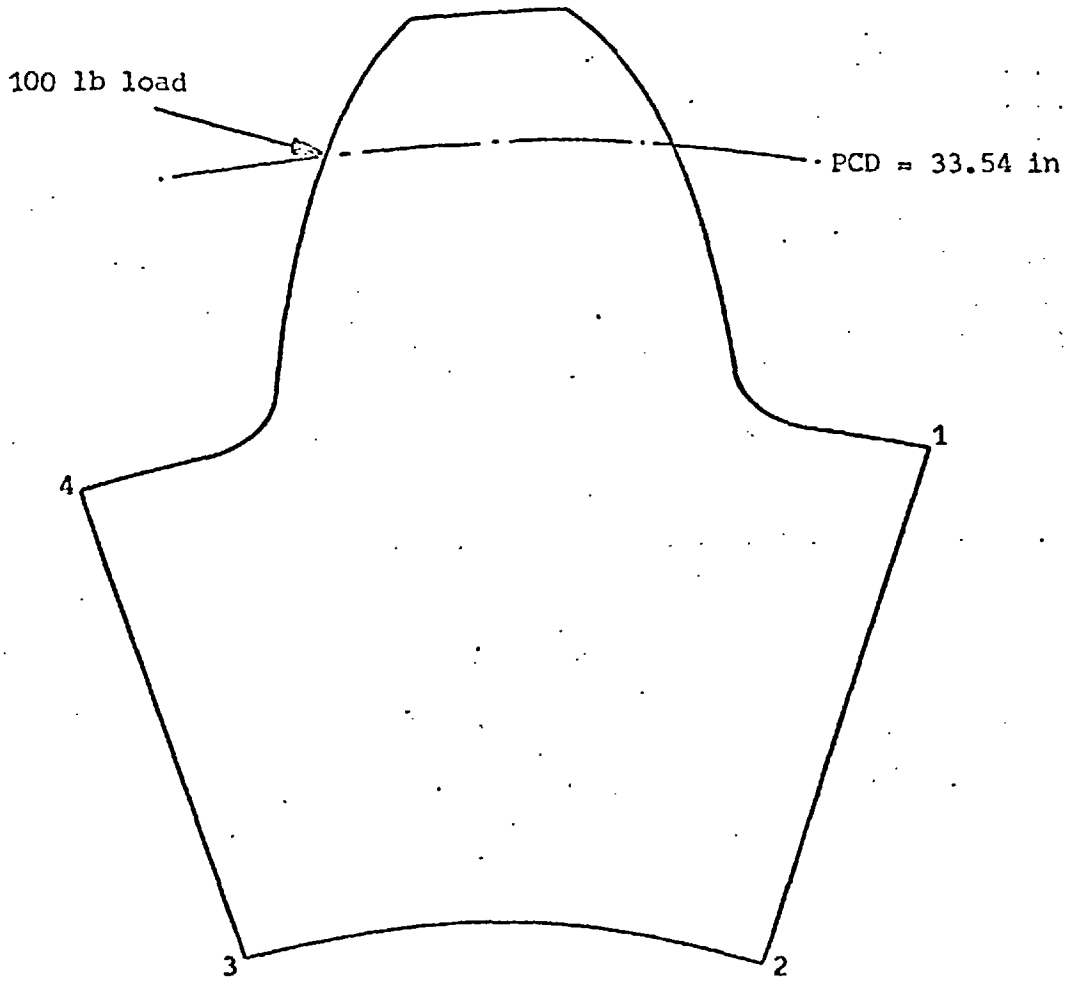

Point 2 is fixed
Points 2-3 lie on a circular arc constrained to move circumferentially about the gear centre
Points 1-2 and 3-4 are allowed to move perpendicular to the radius from the gear centre

Fig. 3.2 Boundary conditions for tooth stress calculations

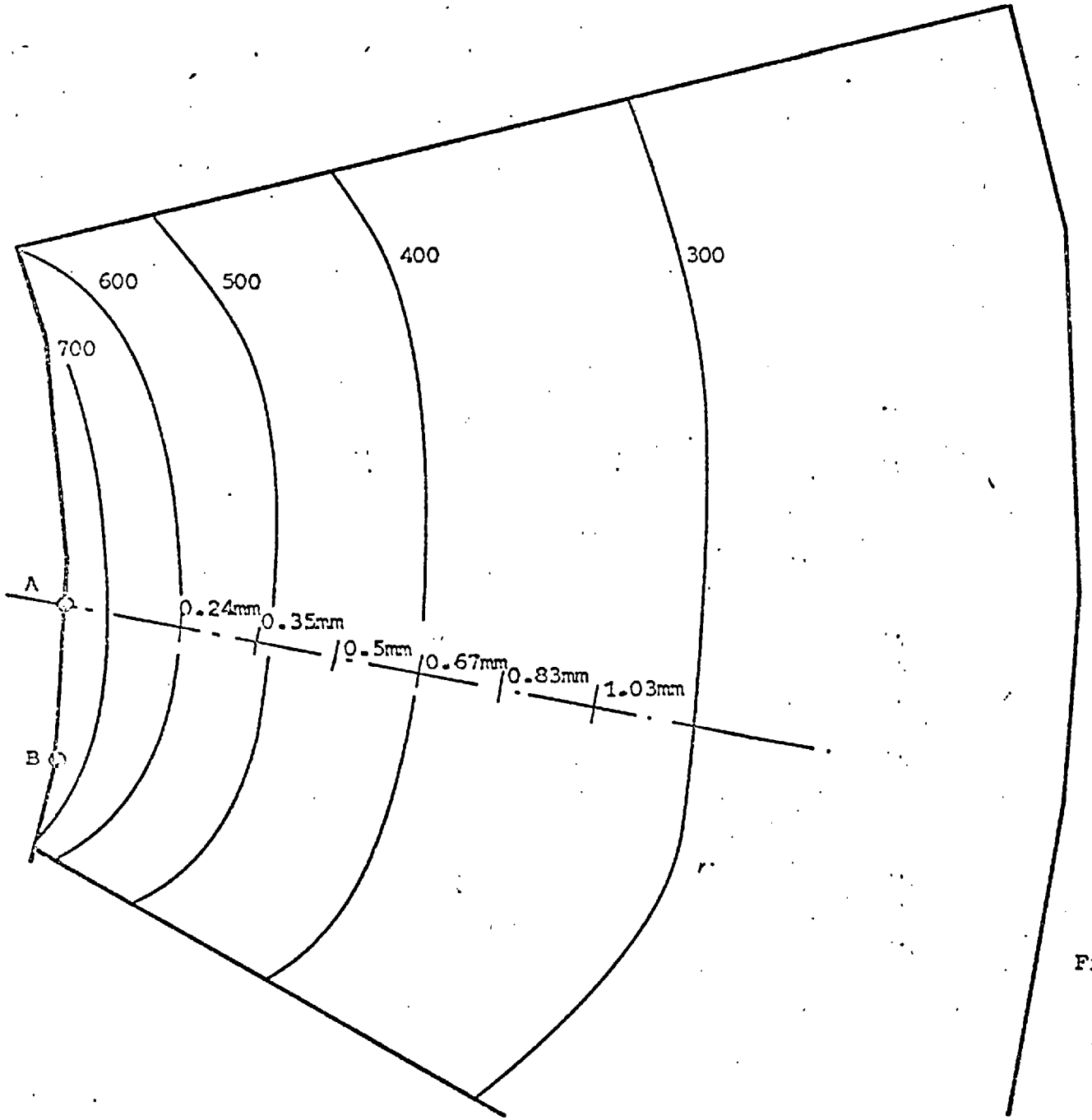

Fig. 3.3 Lines of maximum principal stress in uncracked tooth root per 100 lb load (lb/in^2)

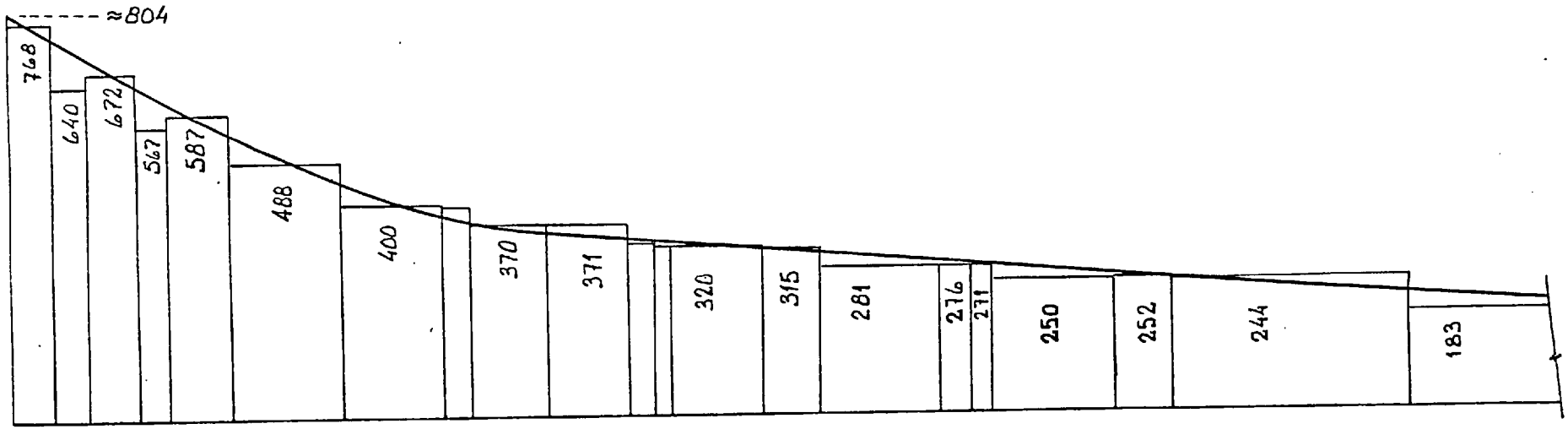

Fig 3.4 Extrapolation to the surface of element stresses in uncracked tooth (lb/in^2)

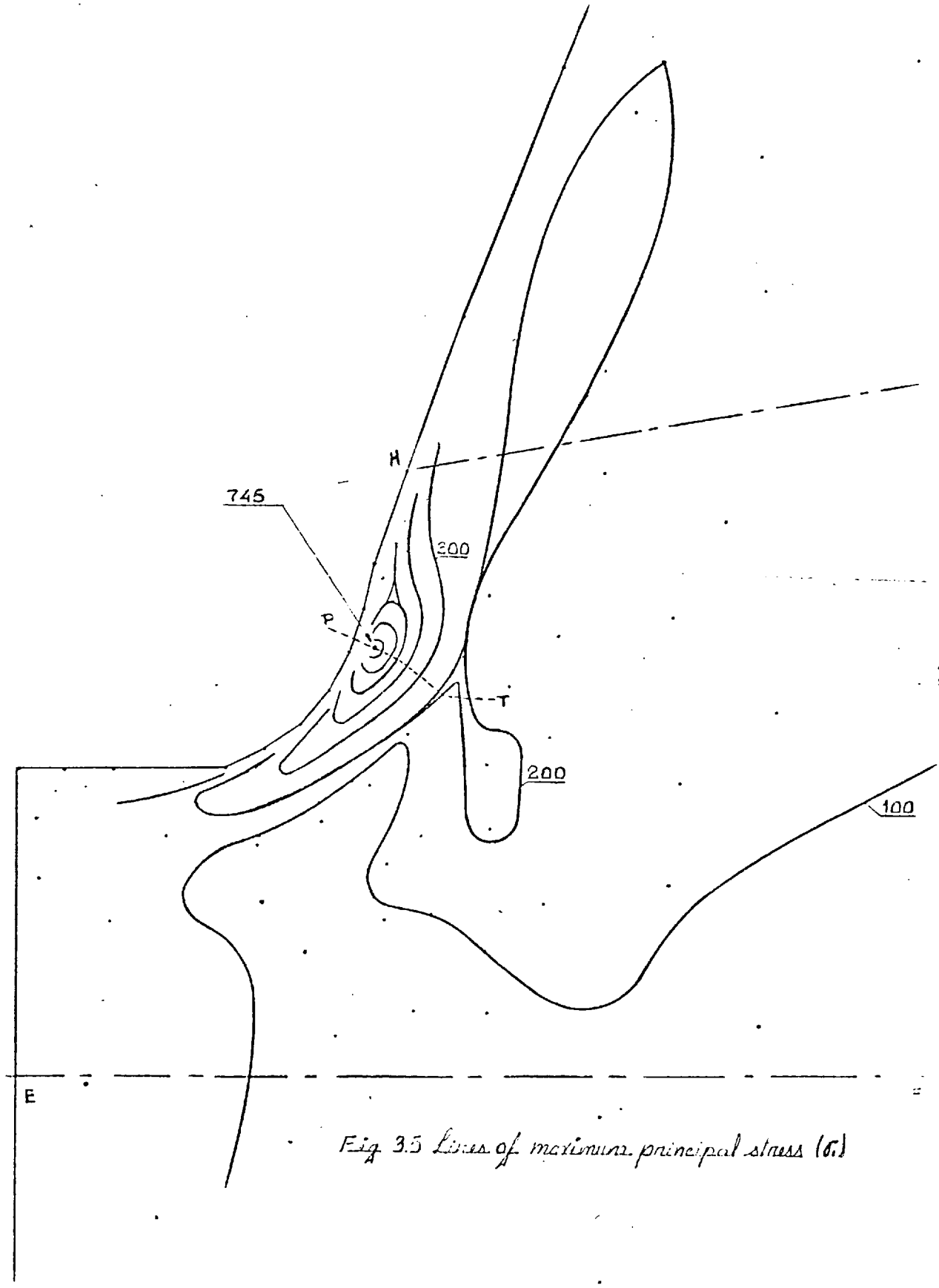

Fig 3.5 Lines of maximum principal stress (σ_1)

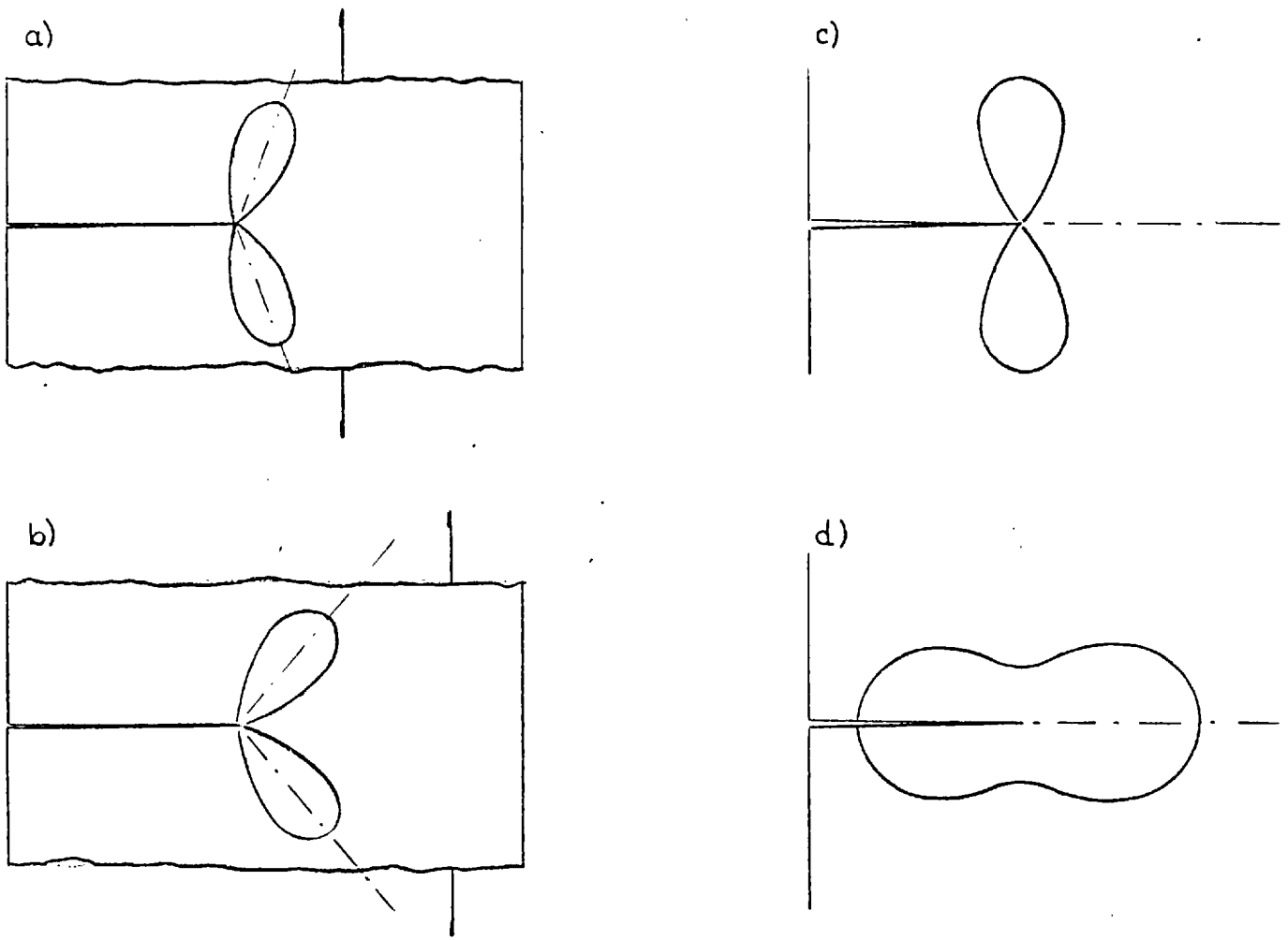

Fig. 3.6 (a), (b) Loading effect on the isochromatics
(c) Symmetric case, (d) Antisymmetric case

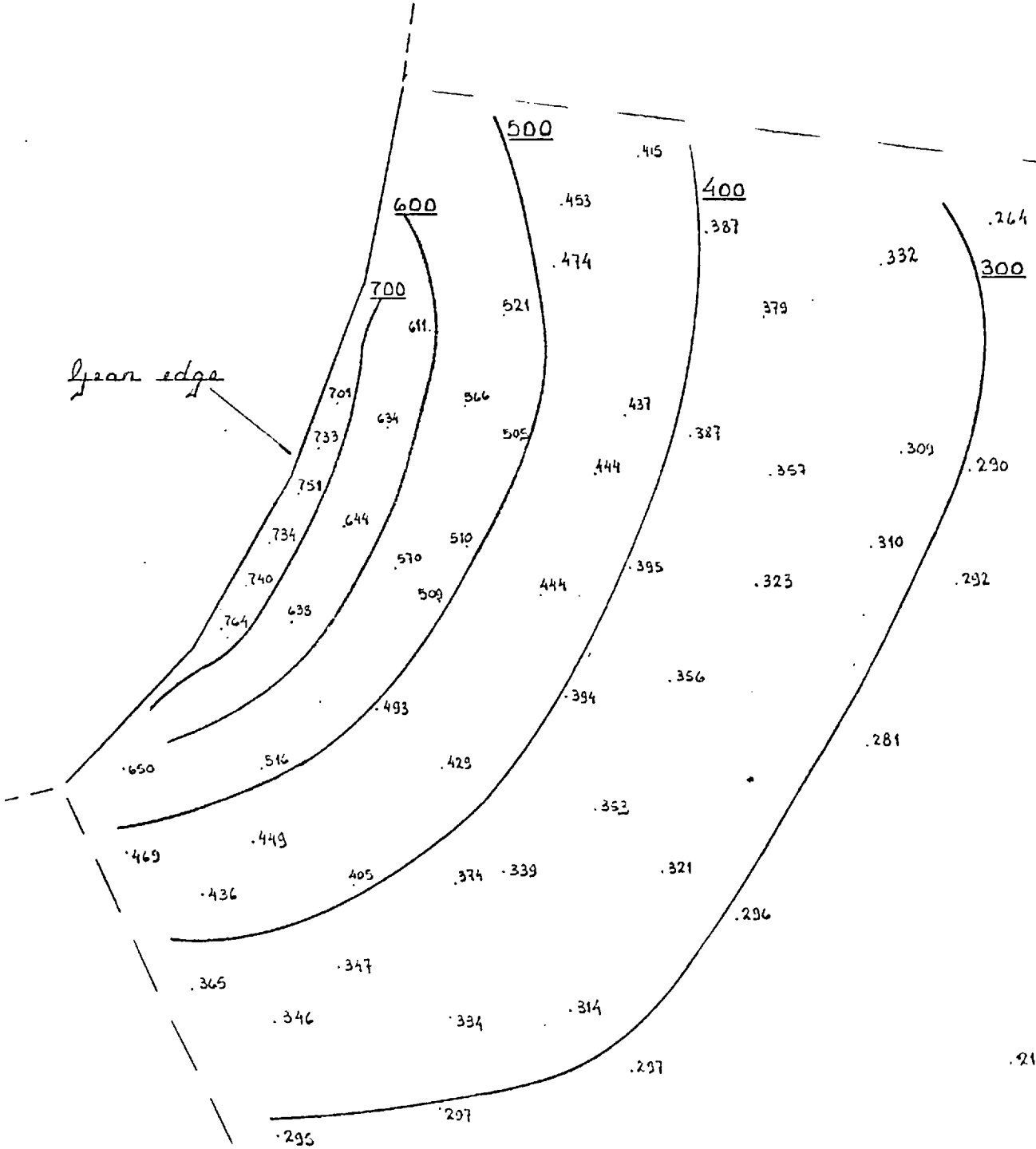

Fig 3.7(a) Lines of maximum principal stress.

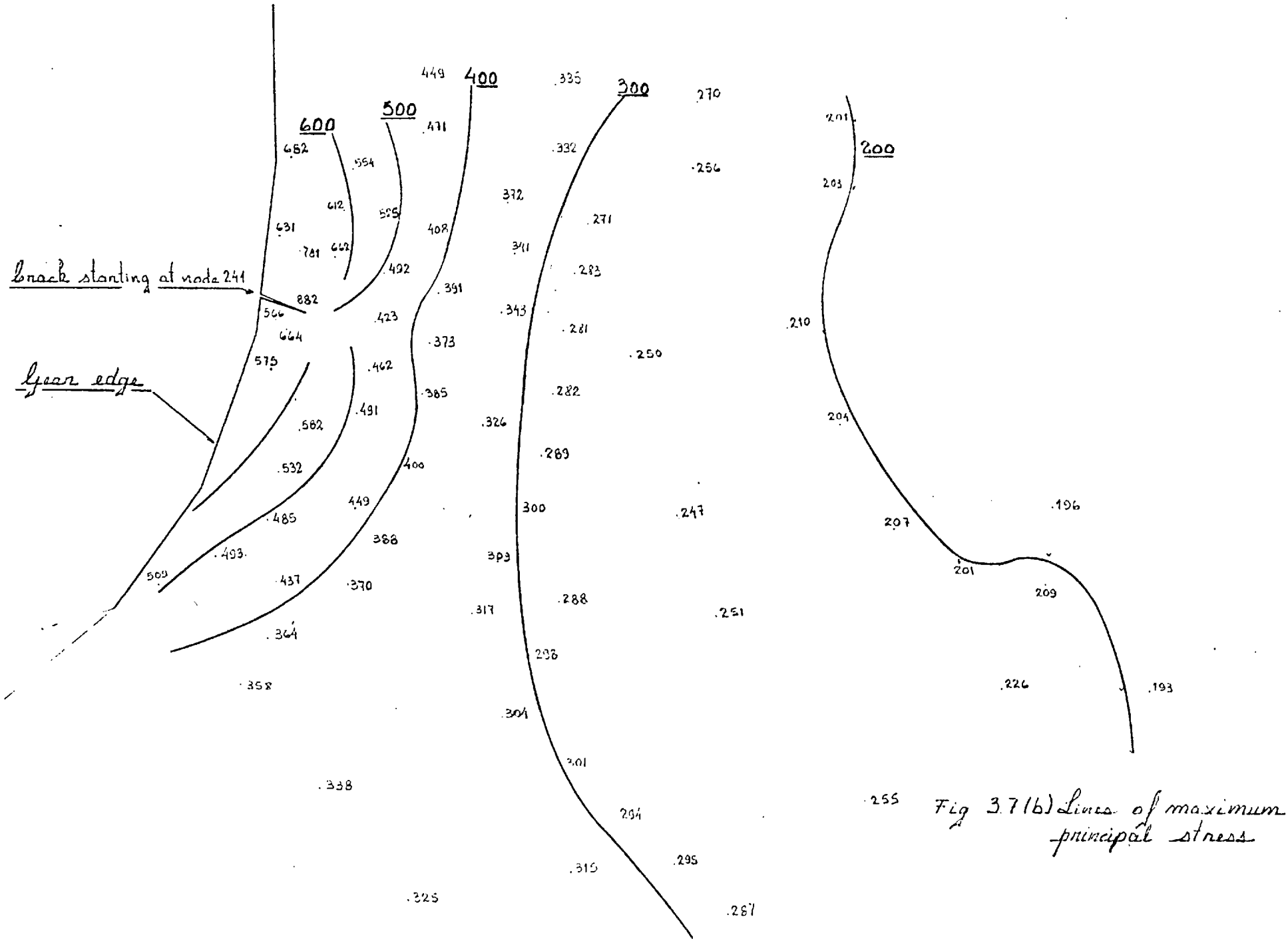

Fig 3.7(b) Lines of maximum principal stress

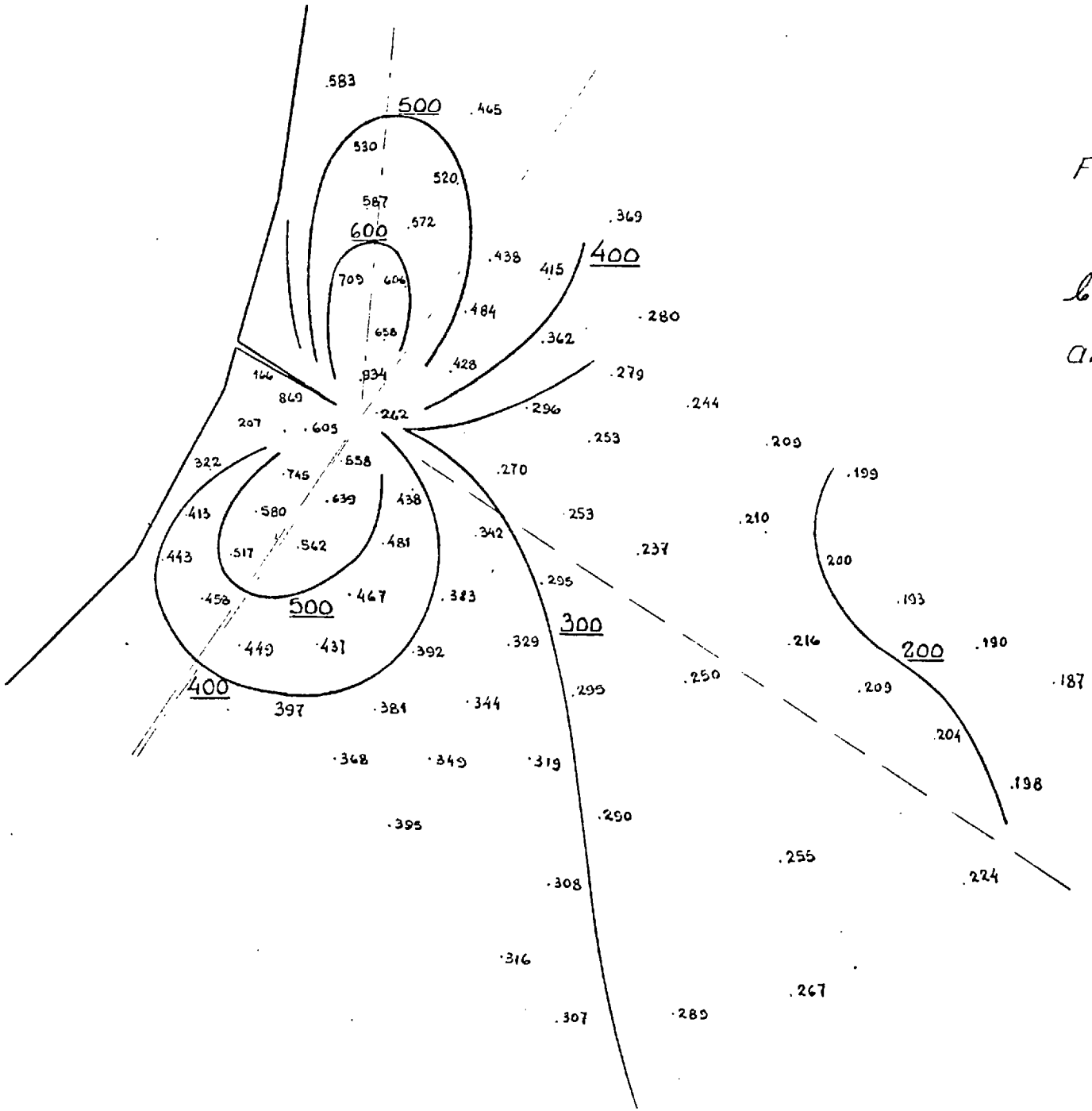

Fig 3.7(c) Lines of maximum principal stress.

Crack extension 0.238 mm.

Angle of crack = 0.97397 rad.

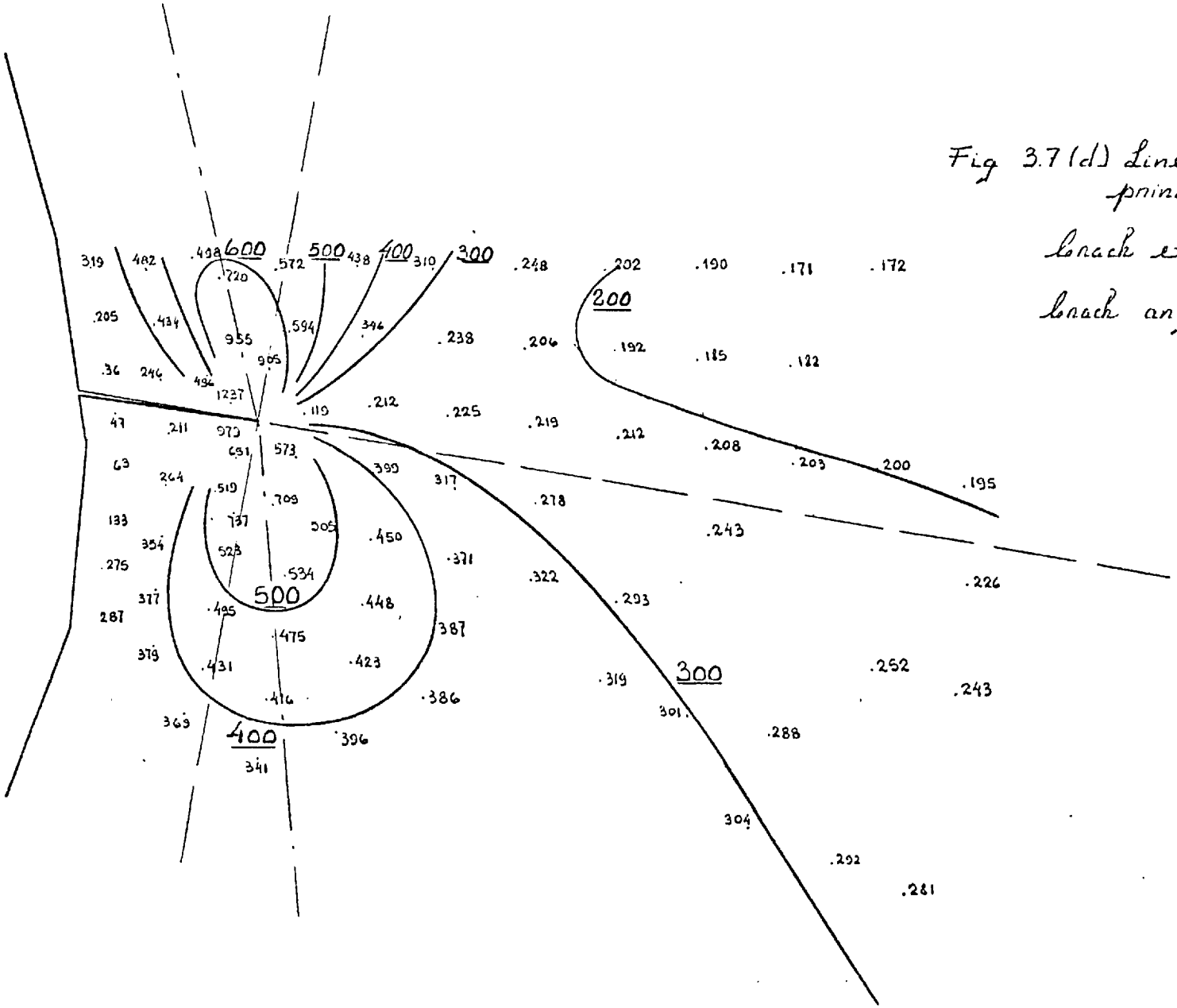

Fig 3.7 (d) Lines of maximum principal stress.

Crack extension 0.36 mm.

Crack angle -0.97397 rad.

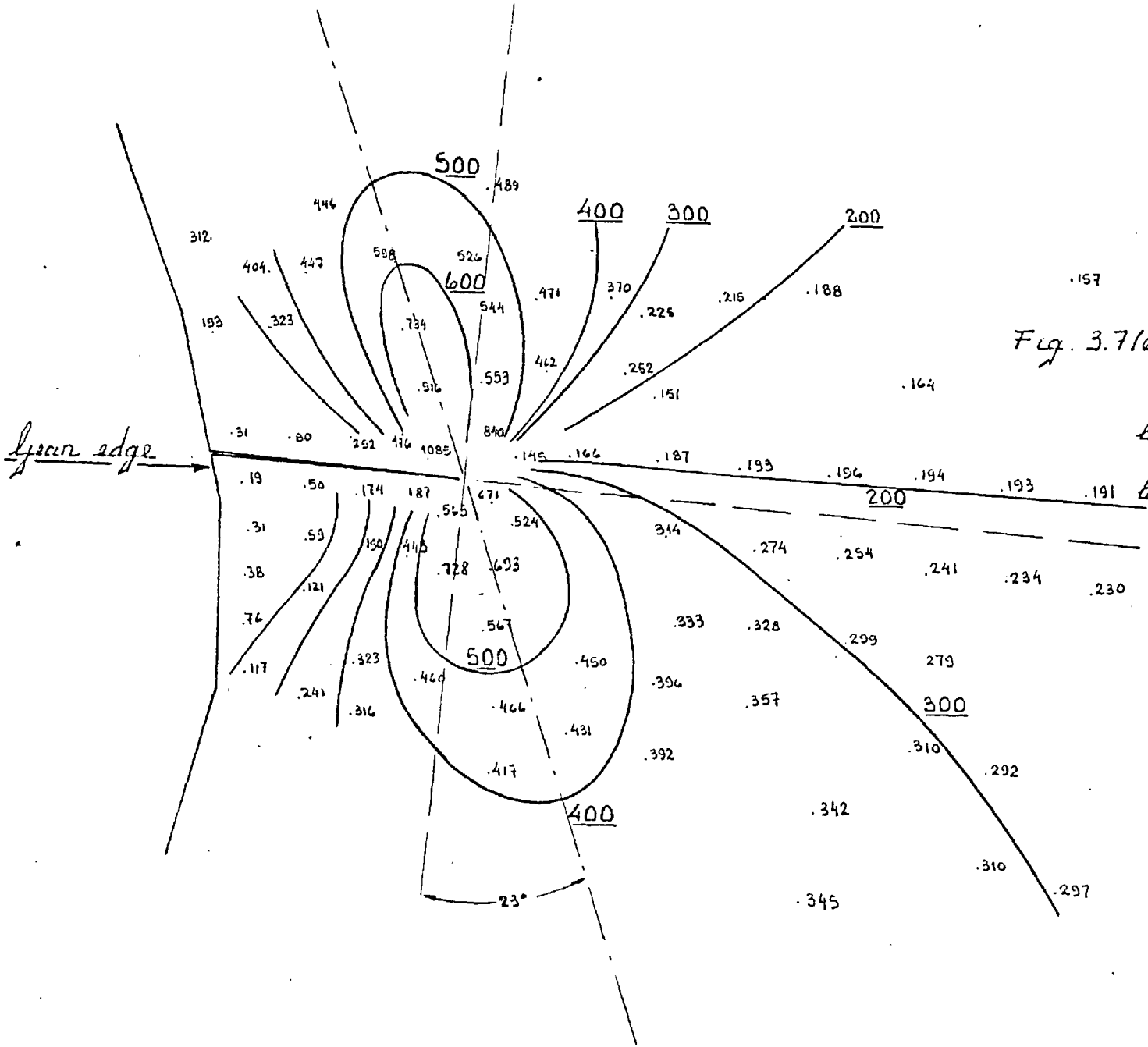

Fig. 3.7(e) Lines of maximum principal stress.

crack extension 0.52 mm.

crack angle = 0.97397 rad.

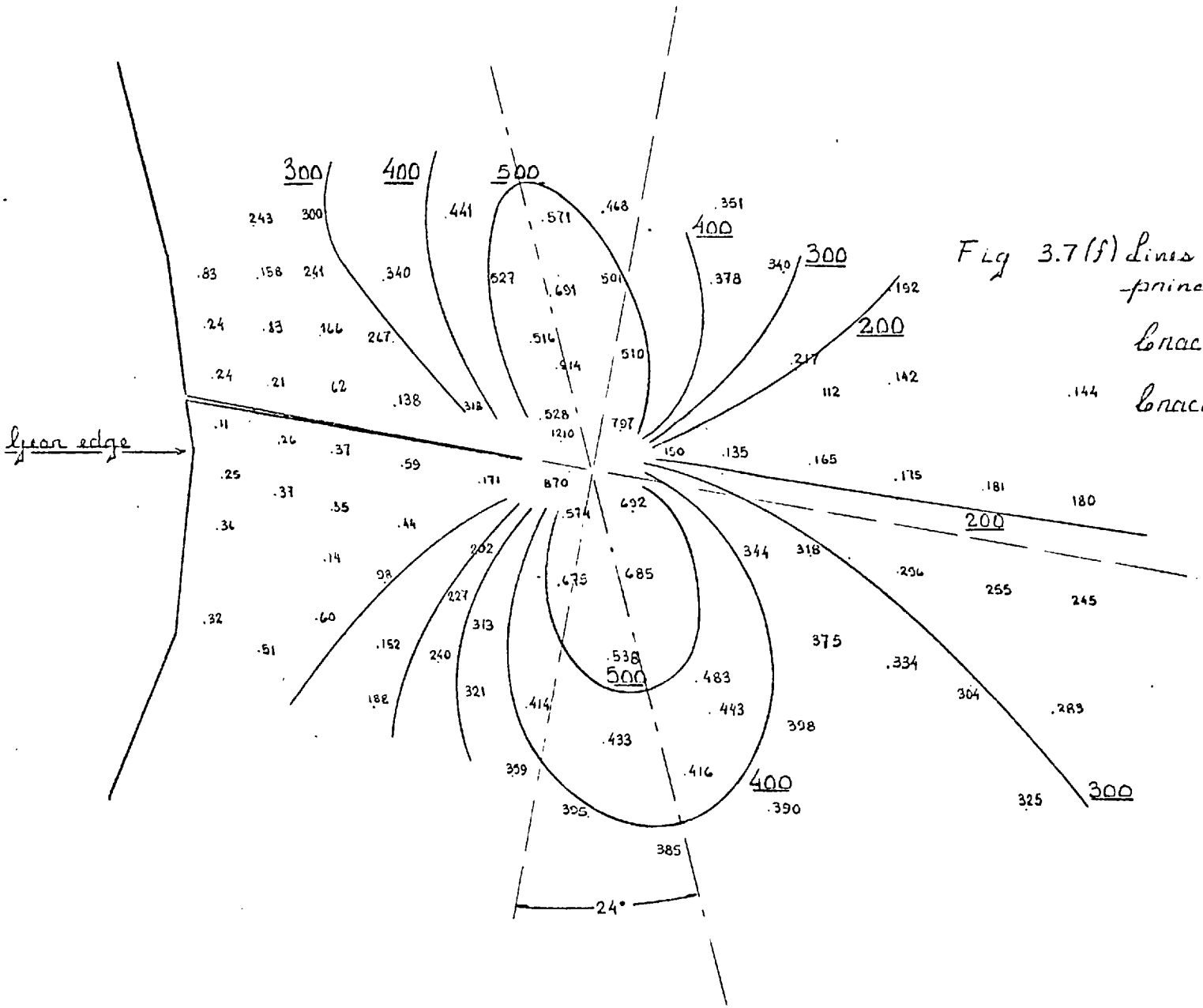

Fig 3.7(f) Lines of maximum principal stress

Crack extension 0.686 mm.

Crack angle _ 0.97397

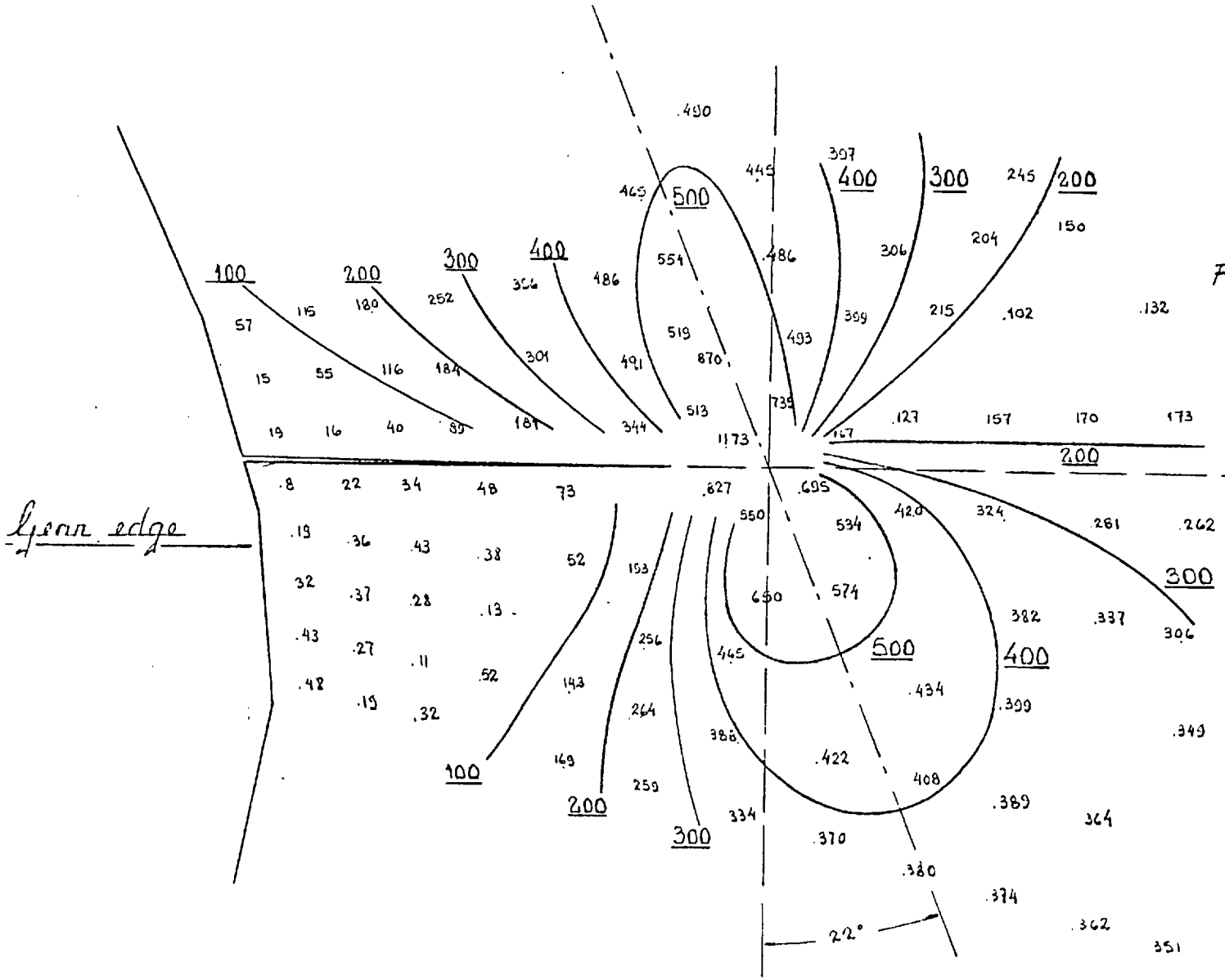

Fig 3.7(g) Lines of maximum principal stress

Crack extension 1.03 mm.

Crack angle -0.97397 rad

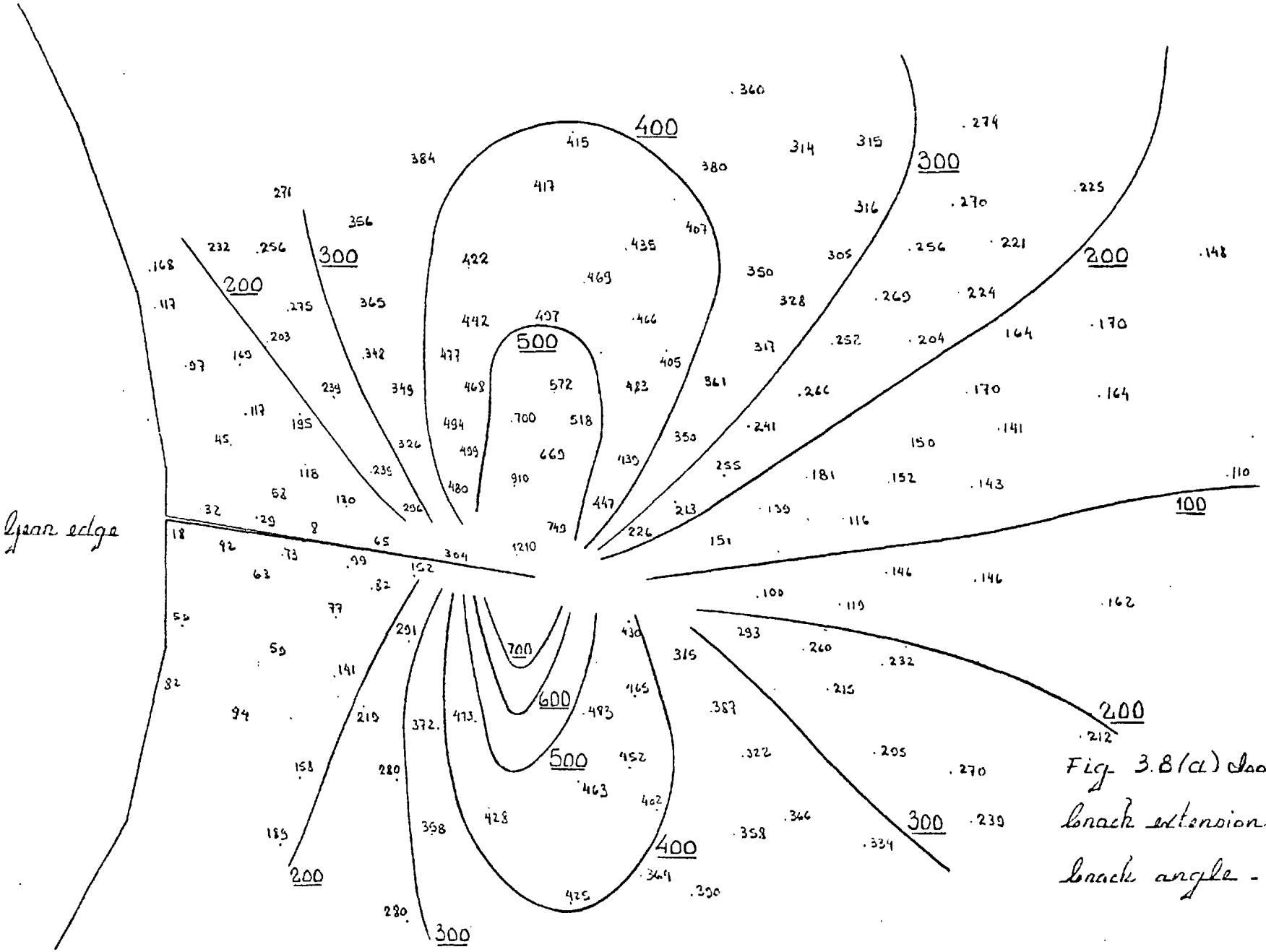

Fig. 3.8(a) Isochromatic field
Knack extension 0.85 mm.
Knack angle - 0.80078 rad.

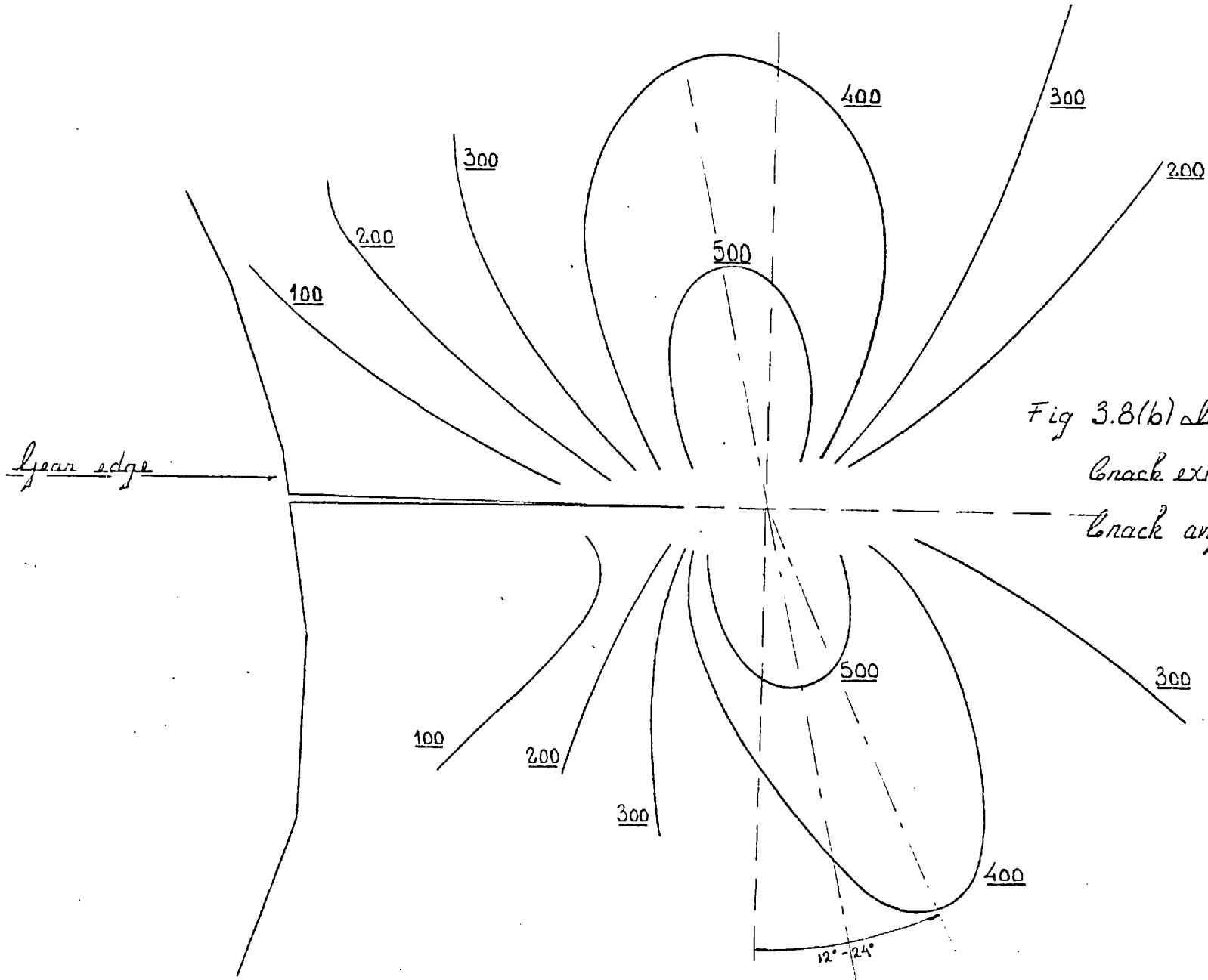

Fig 3.8(b) Isochromatic field
Crack extension 1.03 mm.
Crack angle - 0.82647 rad.

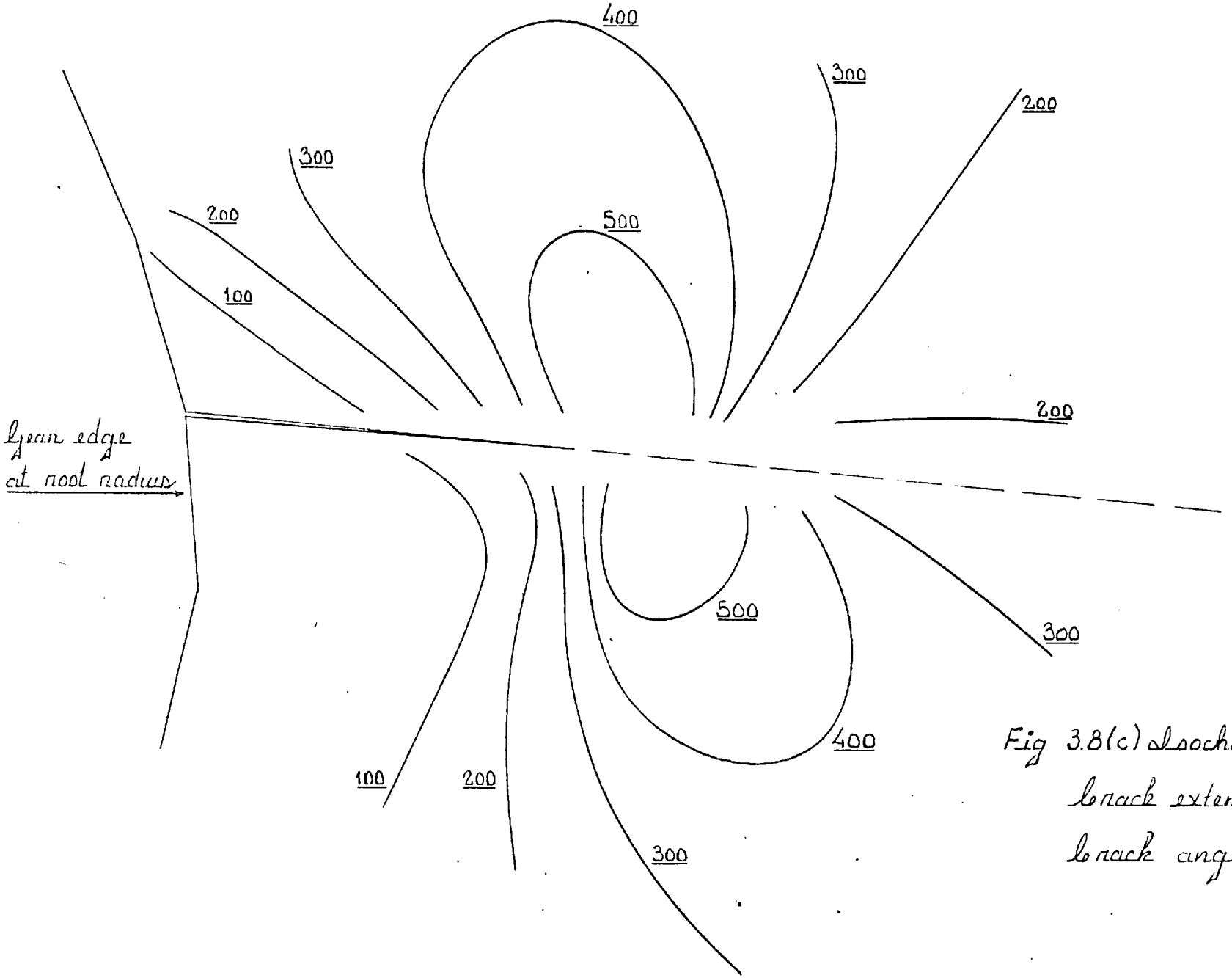

Fig 3.8(c) Isochromatic field
Crack extension 1.03 mm
Crack angle 1.09140 rad.

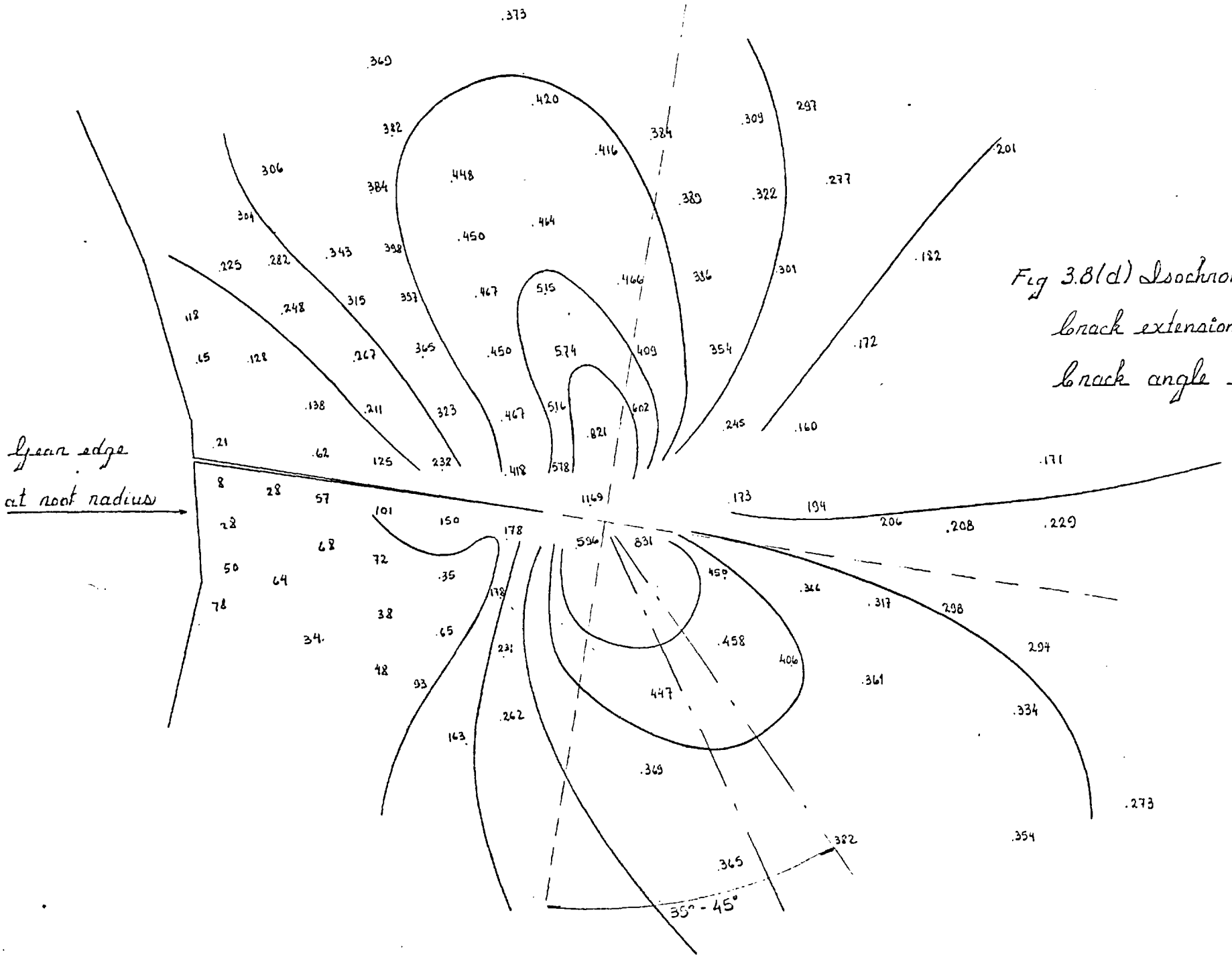

Fig 3.8(d) Isochromatic field
Crack extension 1.03 mm.
Crack angle - 1.10256 rad.

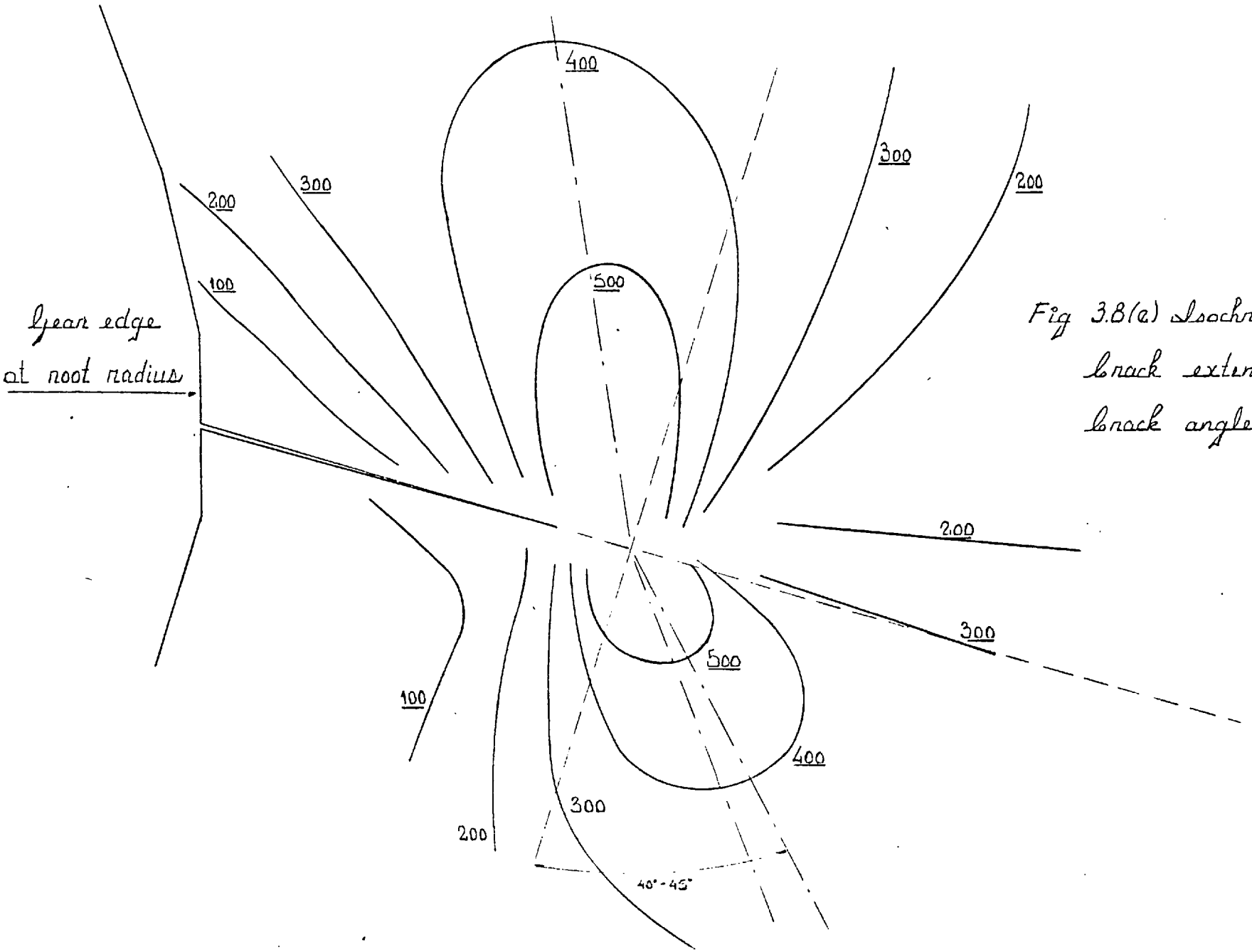

Fig 3.8(a) Isochromatic field
Crack extension 1.03 mm.
Crack angle - 1.13479 rad.

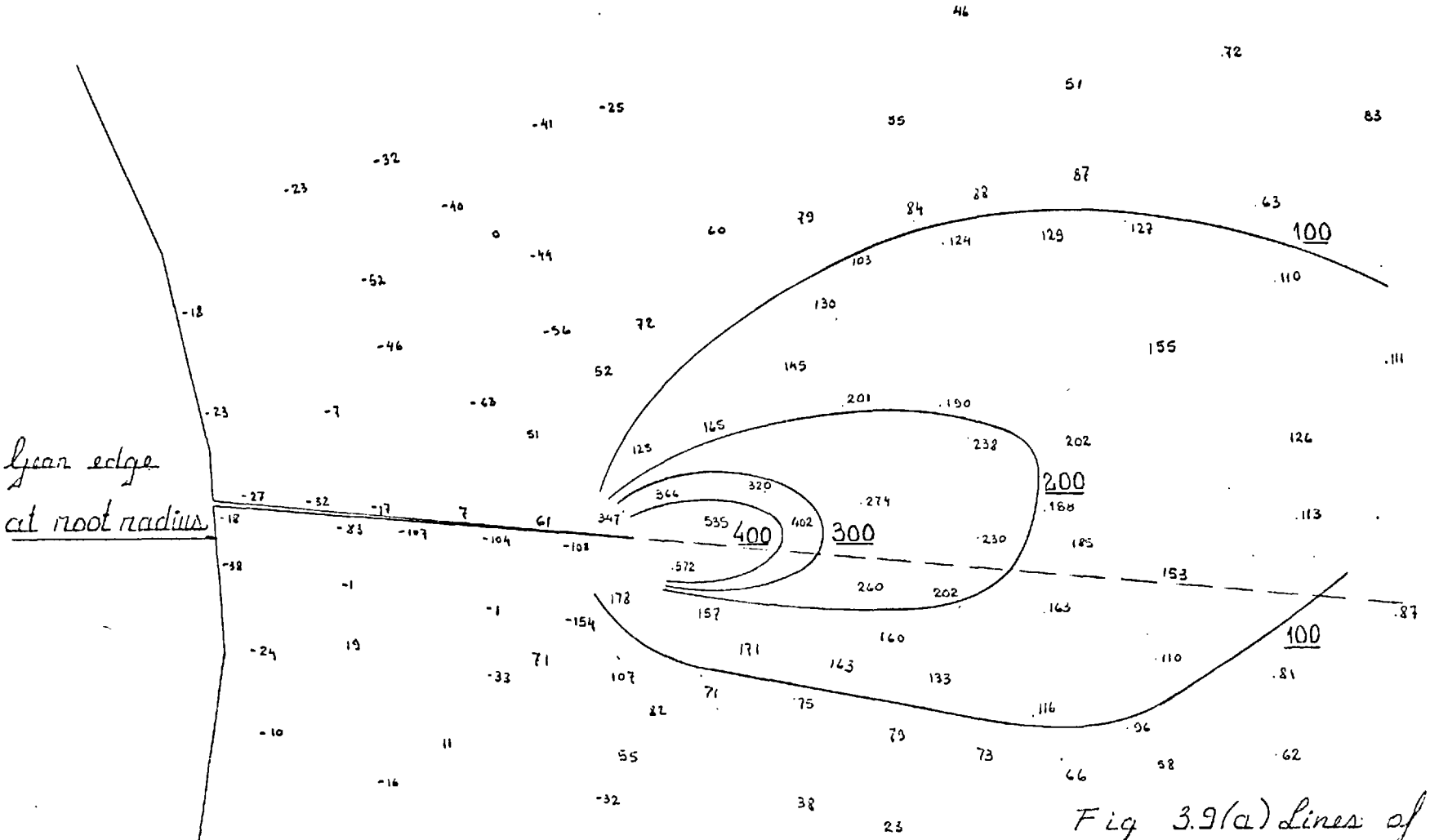

Fig 3.9(a) Lines of minimum principal stress

Crack extension 1.03 mm.

Crack angle - 0.80078 rad.

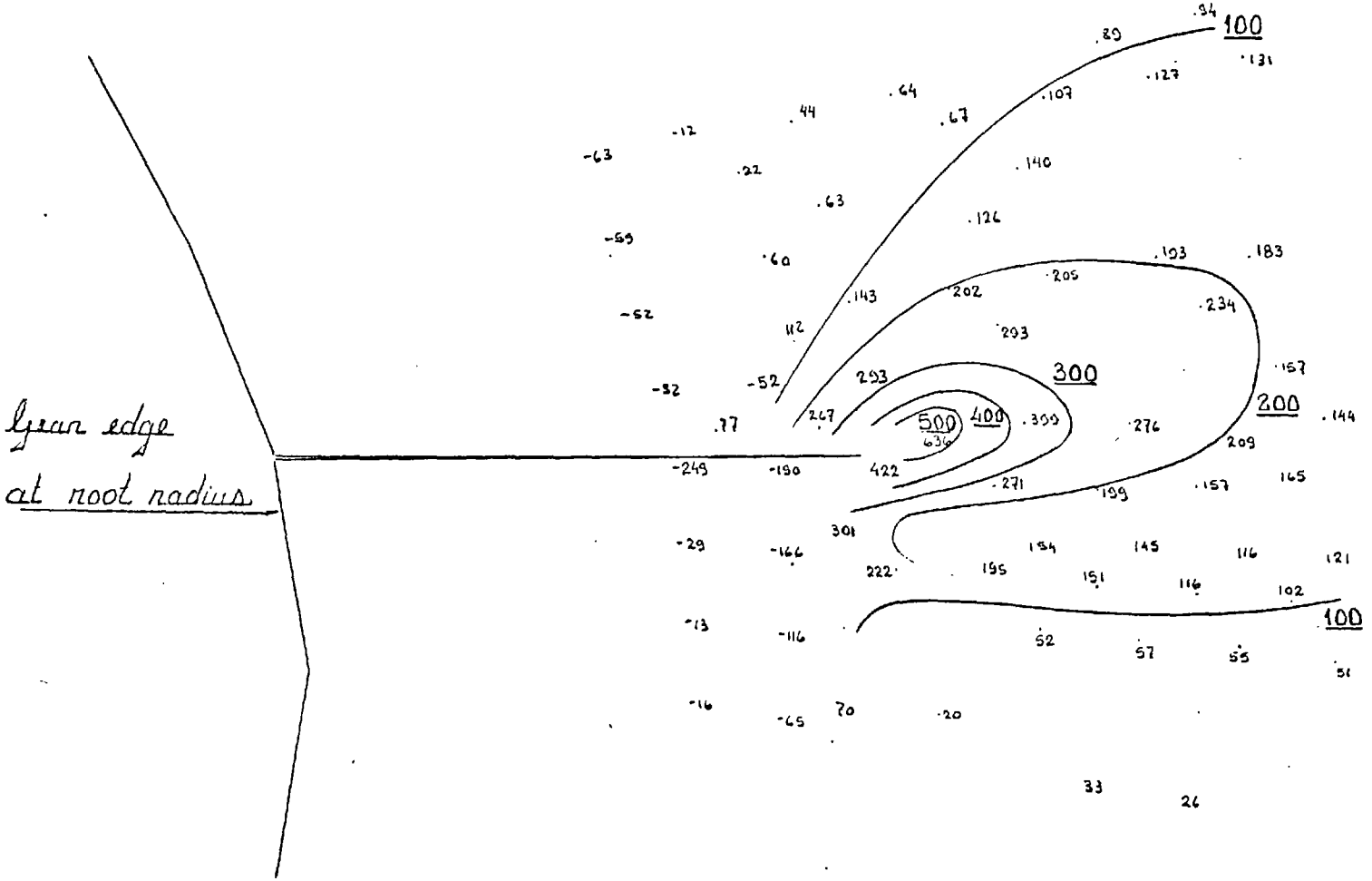

Fig 3.9(b) Lines of minimum principal stress.
Crack extension 1.03 mm.
Crack angle - 1.09140 rad.

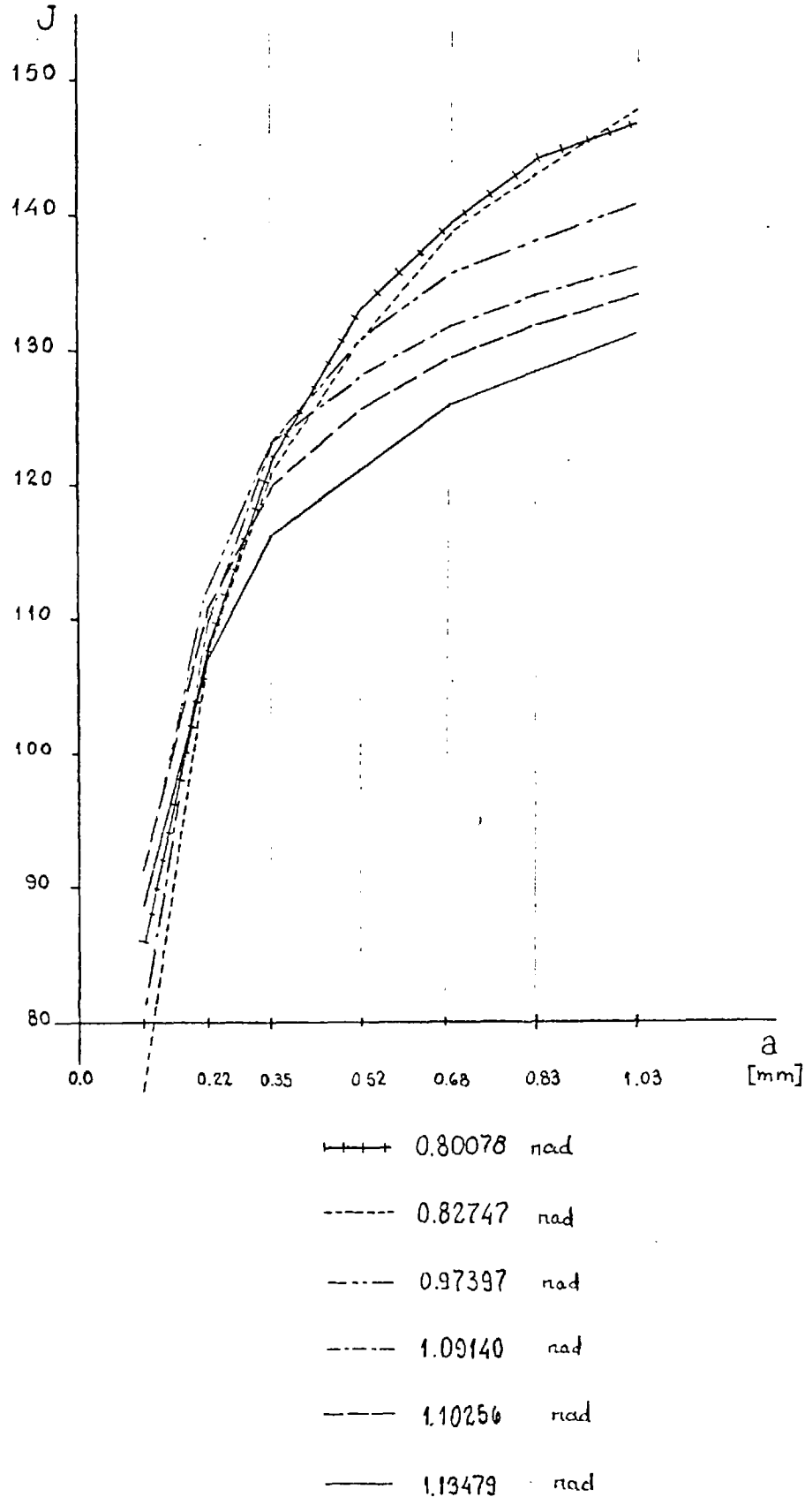

Fig 3.10 Values of the J contour Integral.

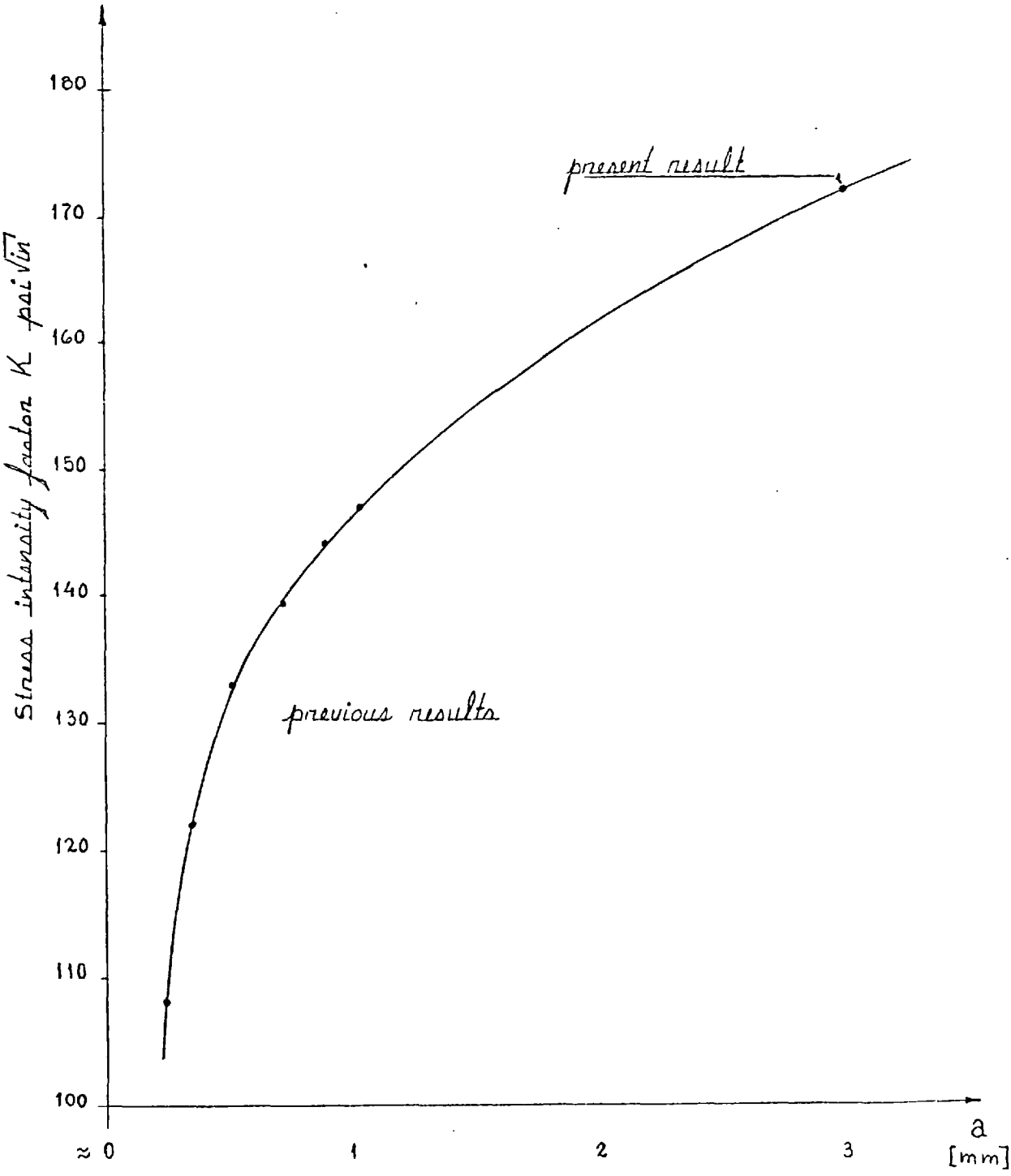

Fig 3.10(a) K values for cracked tooth form.

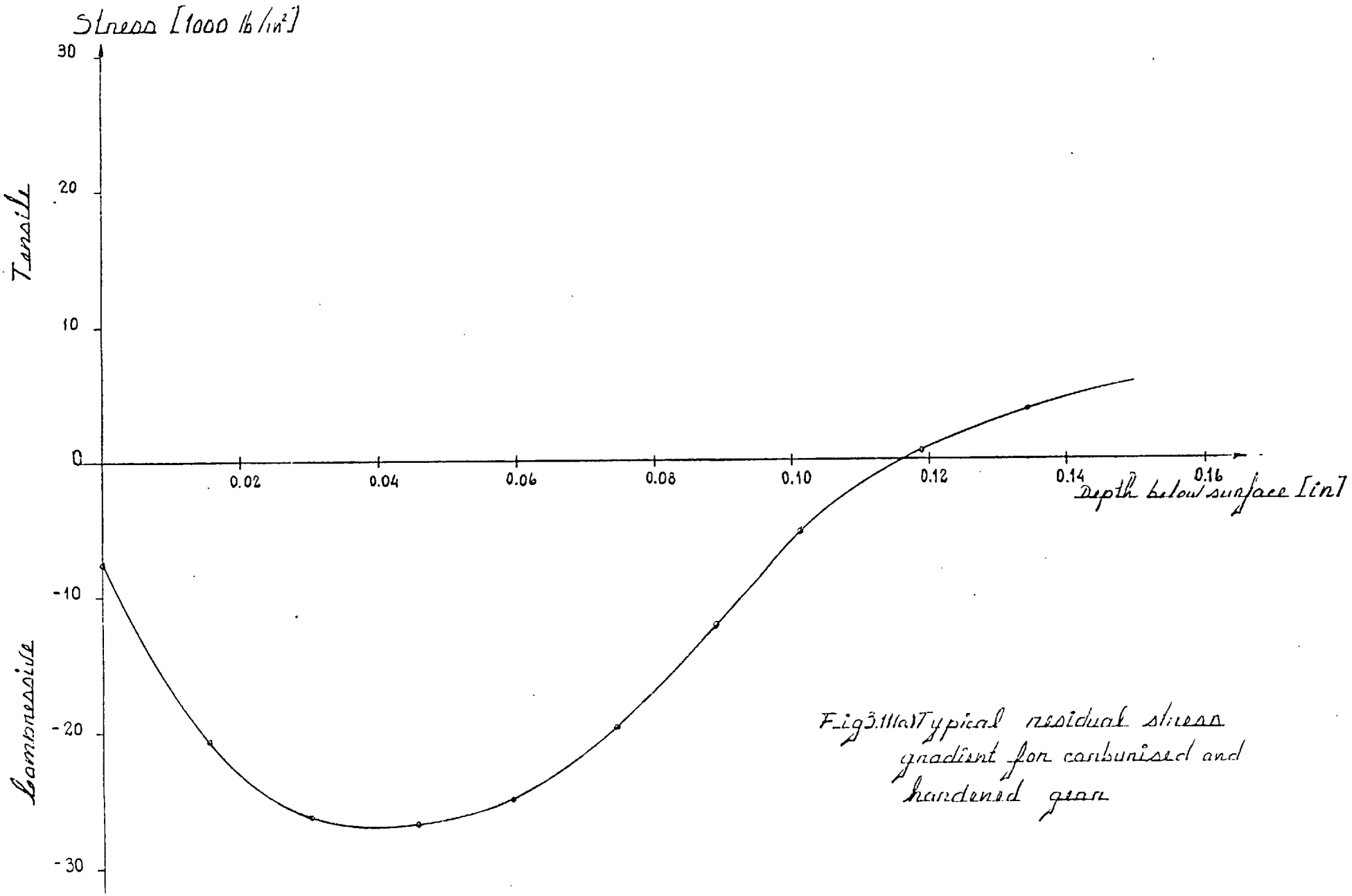

Fig 3.11(a) Typical residual stress gradient for carburised and hardened gear

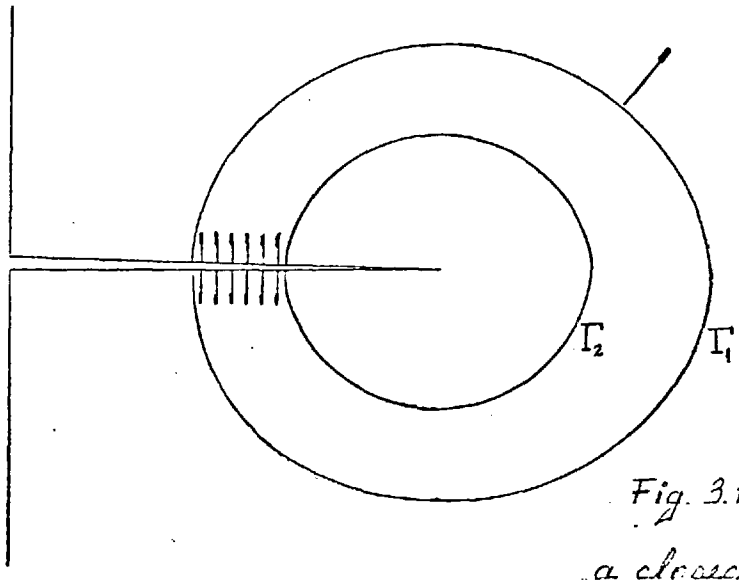

Fig. 3.11(b) Paths for a closed integral

Fig 3.12 A cracked arbitrary body subject to loading

a) Before } Virtual crack extension
b) After } Physical boundary conditions

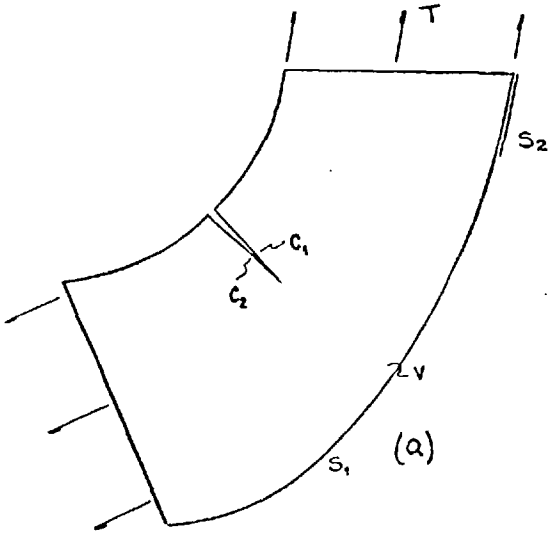

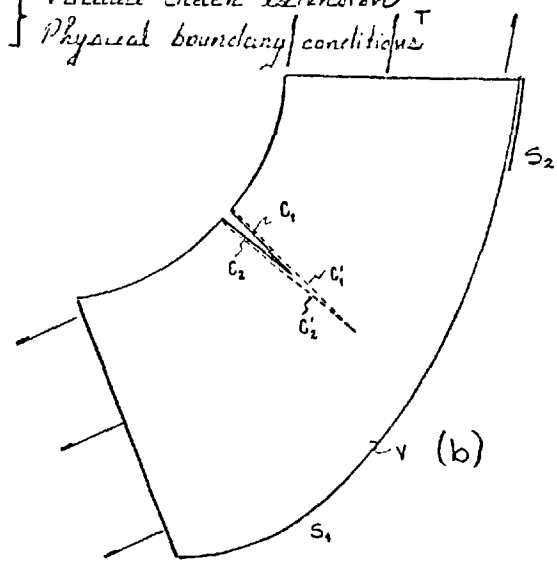

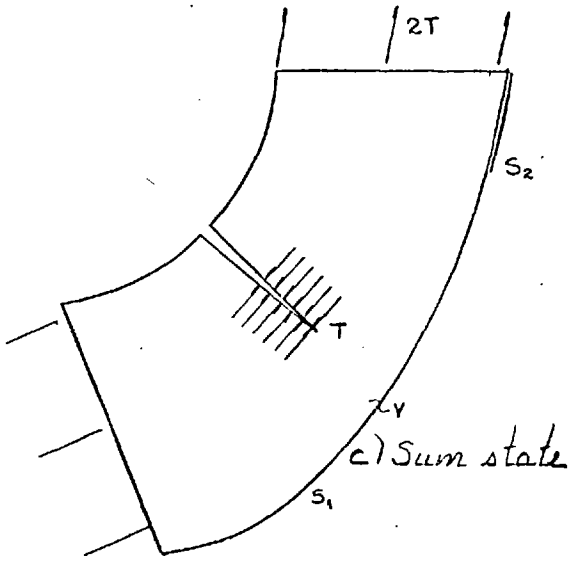

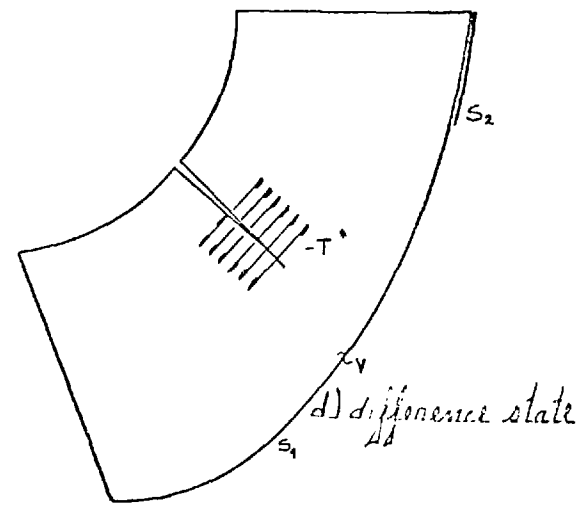

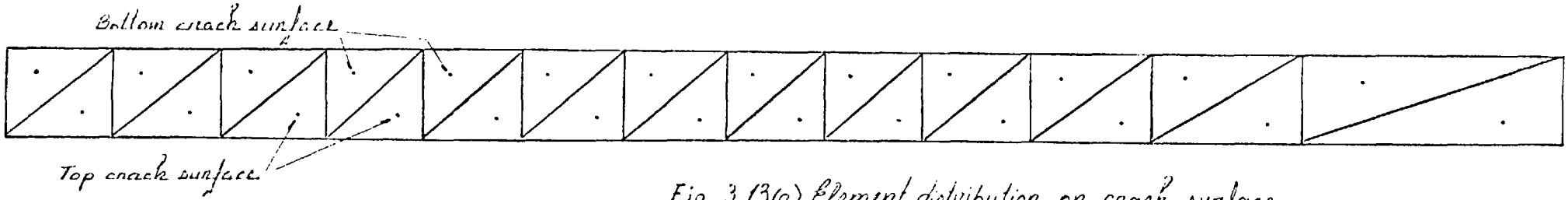

Fig. 3.13(a) Element distribution on crack surface

The stresses considered are those from the elements which centroid is the nearest to the crack surface

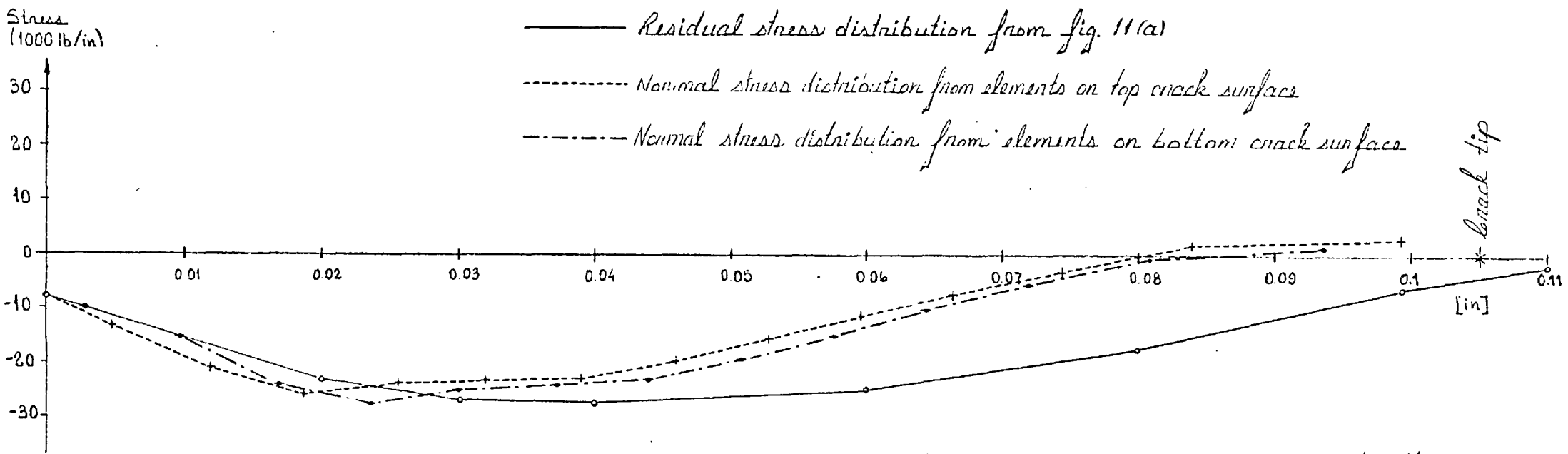

Fig 3.13(b) Stress distribution obtained from the finite element method

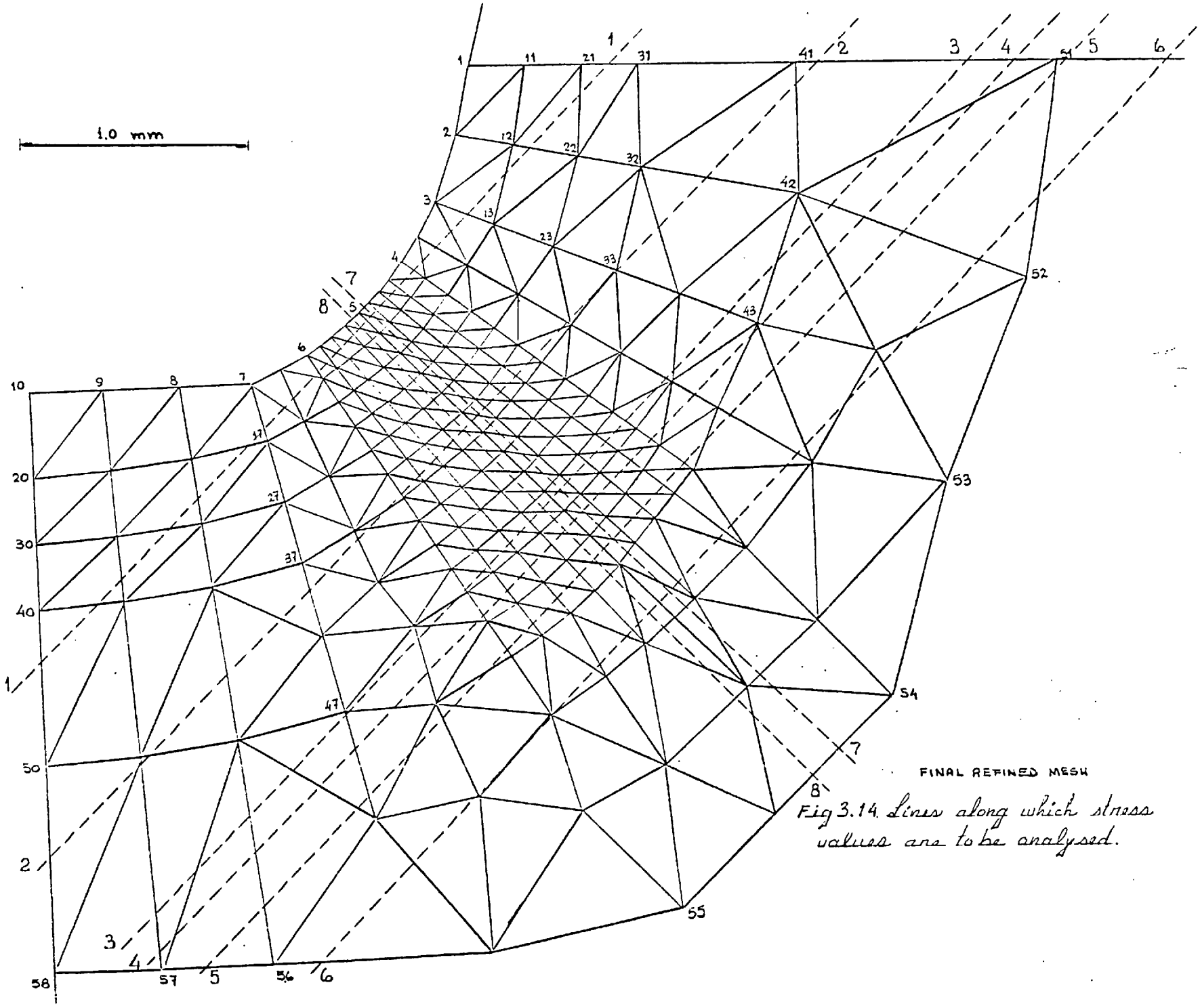

FINAL REFINED MESH

Fig 3.14 Lines along which stress values are to be analysed.

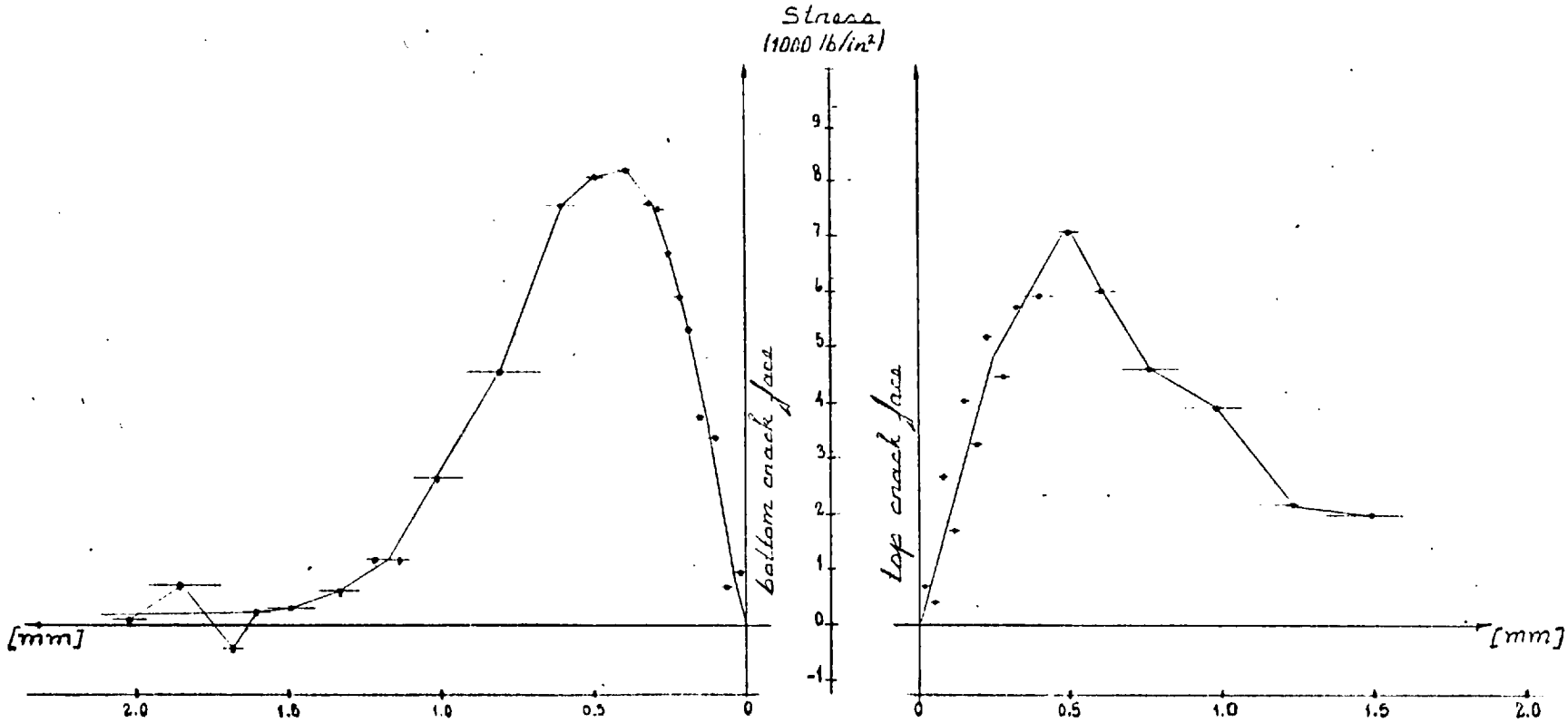

Fig. 3.15(a) Shear stress values along line number 1 from fig. 3.14

• actual stress value at the centroid of the element considered.

—— stress distribution

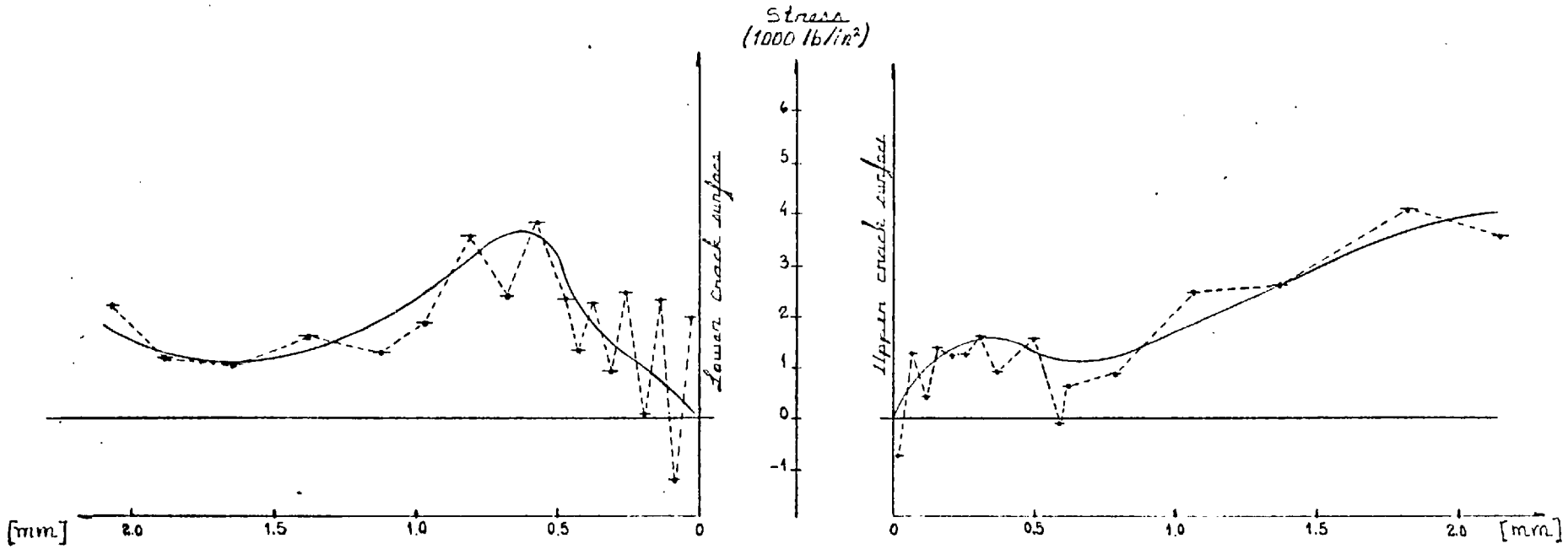

Fig. 3.15(b) Shear stress values along line number 3 from fig. 3.14

+ actual stress value at the centroid of the element considered.

—— stress distribution

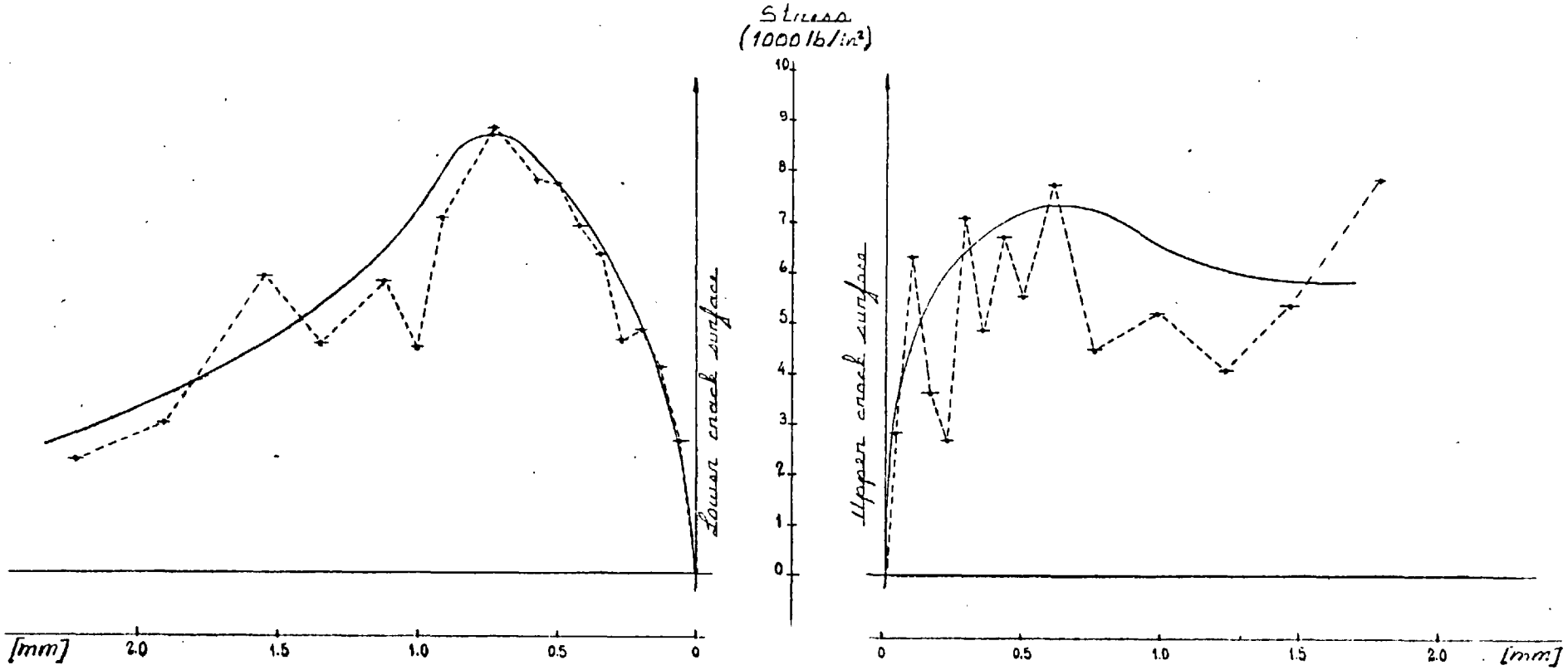

Fig 3.15(c) Shear stress values along line number 5 from fig 3.14

• actual stress value at the centroid of the element considered

— stress distribution

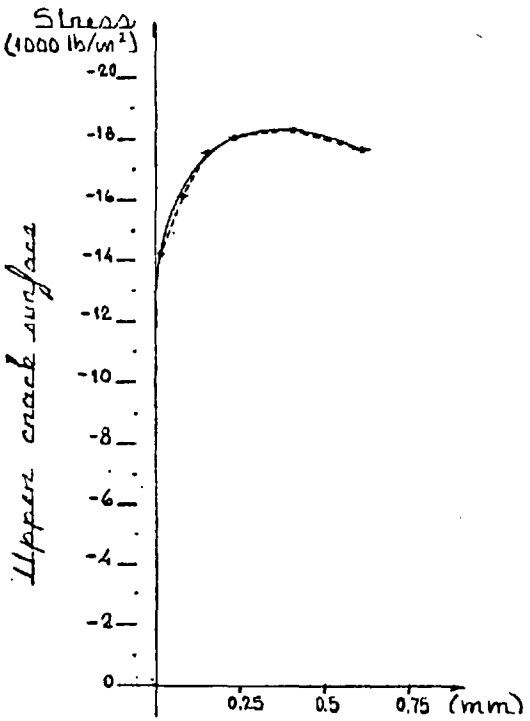

Fig. 3.15(d) Normal stress values along line number 1

• actual stress value at the centroid of the element

—— stress distribution

The tendency of the stress curves is towards the expected values

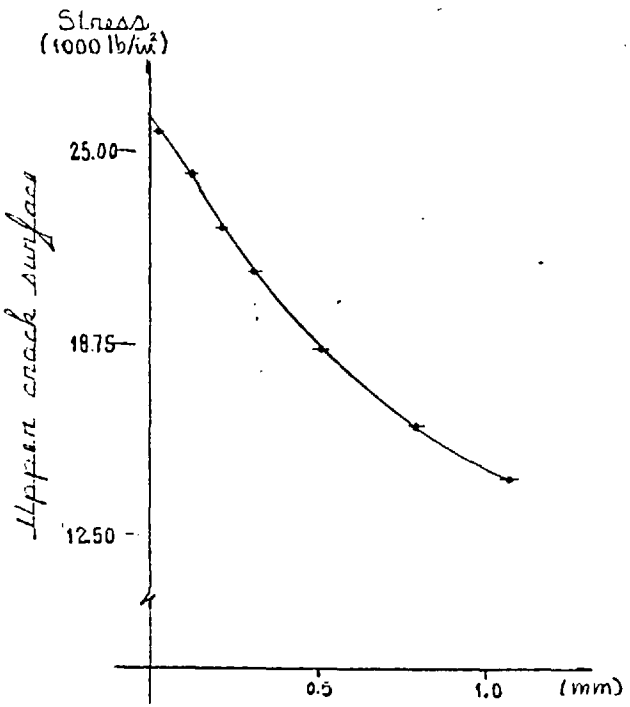

Fig. 3.15(a) Normal stress values along line number 2

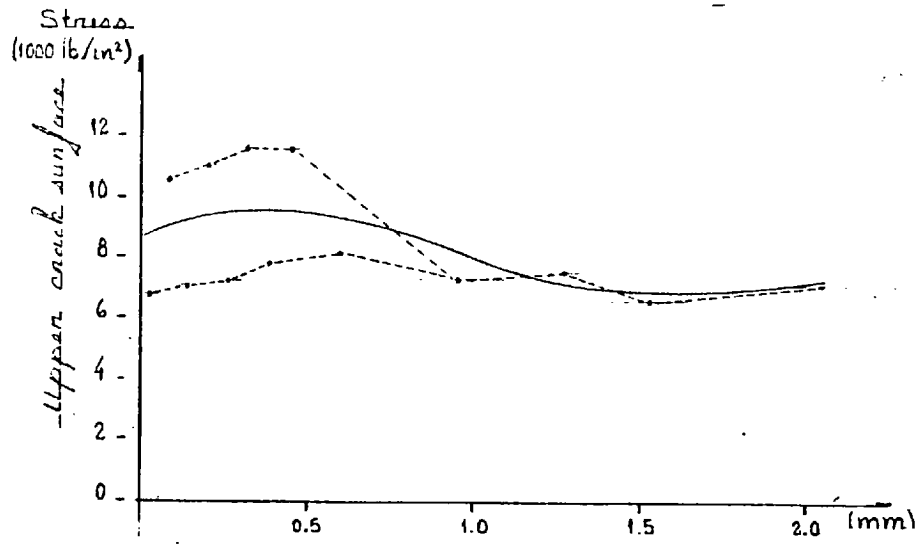

Fig 3.15(f) Normal stress values along line No. 3

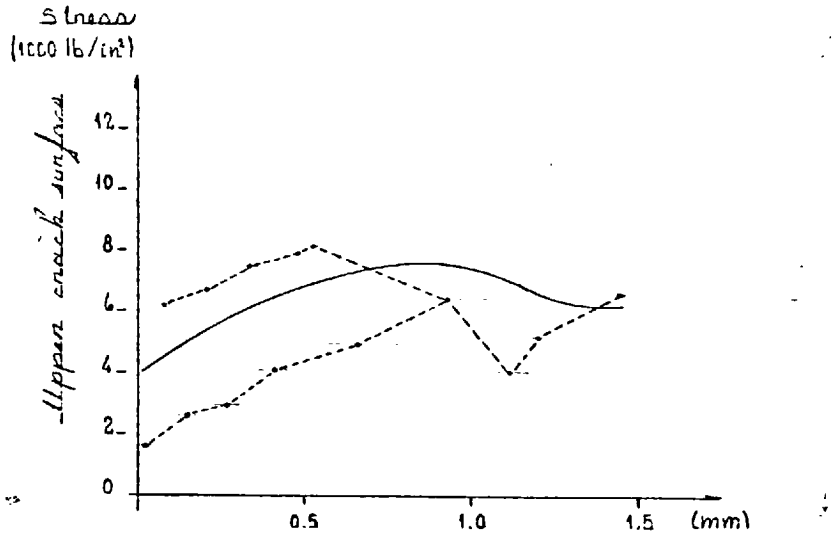

Fig 3.15(g) Normal stress values along line N°4

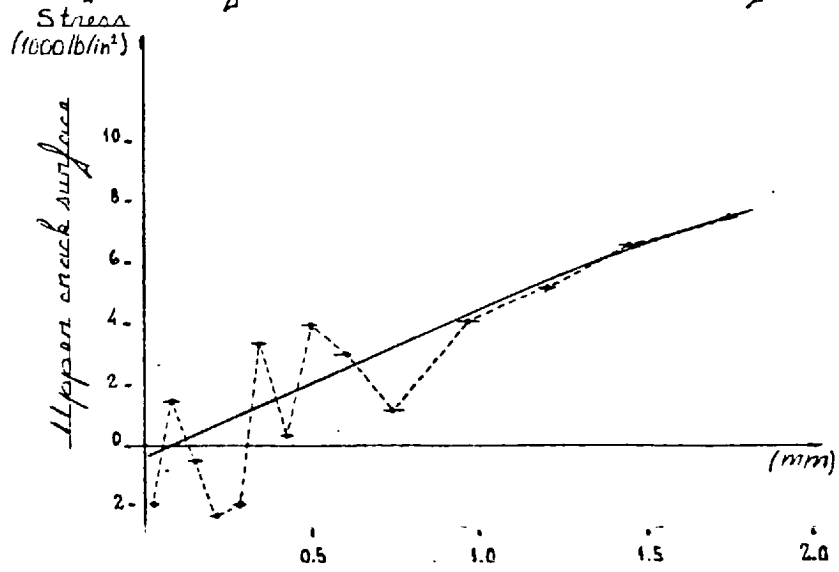

Fig 3.15(h) Normal stress values along line N°5

— actual stress value at the centroid of the element

— stress distribution

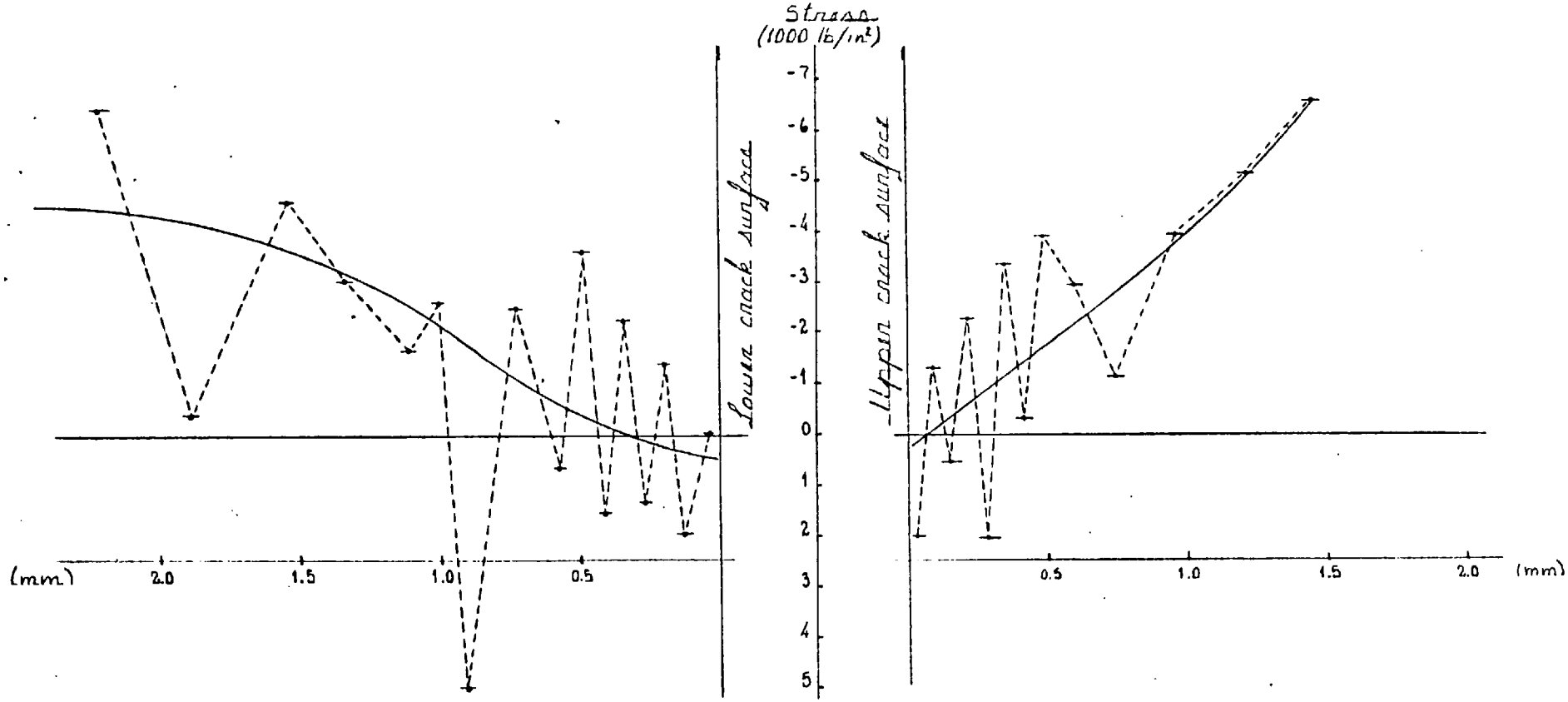

Fig 3.15(i) Normal stress values along line number 5 from fig. 3.14

• actual stress value at the centroid of the element considered.

—— probable stress distribution

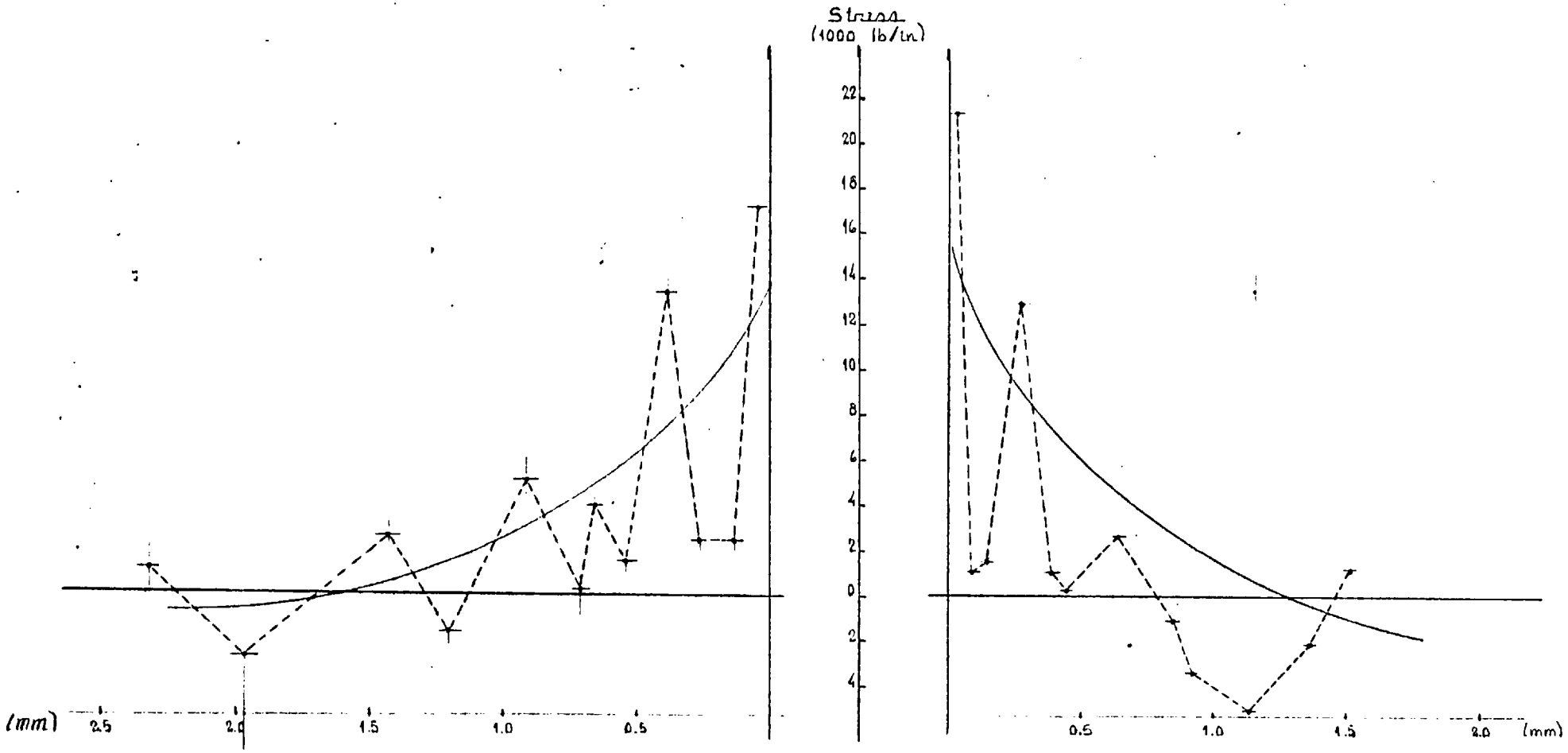

Fig. 3.15(j) Normal stress values along line number 6 from fig. 3.14

— actual stress value at the centroid of the element considered.

—— Stress distribution

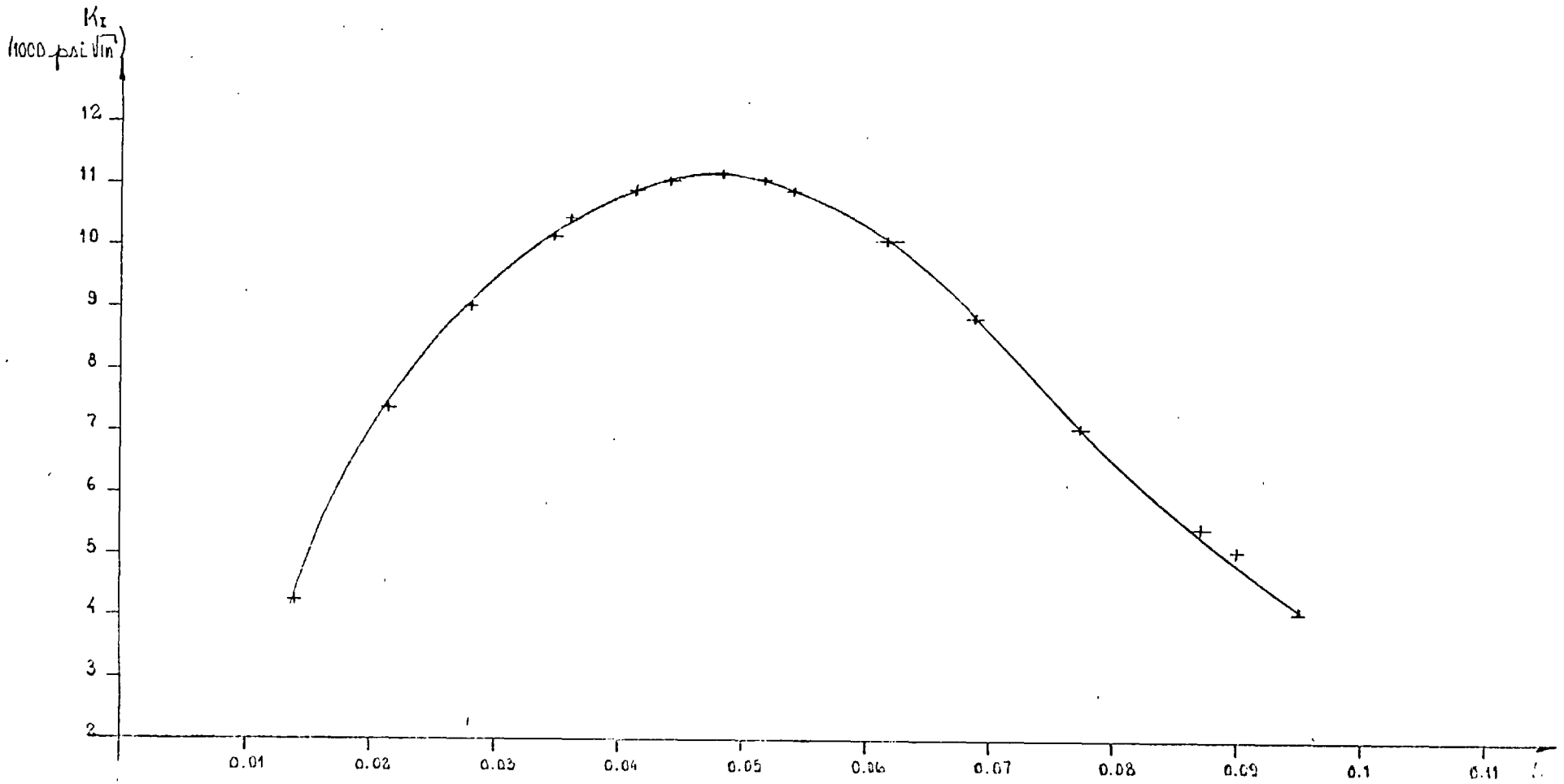

Fig 3.16 K_I values as given by a fitting polynomial of seventh order

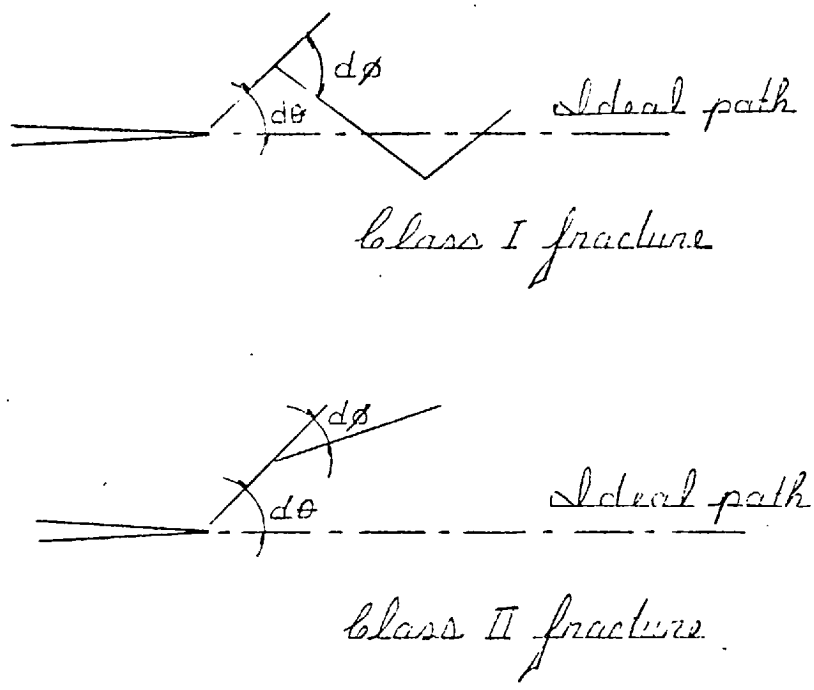

Fig 5.1 Fracture path

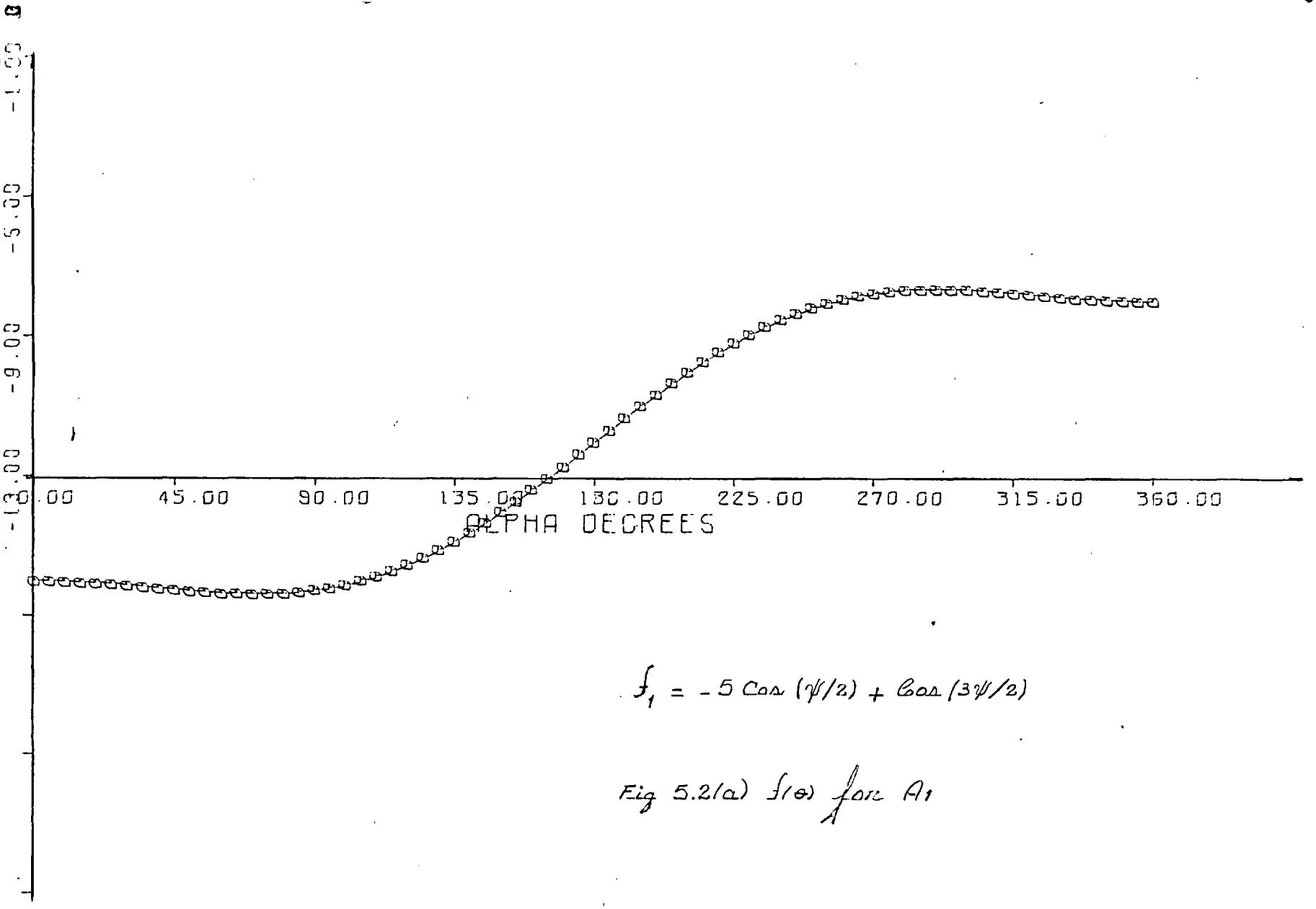

$$f_1 = -5 \cos(\psi/2) + \cos(3\psi/2)$$

Fig 5.2(a) $f(\theta)$ for A_1

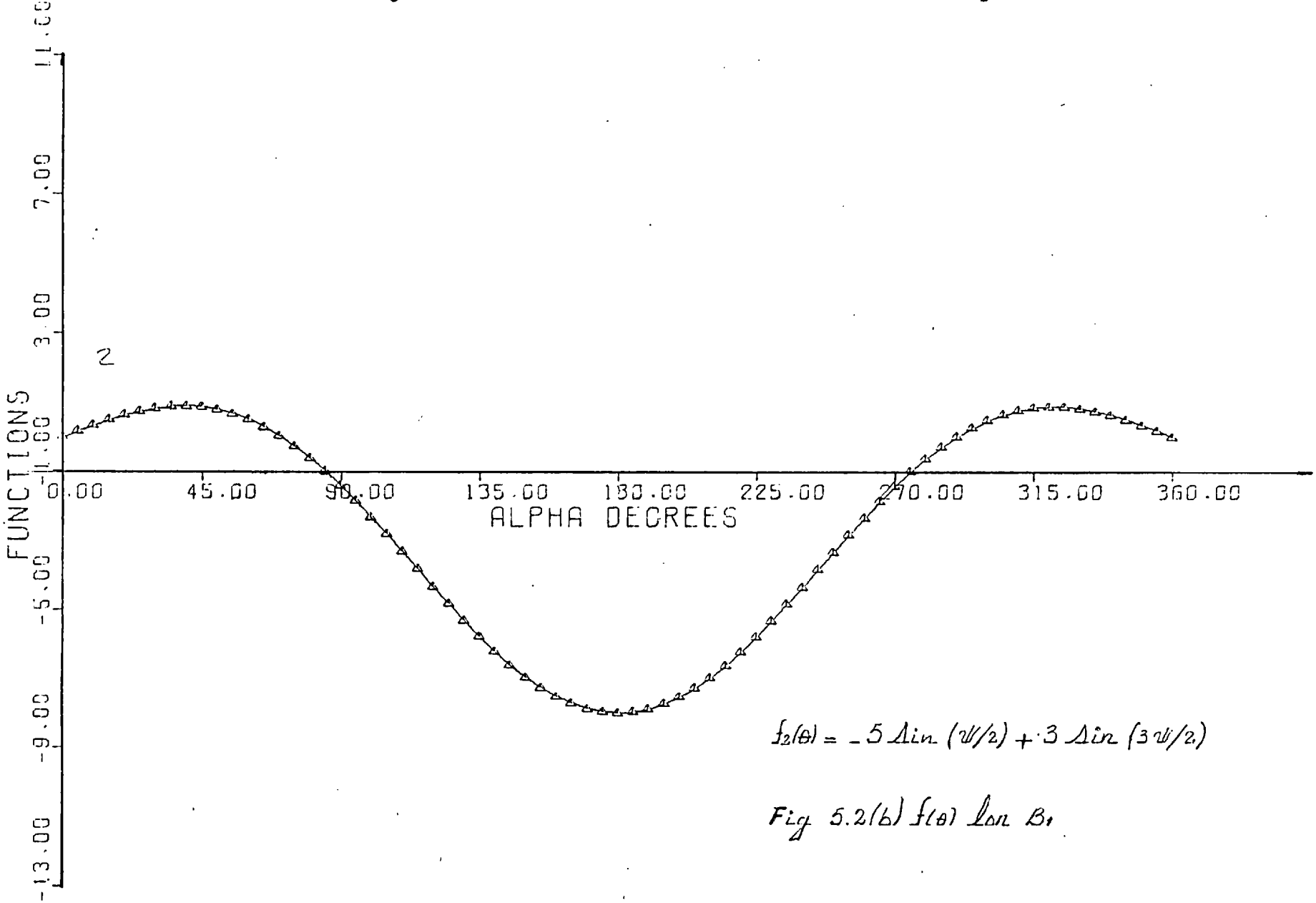

$f_2(\theta) = -.5 \sin(\theta/2) + .3 \sin(3\theta/2)$

Fig 5.2(b) $f(\theta)$ for B_1

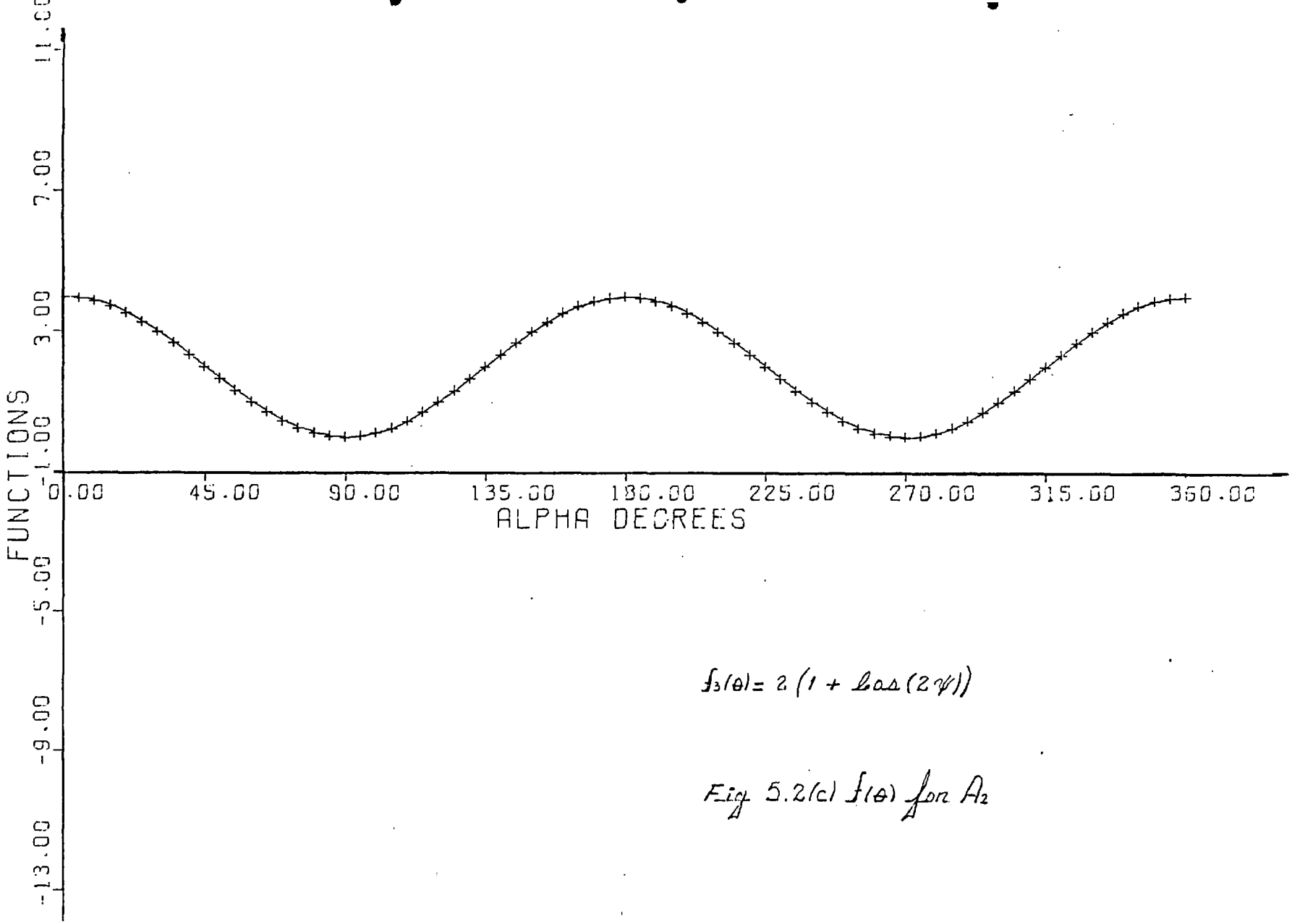

$f_3(\theta) = 2\,(1 + \cos(2\psi))$

Fig 5.2(c) $f(\theta)$ for A_2

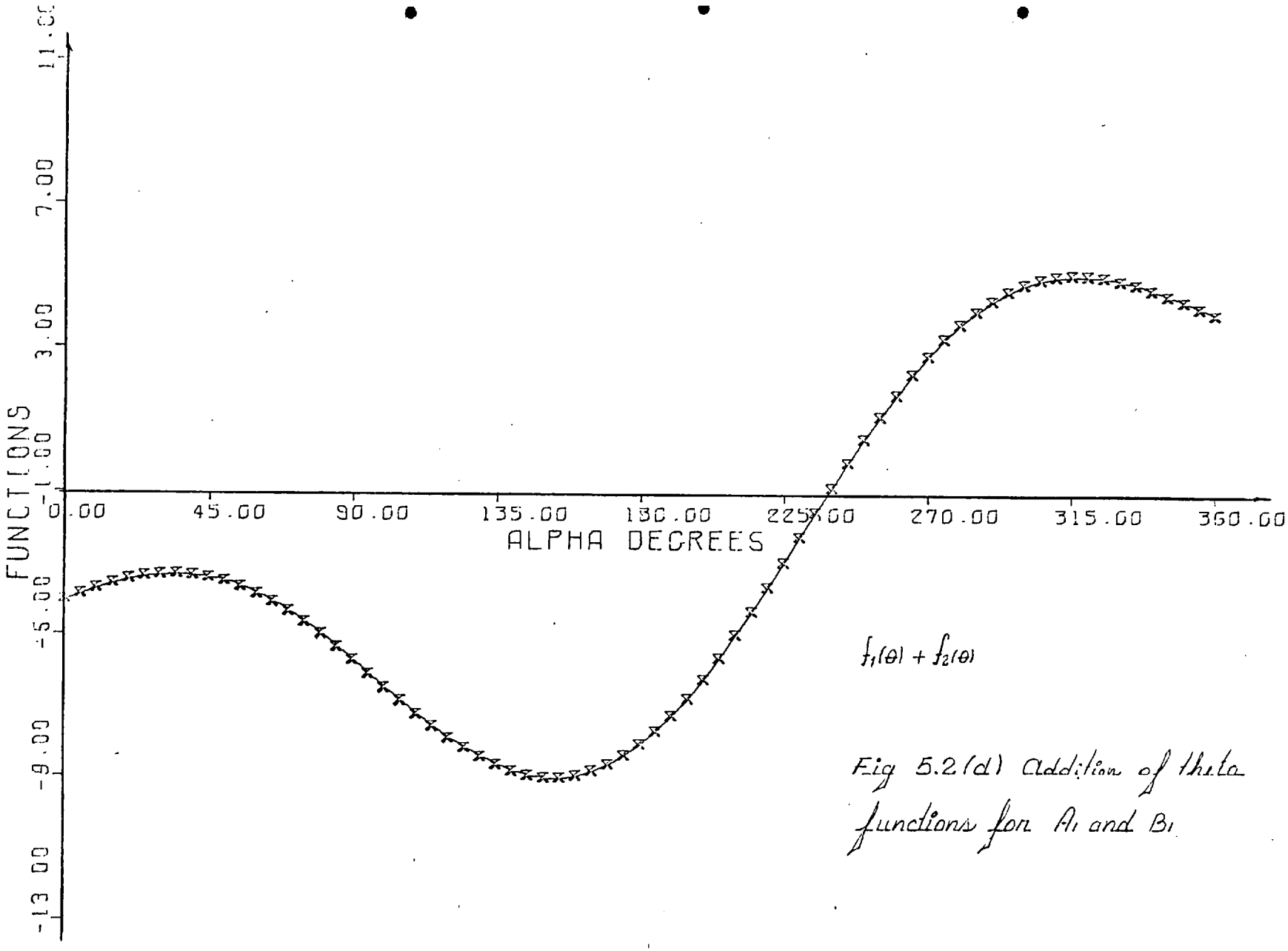

$f_1(\theta) + f_2(\theta)$

Fig 5.2(d) Addition of theta functions for A_1 and B_1

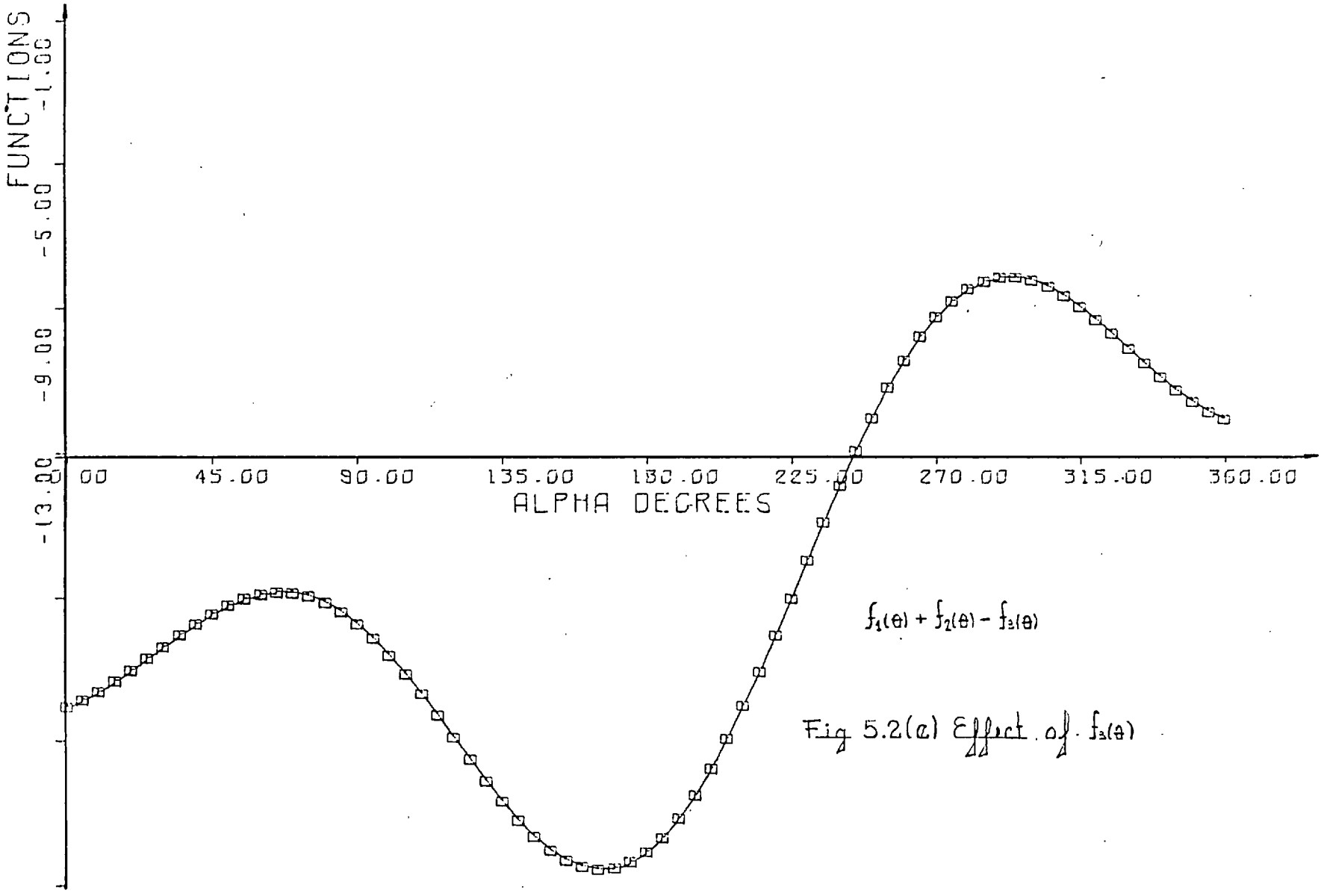

Fig 5.2(a) Effect of $f_3(\theta)$

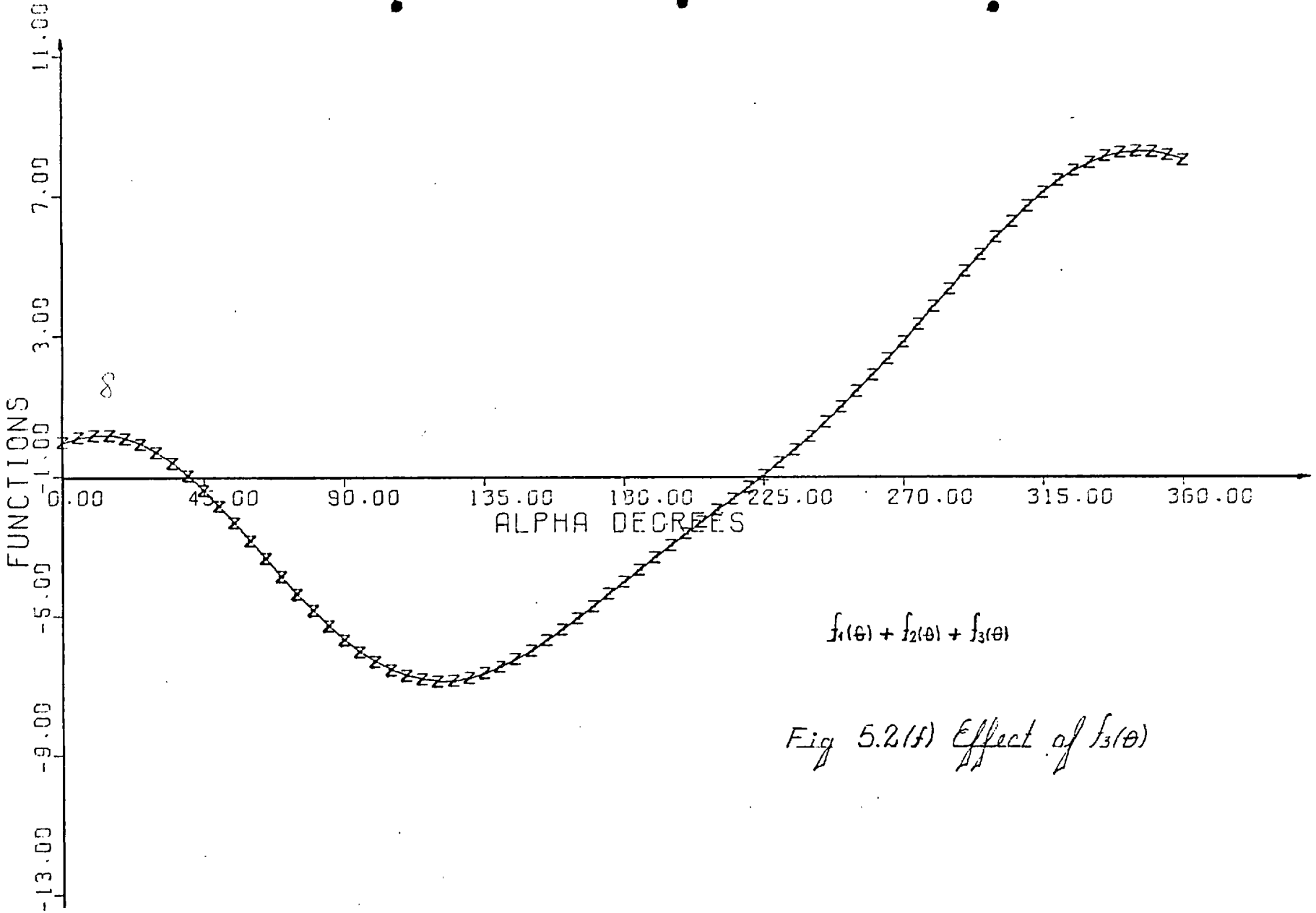

Fig 5.2(f) Effect of $f_3(\theta)$

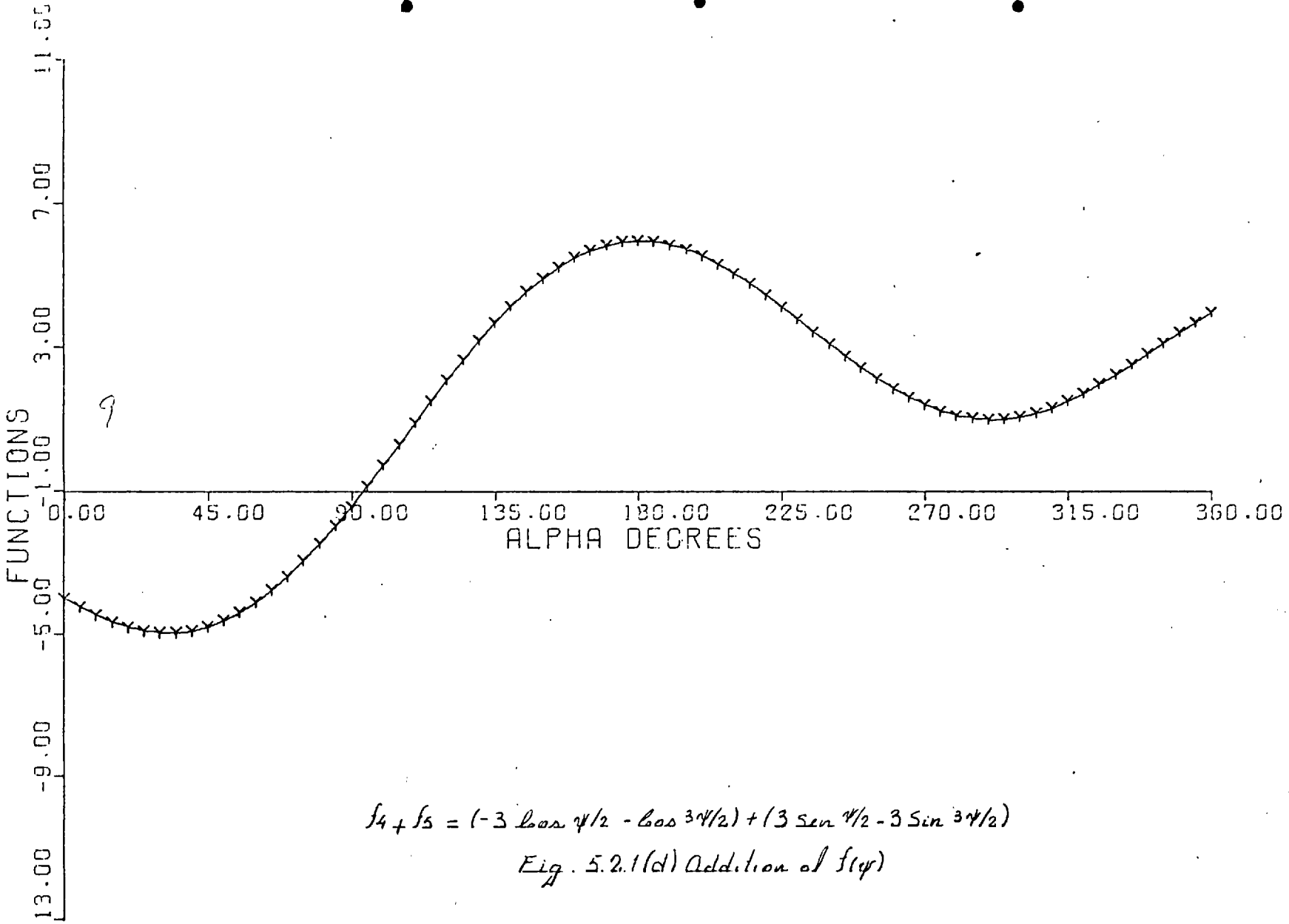

$f_4 + f_5 = (-3 \cos \psi/2 - \cos 3\psi/2) + (3 \operatorname{sen} \psi/2 - 3 \operatorname{Sin} 3\psi/2)$

Fig. 5.2.1(d) Addition of $f(\psi)$

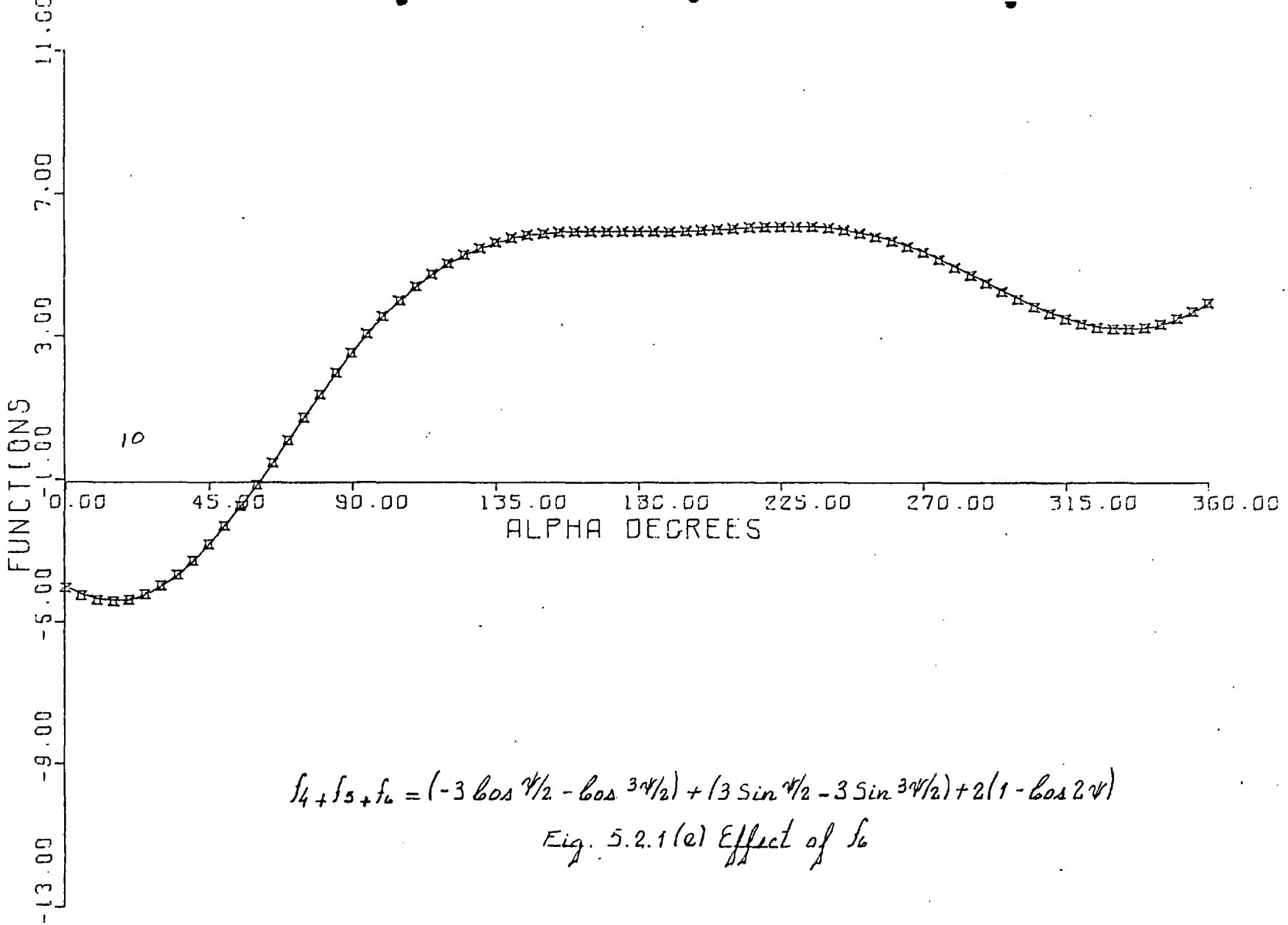

$$f_4 + f_5 + f_6 = (-3\cos\psi/2 - \cos 3\psi/2) + (3\sin\psi/2 - 3\sin 3\psi/2) + 2(1 - \cos 2\psi)$$

Fig. 5.2.1(e) Effect of f_6

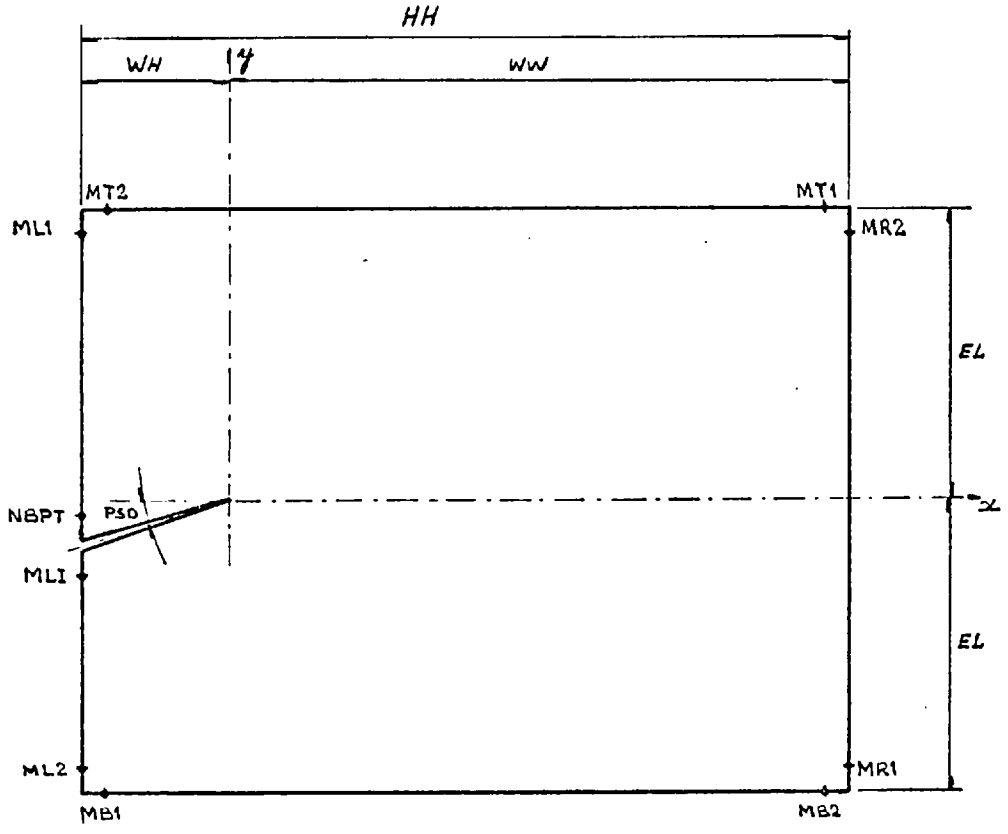

Fig 5.3 Specimen dimensions and position of some of the boundary stations as defined in programme ANGCRK

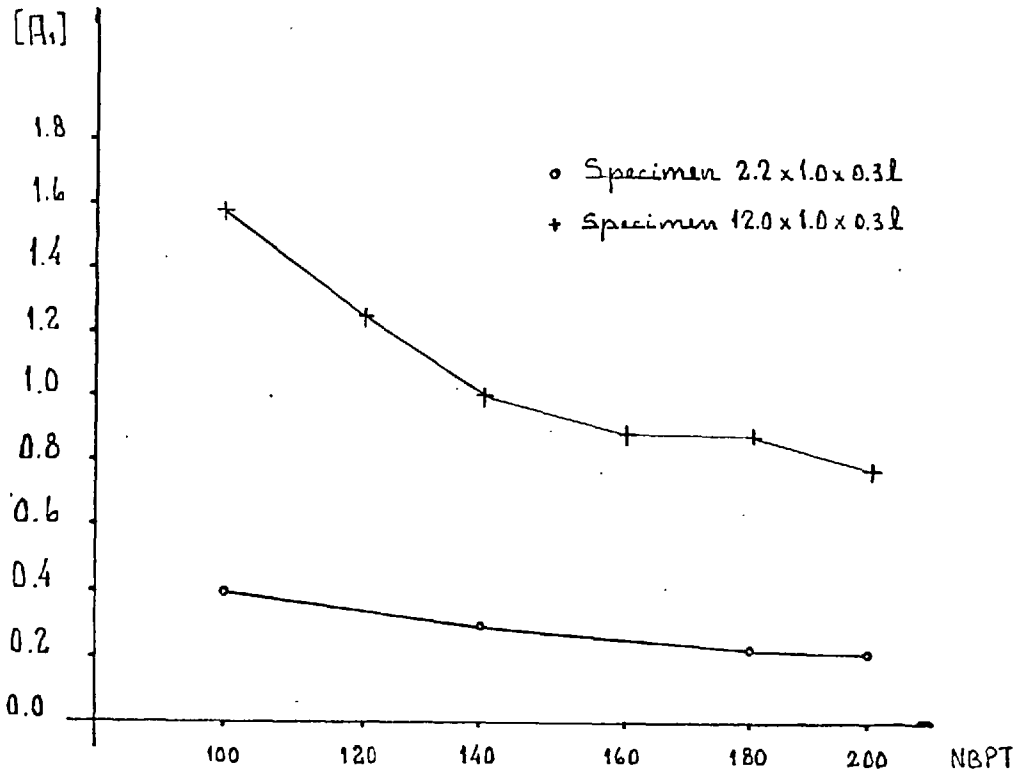

Fig. 5.4(a) Convergence for A_1 values.

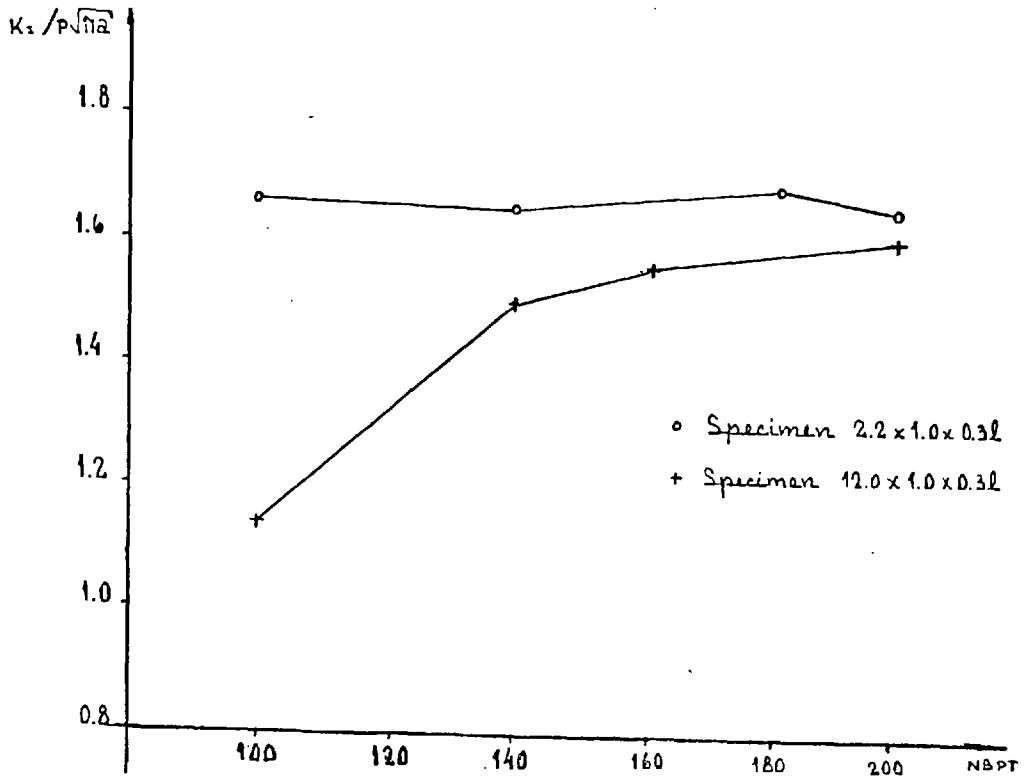

Fig. 5.4(b) Convergence for K_I

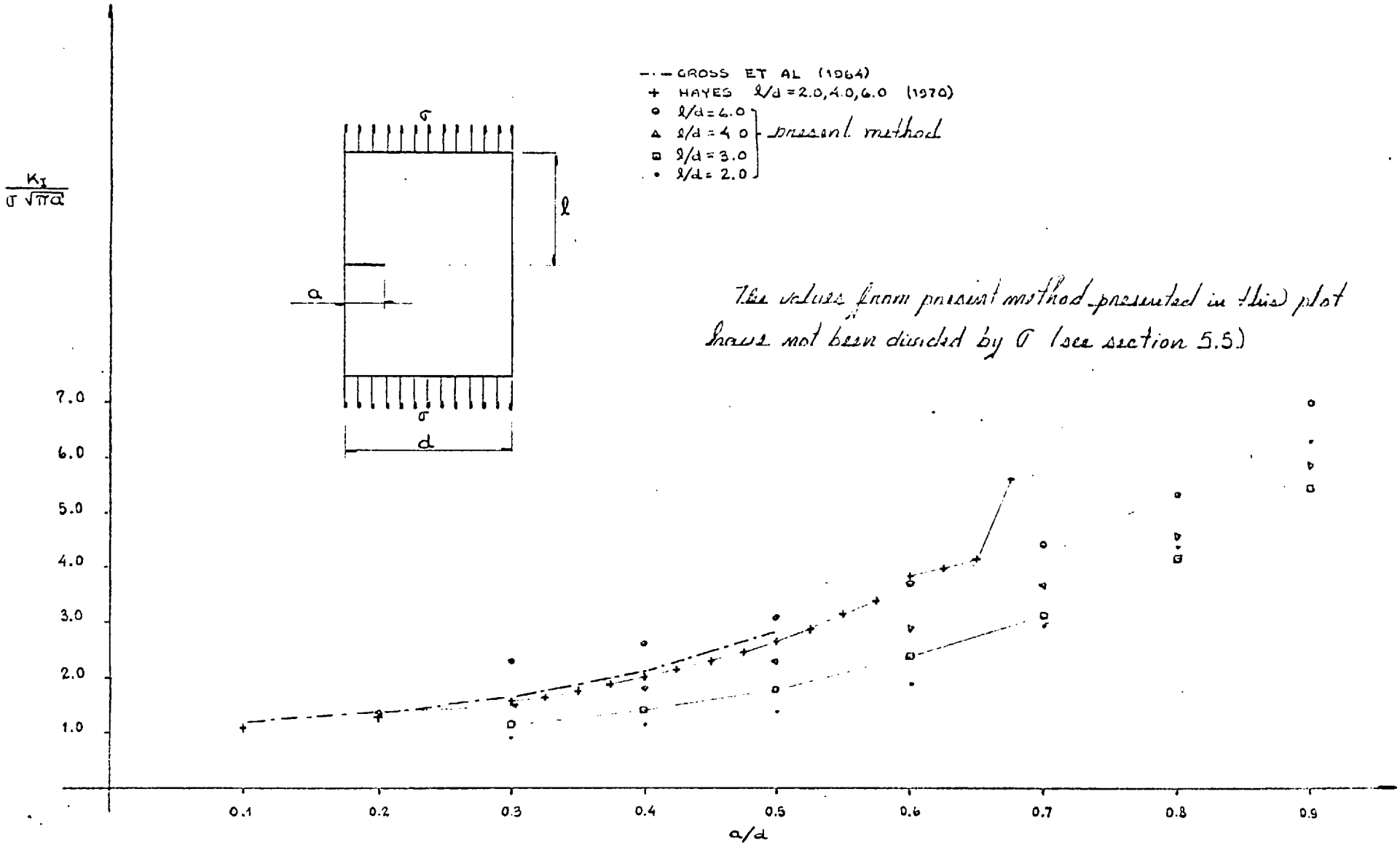

FIG 5.5 STRESS INTENSITY FACTORS FOR UNIFORMLY LOADED SINGLE EDGE CRAKED PLATE.

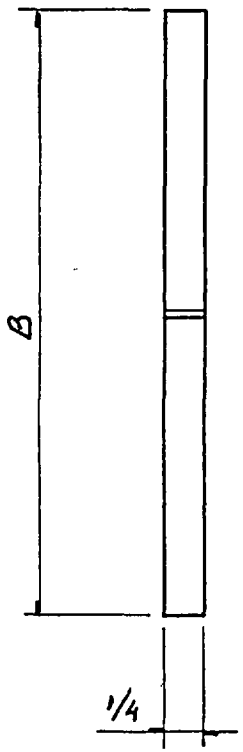

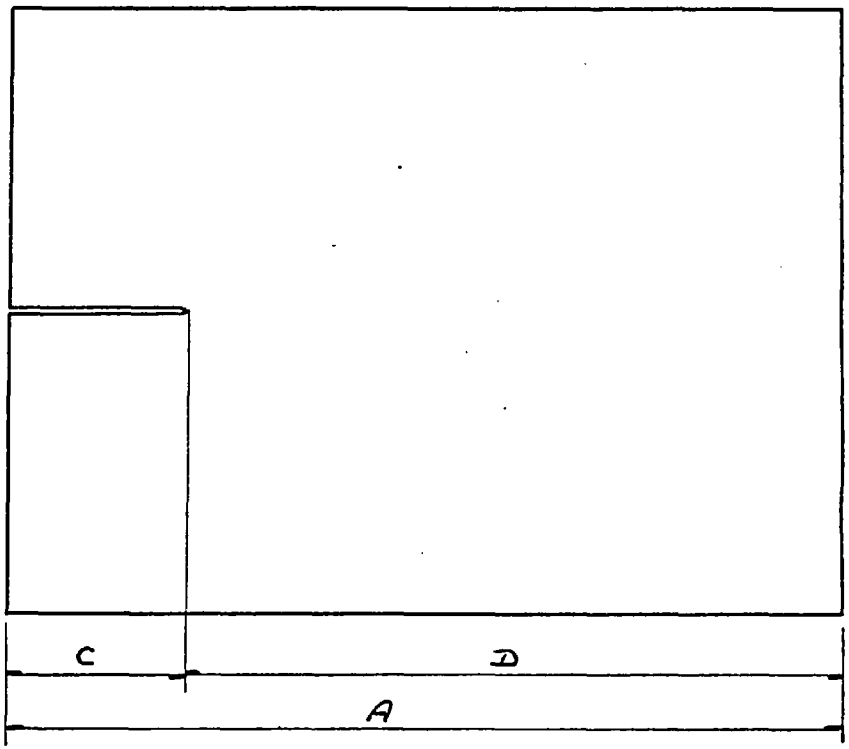

A = 12 to 4 [in]
B = 4 to 1 [in]
C = 0.3 A [in]

FIG. Nº 6.1 Specimen dimensions.

UNLESS SPECIFIED

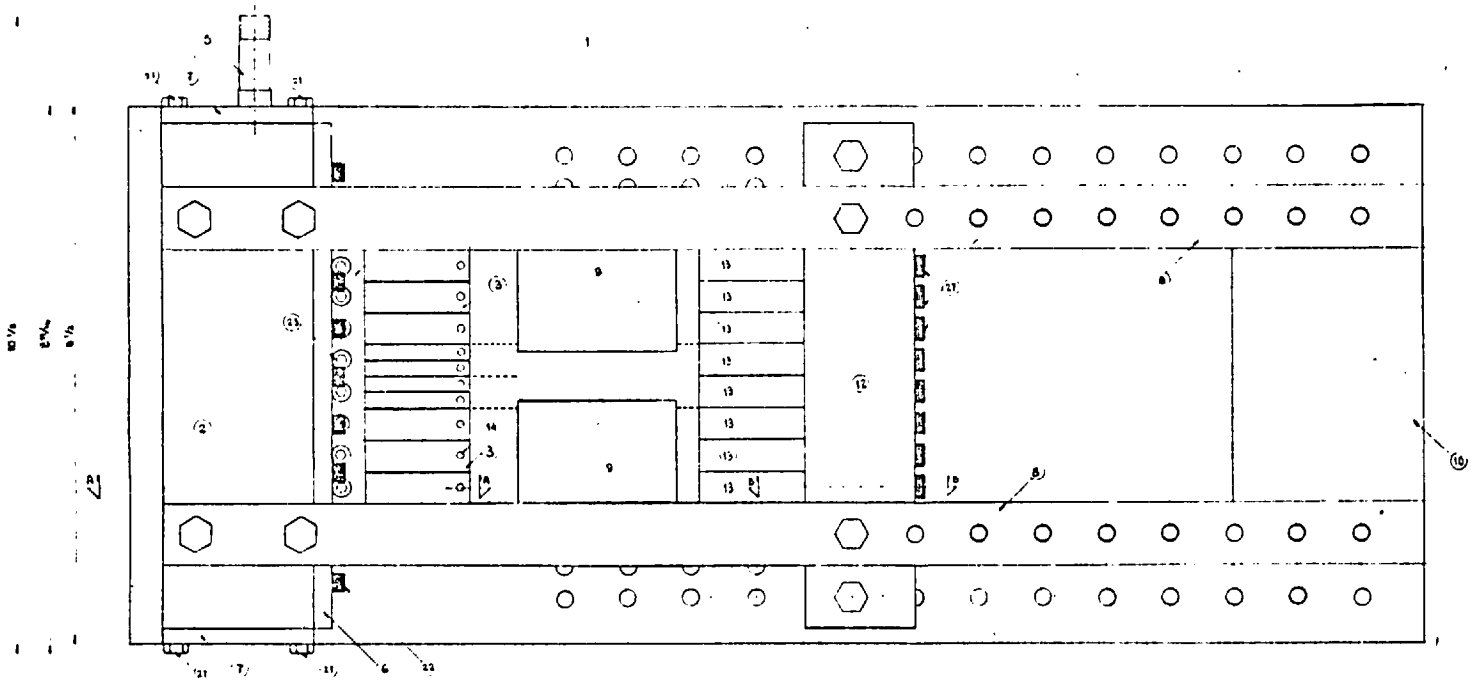

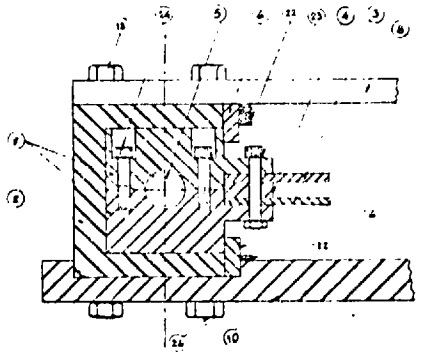

SECTION AA

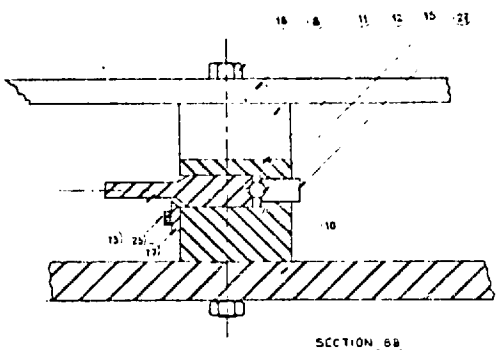

SECTION BB

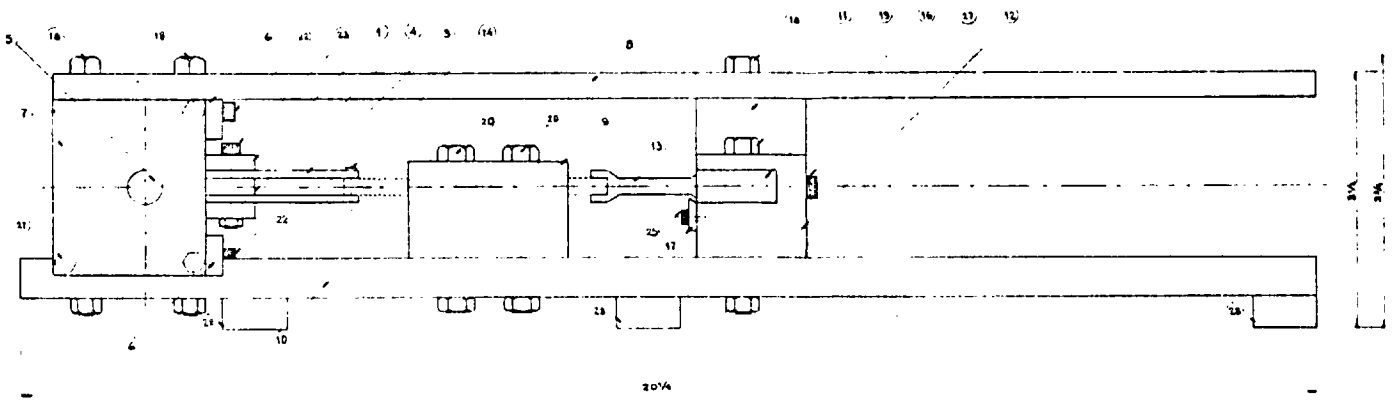

Fig. 6.2 Fracture rig for biaxial loading

PART No	No OFF	DESCRIPTION	MATERIAL	REMARKS

Mechanical Engineering Dept.	DRAWN		SCALE	TITLE	FRACTURE RIG FOR BIAXIAL LOADING	CLASS	DRAWING NUMBER
Imperial College,	APPROVED						
London SW7 2BX	TRACED		DATE	AMMDTS		GROUP	NAME
	CHECKED					FRACTURE	ASSEMBLY

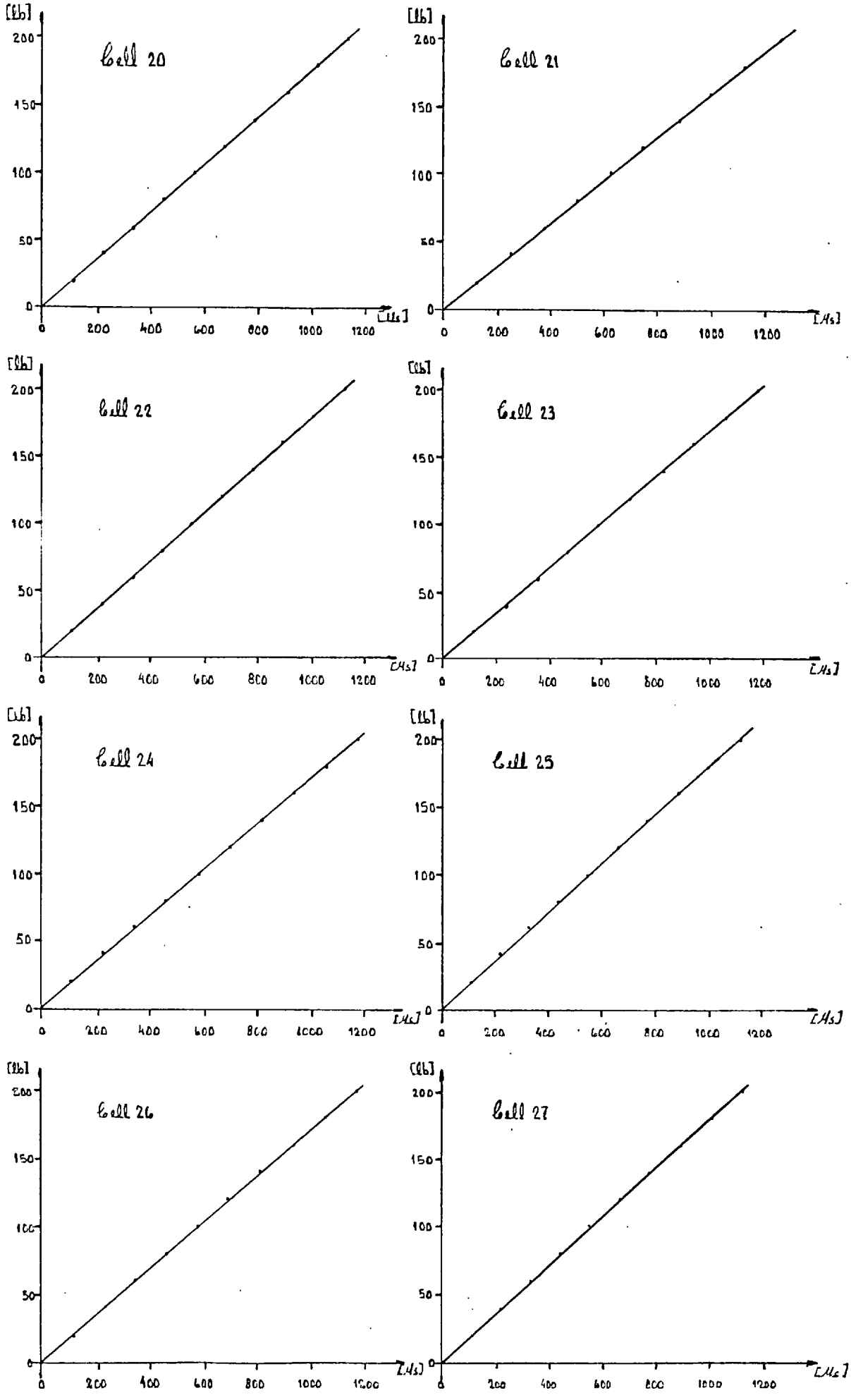

Fig. 6.3(a) Load calibration for transverse load cells

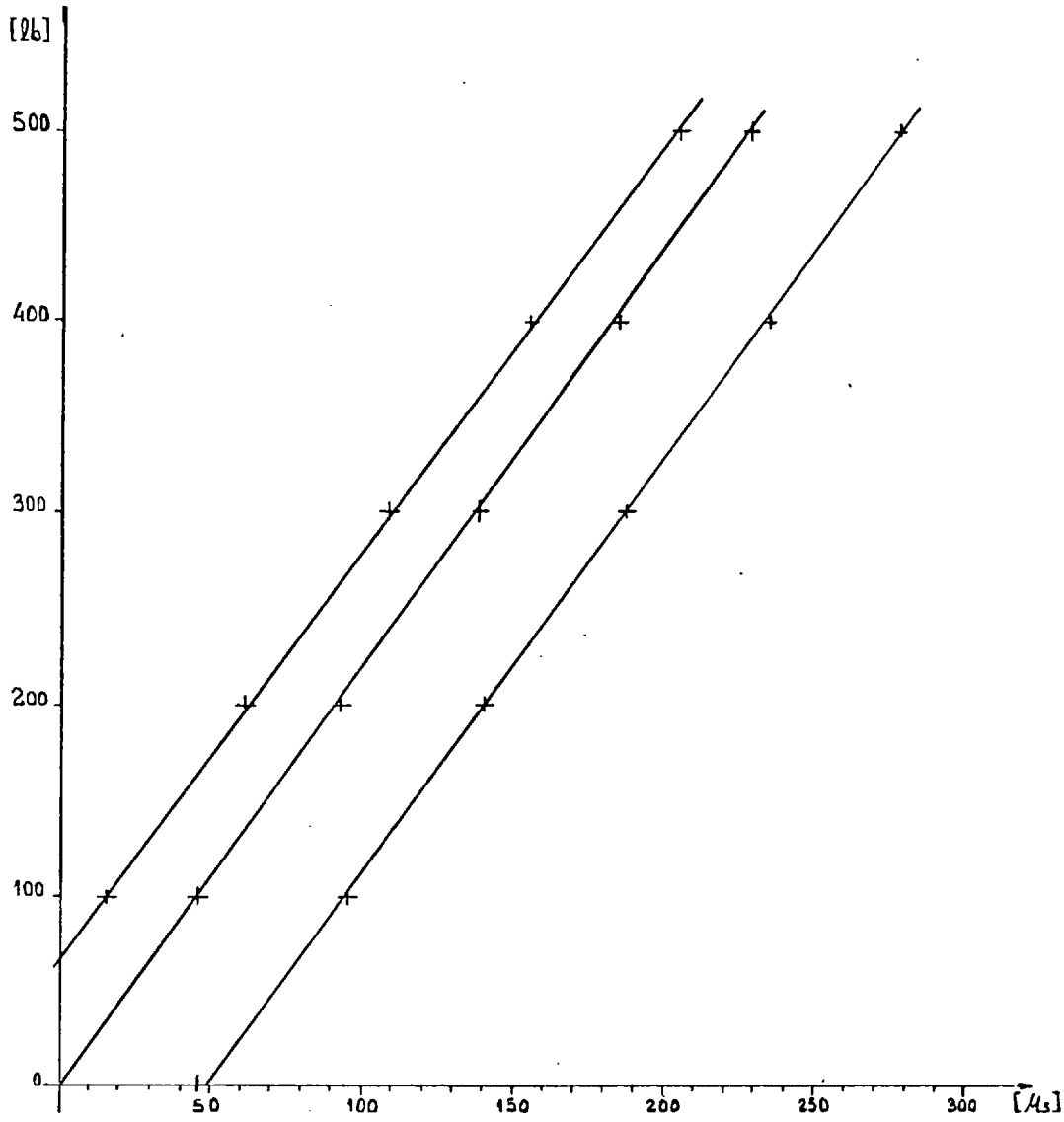

Fig 6.3(b) Load calibration for opening load cell different transverse loading conditions.

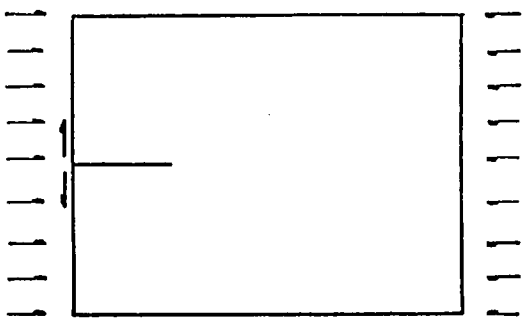

(a)

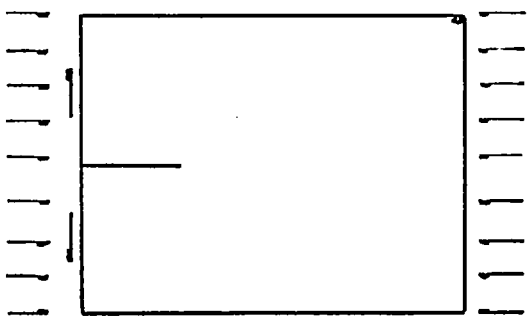

(b)

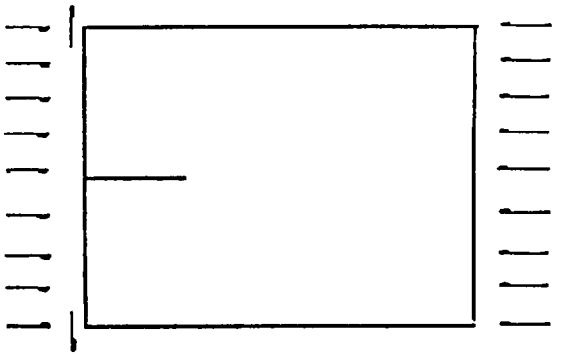

(c)

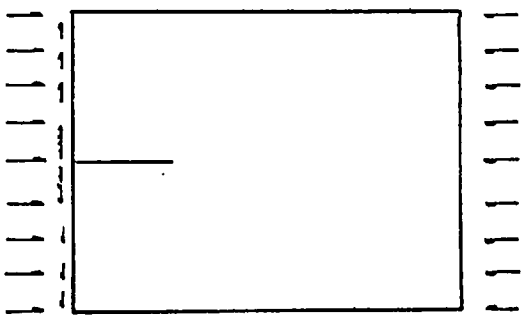

(d)

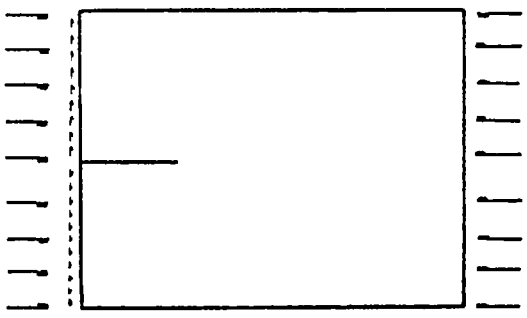

(e)

Fig 6.4 Description of loading conditions for testing loading effects.

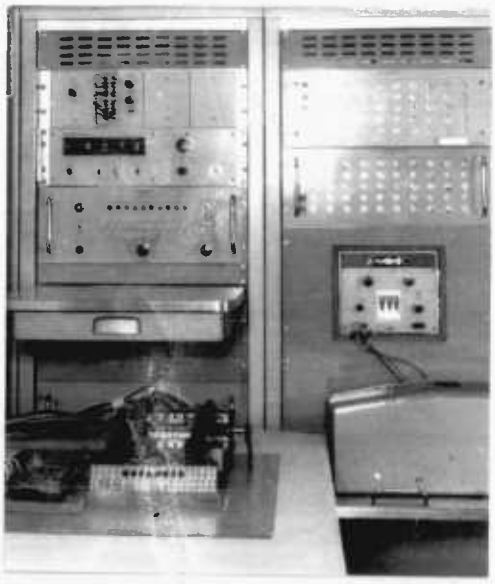

Fig 6.5 Data log and experimental rig

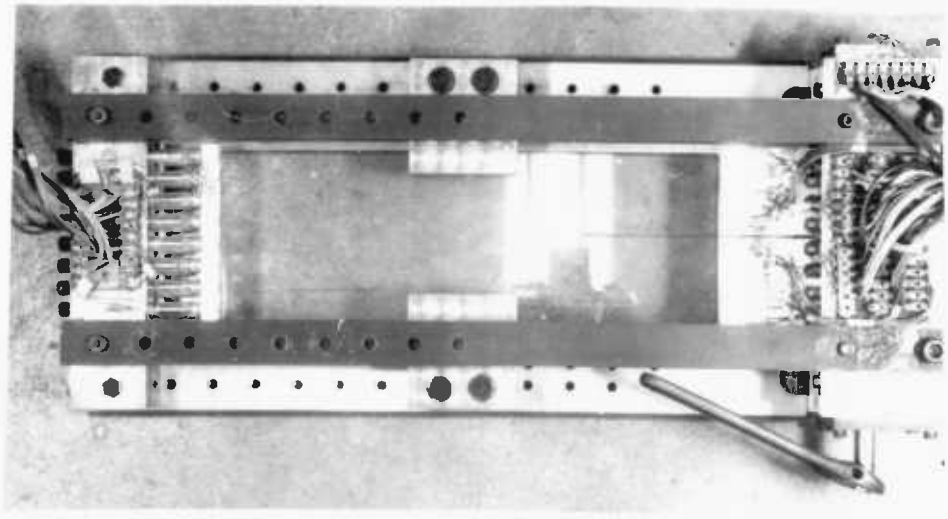

Fig 6.5(a) Calibration of strain gauges for transverse load

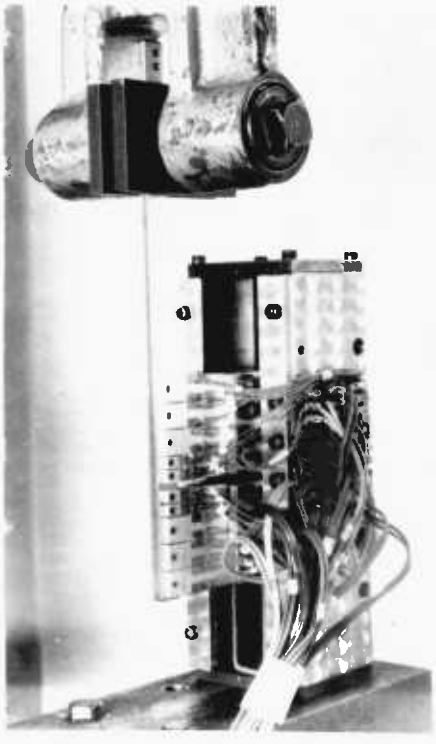

Fig 6.5(b) Detail

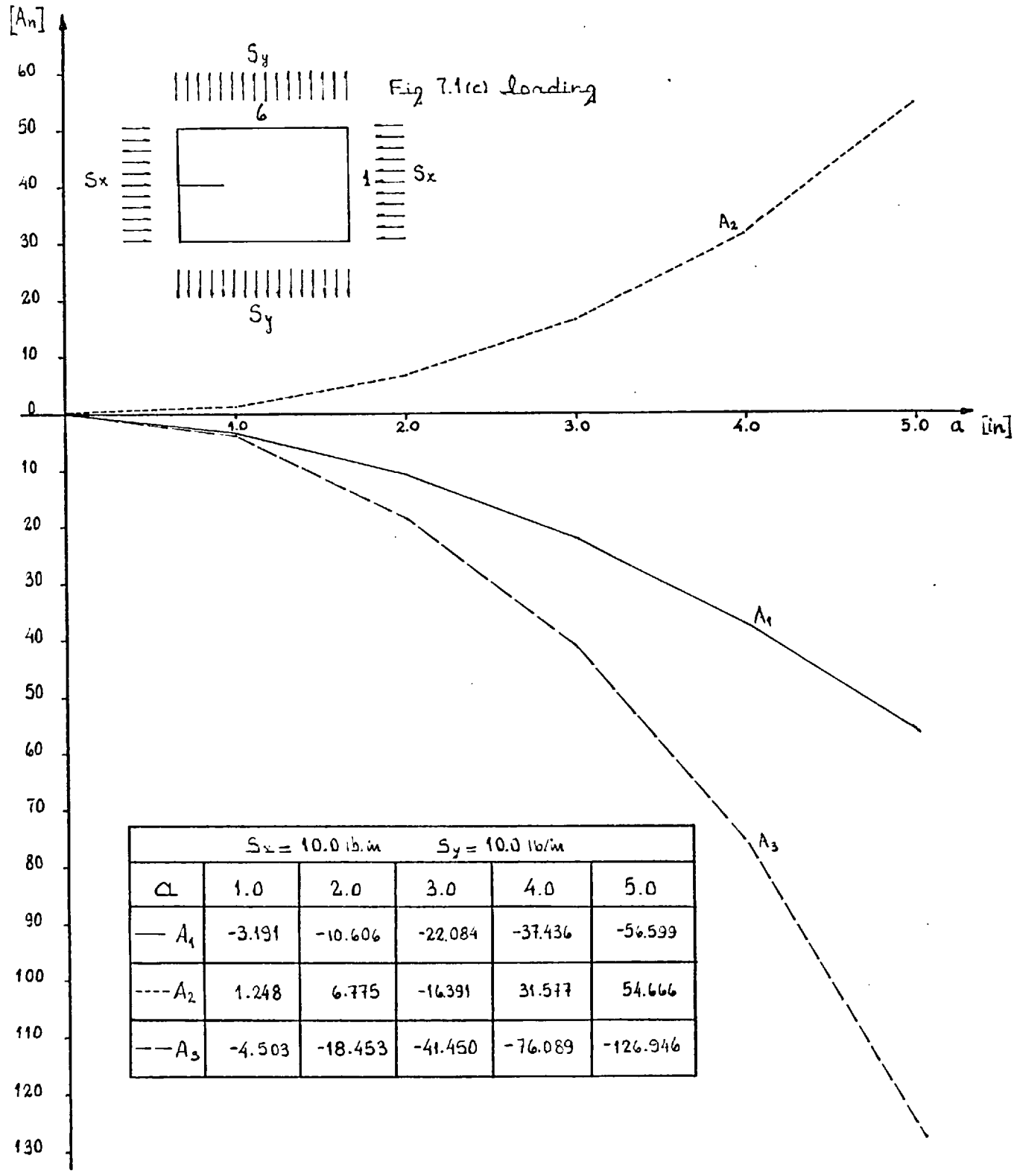

Sx = 10.0 lb.in Sy = 10.0 lb/in					
a	1.0	2.0	3.0	4.0	5.0
— A_1	-3.191	-10.606	-22.084	-37.436	-56.599
---- A_2	1.248	6.775	-16.391	31.577	54.666
— — A_3	-4.503	-18.453	-41.450	-76.089	-126.946

Fig. 7.1(a) Coefficients values for specimen 6x1

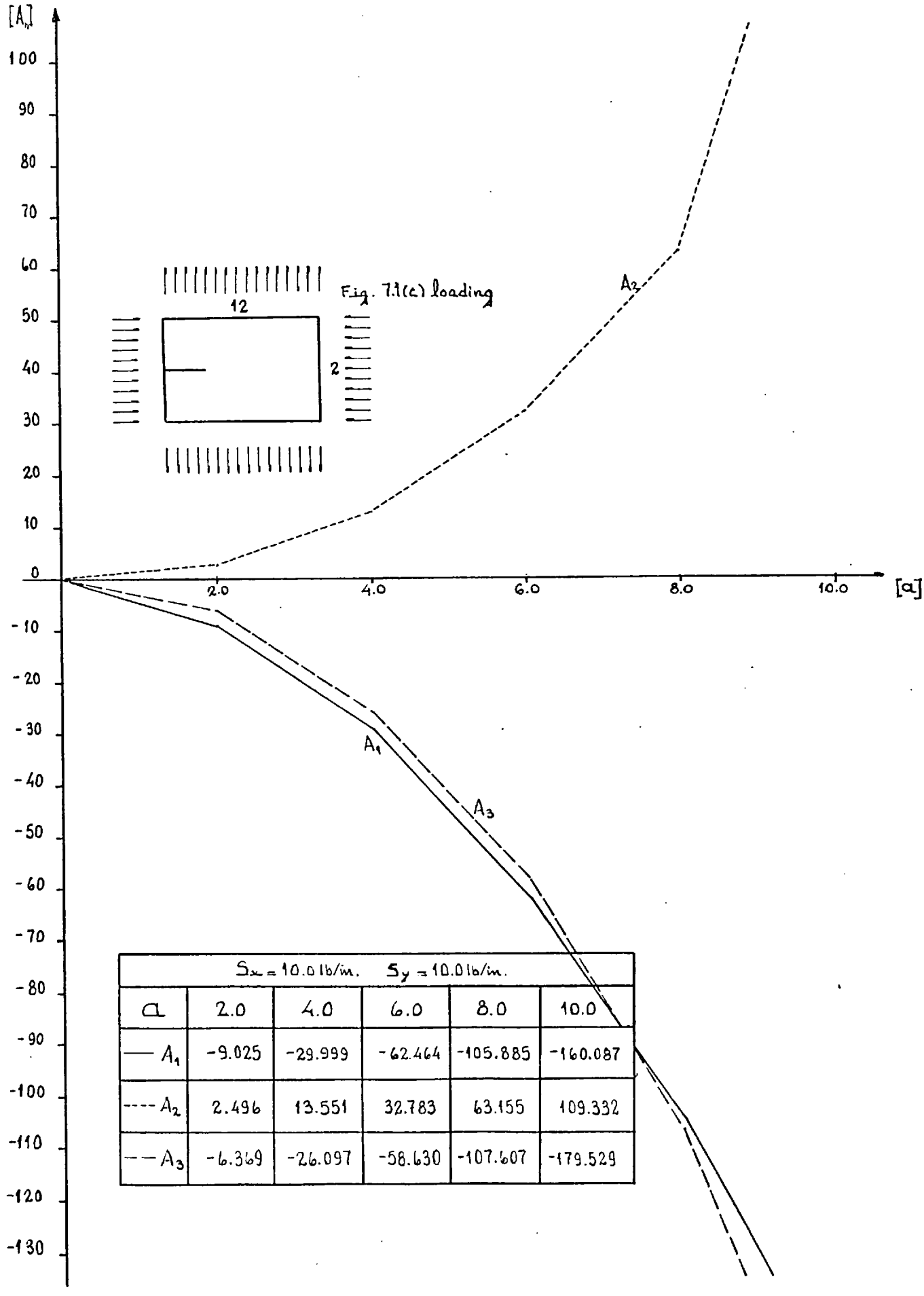

S_x = 10.0 lb/in. S_y = 10.0 lb/in.					
a	2.0	4.0	6.0	8.0	10.0
—— A_1	-9.025	-29.999	-62.464	-105.885	-160.087
---- A_2	2.496	13.551	32.783	63.155	109.332
– – A_3	-6.369	-26.097	-58.630	-107.607	-179.529

Fig. 7.1(b) Coefficients values for specimen 12×2

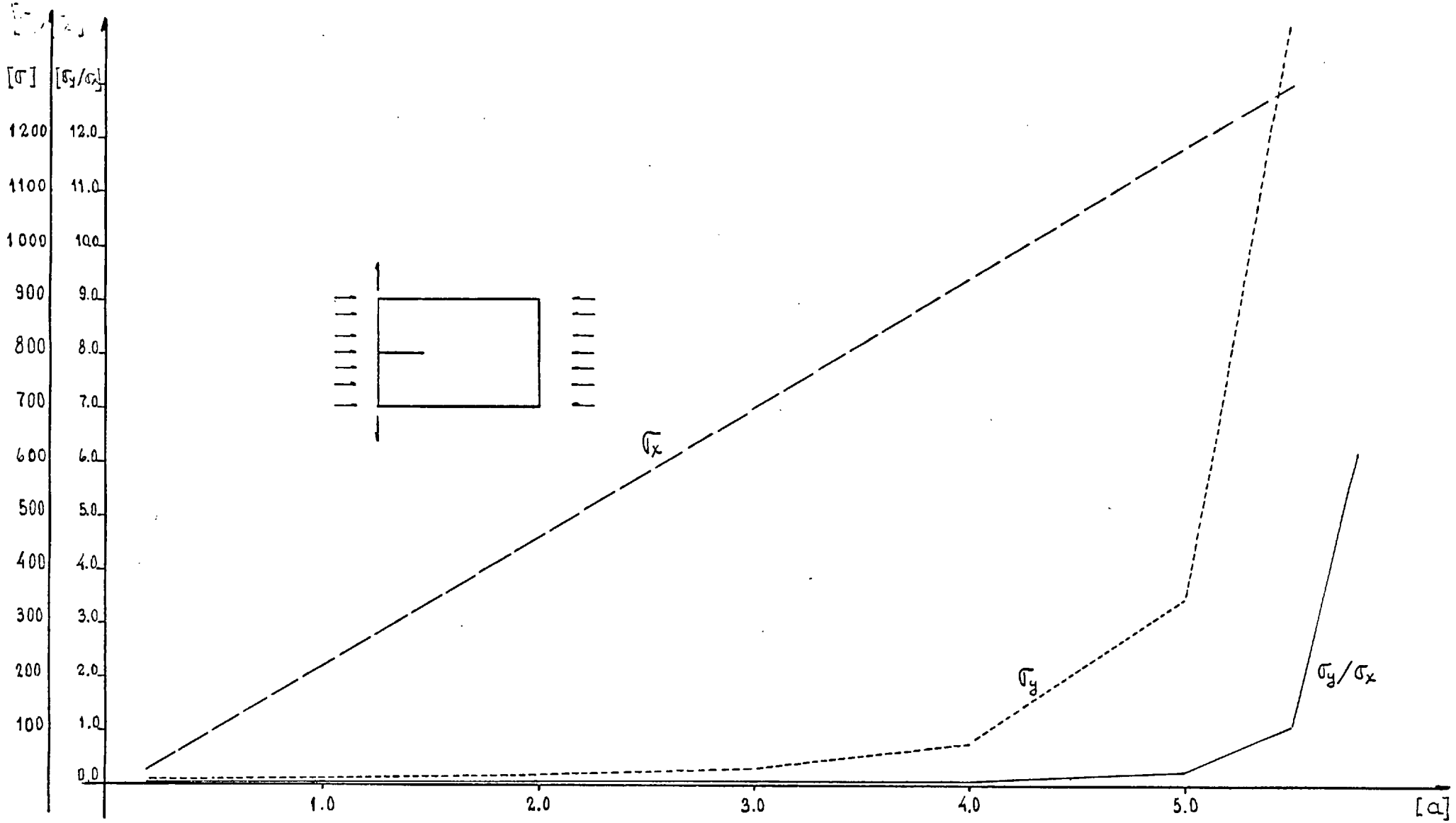

Fig. 7.2 Stresses at the crack tip as calculated by beam theory.

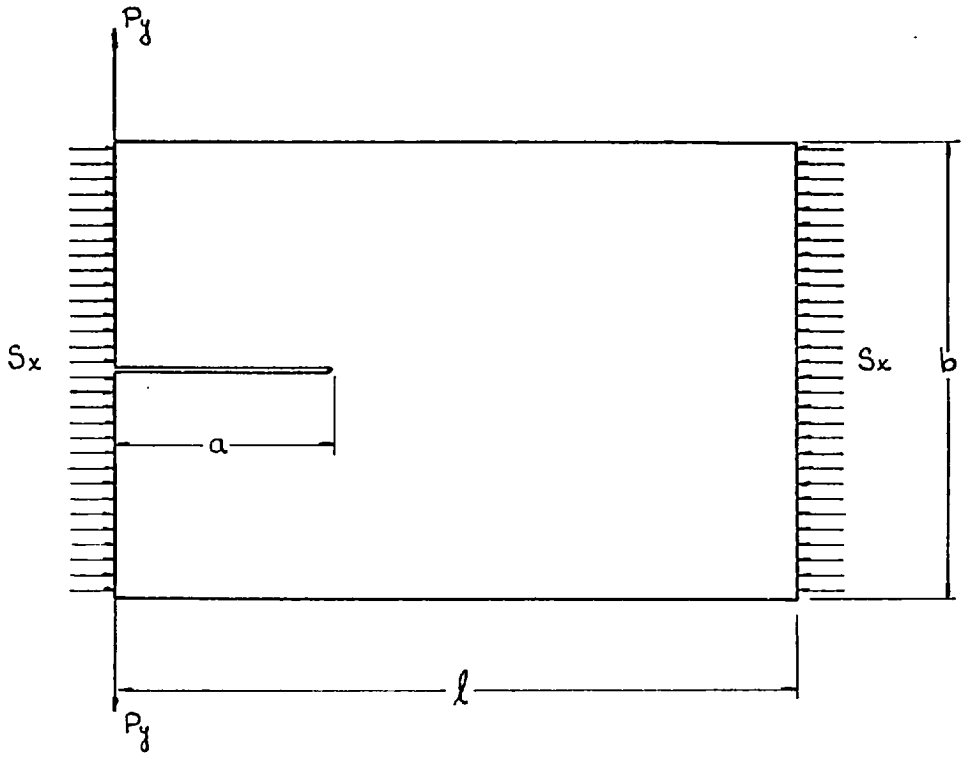

Fig 7.3 Loading and dimensions as factors that affect the coefficients values

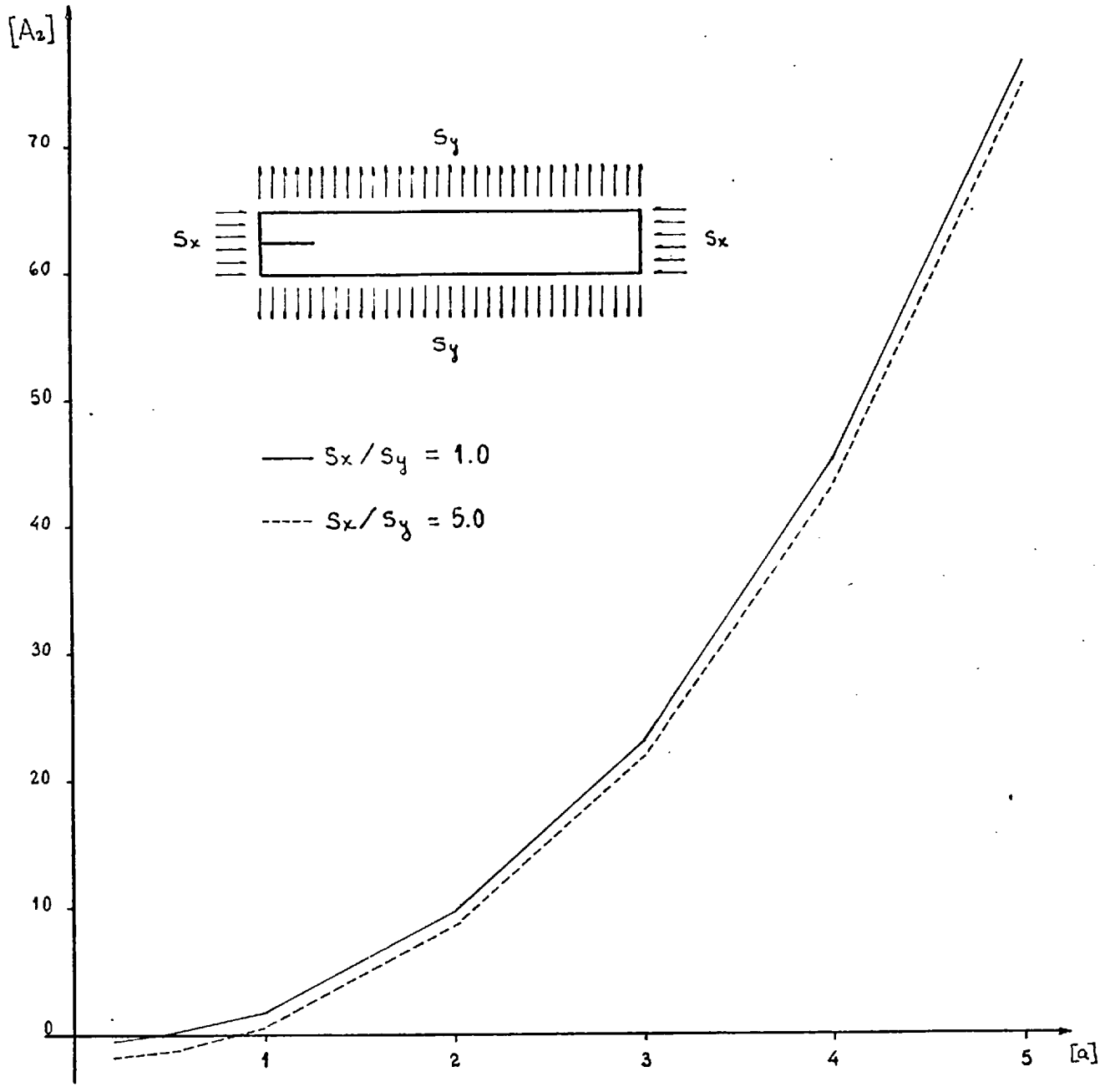

Fig. 7.4(a) A_2 coefficient values for different crack lengths
Specimen 6x1

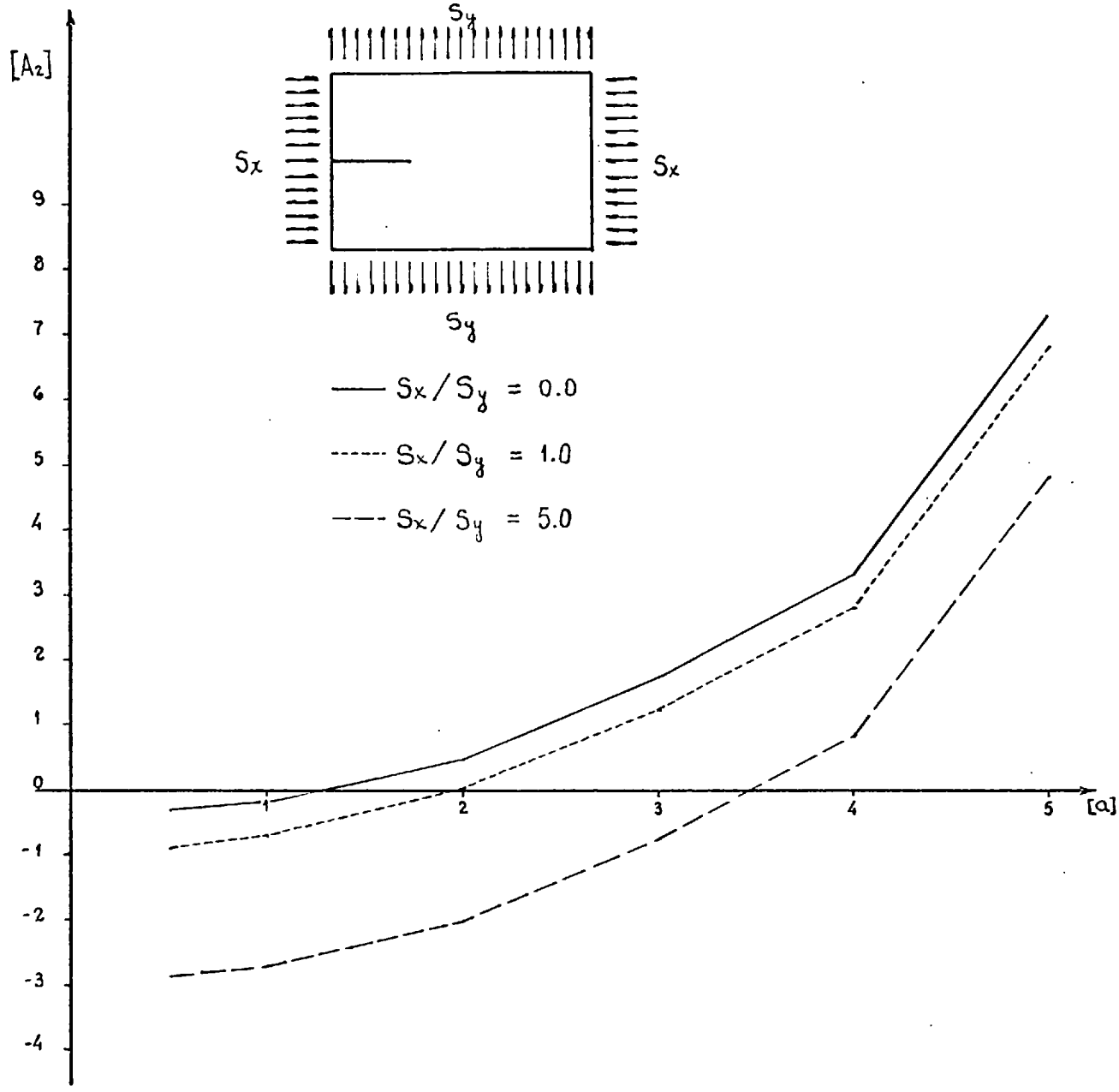

Fig 7.4(b) A_2 coefficients values for different crack lengths
Specimen 6 x 4

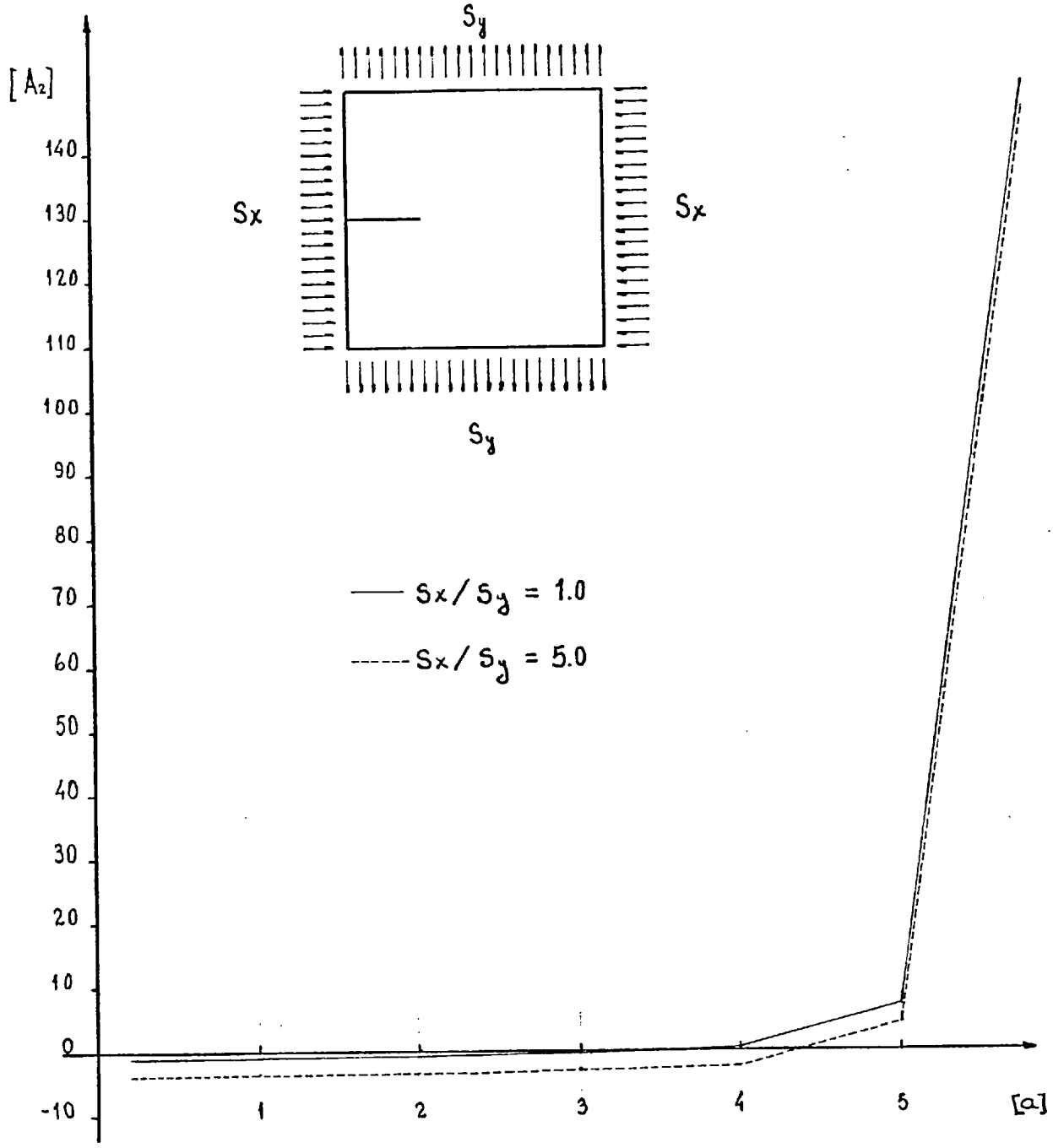

Fig 7.4(c) A2 coefficients values for different crack lengths

Specimen 6x6

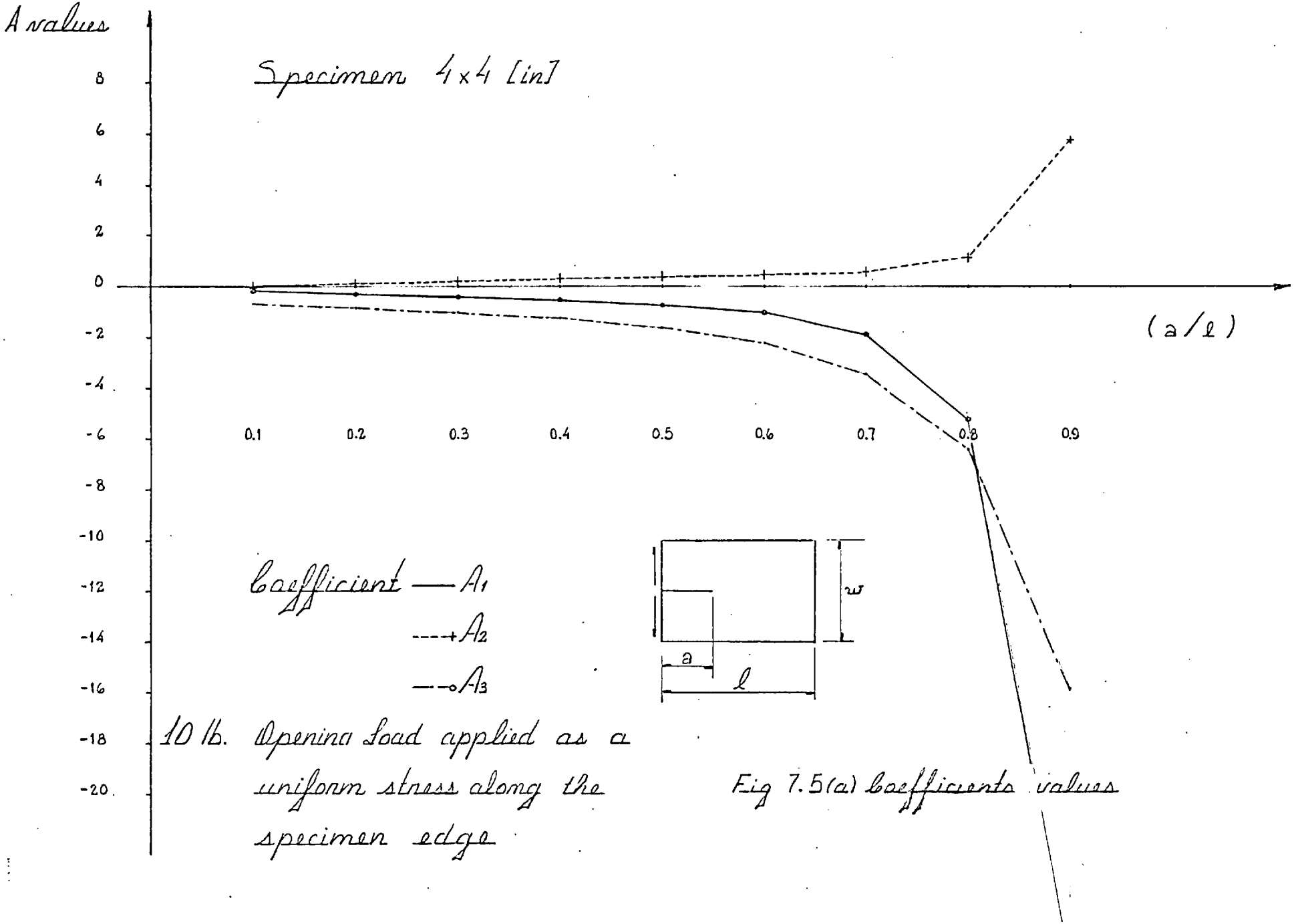

10 lb. Opening load applied as a uniform stress along the specimen edge

Fig 7.5(a) Coefficients values

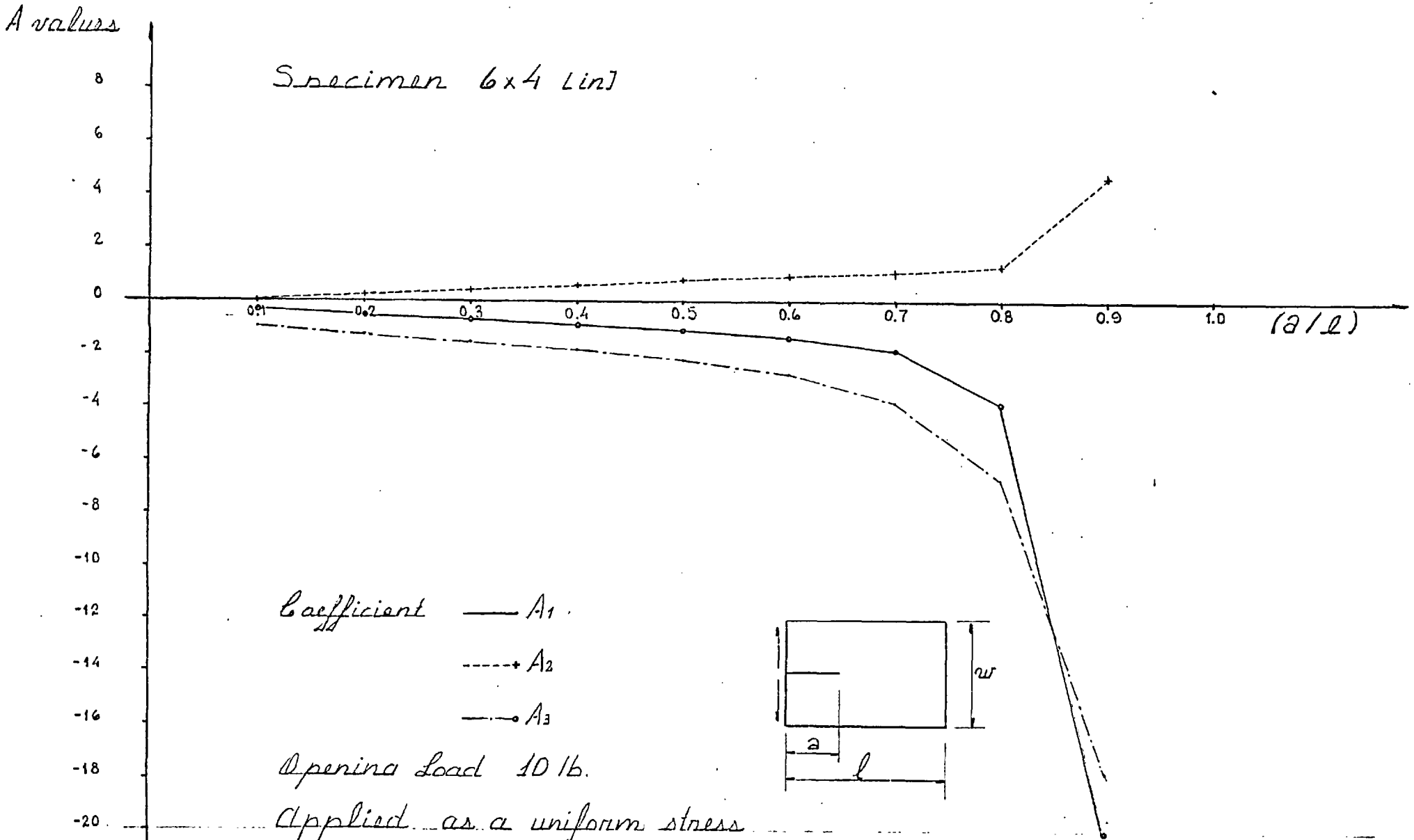

Fig 7.5(b) Coefficients values

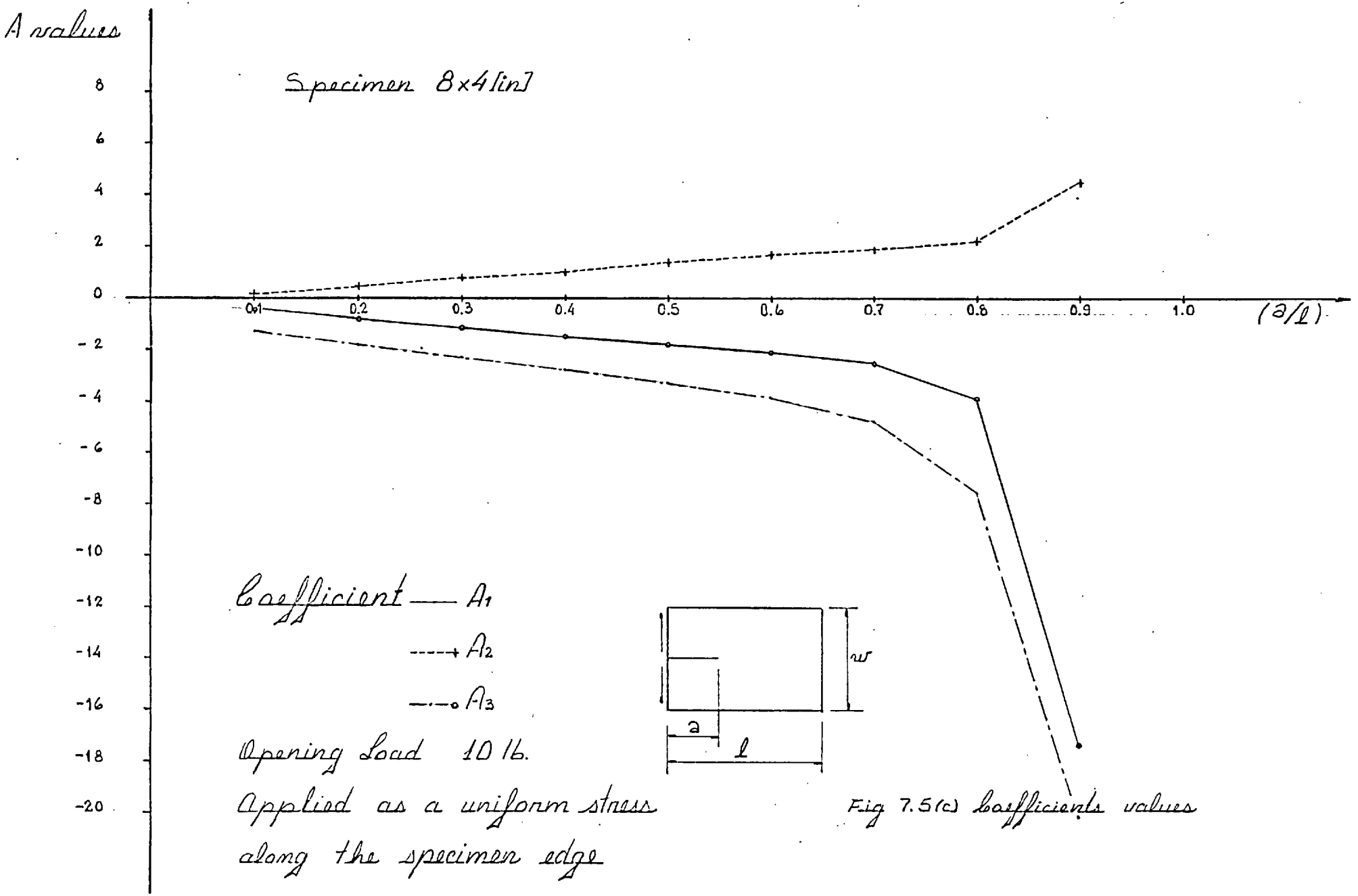

Fig 7.5(c) Coefficients values

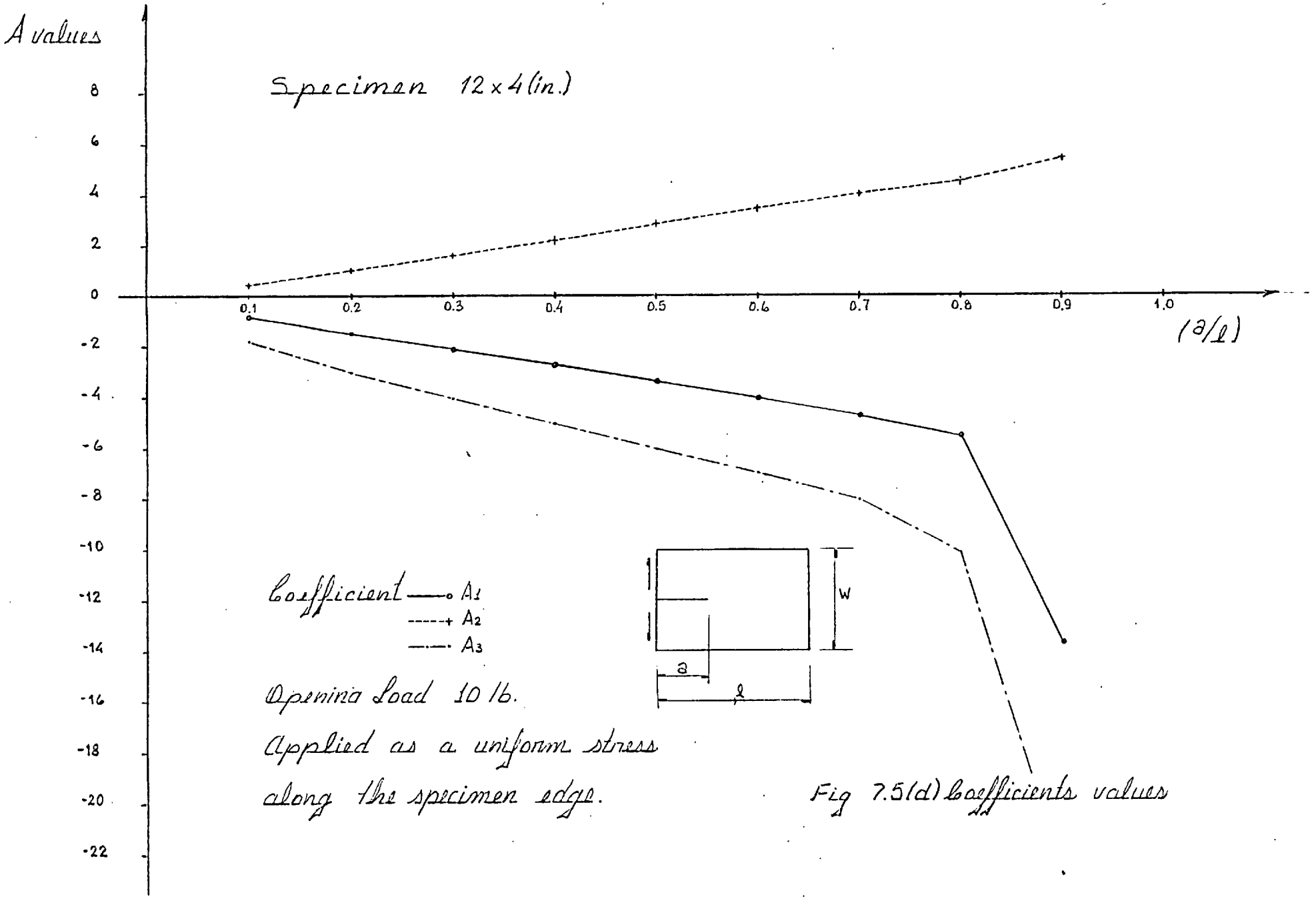

Fig 7.5(d) Coefficients values

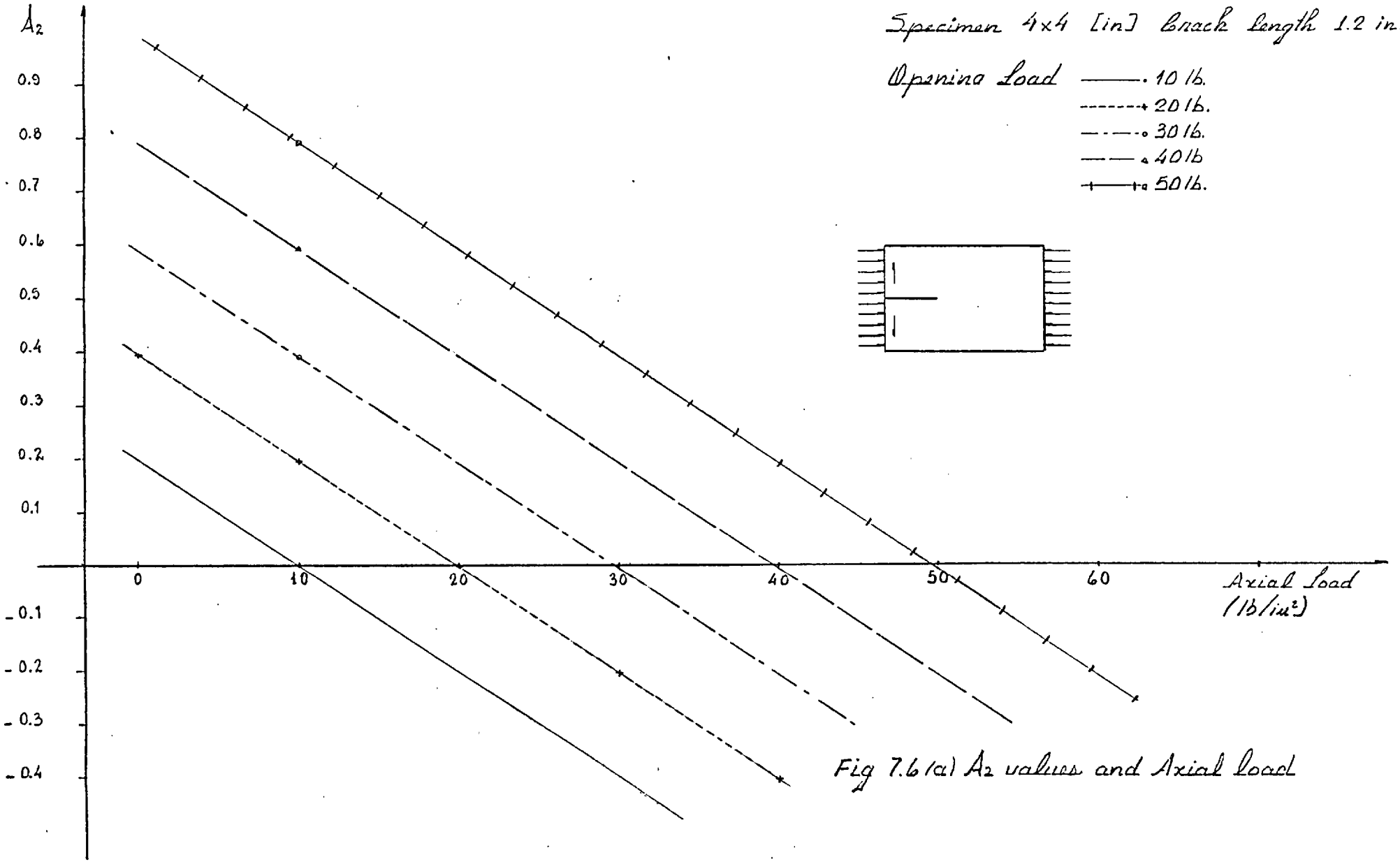

Fig 7.6 (a) A_2 values and Axial load

Specimen 6×4 [in] Crack length 1.8 in

Fig 7.6(b) A_2 values and Axial load

Opening Load
- 10 lb.
- 20 lb.
- 30 lb.
- 40 lb.
- 50 lb.

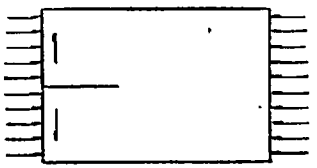

A_2

2.5

2.0

1.5

1.0

0.5

0 10 20 30 40 50 60 70

Axial load (lb/in^2)

Specimen 8×4 (in) Crack length 2.4 in

Opening Load —— 10 lb.
----+ 20 lb.
----• 30 lb.
——→ 40 lb.
+—+—+ 50 lb.

Fig 7.6(c) A_2 values and Axial load

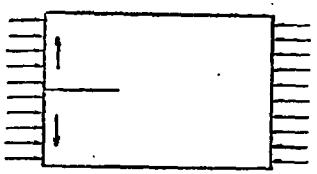

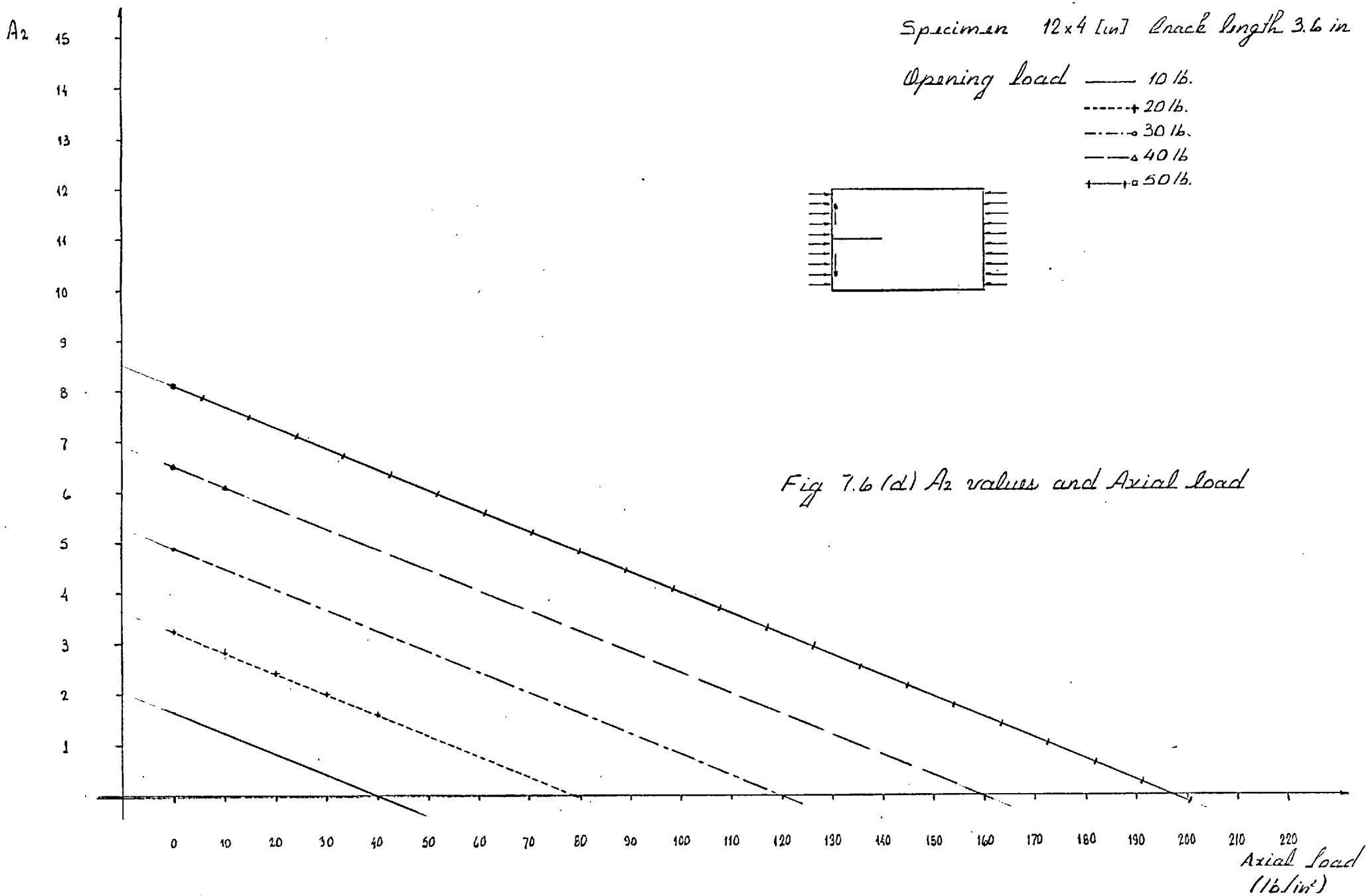

Fig 7.6 (d) A_2 values and Axial load

Fig 7.7 (A_2 vs Axial load) for different specimens

Opening load 20 lb.

Axial load applied as a uniform distributed stress along the specimen edges

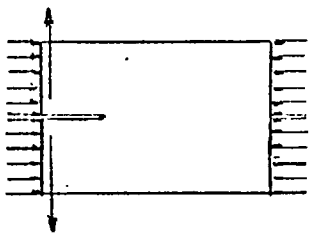

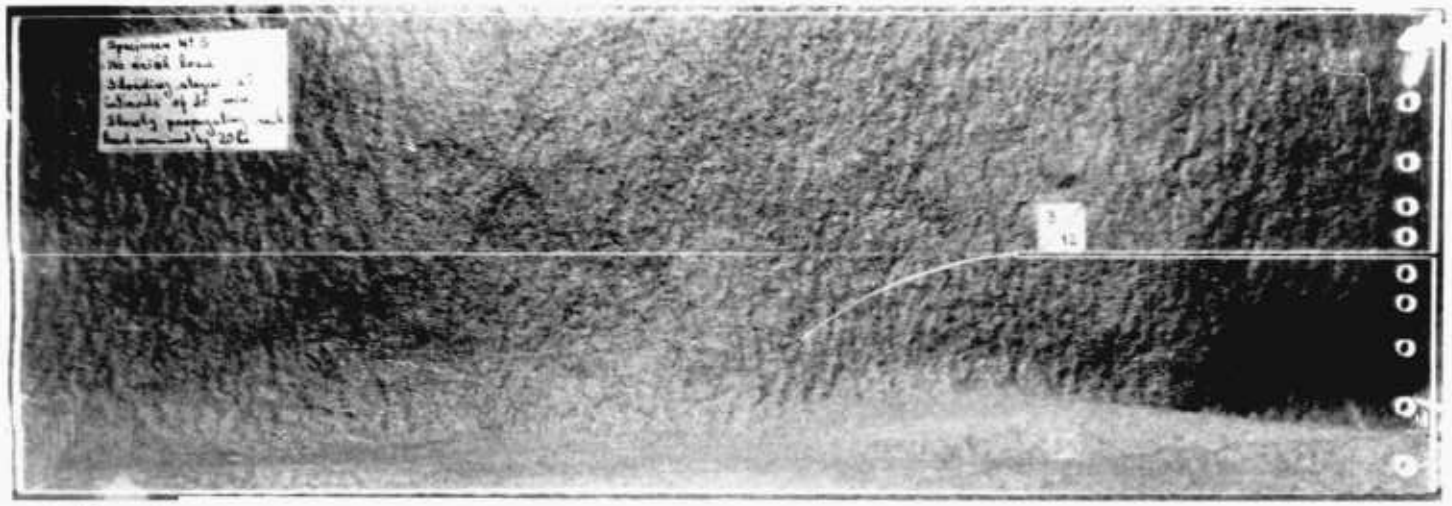

a) 12 x 4

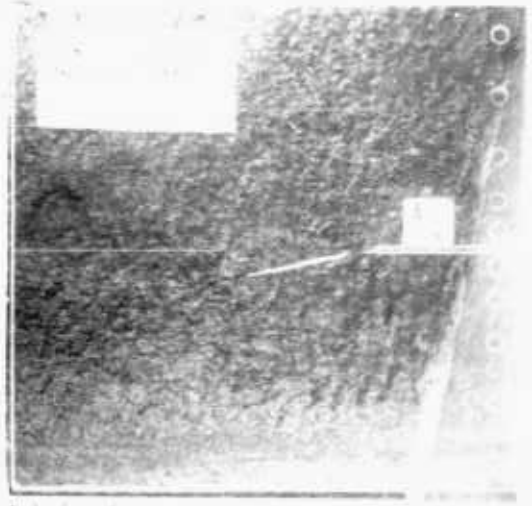

b) 4 x 4

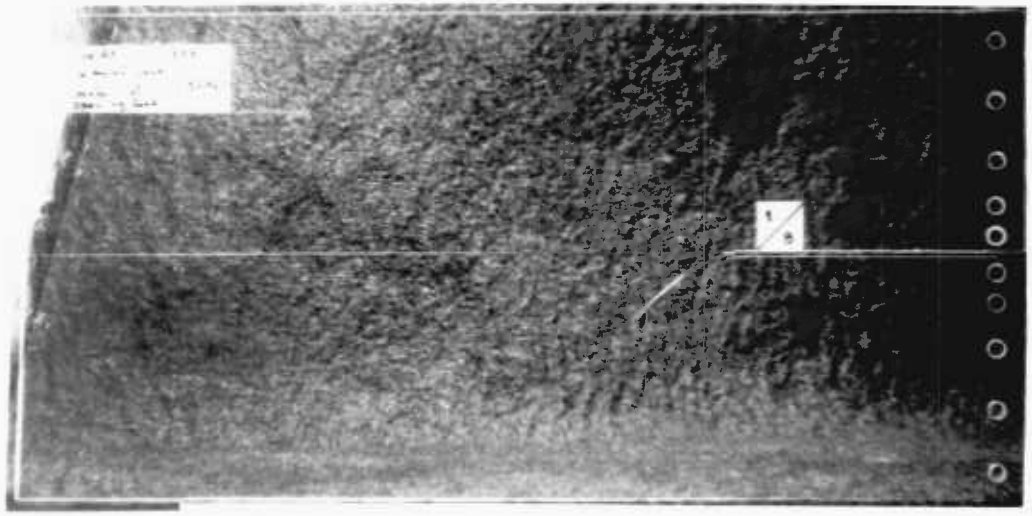

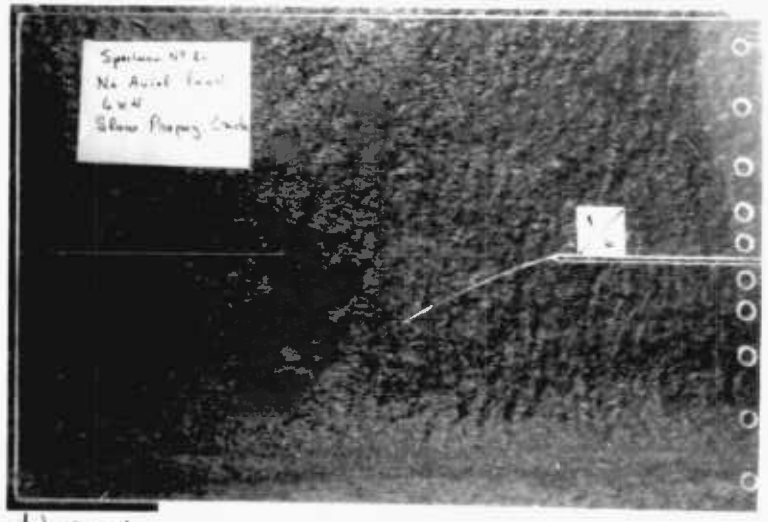

d) 6x4

Fig 7.8 Cracked specimins

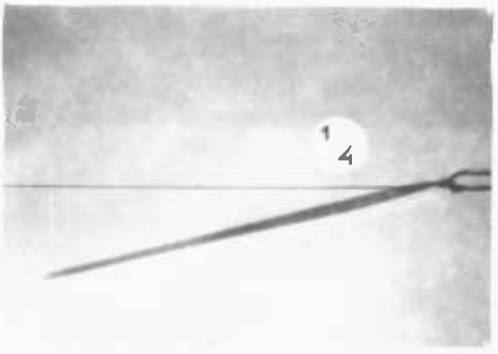

a) No axial load
Specimen 4x4

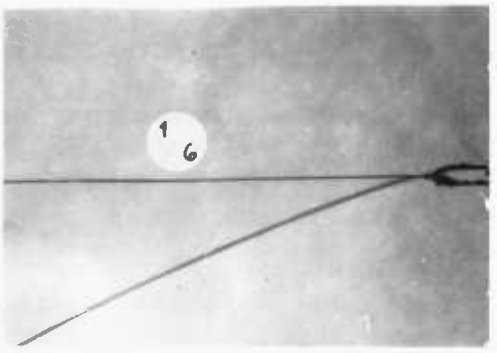

b) No axial load
Specimen 6x4

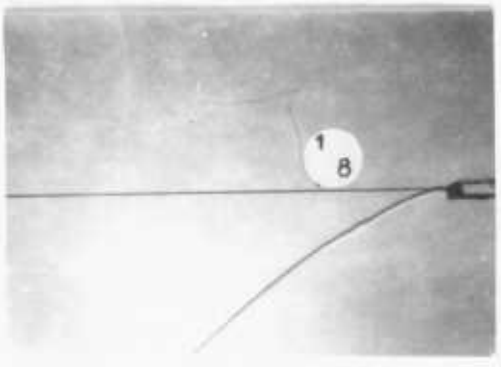

c) No axial load
Specimen 8x4

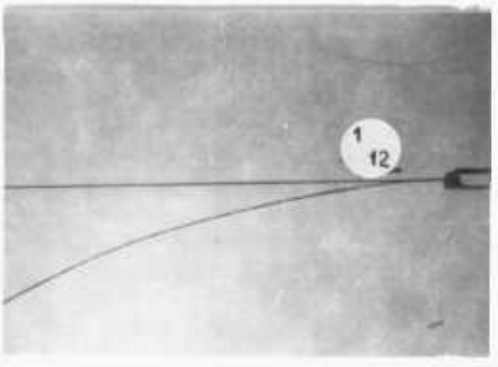

d) No axial load
Specimen 12x4

Fig. 7.8 Crack path and Specimen dimensions

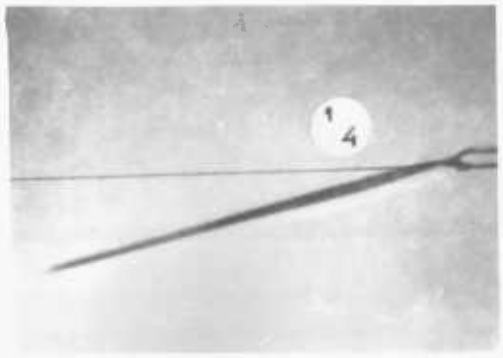

a) No axial load

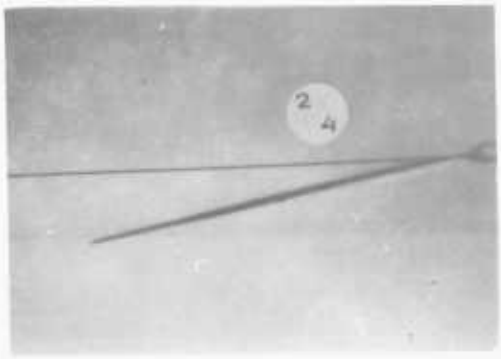

b) No axial load

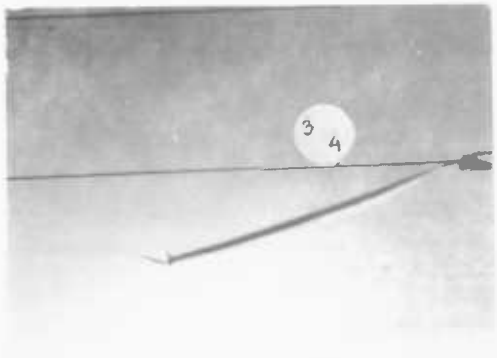

c) Axial load 80 lb

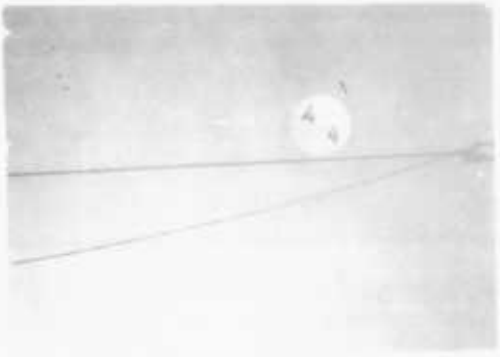

d) Axial load 100 lb.

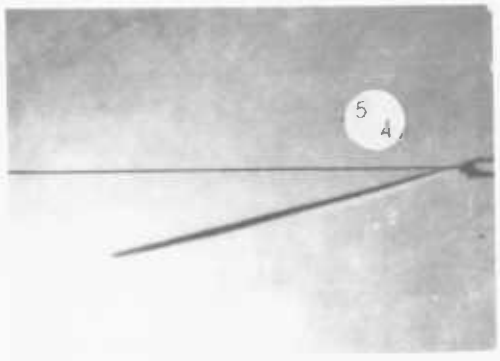

e) Axial load 100 lb.

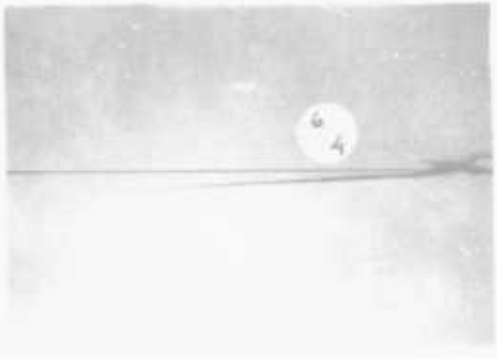

f) Axial load 160 lb.

Fig. 7.9 Crack path for Specimen 4x4

a) No axial load

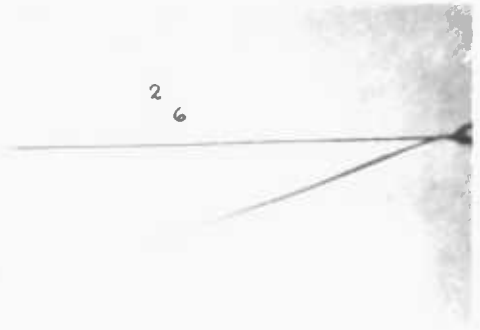

b) Axial load 160 lb.

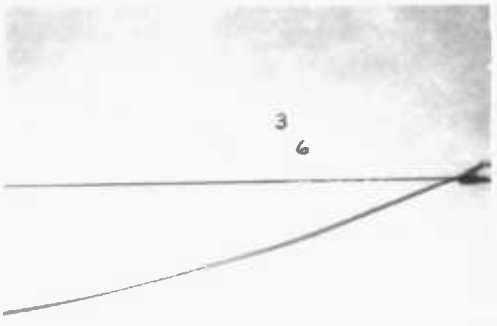

c) Axial load 160 lb.

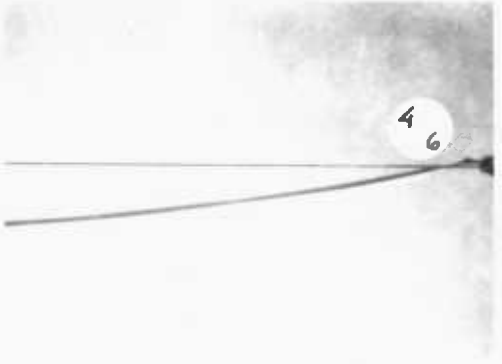

d) Axial load 160 lb.

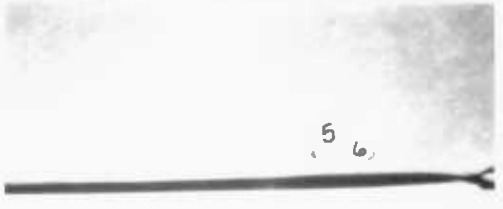

e) Axial load 360 lb

Fig 7.10 Crack for Specimens 6 x 6

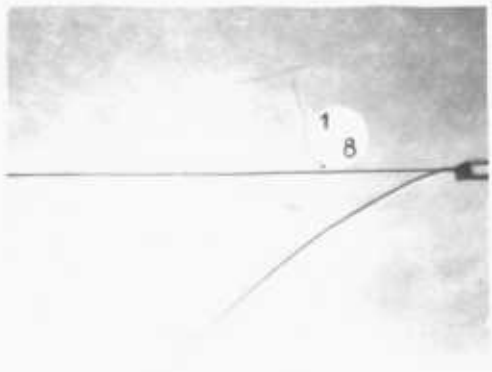

a) No axial load

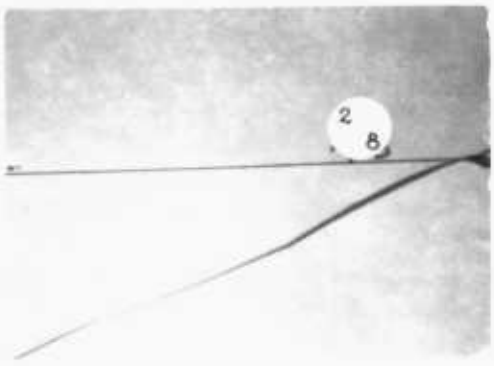

b) No axial load

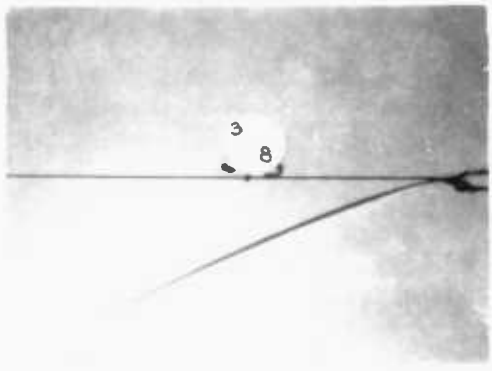

c) No axial load

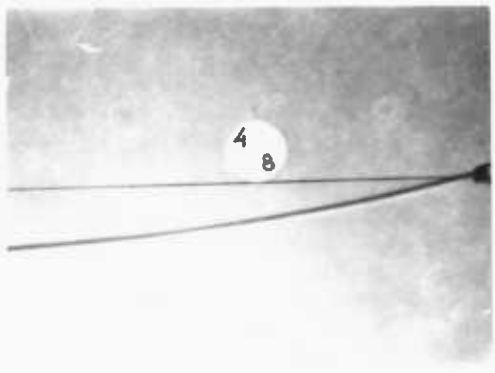

d) Axial load 240 lb.

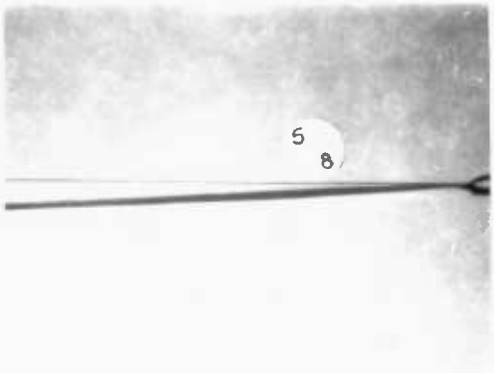

e) Axial load 850 lb.

Fig. 7.11 Crack path for Specimens 3×4

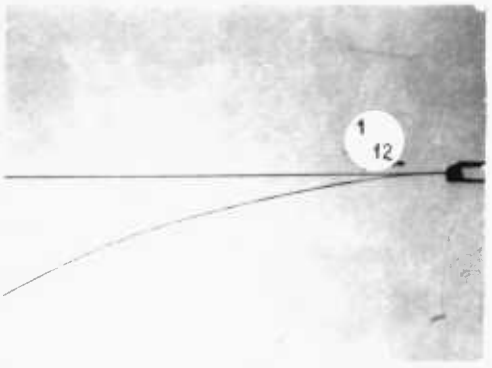

a) No axial load

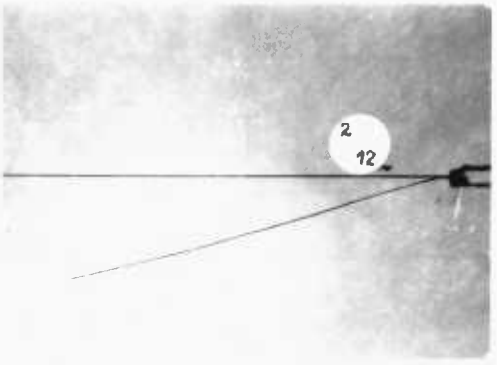

b) Axial load 360 lb.

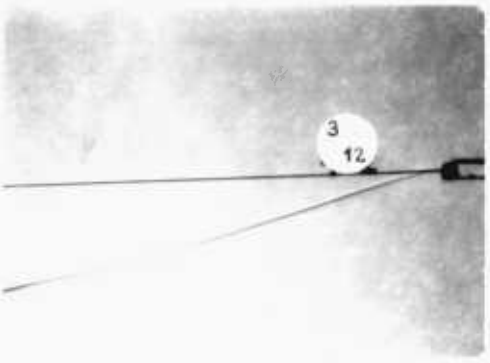

c) Axial load 360 lb.

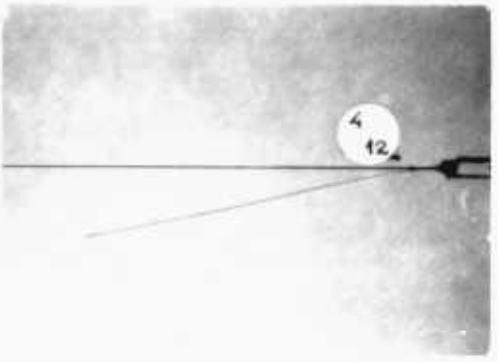

d) Axial load 360 lb.

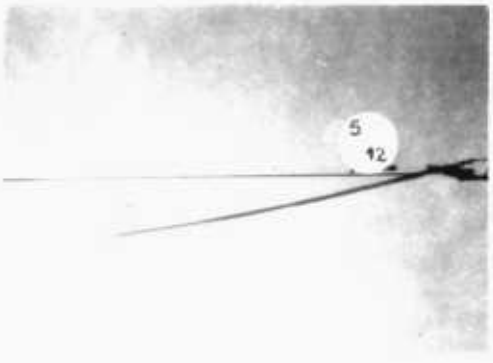

e) Axial load 500 lb.

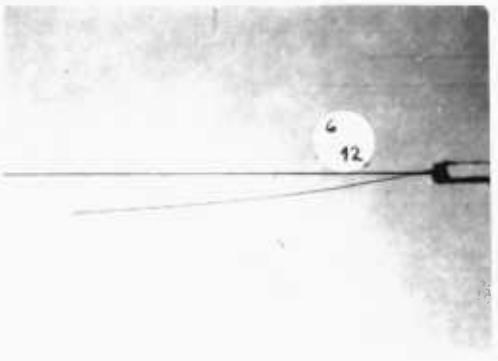

f) Axial load 700 lb.

Fig 7.1 Crack for specimens 12 x 4

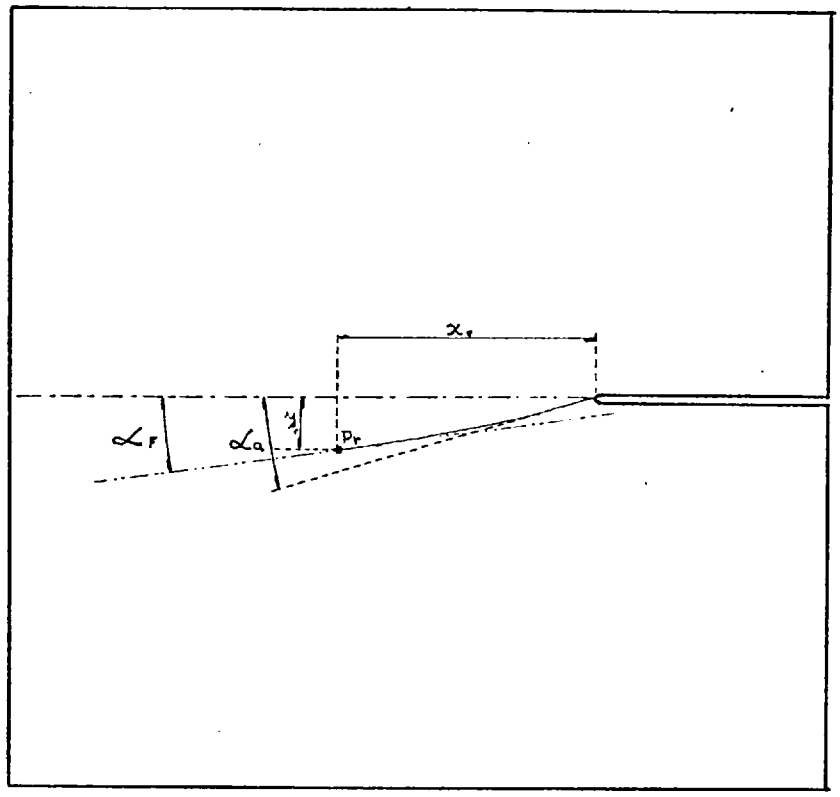

FIG. 7.13 INITIAL AND FINAL ANGLES OF CRACK PROPAGATION (EXPERIMENTAL RESULTS)

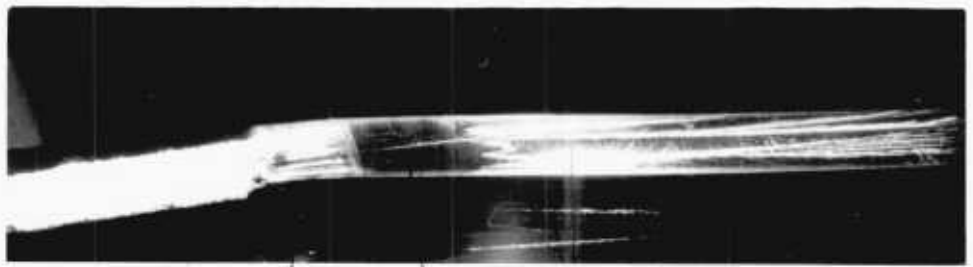

Fig 7.14 Fracture Surfaces

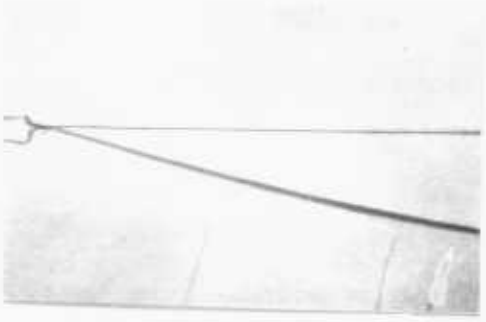

Transverse Load 160 lb/in (a)

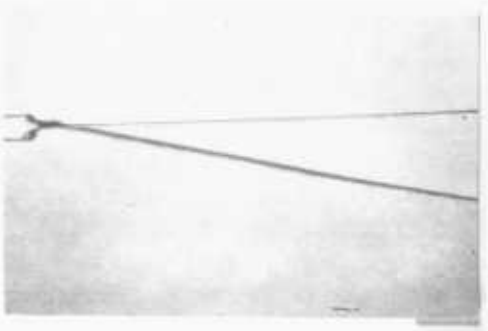

Transverse Load 240 lb/in (b)

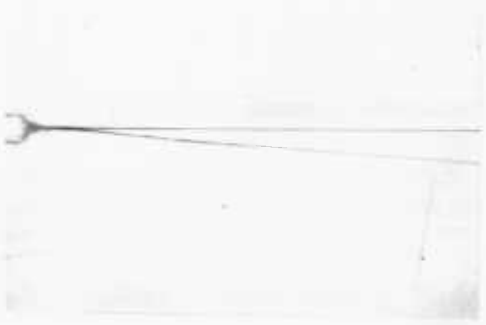

Transverse Load 280 lb/in (c)

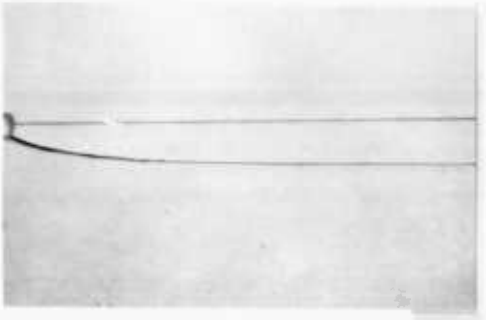

Transverse Load 320 lb/in (d)

Transverse Load 320 lb/in (e)

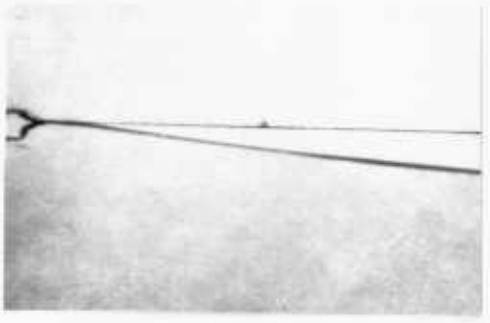

Transverse Load 320 lb/in (f)

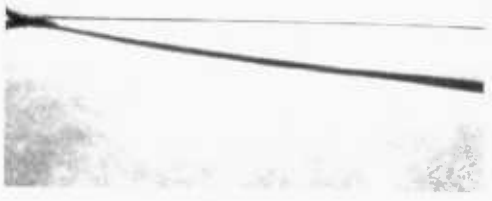

Transverse Load 400 lb/in (g)

Transverse Load 440 lb/in (h)

Fig 7.15 Crack path for specimen 12×4 (no mode II)

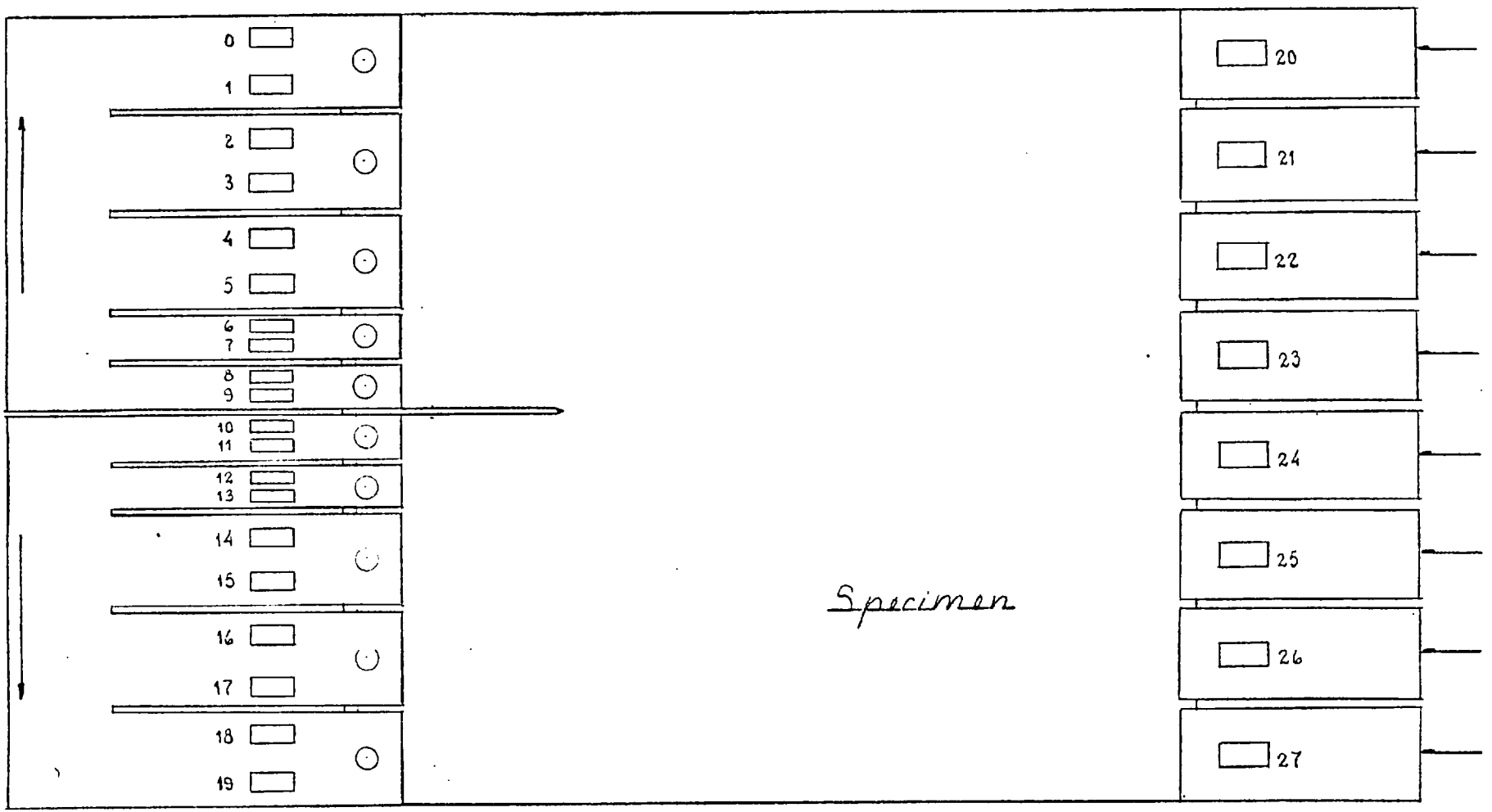

Fig 7.16 Gauges distribution and loading.

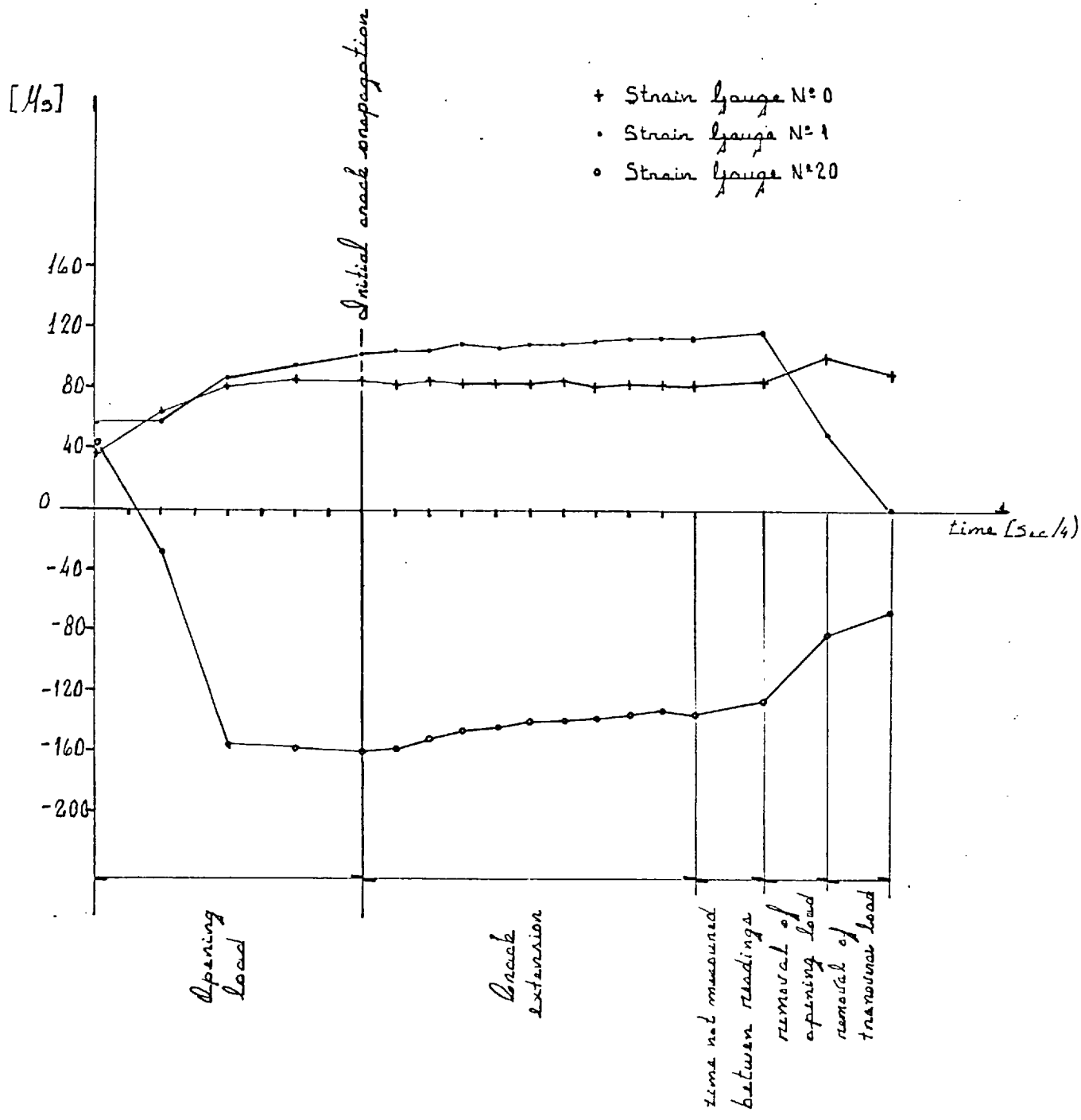

Fig. 7.17(a) Loading record for specimen 4/6

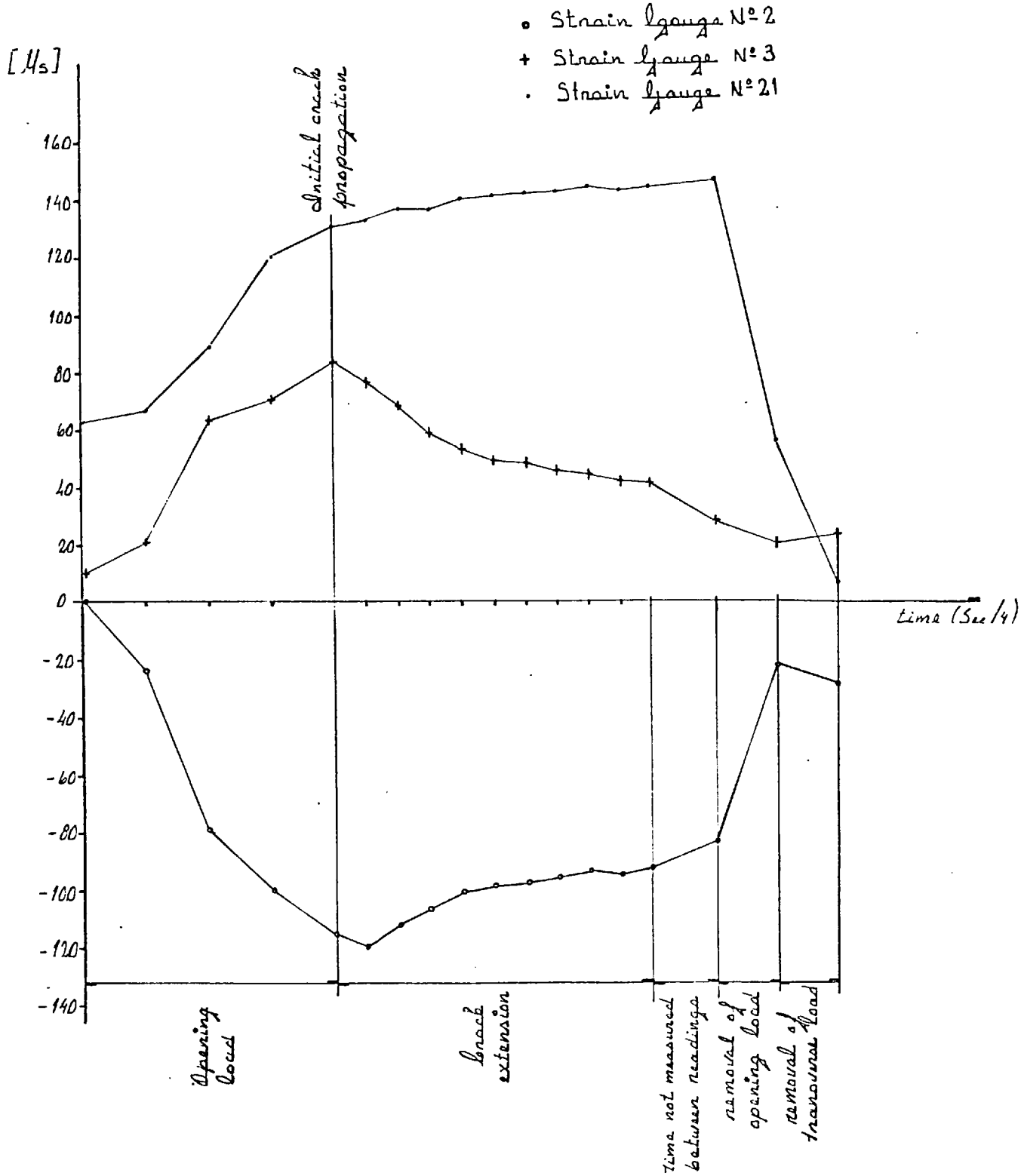

Fig. 7.17(b) Loading record for specimen 4/6

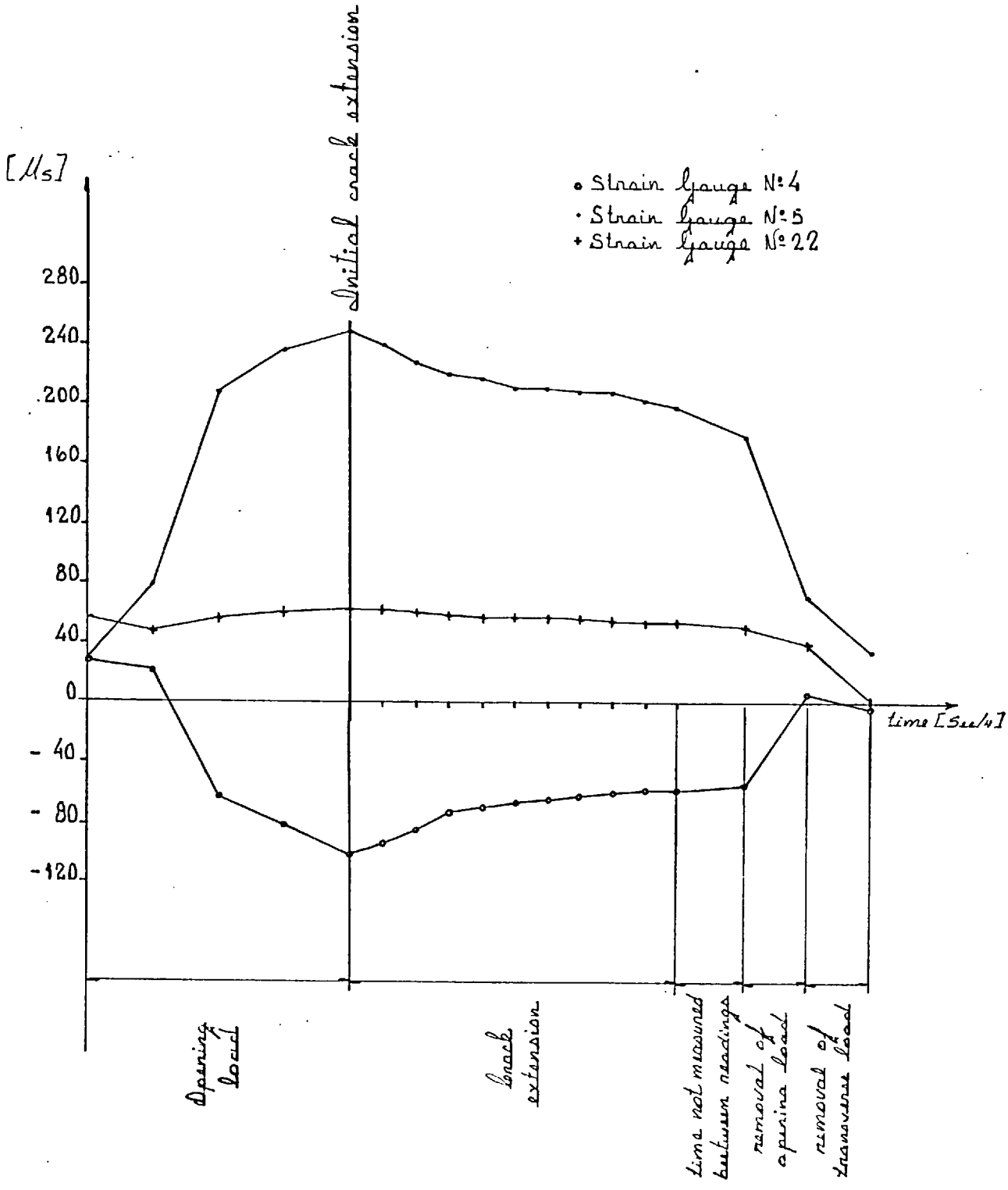

Fig 7.17(c) Loading record for specimen 4/6

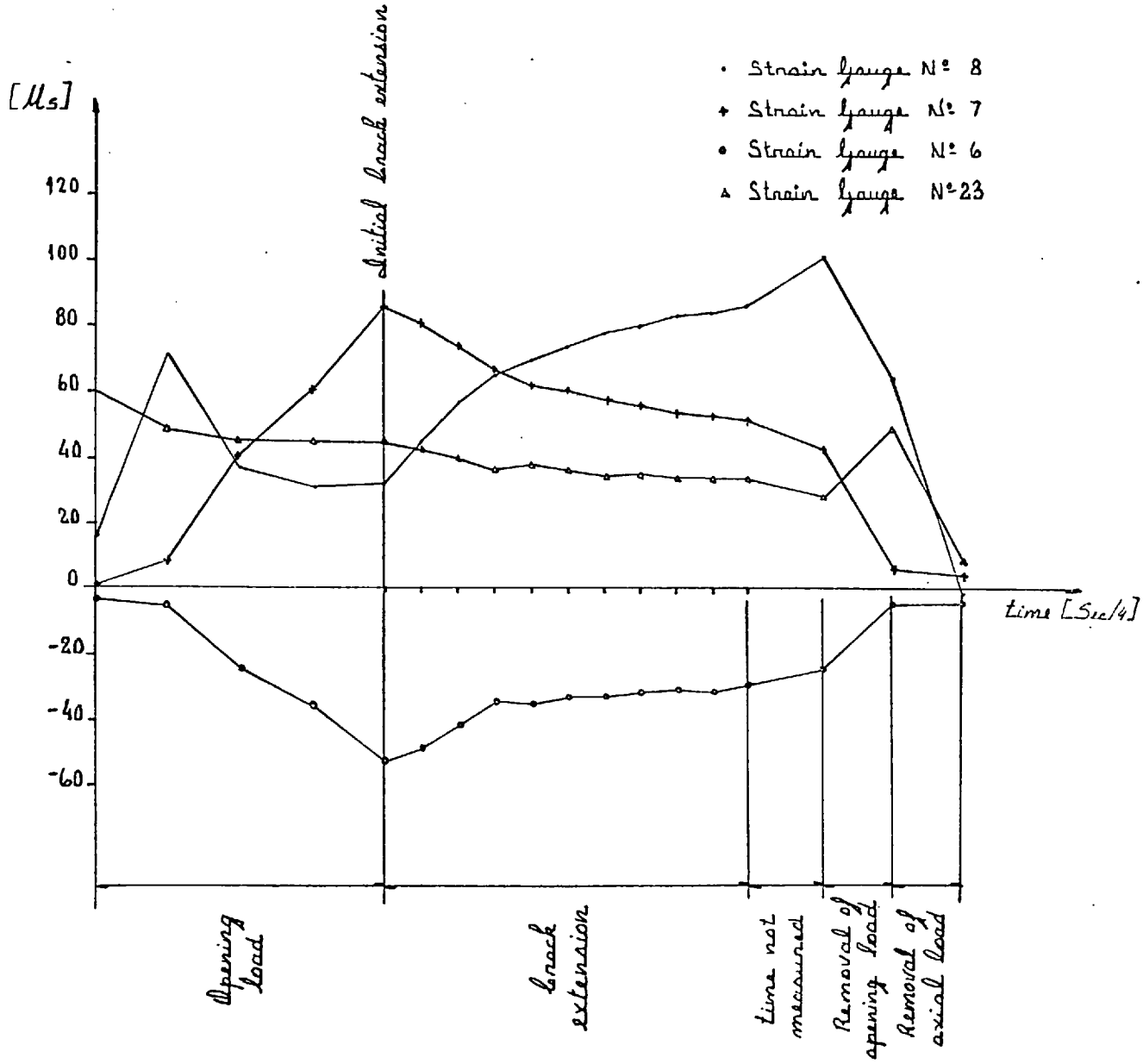

Fig. 7.17 (d) Loading record for specimen 4/6

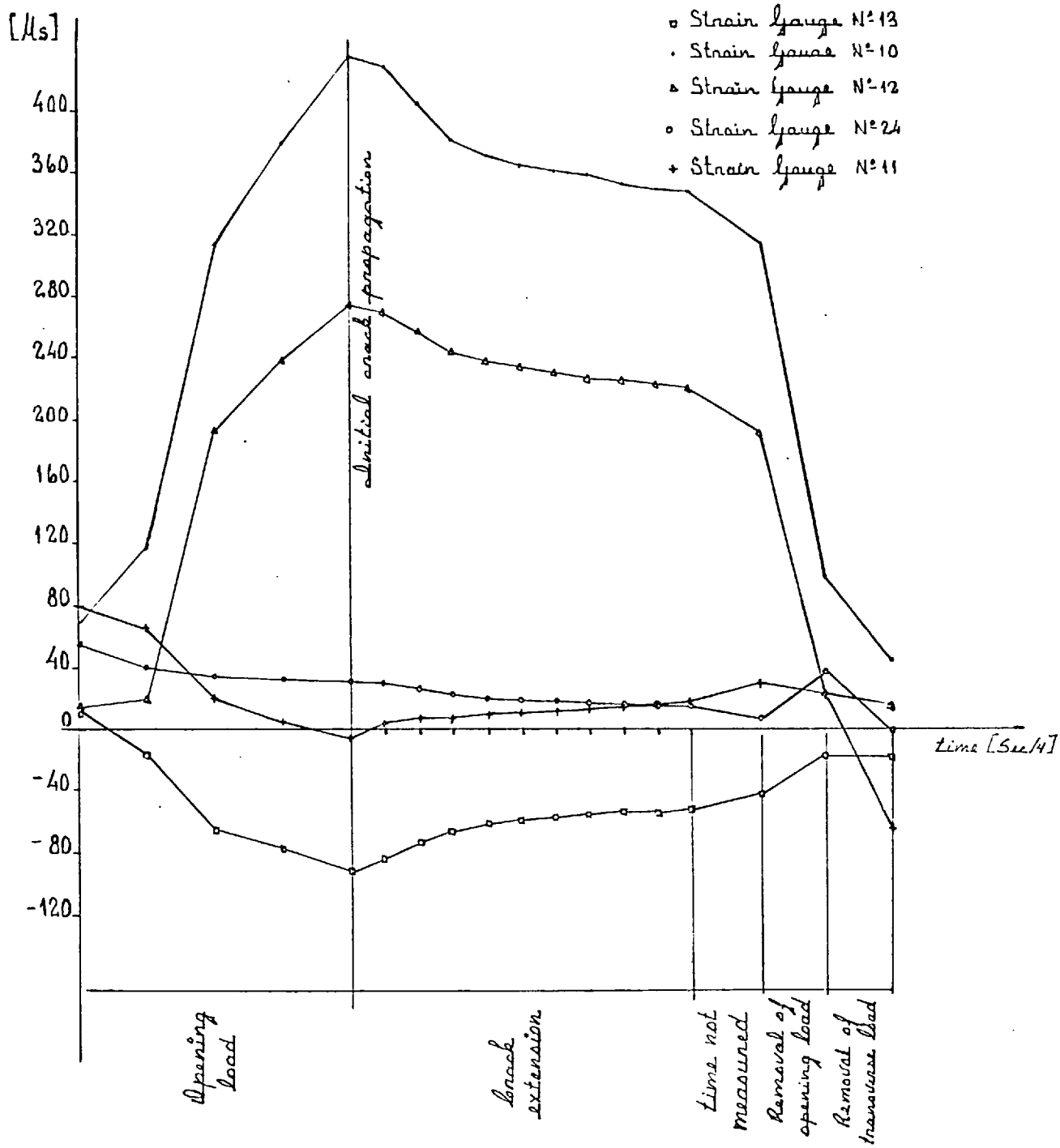

Fig 7.17(e) Loading record for specimen 4/6

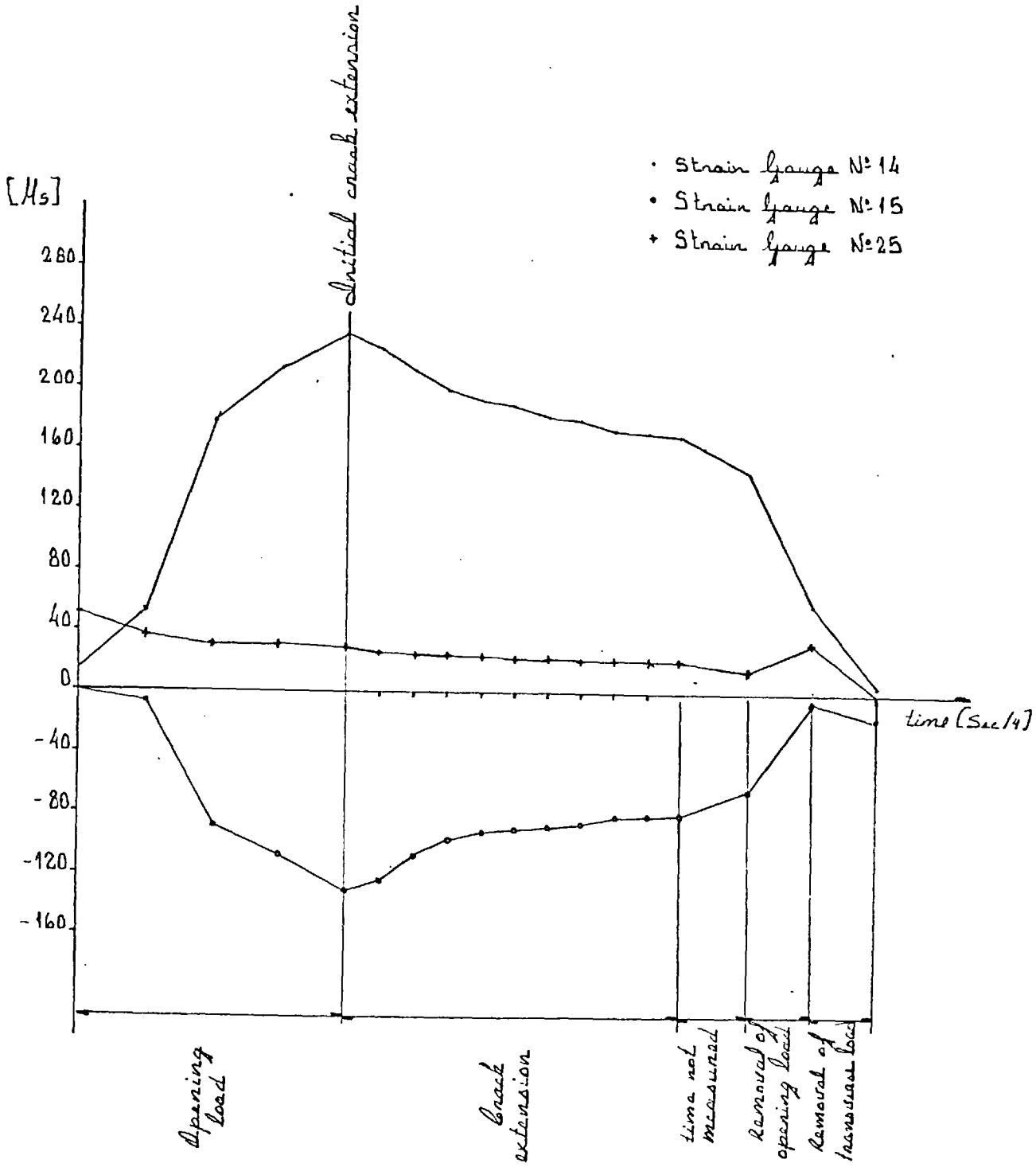

Fig 7.17(f) Loading record for specimen 6/4

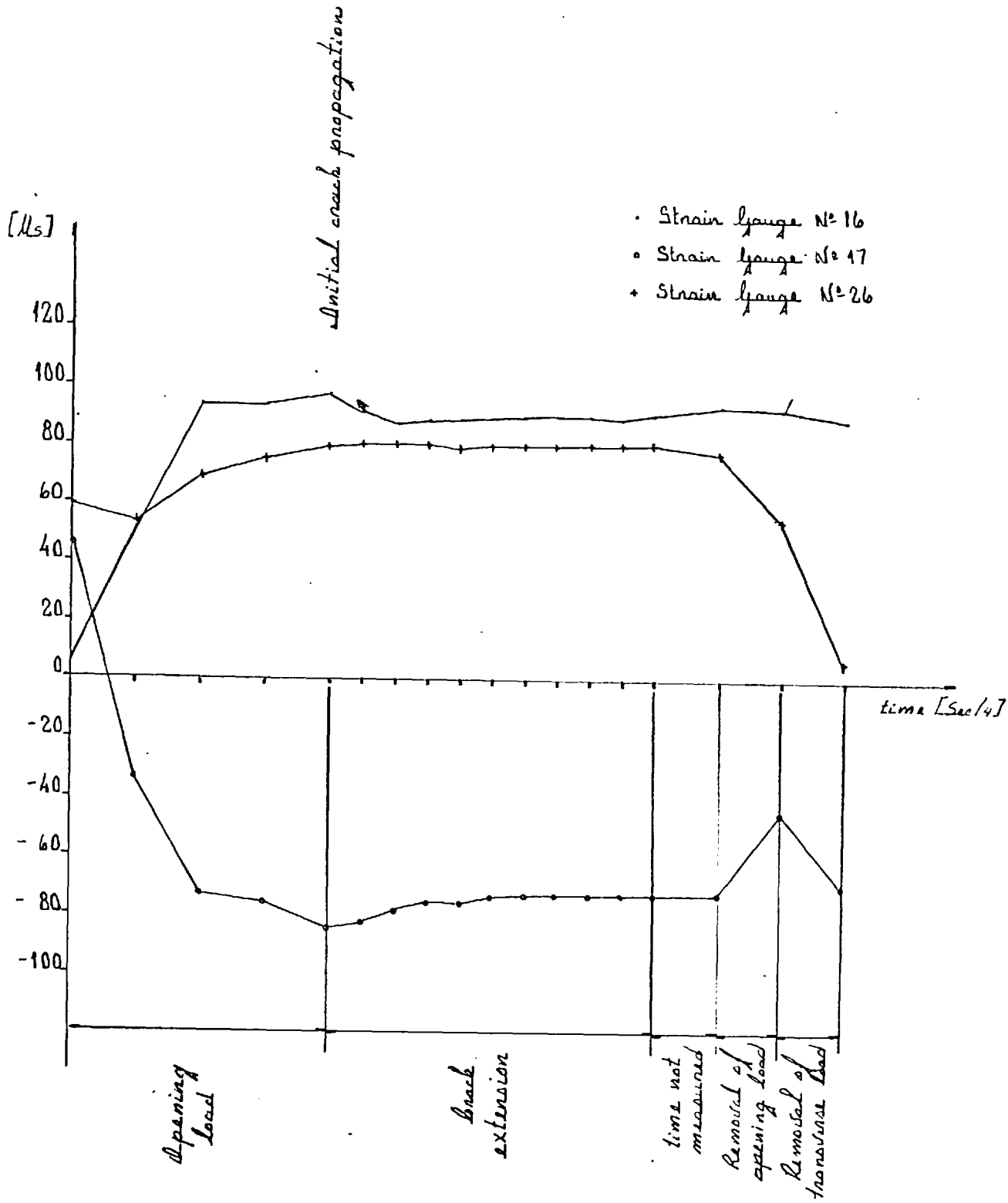

Fig. 7.17(g) Loading record for specimen 6/4

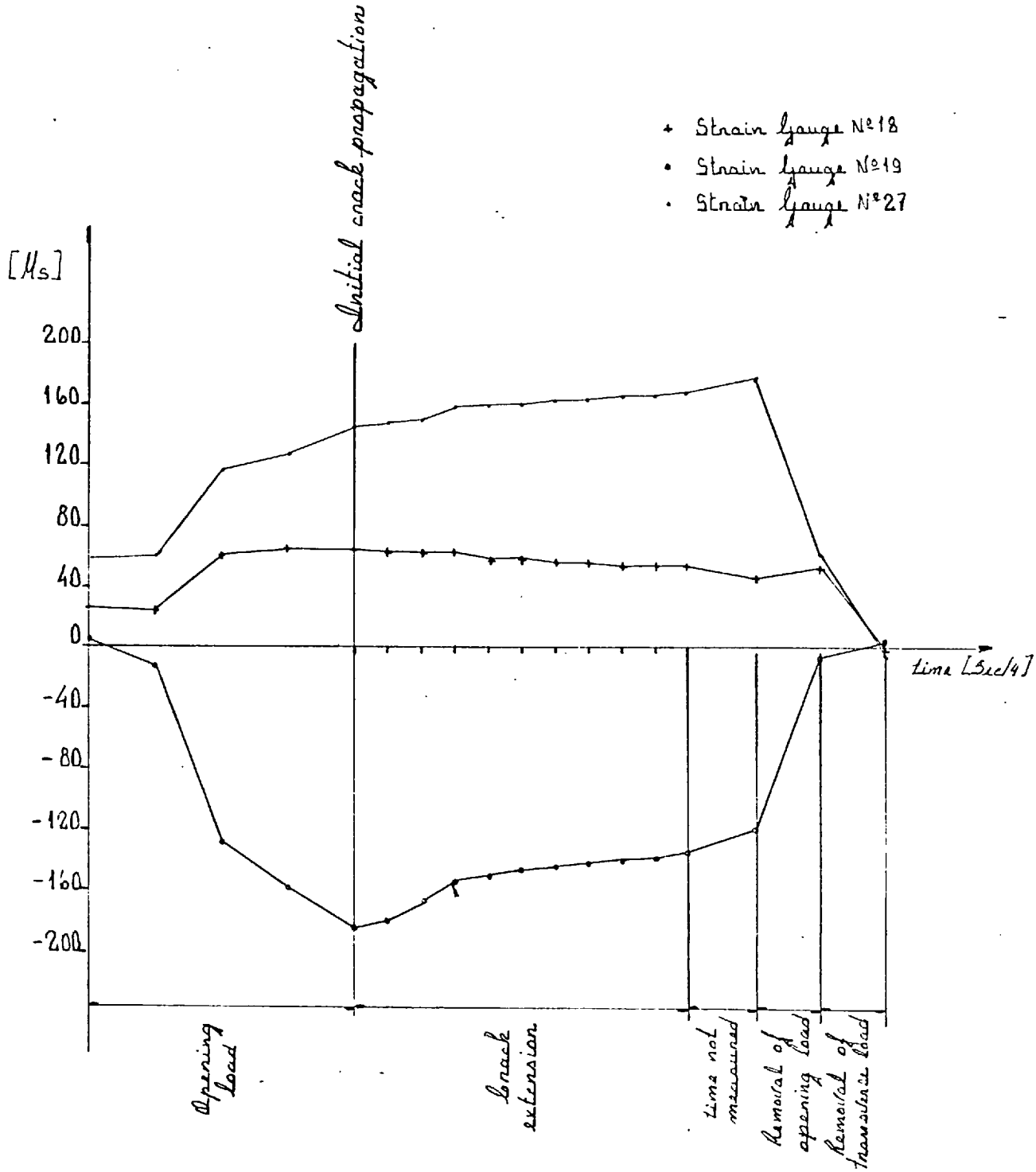

Fig 7.17(h) Loading record for specimen 6/4

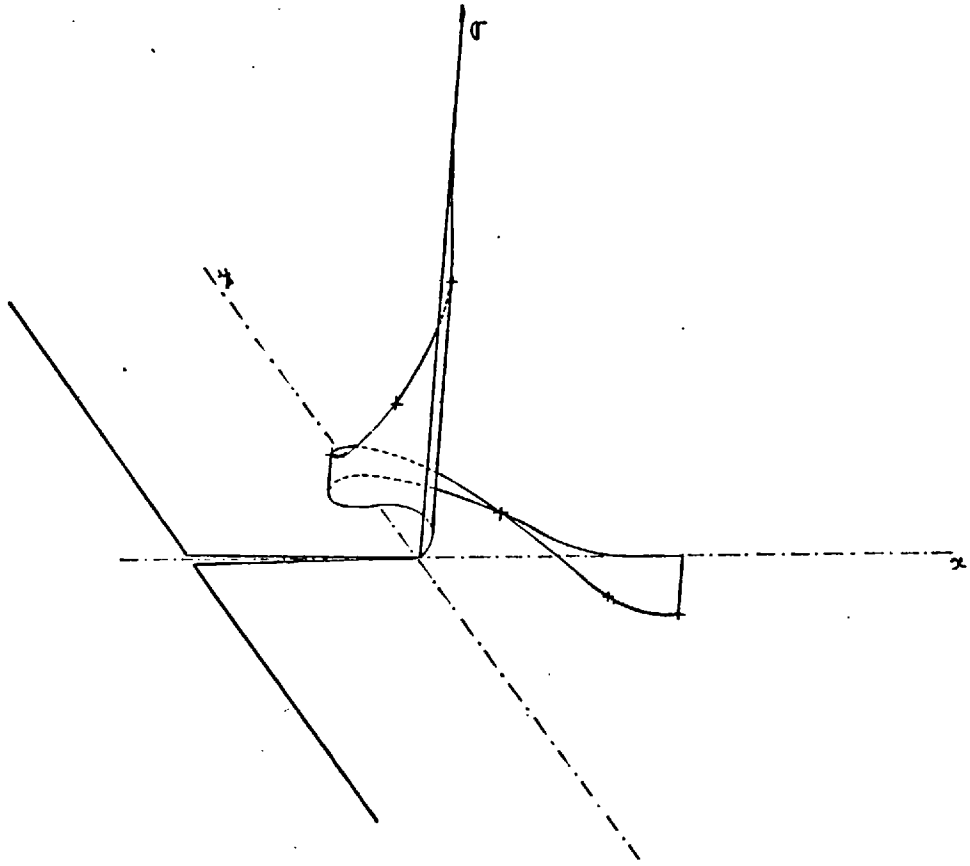

Fig. 7.18 Maximum values of stress (σ_ψ) as defined from the Williams series at r (cone radius) and ψ

(a)

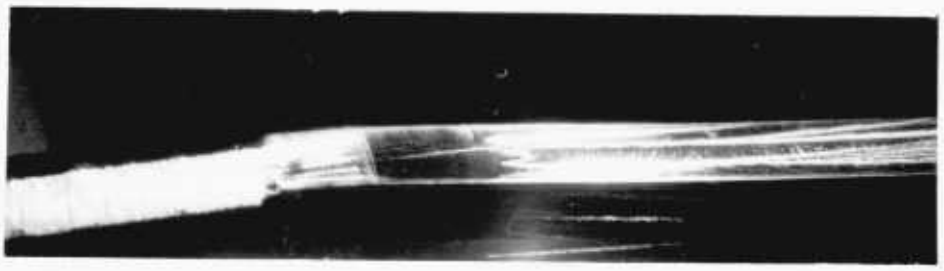

(b)

(c)

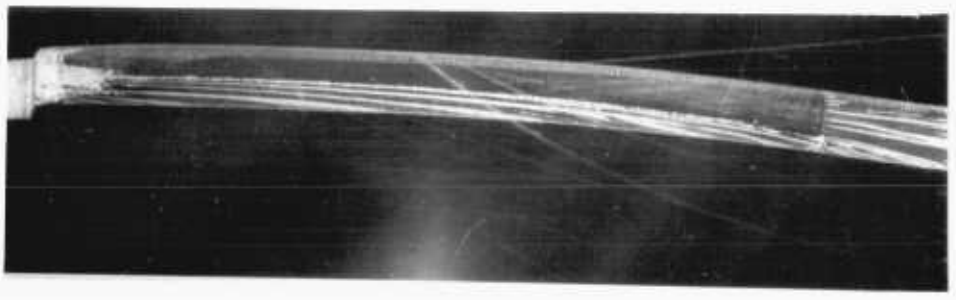

(d)

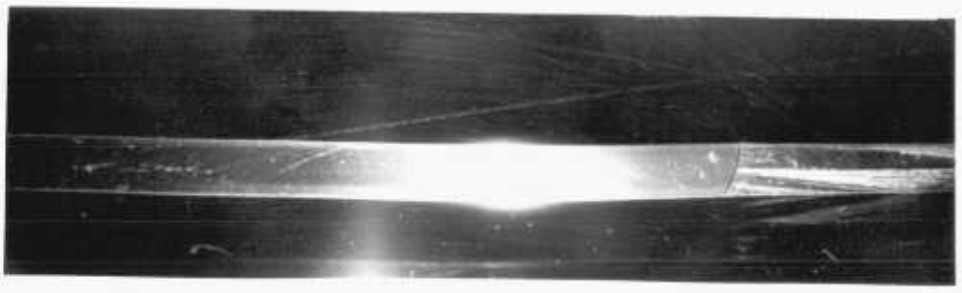

(e)

Fig. 8.1 Length of tusk emission for different operating base pressures

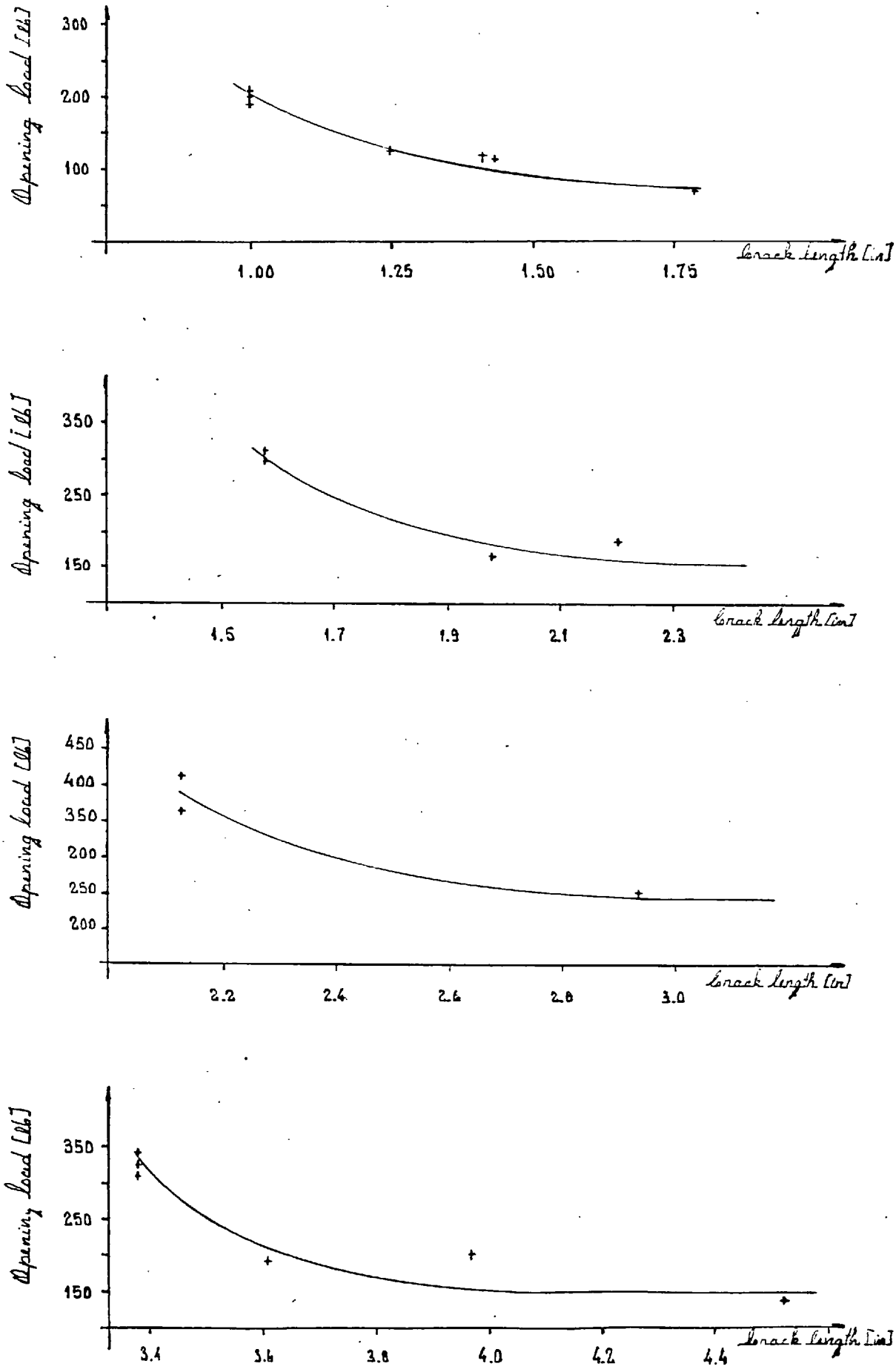

Fig. 6.2 Opening load values for different crack lengths

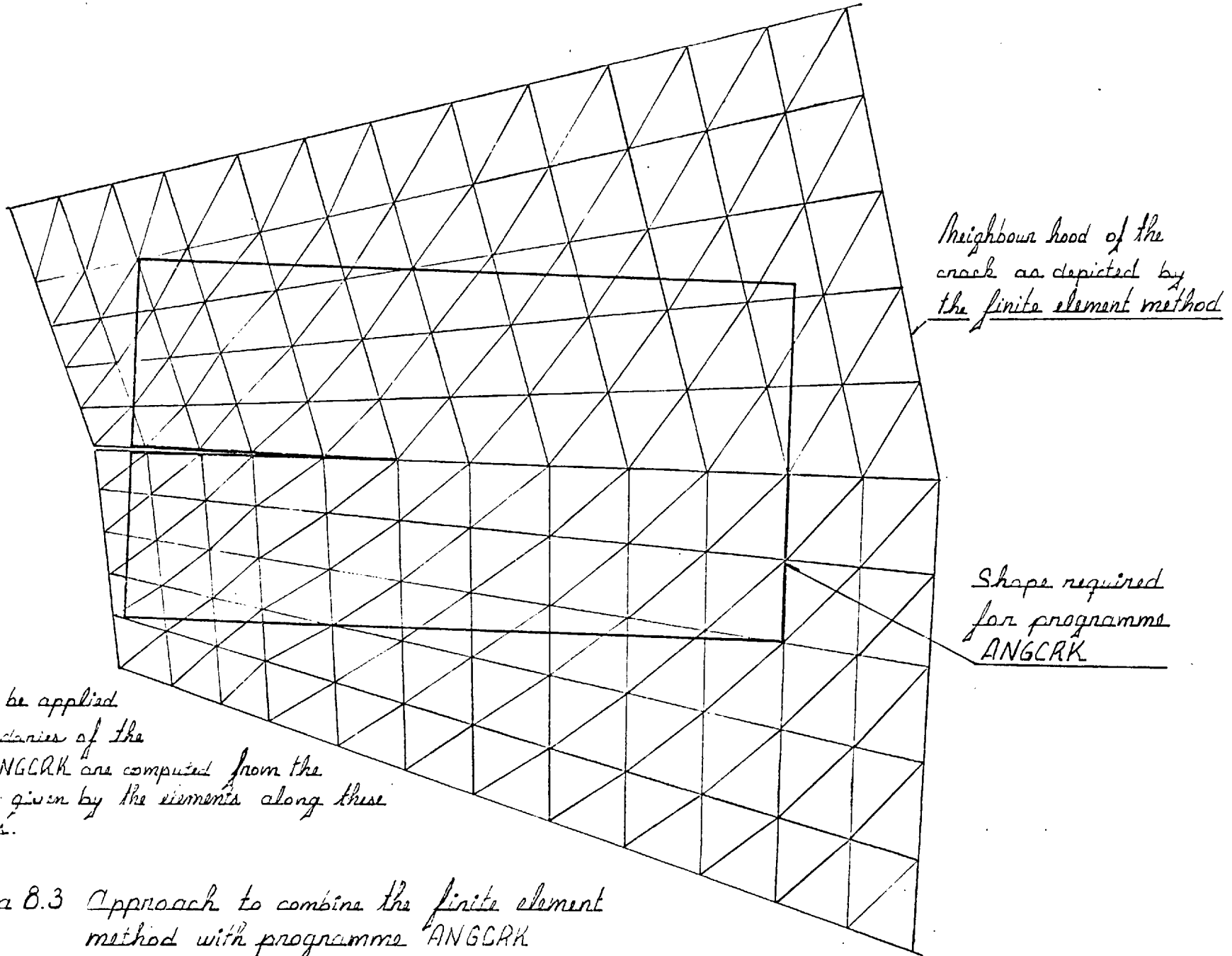

Fig 8.3 Approach to combine the finite element method with programme ANGCRK

APPENDIX 3

(a) Study on determination of direction of crack propagation.

(b) Determination of stress intensity factors.

This study involves: finite elements, computation, programming, automatic mesh generation for the gear.

The program developed works as follows.

Data: Diametral pitch, pitch diameter, number of teeth, helic angle, pressure angle, boundary conditions, loading.

It

(a) computes the tooth profile, isolates a gear section;

(b) generates a mesh suitable to be used in conjunction with program FLAP3, and applies the load;

(c) cracks the tooth;

(d) 1. by using Rice's contour integral, computes K

or

2. by using Bueckner's method, computes K.

Additionally, the data supplied by FLAP 3 can be used to trace isostatics, isoentatics, isopaclines, isochromatics, etc. These were done manually when required and is a length process but it is very useful for the analyst to know deeply what is going on in the material and these fields show clearly critical zones.

APPENDIX 3a

Pitch circle diameter	= 33.54"
Normal pitch	= 0.8"
Base circle diameter	= 31.074"
Addendum circle diameter	= 34.05"
Dedendum circle diameter	= 32.78"
Number of teeth	= 118
Face width	= 8.5"
Axial pitch	= 1.8"
Normal p.a.	= 20^{o}
Helix angle	= 26^{o} 23"
Thickness of rim below dedendum circle	= 2.14"
Grinding allowance	= 0.015"

Carburised to D.G.S. 6017E to give 0.085 effective case depth and hardened to a surface level of 650 to 775 D.P.N. The gears are designed for a Lloyd's 'K' value of 424 i.e. a tangential tooth load of 2727 lb/in face width.

APPENDIX 3b

Circumferential component of 100 lb load = 92.6 lb

Radial component of 100 lb load = 37.2 lb

For point A: moment arm to pitch circle = 0.353 in

root width = 0.702 in

eccentricity of radial load = 0.128 in

Simple bending stress = My/I

$$= \frac{92.6 \times 0.353 \times 3}{0.351 \times 0.351 \times 2}$$

$$= + 398 \text{ lb/in}^2$$

Direct stress = W/A

$$= -37.2/0.702 = -53 \text{ lb/in}^2$$

Eccentric bending stress = $(We)y/I$

$$= 37.2 \times 0.128 \times 3/2$$

$$(.351)^2$$

$$= -58 \text{ lb/in}^2$$

$\therefore$ Simple bending stress = $+398 \text{ lb/in}^2$

Simple combined stresses = 287 lb/in^2

11/4/9 JLS

Appendix 5a

Expressions for displacements "u" and "v" as obtained by Prof. J.L. Swedlow (1974)

Suppose at some point (r,θ)

$$\begin{Bmatrix} \sigma_r \\ \sigma_\theta \\ \tau_{r\theta} \end{Bmatrix} = \{\sigma(r,\theta)\}$$

We have, however, the relation

$$\{\sigma(r,\theta)\} = [C(r,\theta)] \begin{Bmatrix} a \\ b \\ a \\ b \end{Bmatrix}$$

The strain energy density at (r,θ) is $\bar{W}(r,\theta)$ given by,

$$2\bar{W}(r,\theta) = \{\sigma^T(r,\theta)\}[F]\{\sigma(r,\theta)\}$$

where

$$[F] = \frac{1}{E}\begin{bmatrix} 1 & -\upsilon & 0 \\ -\upsilon & 1 & 0 \\ 0 & 0 & 2(1+\upsilon) \end{bmatrix} \text{ or } \frac{1}{8\mu}\begin{bmatrix} \kappa+1 & \kappa-3 & 0 \\ \kappa-3 & \kappa+1 & 0 \\ 0 & 0 & 8 \end{bmatrix}$$

Hence

$$2\bar{W}(r,\theta) = \{a\ b\ a\ b\}[C^T(r,\theta)][F][C(r,\theta)]\begin{Bmatrix} a \\ b \\ a \\ b \end{Bmatrix}$$

Define

$$[B] = \int_{-\pi}^{\pi}\int_{0}^{r_e(\theta)} [C^T(r,\theta)][F][C(r,\theta)]\, r\,dr\,d\theta$$

Then

$$2\bar{U} = \{a\ b\ a\ b\}[B]\begin{Bmatrix} a \\ b \\ a \\ b \end{Bmatrix}$$

Let

$$\begin{Bmatrix} u(r,t) \\ v(r,t) \end{Bmatrix} = \{\underline{u}(r,t)\} = [D(r,t)] \begin{Bmatrix} q_1 \\ q_2 \\ q_3 \\ q_4 \end{Bmatrix}$$

and if

$$P = \int_{S_1}^{S_2} \{t^T\} \{\underline{u}(r,t)\} ds$$

then

$$P = \int_{S_1}^{S_2} \{t^T\} [D(r,t)] ds \cdot \begin{Bmatrix} q_1 \\ q_2 \\ q_3 \\ q_4 \end{Bmatrix} = [A] \begin{Bmatrix} q_1 \\ q_2 \\ q_3 \\ q_4 \end{Bmatrix}$$

or

$$[A] = \int_{S_1}^{S_2} \{t^T\} [D(r,t)] ds \equiv \{D^T\}$$

Now

$$\Pi = \frac{1}{2} \{a_1 a_2 a_3 a_4\} [B] \begin{Bmatrix} q_1 \\ q_2 \\ q_3 \\ q_4 \end{Bmatrix} - [A] \begin{Bmatrix} q_1 \\ q_2 \\ q_3 \\ q_4 \end{Bmatrix}$$

Since $\partial \Pi / \partial \begin{Bmatrix} q_1 \\ q_2 \\ q_3 \\ q_4 \end{Bmatrix} = 0$

we require

$$\boxed{[B] \begin{Bmatrix} q_1 \\ q_2 \\ q_3 \\ q_4 \end{Bmatrix} = \{D\}}$$

we need $[D(r,t)]$

if stress fcn $\phi = \Re\left[\bar{z}\,\psi(z) + \chi(z)\right]$ T&G^3 p 179

$$2\mu(u+iv) = \kappa\psi(z) - z\overline{\psi'(z)} - \overline{\chi'(z)}$$

or, in our notation

$$\chi = \Re\left[\bar{z}\,\phi(z) + \theta(z)\right]$$

$$2\mu(u+iv) = \kappa\phi - z\overline{\phi'} - \overline{\theta'}$$

Now, for <u>every</u> part

$$\chi = \sum_{n=1} \left\{ (-)^{n-1} a_{2n-1}\, r^{n+\frac{1}{2}} \left[-\cos\left(n-\tfrac{3}{2}\right)\psi + \frac{n-3/2}{n+1/2}\cos\left(n+\tfrac{1}{2}\right)\psi \right] \right.$$
$$\left. + (-)^{n} a_{2n}\, r^{n+1} \left[-\cos(n-1)\psi + \cos(n+1)\psi \right] \right\}$$

$$= \sum_{n=1} \left\{ (-)^{n-1} a_{2n-1} \left[\Re\left(-\bar{z}\, z^{n-3/2}\right) + \frac{n-3/2}{n+1/2}\,\Re\left(z^{n+1/2}\right) \right] \right.$$
$$\left. + (-)^{n} a_{2n} \left[\Re\left(-z\bar{z}\, z^{n-1}\right) + \Re\left(z^{n+1}\right) \right] \right\}$$

or apart from summation

$$\phi_n(z) = -\left[(-)^{n-1} a_{2n-1}\, z^{n-1/2} + (-)^{n} a_{2n}\, z^{n} \right]$$

$$\theta_n(z) = \left[(-)^{n-1} a_{2n-1}\, z^{n+1/2}\, \frac{n-3/2}{n+1/2} + (-)^{n} a_{2n} z^{n+1} \right]$$

$$\varphi' = -\left[(-)^{n-1} a_{2n-1} (n-1/2)\, z^{n-3/2} + (-)^n a_{2n}(n)\, z^{n-1}\right]$$

$$-\overline{\varphi'} = \left[(-)^{n-1} a_{2n-1} (n-1/2)\, \bar{z}^{n-3/2} + (-)^n a_{2n}(n)\, \bar{z}^{n-1}\right]$$

$$\psi' = \left[(-)^{n-1} a_{2n-1} (n+1/2)\, \frac{n-3/2}{n+1/2}\, z^{n-1/2} + (-)^n a_{2n}(n+1)\, z^n\right]$$

$$-\overline{\theta'} = -\left[(-)^{n-1} a_{2n-1} (n-3/2)\, \bar{z}^{n-1/2} + (-)^n a_{2n}(n+1)\, \bar{z}^n\right]$$

$$\mathcal{J}\mu(u+iv) = \sum_{n=1} \Big\{ -\kappa \left[(-)^{n-1} a_{2n-1}\, z^{n-1/2} + (-)^n a_{2n}\, z^n\right]$$

$$+ \left[(-)^{n-1} a_{2n-1}(n-1/2)\, z\, \bar{z}^{n-3/2} + (-)^n a_{2n}(n)\, z\, \bar{z}^{n-1}\right]$$

$$- \left[(-)^{n-1} a_{2n-1}(n-3/2)\, \bar{z}^{n-1/2} + (-)^n a_{2n}(n+1)\, \bar{z}^n\right] \Big\}$$

$$= \sum_{n=1} \Big\{ (-)^{n-1} a_{2n-1} \left[-\kappa z^{n-1/2} + (n-1/2)\, z\, \bar{z}^{n-3/2} - (n-3/2)\, \bar{z}^{n-1/2}\right]$$

$$+ \Big\{ (-)^n a_{2n} \left[-\kappa z^n + n\, z\, \bar{z}^{n-1} - \bar{z}^n (n+1)\right] \Big\}$$

$$= \sum_{n=1}^{\infty} \Big\{ (-)^{n-1} a_{2n-1} \Big[-K r^{n-1/2} e^{i(n-\frac{1}{2})t} + (n-\tfrac{1}{2}) r^{n-1/2} e^{-i(n-\frac{1}{2})t} - (n-\tfrac{3}{2}) r^{n-1/2} e^{-i(n-\frac{3}{2})t} \Big]$$

$$+ (-)^{n} a_{2n} r^{n} \Big[-K e^{int} + n e^{-i(n-1)t} - (n+1) e^{-int} \Big] \Big\}$$

$$= \sum_{n=1}^{\infty} \Big\{ (-)^{n-1} a_{2n-1} r^{n-\frac{1}{2}} \Big[-K e^{i(n-\frac{1}{2})t} + (n-\tfrac{1}{2}) e^{-i(n-\frac{3}{2})t} - (n-\tfrac{3}{2}) e^{-i(n-\frac{1}{2})t} \Big]$$

$$+ (-)^{n} a_{2n} r^{n} \Big[\qquad\qquad\qquad\qquad\qquad\qquad \Big]$$

$$= \sum_{n=1}^{\infty} \Big\{ (-)^{n-1} a_{2n-1} r^{n-\frac{1}{2}} \Big[-(K+n-\tfrac{3}{2}) \cos(n-\tfrac{1}{2})t - i(K-n+\tfrac{3}{2}) \sin(n-\tfrac{1}{2})t$$
$$+ (n-\tfrac{1}{2}) \cos(n-\tfrac{3}{2})t - i(n-\tfrac{1}{2}) \sin(n-\tfrac{3}{2})t \Big]$$

$$(-)^{n} a_{2n} r^{n} \Big[-(K+n+1) \cos nt - i(K-n-1) \sin nt$$
$$+ n \cos(n-2)t - i n \sin(n-2)t \Big] \Big\}$$

$$2\mu u = \sum_{n=1}^{\infty} \Big\{ (-)^{n-1} a_{2n-1} r^{n-\frac{1}{2}} \Big[-(K+n-\tfrac{3}{2}) \cos(n-\tfrac{1}{2})t + (n-\tfrac{1}{2}) \cos(n-\tfrac{3}{2})t \Big]$$
$$+ (-)^{n} a_{2n} r^{n} \Big[-(K+n+1) \cos nt + n \cos(n-2)t \Big] \Big\}$$

$$2\mu v = \sum_{n=1}^{\infty} \Big\{ (-)^{n-1} a_{2n-1} r^{n-\frac{1}{2}} \Big[-(K+1-n+\tfrac{1}{2}) \sin(n-\tfrac{1}{2})t - (n-\tfrac{1}{2}) \sin(n-\tfrac{3}{2})t \Big]$$
$$+ (-)^{n} a_{2n} r^{n} \Big[-(K-1-n) \sin nt - n \sin(n-2)t \Big] \Big\}$$

$k=1$

$$2\mu u = a_1 r^{1/2}\left[-(k-\tfrac{1}{2})\cos\tfrac{\theta}{2} + \tfrac{1}{2}\cos\tfrac{3\theta}{2}\right] + a_2 r\left[(k+1)\cos\theta - \cos\theta\right]$$

$$2\mu v = a_1 r^{1/2}\left[-(k+\tfrac{1}{2})\sin\tfrac{\theta}{2} + \tfrac{1}{2}\sin\tfrac{3\theta}{2}\right] + a_2 r\left[(k-3)\sin\theta + \sin\theta\right]$$

---

grad terms $\quad 2\mu u = a_2(k+1)x \qquad 2\mu v = a_2(k-3)y$

$2\mu\varepsilon_x = (k+1)a_2 \qquad 2\mu\varepsilon_y = (k-3)a_2$

$E\varepsilon_x = a_2$

$E\varepsilon_y = -3a_2$

& look ok

1st at $\theta=0$ $\quad 2\mu u = a_1 r^{1/2}(-k+1) = -a_1 r^{1/2}(k-1)$

$2\mu v = 0$

$\theta=\pi$ $\quad 2\mu u = 0$

$2\mu v = -a_1 r^{1/2}(k+1)$

$\theta=\frac{\pi}{2}$ $\quad 2\mu u = -a_1 (r/2)^{1/2} k$

$2\mu v = -a_1 (r/2)^{1/2} k$

nice $\quad \theta=0$ $\quad 2\mu u_r = -a_1 \sqrt{r}\,(k-1)$

$2\mu v_\theta = 0$

$\theta=\pi$ $\quad 2\mu v_r = 0$

$2\mu v_\theta = a_1\sqrt{r}\,(k+1)$

$\theta=\pi/2$ $\quad 2\mu u_r = -k a_1 \sqrt{r/2}$

$2\mu v_\theta = a_1 k\sqrt{r/2}$

from HW

$$2\mu u_r = a_1 r^{1/2}\left[-(\kappa-\tfrac{1}{2})\cos\tfrac{\theta}{2} + \tfrac{1}{2}\cos 3\tfrac{\theta}{2}\right]$$

$$2\mu v_\theta = a_1 r^{1/2}\left[(\kappa+\tfrac{1}{2})\sin\tfrac{\theta}{2} - \tfrac{1}{2}\sin 3\tfrac{\theta}{2}\right]$$

$$u = u_r\cos\theta - v_\theta\sin\theta$$

$$v = u_r\sin\theta + v_\theta\cos\theta$$

neglect $a_1 r^{1/2}$

$$-(\kappa-\tfrac{1}{2})\cos\tfrac{\theta}{2}\cos\theta + \tfrac{1}{2}\cos 3\tfrac{\theta}{2}\cos\theta$$
$$-(\kappa+\tfrac{1}{2})\sin\tfrac{\theta}{2}\sin\theta + \tfrac{1}{2}\sin 3\tfrac{\theta}{2}\sin\theta$$

$$-\kappa\cos\tfrac{\theta}{2} + \tfrac{1}{2}\cos 3\tfrac{\theta}{2} + \tfrac{1}{2}\cos\tfrac{\theta}{2} \quad \checkmark$$

~~$(\kappa+\frac{1}{2})\sin\frac{\theta}{2}\sin\theta \quad \frac{1}{2}\sin 3\frac{\theta}{2}\sin\theta$~~

$$-(\kappa-\tfrac{1}{2})\cos\tfrac{\theta}{2}\sin\theta + \tfrac{1}{2}\cos 3\tfrac{\theta}{2}\sin\theta$$
$$(\kappa+\tfrac{1}{2})\sin\tfrac{\theta}{2}\cos\theta - \tfrac{1}{2}\sin 3\tfrac{\theta}{2}\cos\theta$$

$$-\kappa\sin\tfrac{\theta}{2} + \tfrac{1}{2}\sin 3\tfrac{\theta}{2} - \tfrac{1}{2}\sin\tfrac{\theta}{2} \quad \checkmark$$

OK

for odd part

$$\chi = \sum_{n=1}^{\infty} \left\{ (-)^{n-1} b_{2n-1} r^{n+\frac{1}{2}} \left[\sin(n-\tfrac{3}{2})\psi - \sin(n+\tfrac{1}{2})\psi \right] \right.$$

$$\left. + (-)^{n} b_{2n} r^{n+1} \left[-\sin(n-1)\psi + \frac{n-1}{n+1} \sin(n+1)\psi \right] \right\}$$

$$= \sum_{n=1}^{\infty} \left\{ (-)^{n-1} b_{2n-1} \left[\Re\left(-i\bar{z}\, z^{n-\frac{1}{2}}\right) + \Re\left(i z^{n+\frac{1}{2}}\right) \right] \right.$$

$$\left. + (-)^{n} b_{2n} \left[\Re\left(i\bar{z}\, z^{n}\right) - \frac{n-1}{n+1} \Re\left(i z^{n+1}\right) \right] \right\}$$

So apart from summation

$$\phi_n(z) = -\left[(-)^{n-1} b_{2n-1}\, i\, z^{n-\frac{1}{2}} - (-)^{n} b_{2n}\, i\, z^{n} \right]$$

$$\theta_n(z) = \left[(-)^{n-1} b_{2n-1}\, i\, z^{n+\frac{1}{2}} - \frac{n-1}{n+1} b_{2n}\, i\, z^{n+1} \right]$$

$$\varphi_n' = -i\left[(-)^{n-1} b_{2n-1}\,(n-\tfrac{1}{2})\,z^{n-\frac{3}{2}} - (-)^n b_{2n}\,(n)\,z^{n-1}\right]$$

$$-\overline{\varphi_n'} = -i\left[(-)^{n-1} b_{2n-1}\,(n-\tfrac{1}{2})\,\bar{z}^{n-3/2} - (-)^n b_{2n}(n)\,\bar{z}^{n-1}\right]$$

$$\theta_n' = i\left[(-)^{n-1} b_{2n-1}(n+\tfrac{1}{2})\,z^{n+\frac{1}{2}} - (-)^n b_{2n}(n-1)\,z^n\right]$$

$$-\bar{\theta}_n' = i\left[(-)^{n-1} b_{2n-1}(n+\tfrac{1}{2})\,\bar{z}^{n-\frac{1}{2}} - (-)^n b_{2n}(n-1)\,\bar{z}^n\right]$$

$$2\mu(u+iv) = K\varphi - z\bar{\varphi}' - \bar{\theta}'$$

$$= \sum_{n=1}^{\infty}\Big\{ -Ki\left[(-)^{n-1} b_{2n-1} z^{n-\frac{1}{2}} - (-)^n b_{2n} z^n\right]$$

$$- iz\left[(-)^{n-1} b_{2n-1}(n-\tfrac{1}{2})\,\bar{z}^{n-3/2} - (-)^n b_{2n}(n)\,\bar{z}^{n-1}\right]$$

$$+ i\left[(-)^n b_{2n-1}(n+\tfrac{1}{2})\,\bar{z}^{n-\frac{1}{2}} - (-)^n b_{2n}(n-1)\,\bar{z}^n\right]\Big\}$$

$$= \sum_{n=1}^{\infty} i\Big\{ (-)^{n-1} b_{2n-1}\left[-K z^{n-\frac{1}{2}} - (n-\tfrac{1}{2})\,z\,\bar{z}^{n-\frac{3}{2}} + (n+\tfrac{1}{2})\bar{z}^{n-\frac{1}{2}}\right]$$

$$+ (-)^n b_{2n}\left[K z^n + n z\,\bar{z}^{n-1} - (n-1)\,\bar{z}^n\right]\Big\}$$

$$2\mu(V-iU) = \sum_{n=1}^{\infty} \Big\{ (-)^{n-1} b_{2n-1} \Big[r^{n-1/2} \Big] \Big[-Ke^{i(n-\frac{1}{2})t} - (n-\tfrac{1}{2}) e^{-i(n-\frac{5}{2})t} + (n+\tfrac{1}{2}) e^{-i(n-\frac{1}{2})t} \Big]$$

$$+ (-)^{n} b_{2n} r^{n} \Big[K e^{int} + n e^{-i(n-2)t} - (n-1) e^{-int} \Big] \Big\}$$

$$= \sum_{n=1}^{\infty} \Big\{ (-)^{n-1} b_{2n-1} r^{n-1/2} \Big[-(K-n+\tfrac{1}{2}) \cos(n-\tfrac{1}{2})t - i(K+n+\tfrac{1}{2}) \sin(n-\tfrac{1}{2})t$$

$$-(n-\tfrac{1}{2}) \cos(n-\tfrac{5}{2})t + i(n-\tfrac{1}{2}) \sin(n-\tfrac{5}{2})t \Big]$$

$$+ (-)^{n} b_{2n} r^{n} \Big[(K-n+1) \cos nt + i(K+n-1) \sin nt$$

$$+ n \cos(n-2)t - in \sin(n-2)t \Big] \Big\}$$

$$2\mu V = \sum_{n=1}^{\infty} \Big\{ (-)^{n-1} b_{2n-1} r^{n-1/2} \Big[-(K-n-\tfrac{1}{2}) \cos(n-\tfrac{1}{2})t - (n-\tfrac{1}{2}) \cos(n-\tfrac{5}{2})t \Big]$$

$$+ (-)^{n} b_{2n} r^{n} \Big[\overset{c}{(K-n+1)} \cos nt + \overset{d}{n} \cos(n-2)t \Big] \Big\}$$

$$2\mu U = \sum_{n=1}^{\infty} \Big\{ (-)^{n-1} b_{2n-1} r^{n-1/2} \Big[(K+n+\tfrac{1}{2}) \sin(n-\tfrac{1}{2})t - (n-\tfrac{1}{2}) \sin(n-\tfrac{5}{2})t \Big]$$

$$+ (-)^{n} b_{2n} r^{n} \Big[\overset{a}{-(K+n-1)} \sin nt + \overset{b}{n} \sin(n-2)t \Big] \Big\}$$

$n=1$

$$\tau_{\mu\alpha} = b_1 r^{1/2}\left[\left(K+\tfrac{3}{2}\right)\sin\tfrac{\phi}{2} + \tfrac{1}{2}\sin\tfrac{3\phi}{2}\right]$$

$$+ b_2 r\left[K\sin\phi + \sin\phi\right] = b_2(K+1)\sin\phi$$

$$\tau_{\mu\nu} = b_1 r^{1/2}\left[-\left(K-\tfrac{3}{2}\right)\cos\tfrac{\phi}{2} - \tfrac{1}{2}\cos\tfrac{3\phi}{2}\right]$$

$$+ b_2 r\left[-K\cos\phi - \cos\phi\right] = -b_2(K+1)\cos\phi$$

$\phi=\pi$ $\quad \tau_{\mu\alpha} = b_1 r^{1/2}\left[K+1\right]$

$\tau_{\mu\nu} = 0$

paper seems in error.

$$\tau_{\mu\nu} = S^*\left\{-\tfrac{1}{2} - (K+\tfrac{1}{2})\right\}$$

$\phi=0$ $\quad \tau_{\mu\alpha} = 0$

$\tau_{\mu\nu} = b_1 r^{K+1}\left[-(K-\tfrac{1}{2})\right]$

$\phi=\pi$ $\quad \tau_{\mu\alpha_2} = b_1 r^{K+1}\left[K+\tfrac{1}{2}\right]$

$\tau_{\mu\nu_2} = 0$

$\phi=\pi/2$ $\quad \tau_{\mu\alpha_3} = \frac{b_1 r^{K+1}}{\sqrt{2}}\left[K+\tfrac{1}{2}\right]$

$\tau_{\mu\nu_3} = \frac{b_1 r^{K+1}}{\sqrt{2}}\left[-K-\tfrac{1}{2}\right]$

$\tau_{\mu\alpha_4} = b_1\sqrt{5}\, r^{K+1}\left[\tfrac{1}{2}-K-\tfrac{1}{3}\right]$

$\tau_{\mu\nu_4} = b_1\sqrt{5}\, r^{K+1}\left[-\tfrac{1}{2}-K-\tfrac{1}{3}\right]$

$\tau_{\mu\alpha_5} = b_1 r^{K+1}\left[\tfrac{1}{2}-K-\tfrac{1}{3}\right]$

$\tau_{\mu\nu_5} = 0$

$\upsilon = 0 \quad K+1 = 1$

$\upsilon = 1/2 \quad K+1 = 1/3$

$\upsilon = .3 \quad 3$

$\upsilon = .5 \quad 2\tfrac{2}{3}$

(1/2) (0)

$\frac{5/2}{3/2} = \frac{5}{3}$ 3

$\frac{3-\upsilon}{1+\upsilon}$ $\quad .3 \quad \frac{2.7}{1.3}$

(1C+1)

$$\mathcal{J}_{\mu u} = \sum_{n=1}^{\infty} \Big\{ (-)^{n-1} a_{2n-1} r^{n-\frac{1}{2}} \Big[-(K+n-\tfrac{3}{2}) \cos(n-\tfrac{1}{2})\psi + (n-\tfrac{1}{2}) \cos(n-\tfrac{5}{2})\psi \Big] \quad 318$$

$$+ (-)^{n-1} b_{2n-1} r^{n-\frac{1}{2}} \Big[(K+n+\tfrac{1}{2}) \sin(n-\tfrac{1}{2})\psi - (n-\tfrac{1}{2}) \sin(n-\tfrac{5}{2})\psi \Big]$$

$$+ (-)^{n} a_{2n} r^{n} \Big[-(K+n+1) \cos n\psi + n \cos(n-2)\psi \Big]$$

$$+ (-)^{n} b_{2n} r^{n} \Big[-(K+n-1) \sin n\psi + n \sin(n-2)\psi \Big] \Big\}$$

$$\mathcal{J}_{\mu v} = \sum_{n=1}^{\infty} \Big\{ (-)^{n-1} a_{2n-1} r^{n-\frac{1}{2}} \Big[-(K-n+\tfrac{3}{2}) \sin(n-\tfrac{1}{2})\psi - (n-\tfrac{1}{2}) \sin(n-\tfrac{5}{2})\psi \Big]$$

$$+ (-)^{n-1} b_{2n-1} r^{n-\frac{1}{2}} \Big[-(K-n-\tfrac{1}{2}) \cos(n-\tfrac{1}{2})\psi - (n-\tfrac{1}{2}) \cos(n-\tfrac{5}{2})\psi \Big]$$

$$+ (-)^{n} a_{2n} r^{n} \Big[-(K-1-n) \sin n\psi - n \sin(n-2)\psi \Big]$$

$$+ (-)^{n} b_{2n} r^{n} \Big[(K-n+1) \cos n\psi + n \cos(n-2)\psi \Big] \Big\}$$

$K \cos\psi r$

$v = -y(K+1)$

APPENDIX 5b

Expressions for the stress field in the crack neighbourhood.

$$\epsilon_x = \frac{\partial u}{\partial x} = \frac{\partial u}{\partial r}\frac{\partial r}{\partial x} + \frac{\partial u}{\partial \psi}\frac{\partial \psi}{\partial x}$$

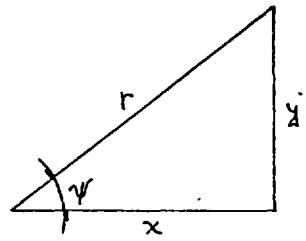

$$r = \sqrt{x^2 + y^2}$$

$$\psi = \mathrm{Tan}^{-1}\,(y/x)$$

$$\frac{\partial r}{\partial x} = \frac{\partial (x^2 + y^2)^{\frac{1}{2}}}{\partial x} = \frac{(x^2 + y^2)^{-\frac{1}{2}}}{2}\frac{d(x^2 + y^2)}{dx}$$

$$= \frac{1}{2(x^2 + y^2)^{\frac{1}{2}}}\frac{dx^2}{dx} = \frac{2x}{2(x^2 + y^2)^{\frac{1}{2}}}\frac{dx}{dx} = \frac{x}{\sqrt{x^2 + y^2}}$$

$$= \frac{x}{r} \doteq \mathrm{Cos}\ \psi \qquad \therefore \frac{\partial r}{\partial x} = \mathrm{Cos}\ \psi$$

in the same way

$$\frac{\partial \psi}{\partial x} = -\frac{\mathrm{Sin}\ \psi}{r} \quad \therefore$$

$$\epsilon_x = \frac{\partial u}{\partial x} = \frac{\partial u}{\partial r}\mathrm{Cos}\ \psi - \frac{\partial u}{\partial \psi}\frac{\mathrm{Sin}\ \psi}{r}\ ;$$

$$\epsilon_y = \frac{\partial v}{\partial y} = \frac{\partial v}{\partial r}\frac{\partial r}{\partial y} + \frac{\partial v}{\partial \psi}\frac{\partial \psi}{\partial y} =$$

$$\epsilon_y = \frac{\partial v}{\partial r}\mathrm{Sin}\ \psi + \frac{\partial v}{\partial \psi}\frac{\mathrm{Cos}\ \psi}{r}$$

and

$$\gamma_{xy} = \frac{\partial u}{\partial y} + \frac{\partial v}{\partial x}$$

that becomes

$$\gamma_{xy} = \frac{\partial u}{\partial r}\mathrm{Sin}\ \psi + \frac{\partial u}{\partial \psi}\frac{\mathrm{Cos}\ \psi}{r} + \frac{\partial \psi}{\partial r}\mathrm{Cos}\ \psi - \frac{\partial v}{\partial \psi}\frac{\mathrm{Sin}\ \psi}{r}$$

u and v are given as shown in Chapter 5 and in order to simplify calculations, constants within the series were represented as follows.

In order to facilitate the handling of the whole expressions

COE1, COE2, etc, are defined as:

$$COE1 = [-(k + n - 3/2)\ Cos\ (n - \tfrac{1}{2})\psi + (n - \tfrac{1}{2})Cos(n - 5/2)\psi]$$

$$\frac{\partial COE1}{\partial \psi} = [(k + n - 3/2)Sin(n - \tfrac{1}{2})\psi - (n - \tfrac{1}{2})(n - 5/2)Sin(n - 5/2)\psi]$$

$$COE5 = [-(k + 3/2 - n)Sin(n - \tfrac{1}{2})\psi - (n - \tfrac{1}{2})Sin(n - 5/2)\psi]$$

$$\frac{\partial COE5}{\partial \psi} = [-(k + 3/2 - n)(n - \tfrac{1}{2})Cos(n - \tfrac{1}{2})\psi - (n - \tfrac{1}{2})(n - 5/2)\ Cos(n - 5/2\psi]$$

So

$$u = \Sigma\{(-1)^{n-1} r^{n-\frac{1}{2}}[a_{2n-1} COE1 + b_{2n-1} COE3] + (-1)^n r^n\ [a_{2n} COE2 + b_{2n} COE4]\}$$

$$v = \Sigma\{(-1)^{n-1} r^{n-\frac{1}{2}}[a_{2n-1} COE5 + b_{n-1} COE7] + (-1)^n r^n\ [a_{2n} COE6 + b_{2n}\ COE8]\}$$

Considering here only those parts of the equations concerning a_{2n-1}

$$\frac{\partial u}{\partial r} = (-1)^{n-1}(n - \tfrac{1}{2}) r^{n-3/2} C_{2n-1} COE1$$

$$\frac{\partial u}{\partial \psi} = (-1)^{n-1} r^{n-\frac{1}{2}} C_{2n-1} \frac{\partial COE1}{\partial \psi}$$

$$\frac{\partial u}{\partial r} Cos\psi = \{(-1)^{n-1}(n - \tfrac{1}{2}) r^{n-3/2} C_{2n-1} COE1\ Cos\psi\}$$

$$\frac{\partial u}{\partial \psi} \frac{Sin\psi}{r} = \{(-1)^{n-1}\ r^{n-3/2}\ C_{2n-1} \frac{\partial COE1}{\partial \psi}\ Sin\ \psi\}$$

$$\frac{\partial v}{\partial r} = \{(-1)^{n-1}(n - \tfrac{1}{2}) r^{n-3/2}\ C_{2n-1}\ COE5\}$$

$$\frac{\partial v}{\partial \psi} = \{(-1)^{n-1}\ r^{n-3/2}\ C_{2n-1} \frac{\partial COE5}{\partial \psi}\ \}$$

$$\frac{\partial v}{\partial r} Sin\psi = \{(-1)^{n-1}(n - \tfrac{1}{2}) r^{n-3/2}\ C_{2n-1}\ COE5\ Sin\ \psi\}$$

$$\frac{\partial v}{\partial \psi} \frac{Cos\psi}{r} = \{(-1)^{n-1}\ r^{n-3/2}\ C_{2n-1} \frac{\partial COE5}{\partial \psi} Cos\psi\}$$

$$\frac{\partial u}{\partial r}\,\mathrm{Sin}\psi = \{(-1)^{n-1}(n-\tfrac{1}{2})r^{n-3/2}C_{2n-1}\mathrm{COE1}\,\mathrm{Sin}\psi\}$$

$$\frac{\partial u}{\partial \psi}\,\frac{\mathrm{Cos}\psi}{r} = \{(-1)^{n-1}r^{n-3/2}\,C_{2n-1}\,\frac{\partial \mathrm{COE1}}{\partial \psi}\,\mathrm{Cos}\psi\}$$

$$\frac{\partial v}{\partial r}\,\mathrm{Cos}\psi = \{(-1)^{n-1}(n-\tfrac{1}{2})\,r^{n-3/2}\,C_{2n-1}\,\mathrm{COE5}\,\mathrm{Cos}\psi\}$$

$$\frac{\partial v}{\partial r}\,\frac{\mathrm{Sin}\psi}{r} = \{(-1)^{n-1}\,r^{n-3/2}\,C_{2n-1}\,\frac{\partial \mathrm{COE5}}{\partial \psi}\,\mathrm{Sin}\psi\}$$

$$\sigma_r = \frac{\sigma_x + \sigma_y}{2} + \frac{\sigma_x - \sigma_y}{2}\,\mathrm{Cos}\,2\psi + \sigma_{xy}\,\mathrm{Sin}\,2\psi$$

$$\frac{\sigma_x + \sigma_y}{2} = \frac{E}{2(1-\nu)}\,(\epsilon_x + \epsilon_y)$$

$$\frac{\sigma_x - \sigma_y}{2} = \frac{E}{2(1+\nu)}\,(\epsilon_x - \epsilon_y)$$

$$\sigma_{xy} = \frac{E}{2(1+\nu)}\,\gamma_{xy}$$

$$\epsilon_x = \frac{\partial u}{\partial x} = \frac{\partial u}{\partial r}\,\frac{\partial r}{\partial x} + \frac{\partial u}{\partial \psi}\,\frac{\partial \psi}{\partial x}$$

$$\epsilon_x = \frac{\partial u}{\partial r}\,\mathrm{Cos}\,\psi - \frac{\partial u}{\partial \psi}\,\frac{\mathrm{Sin}\,\psi}{r}$$

$$\epsilon_x = \{[(-1)^{n-1}(n-\tfrac{1}{2})r^{n-3/2}C_{2n-1}\,\mathrm{COE1}\,\mathrm{Cos}\psi] - [(-1)^{n-1}r^{n-3/2}\,C_{2n-1}\,\frac{\partial \mathrm{COE1}}{\partial \psi}\,\mathrm{Sin}\psi]$$

$$\epsilon_y = \frac{\partial v}{\partial y} = \frac{\partial v}{\partial r}\,\frac{\partial r}{\partial y} + \frac{\partial v}{\partial \psi}\,\frac{\partial \psi}{\partial y} = \frac{\partial v}{\partial r}\,\mathrm{Sin}\psi + \frac{\partial v}{\partial \psi}\,\frac{\mathrm{Cos}\psi}{r}$$

$$\epsilon_y = \{[(-1)^{n-1}(n-\tfrac{1}{2})r^{n-3/2}C_{2n-1}\mathrm{COE5}\,\mathrm{Sin}\psi]$$

$$+\,[)-1)^{n-1}r^{n-3/2}C_{2n-1}\,\frac{\partial \mathrm{COE5}}{\partial \psi}\,\mathrm{Cos}\psi]$$

$$\gamma_{xy} = \frac{\partial u}{\partial y} + \frac{\partial v}{\partial x} = \frac{\partial u}{\partial r}\,\mathrm{Sin}\psi + \frac{\partial u}{\partial \psi}\,\frac{\mathrm{Cos}\psi}{r} + \frac{\partial v}{\partial r}\,\mathrm{Cos}\psi - \frac{\partial v}{\partial \psi}\,\frac{\mathrm{Sin}\psi}{r}$$

$$\gamma_{xy} = \{[(-1)^{n-1}(n - \tfrac{1}{2})r^{n-3/2}C_{2n-1}COE1\ Sin\psi]$$

$$+ [(-1)^{n-1}\ r^{n-3/2}C_{2n-1}\ \frac{\partial COE1}{\partial\psi}\ Cos\psi]$$

$$+ [(-1)^{n-1}(n-\tfrac{1}{2})r^{n-3/2}C_{2n-1}\ COE5\ Cos\psi]$$

$$- [(-1)^{n-1}r^{n-3/2}C_{2n-1}\ \frac{\partial COE5}{\partial\psi}\ Sin\psi]\}$$

$$\epsilon_x \pm \epsilon_y = \{[(-1)^{n-1}(n - \tfrac{1}{2})r^{n-3/2}C_{2n-1}COE1\ Cos\psi]$$

$$- [(-1)^{n-1}r^{n-3/2}C_{2n-1}\ \frac{\partial COE1}{\partial\psi}\ Sin\psi]$$

$$\pm [(-1)^{n-1}(n - \tfrac{1}{2})r^{n-3/2}C_{2n-1}\ COE5\ Sin\psi]$$

$$\pm [(-1)^{n-1}\ n-3/2C_{2n-1}\ \frac{\partial COE5}{\partial\psi}\ Cos\ \psi]\}$$

$$\zeta = (-1)^{n-1}\ r^{n-3/2}C_{2n-1}$$

$$\epsilon_x + \epsilon_y = \zeta\ [(n - \tfrac{1}{2})\ COE1\ Cos\psi - \frac{\partial COE1}{\partial\psi}\ Sin\psi + (n - \tfrac{1}{2})COE5\ Sin\psi$$

$$+ \frac{\partial COE5}{\partial\psi}\ Cos\psi]$$

$$\epsilon_x - \epsilon_y = \zeta[(n - \tfrac{1}{2})\ COE1\ Cos\psi - \frac{\partial COE1}{\partial\psi}\ Sin\psi - (n - \tfrac{1}{2})\ COE5\ Sin\psi$$

$$- \frac{\partial COE5}{\partial\psi}\ Cos\psi]$$

$$\frac{\sigma_x - \sigma_y}{2}\ Cos\ 2\psi = \frac{E}{2(1+\nu)}\ (\epsilon_x - \epsilon_y)Cos2\psi = \frac{E}{2(1+\nu)}(\epsilon_x - \epsilon_y)(1 - 2Sin^2\psi)$$

$$(\epsilon_x - \epsilon_y)(1-2Sin^2\partial) = \zeta[(n - \tfrac{1}{2})COE1\ Cos\psi - \frac{\partial COE1}{\partial\psi}\ Sin\psi - (n - \tfrac{1}{2})COE5Sin\psi$$

$$- \frac{\partial COE5}{\partial\psi}\ Cos\psi] + [-2(m - \tfrac{1}{2})COE1\ Cos\psi\ Sin^2\psi$$

$$+ 2(n - \tfrac{1}{2})COE5\ Sin^3\psi + 2\ \frac{\partial COE5}{\partial\psi}\ Cos\psi\ Sin^2\psi]$$

$$\sigma_{xy}Sin2\psi = \frac{E}{2(1+\nu)}\ \gamma_{xy}Sin2\psi = \frac{E}{2(1+\nu)}\ \ _{xy}2Sin\psi\ Cos\psi$$

$$\gamma_{xy} = \zeta\{(n - \tfrac{1}{2})COE1Sin\psi + \frac{\partial COE1}{\partial\psi}\ Cos\psi + (n - \tfrac{1}{2})COE5\ Cos\psi - \frac{\partial COE5}{\partial\psi}\ Sin\psi\}$$

$$\gamma_{xy}\, 2\mathrm{Sin}\psi\mathrm{Cos}\psi = \zeta\,\{2(n-\tfrac{1}{2})\mathrm{COE1}\mathrm{Sin}^2\psi + 2\frac{\partial \mathrm{COE1}}{\partial\psi}\mathrm{Cos}^2\psi\mathrm{Sin}\psi$$

$$+ 2(n-\tfrac{1}{2})\mathrm{COE5}\,\mathrm{Cos}^2\psi\mathrm{Sin}\psi - 2\frac{\partial \mathrm{COE5}}{\partial\psi}\mathrm{Sin}^2\psi\mathrm{Cos}\psi\,\}$$

$$(\epsilon_x - \epsilon_y)(1 - 2\mathrm{Sin}^2\psi) + \gamma_{xy}2\mathrm{Sin}\psi\mathrm{Cos}\psi = \zeta\,\{(n-\tfrac{1}{2})\mathrm{COE1}\mathrm{Cos}\psi$$

$$- \frac{\partial \mathrm{COE1}}{\partial\psi}\mathrm{Sin}\psi - (n-\tfrac{1}{2})\mathrm{COE5}\mathrm{Sin}\psi - \frac{\partial \mathrm{COE5}}{\partial\psi}\mathrm{Cos}\psi$$

$$+ 2\frac{\partial \mathrm{COE1}}{\partial\psi}\mathrm{Cos}^2\psi\mathrm{Sin}\psi + 2\frac{\partial \mathrm{COE1}}{\partial\psi}\mathrm{Sin}^3\psi + 2(n-\tfrac{1}{2})\mathrm{COE5}\mathrm{Cos}^2\psi\mathrm{Sin}\psi$$

$$+ 2(n-\tfrac{1}{2})\,\mathrm{COE5}\mathrm{Sin}^3\psi\} = \zeta\,\{(n-\tfrac{1}{2})\mathrm{COE1}\mathrm{Cos}\psi - \frac{\partial \mathrm{COE1}}{\partial\psi}\mathrm{Sin}\psi$$

$$[1 - 2(\mathrm{Cos}^2\psi + \mathrm{Sin}^2\psi)] - (n-\tfrac{1}{2})\mathrm{COE5}\mathrm{Sin}\psi\,[1 - 2\,(\mathrm{Cos}^2\psi + \mathrm{Sin}^2\psi)]$$

$$- \frac{\partial \mathrm{COE5}}{\partial\psi}\mathrm{Cos}\psi\}$$

$$= \zeta\,[(n-\tfrac{1}{2})\mathrm{COE1}\mathrm{Cos}\psi + \frac{\partial \mathrm{COE1}}{\partial\psi}\mathrm{Sin}\psi + (n-\tfrac{1}{2})\mathrm{COE5}\mathrm{Sin}\psi - \frac{\partial \mathrm{COE5}}{\partial\psi}\mathrm{Cos}\psi]$$

$$= \zeta\,(n-\tfrac{1}{2})\{[-(k+n-3/2)\mathrm{Cos}(n-\tfrac{1}{2})\psi + (n-\tfrac{1}{2})\mathrm{Cos}(n-5/2)\psi]\mathrm{Cos}\psi$$

$$+ [(k+n-3/2)\mathrm{Sin}(n-\tfrac{1}{2})\psi - (n-5/2)\mathrm{Sin}(n-5/2)\psi]\mathrm{Sin}\psi$$

$$+ [-(k+3/2-n)\mathrm{Sin}(n-\tfrac{1}{2})\psi - (n-\tfrac{1}{2})\mathrm{Sin}(n-5/2)\psi]\mathrm{Sin}\psi$$

$$- [-(k+3/2-n)\mathrm{Cos}(n-\tfrac{1}{2})\psi - (n-5/2)\mathrm{Cos}(n-5/2)\psi]\mathrm{Cos}\psi\,\}$$

$$= \zeta(n-\tfrac{1}{2})[-2(n-3/2)\mathrm{Cos}\psi\,\mathrm{Cos}(n-\tfrac{1}{2})\psi + 2(n-3/2)\mathrm{Cos}\psi\mathrm{Cos}(n-5/2)\psi$$

$$+ 2(n-3/2)\mathrm{Sin}\psi\mathrm{Sin}(n-\tfrac{1}{2})\psi - 2(n-3/2)\mathrm{Sin}\psi\mathrm{Sin}(n-5/2)\psi\,]$$

$\alpha_1 = (n-\tfrac{1}{2})\psi$; $\quad = \psi\,\alpha_1-\alpha_2 = (n-3/2)\psi\;\alpha_1+\alpha_2 = (n+\tfrac{1}{2})\psi$

$\alpha_3 = (n-5/2)\psi\;\alpha_4 = \psi\,\alpha_3-\alpha_4 = (n-7/2)\alpha_3+\alpha_4 = (n-3/2)$

$$= \zeta(n-\tfrac{1}{2})2(n-3/2)\,\{-\tfrac{1}{2}\,\mathrm{Cos}(n-3/2)\psi - \tfrac{1}{2}\,\mathrm{Cos}(n+\tfrac{1}{2})\psi$$

$$+ \tfrac{1}{2}\,\mathrm{Cos}(n-7/2)\psi + \tfrac{1}{2}\,\mathrm{Cos}(n-3/2)\psi$$

$$+ \tfrac{1}{2}\,\mathrm{Cos}(n-3/2)\psi - \tfrac{1}{2}\,\mathrm{Cos}(n+\tfrac{1}{2})\psi - \tfrac{1}{2}\,\mathrm{Cos}(n-7/2)\psi + \tfrac{1}{2}\,\mathrm{Cos}(n-3/2)\psi\}$$

$$= \zeta\,(n-\tfrac{1}{2})2(n-3/2)\,[-\mathrm{Cos}(n+\tfrac{1}{2})\psi + \mathrm{Cos}(n-3/2)\psi]$$

$$(\epsilon_x - \epsilon_y)\mathrm{Cos}2\psi + \gamma_{xy}\mathrm{Sin}2\psi = (-1)^{n-1}\;{}^{n-3/2}C_{2n-1}(n-\tfrac{1}{2})2(n-3/2)$$

$$[\mathrm{Cos}(n-3/2)\psi - \mathrm{Cos}(n+\tfrac{1}{2})\psi]$$

This is being multiplied by $\dfrac{E}{2(1+\nu)}$

$$\frac{\epsilon_x + \epsilon_y}{2} = \zeta\,[(n-\tfrac{1}{2})\mathrm{COE1}\mathrm{Cos}\psi - \frac{\partial \mathrm{COE1}}{\partial\psi}\mathrm{Sin}\psi + (n-\tfrac{1}{2})\mathrm{COE5}\,\mathrm{Sin}\psi + \frac{\partial \mathrm{COE5}}{\partial\psi}\mathrm{Cos}\psi]$$

$$= \zeta(n - \tfrac{1}{2}) \{[-(k + n - 3/2)\cos(n - \tfrac{1}{2})\psi + (n - \tfrac{1}{2})\cos(n - 5/2)\psi]\cos\psi$$

$$-[(k + n - 3/2)\sin(n - \tfrac{1}{2})\psi - (n - 5/2)\sin(n - 5/2)\psi]\sin\psi$$

$$+[-(k + 3/2 - n)\sin(n - \tfrac{1}{2})\psi - (n - \tfrac{1}{2})\sin(n - 5/2)\psi]\sin\psi$$

$$+[-(k + 3/2 - n)\cos(n - \tfrac{1}{2})\psi - (n - 5/2)\cos(n - 5/2)\psi]\cos\psi\}$$

$$= \zeta(n - \tfrac{1}{2}) \{-2k\cos\psi\cos(n - \tfrac{1}{2})\psi + 2\cos\psi\cos(n - 5/2)\psi$$

$$-2k\sin\psi\sin(n - \tfrac{1}{2})\psi - 2\sin\psi\sin(n - 5/2)\psi$$

$\alpha_1 = (n - \frac{1}{2})\psi$; $\alpha_1 - \alpha_2 = n - 3/2$ $\alpha_3 = (n - 5/2)\psi$ $\alpha_3 - \alpha_4 = (n - 7/2)\psi$

$\alpha_2 = \psi$ $\alpha_1 + \alpha_2 = n + \frac{1}{2}$ $\alpha_4 = \psi$ $\alpha_3 + \alpha_4 = \psi$

$$= -\zeta(n-\tfrac{1}{2}) \quad k\begin{bmatrix} \cos(n-3/2)\psi + \cos(n+\frac{1}{2})\psi & + & \cos(n-7/2)\psi + \cos(n-3/2)\psi \\ +\cos(n-3/2)\psi - \cos(n+\frac{1}{2})\psi & & -\cos(n-7/2)\psi + \cos(n-3/2)\psi \end{bmatrix}$$

$$= \zeta(n-\tfrac{1}{2}) [-2\,k\,\cos(n - 3/2)\psi + 2\,\cos(n - 3/2)\psi]$$

$$= \zeta(n-\tfrac{1}{2}) [-2(k - 1)\,\cos(n - 3/2)\psi]$$

and

$$K = \frac{3 - \nu}{1 + \nu} \quad \therefore$$

$$-2(k - 1) = -2\left[\frac{3 - \nu}{1 + \nu} - 1\right] = \frac{-6 + 2\nu}{1 + \nu} + 2 = \frac{-6 + 2\nu + 2 + 2\nu}{1 + \nu}$$

$$= \frac{-4 + 4\nu}{1 + \nu} = \frac{-4(1 - \nu)}{1 + \nu}$$

$$\epsilon_x + \epsilon_y = \zeta(n - \tfrac{1}{2}) \left[\frac{-4(1 - \nu)}{1 + \nu} \cos(n - 3/2)\psi\right]$$

$$\frac{\sigma_x + \sigma_y}{2} = \frac{E}{2(1 - \nu)} (\epsilon_x + \epsilon_y) = \frac{E}{2(1 + \nu)} \zeta\,(n - \tfrac{1}{2})(-4\cos(n - 3/2)\psi)$$

$$\frac{\sigma_x - \sigma_y}{2} \cos 2\psi + \sigma_{xy} \sin 2\psi = \zeta(n - \tfrac{1}{2})2(n - 3/2)[\cos(n - 3/2)\psi$$

$$- \cos(n + \tfrac{1}{2})\psi] \frac{E}{2(1 + \nu)}$$

$$\sigma_r = \frac{\sigma_x + \sigma_y}{2} + \frac{\sigma_x - \sigma_y}{2} \cos\psi + \sigma_{xy}\sin 2\psi$$

$$= \frac{E}{2(1 + \nu)} \zeta(n - \tfrac{1}{2}) [(2(n - 3/2) - 4)\cos(n - 3/2)\psi -$$

$$- 2(n - 3/2)\cos(n + \tfrac{1}{2})\psi]$$

$$= \frac{E}{2(1+\nu)} \zeta(n - \tfrac{1}{2})[(2n - 6/2 - 4)\ \mathrm{Cos}\ (n - 3/2)\psi - 2(n - 3/2)\ \mathrm{Cos}\ (n + \tfrac{1}{2})\psi]$$

$$= \frac{E}{2(1+\nu)} \zeta(n - \tfrac{1}{2})[2(n - 7/2)\mathrm{Cos}(n - 3/2)\psi - 2(n - 3/2)\mathrm{Cos}(n + \tfrac{1}{2})\psi]$$

if n = 1

$$\sigma_r = \frac{E}{(1+\nu)} \frac{\zeta}{4} (-5\ \mathrm{Cos}(-\frac{\psi}{2}) + \mathrm{Cos}\ \frac{3\psi}{2})$$

As given by Williams

Proceeding in the same way it was done, but for those terms with A_{2n}

$$\mathrm{COE2} = [-(k + n + 1)\mathrm{Cos}\ n\ \psi + n\ \mathrm{Cos}(n - 2)\psi]$$

$$\frac{\partial \mathrm{COE2}}{\partial \psi} = [(k + n + 1)n\ \mathrm{Sin}\ n\psi - n(n - 2)\mathrm{Sin}(n - 2)\psi]$$

$$\mathrm{COE6} = [-(k - 1 - n)\mathrm{Sin}\ n\psi - n\ \mathrm{Sin}\ (n - 2)\psi]$$

$$\frac{\partial \mathrm{COE6}}{\partial \psi} = [-(k - 1 - n)n\ \mathrm{Cos}\ n\psi - n(n - 2)\mathrm{Cos}(n - 2)\psi]$$

$$\frac{\partial u}{\partial r} = (-1)^n n\ r^{n-1} A_{2n}\ \mathrm{COE2}$$

$$\frac{\partial u}{\partial \psi} = (-1)^n\ r^{n-1} A_{2n} \frac{\partial \mathrm{COE2}}{\partial \psi}$$

$$\frac{\partial u}{\partial r}\mathrm{Cos}\psi = [(-1)^n\ n\ r^{n-1} A_{2n}\ \mathrm{COE2}\ \mathrm{Cos}\psi]$$

$$\frac{\partial u}{\partial \psi}\frac{\mathrm{Sin}\psi}{r} = [(-1)^n\ r^{n-1} A_{2n} \frac{\partial \mathrm{COE2}}{\partial \psi}\ \mathrm{Sin}\psi]$$

$$\frac{\partial v}{\partial r}\mathrm{Sin}\psi = [(-1)^n n\ r^{n-1} A_{2n}\ \mathrm{COE6}\ \mathrm{Sin}\psi]$$

$$\frac{\partial v}{\partial \psi}\frac{\mathrm{Cos}\psi}{r} = [(-1)^n\ r^{n-1} A_{2n} \frac{\partial \mathrm{COE6}}{\partial \psi}\ \mathrm{Cos}\psi]$$

$$\frac{\partial u}{\partial r}\mathrm{Sin}\psi = [(-1)^n\ n\ r^{n-1} A_{2n}\ \mathrm{COE2}\ \mathrm{Sin}\psi]$$

$$\frac{\partial u}{\partial \psi}\frac{\mathrm{Cos}\psi}{r} = [(-1)^n\ r^{n-1} A_{2n} \frac{\partial \mathrm{COE2}}{\partial \psi}\ \mathrm{Cos}\psi]$$

$$\frac{\partial v}{\partial r}\mathrm{Cos}\psi = [(-1)^n\ n\ r^{n-1} A_{2n}\ \mathrm{COE6}\ \mathrm{Cos}\psi]$$

$$\frac{\partial v}{\partial \psi}\frac{\mathrm{Sin}\psi}{r} = [(-1)^n\ r^{n-1} A_{2n} \frac{\partial \mathrm{COE6}}{\partial \psi}\ \mathrm{Sin}\psi]$$

$$\epsilon_x = \frac{\partial u}{\partial r}\,\mathrm{Cos}\psi - \frac{\partial u}{\partial \psi}\,\frac{\mathrm{Sin}\psi}{r} \quad ; \quad \epsilon_y = \frac{\partial v}{\partial r}\,\mathrm{Sin}\psi + \frac{\partial u}{\partial \psi}\,\frac{\mathrm{Cos}\psi}{r}$$

$$\epsilon_x \pm \epsilon_y = \{(-1)^n\, n\, r^{n-1}\, A_{2n}\, \mathrm{COE2}\, \mathrm{Cos}\psi - (-1)^n\, r^{n-1}\, A_{2n}\, \frac{\partial \mathrm{COE2}}{\partial \psi}\, \mathrm{Sin}\psi\}$$

$$\pm \{(-1)^n\, n\, r^{n-1}\, A_{2n}\, \mathrm{COE6}\, \mathrm{Cos}\psi + (-1)^n\, r^{n-1}\, A_{2n}\, \frac{\partial \mathrm{COE6}}{\partial \psi}\, \mathrm{Sin}\psi\}$$

$$\zeta_{2n} = (-1)^n\, r^{n-1}\, A_{2n}$$

$$\epsilon_x + \epsilon_y = \zeta_{2n}[n\, \mathrm{COE2}\, \mathrm{Cos}\psi - \frac{\partial \mathrm{COE2}}{\partial \psi}\, \mathrm{Sin}\psi + n\, \mathrm{COE6}\, \mathrm{Sin}\psi + \frac{\partial \mathrm{COE6}}{\partial \psi}\, \mathrm{Cos}\psi]$$

$$\epsilon_x - \epsilon_y = \zeta_{2n}[n\, \mathrm{COE2}\, \mathrm{Cos}\psi - \frac{\partial \mathrm{COE2}}{\partial \psi}\, \mathrm{Sin}\psi - n\, \mathrm{COE6}\, \mathrm{Sin}\psi - \frac{\partial \mathrm{COE6}}{\partial \psi}\, \mathrm{Cos}\psi]$$

$$\gamma_{xy} = \frac{\partial u}{\partial r}\,\mathrm{Sin}\psi + \frac{\partial u}{\partial \psi}\,\frac{\mathrm{Cos}\psi}{r} + \frac{\partial v}{\partial r}\,\mathrm{Cos}\psi - \frac{\partial v}{\partial \psi}\,\frac{\mathrm{Sin}\psi}{r}$$

$$\gamma_{xy} = \zeta_{2n}[n\, \mathrm{COE2}\, \mathrm{Sin}\psi + \frac{\partial \mathrm{COE2}}{\partial \psi}\, \mathrm{Cos}\psi + n\, \mathrm{COE6}\, \mathrm{Cos}\psi - \frac{\partial \mathrm{COE6}}{\partial \psi}\, \mathrm{Sin}\psi]$$

$$\frac{\sigma_x - \sigma_y}{2}\,\mathrm{Cos}2\psi = \frac{E}{2(1+\nu)}\,\epsilon_x - \epsilon_y\,\mathrm{Cos}2\psi = \frac{E}{2(1+\nu)}\,(\epsilon_x - \epsilon_y)(1 - 2\,\mathrm{Sin}^2\psi)$$

$$= \zeta_{2n}[n\, \mathrm{COE2}\, \mathrm{Cos}\psi - \frac{\partial \mathrm{COE2}}{\partial \psi}\, \mathrm{Sin}\psi - n\, \mathrm{COE6}\, \mathrm{Sin}\psi - \frac{\partial \mathrm{COE6}}{\partial \psi}\, \mathrm{Cos}\psi]$$

$$+ [-2n\, \mathrm{COE2}\, \mathrm{Sin}^2\psi\, \mathrm{Cos}\psi + 2\,\frac{\partial \mathrm{COE2}}{\partial \psi}\, \mathrm{Sin}^3\psi + 2n\, \mathrm{COE6}\, \mathrm{Sin}^3\psi + 2\,\frac{\partial \mathrm{COE6}}{\partial \psi}$$

$$\mathrm{Cos}\psi\, \mathrm{Sin}^2\psi]$$

$$\sigma_{xy}\,\mathrm{Sin}2\psi = \frac{E}{2(1+\nu)}\,\gamma_{xy}\,\mathrm{Sin}2\psi = \frac{E}{2(1+\nu)}\,\gamma_{xy} 2\mathrm{Sin}\psi\,\mathrm{Cos}\psi$$

$$= \zeta_{2n}\,[2n\, \mathrm{COE2}\, \mathrm{Cos}\psi\, \mathrm{Sin}^2\psi + 2\,\frac{\partial \mathrm{COE2}}{\partial \psi}\, \mathrm{Sin}\psi\, \mathrm{Cos}^2\psi + 2n\, \mathrm{COE6}\, \mathrm{Cos}^2\psi \mathrm{Sin}\psi$$

$$- 2\,\frac{\partial \mathrm{COE6}}{\partial \psi}\, \mathrm{Sin}^2\psi\, \mathrm{Cos}\psi]$$

$$\frac{\sigma_x - \sigma_y}{2}\,\mathrm{Cos}2\psi + \sigma_{xy}\,\mathrm{Sin}2\psi =$$

$$\zeta_{2n}[n\, \mathrm{COE2}\, \mathrm{Cos}\psi - \frac{\partial \mathrm{COE2}}{\partial \psi}\, \mathrm{Sin}\psi - n\, \mathrm{COE6}\, \mathrm{Sin}\psi - \frac{\partial \mathrm{COE6}}{\partial \psi}\, \mathrm{Cos}\psi]$$

$$+ [+ 2\,\frac{\partial \mathrm{COE2}}{\partial \psi}\, \mathrm{Sin}^3\psi + 2\,\frac{\partial \mathrm{COE2}}{\partial \psi}\, \mathrm{Sin}\psi\, \mathrm{Cos}^2\psi + 2n\, \mathrm{COE6}\, \mathrm{Sin}^3\psi$$

$$+ 2n\, \mathrm{COE6}\, \mathrm{Cos}^2\psi\, \mathrm{Sin}\psi]$$

$$= \zeta_{2n}\,[n\, \mathrm{COE2}\, \mathrm{Cos}\psi - \frac{\partial \mathrm{COE2}}{\partial \psi}\, \mathrm{Sin}\psi\,[1-2(\mathrm{Sin}^2\psi + \mathrm{Cos}^2\psi) - n\, \mathrm{COE6}\, \mathrm{Sin}\psi$$

$$[1-2(\mathrm{Sin}^2\psi + \mathrm{Cos}^2\psi)] - \frac{\partial \mathrm{COE6}}{\partial \psi}\, \mathrm{Cos}\psi]$$

$$= \zeta_{2n} \{ \text{nCOE2 Cos}\psi + \frac{\partial \text{COE2}}{\partial \psi} \text{Sin}\psi + \text{nCOE6 Sin}\psi - \frac{\partial \text{COE6}}{\partial \psi} \text{Cos}\psi \}$$

$$= \zeta_{2n}\, n[-(k + n + 1)\text{Cos } n\psi + n \text{ Cos}(n - 2)\psi]\text{Cos}\psi$$

$$[(k + n + 1) \text{ Sin } n\psi - (n - 2)\text{Sin}(n - 2)\psi]\text{Sin}\psi$$

$$[-(k - 1 - n)\text{Sin } n\psi - n \text{ Sin}(n - 2)\psi]\text{Sin}\psi$$

$$- [-(k - 1 - n)\text{Cos } n\psi - (n - 2)\text{Cos}(n - 2)\psi]\text{Cos}\psi]$$

$$= \zeta_{2n}\, n \left\{ \begin{array}{l} -2(n + 1)\text{Cos}\psi\text{Cos } n\psi + 2(n - 1)\text{Sin}\psi(n - 2)\psi \\ + 2(n + 1)\text{Sin}\psi\text{Sin } n\psi - 2(n - 1)\text{Sin}\psi\text{Sin}(n - 2)\psi \end{array} \right\}$$

$$= \zeta_{2n}\, n[-2(n + 1)\text{Cos}(n + 1)\psi + 2(n - 1)\text{Cos}(n - 1)\psi]$$

$$\epsilon_x - \epsilon_y)\text{Cos}^2\psi + \gamma_{xy}\text{Sin } 2\psi = (-1)^n r^{n-1} A_{2n} 2n[-(n + 1)\text{Cos}(n + 1)\psi$$

$$+ (n - 1)\text{Cos}(n - 1)\psi]$$

$$(-1)A_{2n} 2(-2)\text{Cos } 2\psi$$

$$4A_{2n}\text{Cos } 2\psi$$

$$\epsilon_x + \epsilon_y = \zeta_{2n} [\text{nCOE2Cos}\psi - \frac{\partial \text{COE2}}{\partial \psi} \text{Sin}\psi + n \text{ COE6 Sin}\psi + \frac{\partial \text{COE6}}{\partial \psi} \text{Cos}\psi]$$

$$= \zeta_{2n}\, n \{[-(k + n + 1)\text{Cos } n\psi + \text{Cos}(n - 2)\psi]\text{Cos}\psi$$

$$-[(k + n + 1)\text{Sin } n\psi - (n - 2)\text{Sin}(n - 2)\psi]\text{Sin}\psi$$

$$+ [-(k - 1 - n)\text{Sin } n\psi - n \text{ Sin}(n - 2)\psi]\text{Sin}\psi$$

$$+ [-(k - 1 - n)\text{Cos } n\psi - (n - 2)\text{Cos}(n - 2)\psi]\text{Cos}\psi \}$$

$$= \zeta_{2n}\, n \quad (-2k \text{ Cos } n\psi + 2\text{Cos}(n - 2)\psi)\text{Cos}\psi$$

$$+(-2k \text{ Sin } n\psi - 2\text{Sin}(n - 2)\psi)\text{Sin}\psi$$

$$= \zeta_{2n}\, n[-2k[\text{cos}(n - 1)\psi] + 2 \text{ Cos}(n - 1)\psi]$$

$$= \zeta_{2n}\, n[-2(k - 1)\text{Cos}(n - 1)\psi] \quad ; \quad k = \frac{3 - \nu}{1 + \nu}$$

$$(k - 1) = \left[\frac{3 - \nu - 1 - \nu}{1 + \nu}\right] = \left[\frac{2 - 2\nu}{1 + \nu}\right] = \frac{2(1 - \nu)}{1 + \nu}$$

$$\zeta_{2n}\, 2n[-2 \frac{(1 - \nu)}{1 + \nu} \text{Cos}(n - 1)\psi]$$

and when it is multiplied by $\frac{E}{2(1 - \nu)}$

$$- \frac{E}{2(1+\nu)} \zeta_{2n}\, 2n[2\,\mathrm{Cos}(n-1)\psi]$$

and

$$\sigma_r = \frac{\sigma_x + \sigma_y}{2} + \frac{\sigma_x - \sigma_y}{2}\mathrm{Cos}\psi + \sigma_{xy}\,\mathrm{Sin}\,2\psi$$

$$\sigma_r = \{(-1)^n r^{n-1} A_{2n}\, 2n[-(n+1)\mathrm{Cos}(n+1)\psi + (n-1)\mathrm{Cos}(n-1)\psi]$$

$$- (-1)^n r^{n-1} A_{2n}\, 2n[2\,\mathrm{Cos}(n-1)\psi]\} \frac{1}{2(1+\nu)}$$

$$\sigma_r = \frac{E}{2(1+\nu)} (-1)^n r^{n-1} A_{2n}\, 2n[-(n+1)\mathrm{Cos}(n+1)\psi + [(n-1)-2]\mathrm{Cos}(n-1)\psi]$$

$$\sigma_r = \frac{E}{2(1+\nu)} (-1)^n r^{n-1} A_{2n}\, 2n[-(n+1)\mathrm{Cos}(n+1)\psi + (n-3)\mathrm{Cos}(n-1)\psi]$$

$$\sigma_r = \frac{E}{1+\nu} (-1)^n r^{n-1} A_{2n}\, n[-(n+1)\mathrm{Cos}(n+1)\psi + (n-3)\mathrm{Cos}(n-1)\psi]$$

for n = 1

$$\sigma_r = \frac{E}{1+\nu} (-1)\, r^{o} A_2\, [-2\,\mathrm{Cos}\,2\psi - 2\,\mathrm{Cos}\,0]$$

$$\sigma_r = \frac{E}{1+\nu} (-1)\, A_2\, [-2(1+\mathrm{Cos}\,2\psi)]$$

$$= - \frac{E}{1+\nu} A_2\, [-2\,[1 + 2\,\mathrm{Cos}2\psi - 1]]$$

$$= + \frac{E}{1+\nu} A_2\, 4\ \mathrm{Cos}2\psi = \frac{E}{1+\nu} 4\, A_2\, \mathrm{Cos}^2\psi$$

$$= \sigma_r = \frac{E}{1+\nu} 4\, A_2\, \mathrm{Cos}^2\psi$$

The same procedure is applied to those terms containing B_{2n-1}, and B_{2n} in order to obtain the full equation defining the radial stress. Stresses σ_ψ, and $\sigma_{r\psi}$, are obtained similarly by applying the corresponding relationships, this was done and the equations given in Section 5 were arrived at.

Appendix 5.c

```
      PROGRAM ANGCRK (INPUT, OUTPUT, TAPE 5 = INPUT, TAPE 6 = OUTPUT)
C     PROGRAM ANGCRK (INPUT, OUTPUT, TAPE 7, TAPE 5 = INPUT,
C    1                                       TAPE 6 = OUTPUT)
CRACK AT AN ANGE PSO IN A SINGLE EDGE NOTCH SPECIMEN
      READ  (5,100) KASE
      DO 20  K = 1, KASE
      KGO = 1
C READS IN DATA, LOCATES BOUNDARY POINTS, SETS LOAD VECTOR (BVEC)
      CALL SET UP (KGO)
      GO TO (10, 20), KGO
C OBTAINS MATRIX OF COEFFICIENTS (A)
   10 CALL MATRIX
C SOLVES EQUATION FOR COEFFICIENTS IN SERIES (XVEC)
      CALL SOLVER
C PREPARES AND PRINTS OUTPUT
      CALL OUTPUT
   20 WRITE (6,200) K, KASE
C     END FILE 7
      STOP
C
  100 FORMAT (I5)
  200 FORMAT (//27X11HEND OF CASE I3, 3H OF I3)
      END
```

```
      SUBROUTINE SET UP (KGO)
      COMMON   COR(5,201),MSID(201), BDYLD(2,201), DUM(2000),D(100,20)
      COMMON / PROBLM /A(20,20),XVEC(20),BVEC(20),NBPT,NTRM,KND
      COMMON / CONSTS / EL, HH, WW, PSO, PI, CRK
      COMMON / MATDAT / GMOD, YMOD, PRAT, CAY, F(3,3)
      COMMON/LOADS/  ML1, ML2, MB1, MB2, MR1, MR2, MT1, MT2
      DIMENSION S1(5),S2(5),L1(5),L2(5)
      DOUBLE PRECISION  A, BVEC
      READ  (5,500) EL, HH, WW, PSO, NBPT, NTRM, KND, IPRNT, LPAR, PAR
      READ  (5,505) PRAT, YMOD
C     READ(5,510)QLOAD,QWEDGE
  510 FORMAT(2F10.5)
      WRITE (6,600) EL, HH, WW, PSO, NBPT, NTRM, KND, IPRNT, LPAR, PAR
      WRITE (6,605) PRAT, YMOD
C     WRITE (7,500) EL, HH, WW, PSO, NBPT, NTRM, KND, IPRNT
C     WRITE (7,505) PRAT, YMOD
C CHECKS DATA TO ENSURE CONFORMABILITY TO PROGRAM LIMITS
      NT = (NTRM / 2) * 2
      IF (NT .GT. 40) NT = 40
      IF (NT .EQ. NTRM) GO TO 02
      WRITE (6,610) NTRM, NT
      NTRM = NT
   02 NB = (NBPT / 2) * 2
      IF (NB .GT. 200) NB = 200
      IF (NB .EQ. NBPT) GO TO 04
      WRITE (6,615) NBPT, NB
      NBPT = NB
   04 IF (PSO .GE. 0.0 .AND. PSO .LT. 90.0) GO TO 06
      WRITE (6,620) PSO
      KGO = 2
      RETURN
   06 IF (NTRM .LT. NBPT) GO TO 07
      KGO = 2
      RETURN
C SETS PARAMETERS
   07 PI = 3.14159265358979
      FA = 180.0 / PI
      ST = 2.0 * (HH + 2.0 * EL)
      DS = ST / NBPT
      WH = WW + HH
      PS1 = PSO / FA
      SPS=SIN(PS1)
      CPS=COS(PS1)
      CRK = -WH / COS(PS1)
C LOCATES BOUNDARY POINTS
      I = 1
      MT1 = I
      COR(1,I) = WW
      COR(2,I) = EL
      MSID(I) = 1
   08 IF (COR(1,I) - DS .LT. WH) GO TO 10
      I = I + 1
      COR(1,I) = COR(1,I-1) - DS
      COR(2,I) = EL
```

```
      MSID(I) = 1
      GO TO 08
   10 MT2 = I
      SH = WW - 0.5 * (HH + COR(1,MT1) + COR(1,MT2))
      DO 12  M = MT1,MT2
   12 COR(1,M) = COR(1,M) + SH
      I = I + 1
      ML1 = I
      COR( ,I) = WH
      COR(2,I) = EL - DS / 100.0
      MSID(I) = 2
   14 IF (COR(2,I) - DS .LT. -EL) GO TO 16
      I = I + 1
      COR(1,I) = WH
      COR(2,I) = COR(2,I-1) - DS
      MSID(I) = 2
      GO TO 14
   16 ML2 = I
      NOL = ML2 - ML1 + 1
      IF ((NOL/2)*2 .EQ. NOL) GO TO 17
      I = I - 1
      ML2 = ML2 - 1
   17 SH = -0.5 * (COR(2,ML1) + COR(2,ML2))
      DO 18  M = ML1,ML2
   18 COR(2,M) = COR(2,M) + SH
      MB1 = I + 1
      MB2 = MT2 - MT1 + MB1
      DO 20  M = MB1,MB2
      I = M
      K = MT1 + MB2 - M
      COR(1,M) = COR(1,K)
      COR(2,M) = -EL
   20 MSID(I) = 3
      MR1 = I + 1
      MR2 = ML2 - ML1 + MR1
      DO 22  M = MR1,MR2
      I = M
      K = ML1 + MR2 - M
      COR(1,M) = WW
      COR(2,M) = COR(2,K)
   22 MSID(I) = 4
      IF (I .EQ. NBPT) GO TO 24
      WRITE (6,617) N PT, I
      NBPT = I
      IF (NBPT .LE. 200) GO TO 24
      WRITE (6,619)
      KGO = 2
      RETURN
   24 DO 26  I = 1,NBPT
      X = COR(1,I)
      Y = COR(2,I)
      R = SQRT(X*X + Y*Y)
      T = ATAN2(Y,X)
      P = T - PS1
      COR(3,I) = R
```

```
      COR(4,I) = T
   26 COR(5,I) = P
      IF (P .LT. -PI) P = P + 2.0 * PI
C PRINTS COORDINATES OF BOUNDARY POINTS (IF IPRNT .NE. 0)
      IF (IPRNT .EQ. 0) GO TO 30
      WRITE (6,630)
      N2 = NBPT / 2
      DO 28  I = 1,N2
      J = I + N2
      T1 = COR(4,I) * FA
      T2 = COR(4,J) * FA
      P2 = COR(5,J) * FA
      P1 = COR(5,I) * FA
      IF (I .EQ. 51) WRITE (6,680)
      WRITE (6,640) I, (COR(L,I),  L = 1,3), T1, P1,
     1              J, (COR(L,J),  L = 1,3), T2, P2
   28 CONTINUE
C INVERSE HOOKEAN MATRIX
   30 GMOD = YMOD / 2.0 / (1.0 + PRAT)
      GMD2 = GMOD * 2.0
      CAY = (3.0 - PRAT) / (1.0 + PRAT)
      F(1,1) = (CAY + 1.0) / (8.0 * GMOD)
      F(2,1) = (CAY - 3.0) / (8.0 * GMOD)
      F(3,1) = 0.0
      F(1,2) = F(2,1)
      F(2,2) = F(1,1)
      F(3,2) = 0.0
      F(1,3) = F(3,1)
      F(2,3) = F(3,2)
      F(3,3) = 1.0 / GMOD
C SETS LOAD VECTOR - VERTICAL LOADING ONLY
C                  ----------------------
      DO 32  J = 1,NBPT
      DO 32  I = 1,2
   32 BDYLD(I,J) = 0.0
      MLJ = 0
      IF(LPAR.EQ.1)GO TO 56
      GO TO (34, 40, 46), KND
C SIMPLE TENSION
   34 DO 36  I = MT1,MT2
   36 BDYLD(2,I) = -1.0 / GMD2
      DO 38  I = MB1,MB2
   38 BDYLD(2,I) = -1.0 / GMD2
      WRITE (6,650)
      GO TO 56
C PURE BENDING
   40 DO 42  I = MT1,MT2
   42 BDYLD(2,I) =  (1.0 + 2.0 * (COR(1,I) - WW) / HH) / GMD2
      DO 44  I = MB1,MB2
   44 BDYLD(2,I) =  (1.0 + 2.0 * (COR(1,I) - WW) / HH) / GMD2
      WRITE (6,660)
      GO TO 56
C SHEAR AS IN CKS GEOMETRY
   46 TH = -CRK * SIN(PS1)
      DO 48  I = ML1,ML2
```

```
      MLI = I
      IF (COR(2,I) .LT. TH) GO TO 50
   48 CONTINUE
   50 J = ML1 + ML2 - I
      MLJ = J
      R = HH / (EL - COR(2,J)) / GMD2
      DO 52  M = ML1,MLJ
   52 BDYLD(2,M) = -R
      DO 54  M = MLI, ML2
   54 BDYLD(2,M) =  R
      WRITE (6,670)
   56 CONTINUE
      IF(LPAR.NE.1)GO TO 57
   57 IF(IPRINT.EQ.0)GO TO 58
      WRITE (6,680)
C SHIFTS ORDER OF STORING COORDINATES TO BEGIN AT LOWER CRACK FLANK
   58 NBP1 = NBPT + 1
      DO 69 I=MT2,NBPT
      IF (COR(5,I).LT.0.0)GO TO 691
      ISHFT=I
   69 CONTINUE
  691 DO 70 I=1,ISHFT
      DO 60  J = 1,5
   60 COR(J,NBP1) = COR(J,1)
      DO 62  J = 1,2
   62 BDYLD(J,NBP1) = BDYLD(J,1)
      MSID(NBP1) = MSID(1)
      DO 68  K = 1,NBPT
      DO 64  J = 1,5
   64 COR(J,K) = COR(J,K+1)
      DO 66  J = 1,2
   66 BDYLD(J,K) = BDYLD(J,K+1)
   68 MSID(K) = MSID(K+1)
      L = I
   70 CONTINUE
   72 NBPL = NBPT - LI
      MT1 = MT1 + NBPL
      MT2 = MT2 + NBPL
      ML1 = ML1 + NBPL
      MLJ = MLJ + NBPL
      MLI = 1
      ML2 = ML2 - L
      MR1=MR1-LI
      MR2=MR2-LI
      MB1 = MB1 - L
      MB2 = MB2 - L
      DO 74  J = 1,NTRM
      BVEC(J) = 0.0D0
      DO 74  I = 1,NTRM
   74 A(I,J) = 0.0D0
C-----------------------------------------------------------------------
C-----------------------------------------------------------------------
      CALL LOADING
C-----------------------------------------------------------------------
C-----------------------------------------------------------------------
```

```
C      PAR=(2.0*QLOAD)/FLOAT(ML2)
       DO 561 I=1,ML2
C      CYM= -COR(2,I)-EL/2.0
C      TSMOM=(2.0*QWEDGE*WH*CYM)/((EL**2)*FLOAT(ML2))
CC     BDYLD(2,I)= (4.0*QWEDGE/FLOAT(ML2))/GMD2
C      BDYLD(2,I)= (    QWEDGE/FLOAT(ML2))/GMD2
  561  CONTINUE
C      PAR=(2.0*QLOAD)/FLOAT(NBPT-ML1+1)
       DO 562 I=ML1,NBPT
C      CYM=COR(2,I)-EL/2.0
C      TSMOM=(2.0*QWEDGE*WH*CYM)/((EL**2)*FLOAT(ML2))
C      BDYLD(2,I)=-(4.0*QWEDGE/FLOAT(ML2))/GMD2
C      BDYLD(2,I)=-(    QWEDGE/FLOAT(ML2))/GMD2
  562  CONTINUE
C      PAR=(4.0*QLOAD)/FLOAT(MR2-MR1+1)
       DO 563 I=MR1,MR2
  563  CONTINUE
C      QCLAMP=(QWEDGE*WH*EL)/((EL**2)*FLOAT(ML2))
C      WRITE(6,746)QLOAD,QWEDGE,QCLAMP
  746  FORMAT(1X,86H THE PRESENT CASE IS A SIMULATION OF THE BENBOW PLATE
     1 WITH LATERAL COMPRESSION LOAD OF//1X,30X,3H Q=,F7.3,3HLB.//1X,30H
     2IT ALSO HAS AN OPENING LOAD OF//1X,30X,8H LWEDGE=,F7.3,3HLB.//5X,3
     34HAND A CLAMPING MOMENT LOAD MLCLAM=,F9.3,3HLB.)
C-----------------------------------------------------------------------
       WRITE(6,630)
       N2= NBPT / 2
       DO  98  I = 1,N2
       J = I + N2
       T1 = COR(4,I) * FA
       T2 = COR(4,J ) * FA
       P1 = COR(5,I) * FA
       P2 = COR(5,J) * FA
       IF (I .EQ. 51) WRITE (6,680)
       WRITE (6,640) I,  (COR(L,I), L = 1,3), T1, P1,
     1               J, (COR(L,J), L = 1,3), T2, P2
   98  CONTINUE
       WRITE(6,690)MT1,MT2,ML1,MLJ,MLI,ML2,MB1,MB2,NBPT,MR1,MR2
  690  FORMAT(/,11I7,/)
       WRITE(6,700)
  700  FORMAT(/42X,51H BOUNDARY LOADS FOR USE IN COMPUTATION ARE
     1 // 40X,4HNODE,2(4X,1HX,5X),4X,2HFX,8X,2HFY//)
       DO 748 I=1,NBPT
       IF(BDYLD(1,I).EQ.0.0.AND.BDYLD(2,I).EQ.0.0)GO TO 748
       XLOAD=BDYLD(1,I)*GMD2
       YLOAD=BDYLD(2,I)*GMD2
       WRITE(6,710)I,(COR(L,I),L=1,2),XLOAD,YLOAD
  748  CONTINUE
  710  FORMAT(1X,39X,I4,4F10.3)
C-----------------------------------------------------------------------
C SETS RVEC
       N4 = NTRM / 2
       GO TO (76 , 76 , 78 , 79 ),KND
   76  LS = 1
       S1(1) = WW
       S2(1) = WH
```

```
      S1(2) = WH
      S2(2) = WW
      L1(1) = MT1
      L2(1) = MT2
      L1(2) = MB1
      L2(2) = MB2
      LESP = 2
      GO TO 80
   78 LS = 2
      TH= -CRK * SIN (PS1)
      S1(1) = EL
      S2(1)=TH
      S1(2) = TH
      S2(2) =-EL
      L1(1) = ML1
      L2(1)=NBPT
      L1(2) = ML1
      L2(2) = ML2
      LESP = 2
      GO TO 80
   79 CONTINUE
      TH=-CRK*SIN(PS1)
      S1(1)=EL & L1(1)=ML1
      S2(1)=TH & L2(1)=NBPT
      S1(2)=TH & L1(2)=1
      S2(2)=-EL & L2(2)=ML2
      S1(3)=WH & L1(3)=MB1
      S2(3)=WW & L2(3)=MB2
      S1(4)=-EL & L1(4)=MR1
      S2(4)=EL & L2(4)=MR2
      S1(5)=WW & L1(5)=MT1
      S2(5)=WH & L2(5)=MT2
      IF(KND.EQ.4)LESP=5
   80 DO 94 I=1,LESP
      N1 = L1(I)
      N2 = L2(I)
      DO 82  N = N1,N2
      R = COR(3,N)
      P = COR(5,N)
      RT = SQRT(R)
      DO 82  M = 1,N4
      M4 = M * 2
      S = M
      S52 = S - 2.5
      S21 = S - 2.0
      S32 = S - 1.5 - CAY
      S11 = S - 1.0 - CAY
      S12 = S - 0.5
      P12 = S + 0.5 - CAY
      P11 = S + 1.0 - CAY
      RI = R ** M
      RR = RI / RT
      R32=S-1.5+CAY
      A12=S+0.5+CAY
      A11=S+1.0+CAY
```

```
      R11=S-1.0+CAY
      SE = -1.0
      IF ((M/2)*2 .EQ. M) SE = 1.0
      SM = - SE
      SS52 = SIN(S52 * P)
      SS21 = SIN(S21 * P)
      SS12 = SIN(S12 * P)
      SS   = SIN(S   * P)
      CS52 = COS(S52 * P)
      CS21 = COS(S21 * P)
      CS12 = COS(S12 * P)
      CS   = COS(S   * P)
      D(N,M4-1) = SM *RR * (  (S32*SS12 - S12*SS52) * CPS
     1                      -(R32*CS12 - S12*CS52) * SPS )* BDYLD(2,N)
      D(N,M4  ) = SE * RI * (  (P11*SS - S*SS21) * CPS
     1                       - (A11*CS - S*CS21) * SPS ) * BDYLD(2,N)
   82 CONTINUE
      DO 94  N = N1,N2
      LS = 2
      IF((N1.EQ.MB1.AND.N2.EQ.MB2).OR.(N1.EQ.MT1.AND.N2.EQ.MT2))LS=1
      DO 92  J = 1,NTRM
      IF (N1 - N) 84, 86, 94
   84 IF (N - N2) 90, 88, 94
   86 X0 = S1(I)
      X1 = COR(LS,N1)
      X2 = COR(LS,N1+1)
      C1 = -X0 + (5.0*X1 + 3.0*X2)/8.0 + 0.5*(X1-X0)*(X1-X0)/(X2-X1)
      C2 = 0.125*(X2-X1)-0.5*(X1-X0)*(X1-X0)/(X2-X1)
      DB = C1 * D(N,J) + C2 * D(N+1,J)
      GO TO 92
   88 XN = S2(I)
      XM = COR(LS,N2)
      XL = COR(LS,N2-1)
      CM = XN - (5.0*XM+3.0*XL)/8.0 + 0.5*(XN-XM)*(XN-XM)/(XM-XL)
      CL = 0.125*(XM-XL) - 0.5*(XN-XM)*(XN-XM)/(XM-XL)
      DB = CM * D(N,J) + CL * D(N-1,J)
      GO TO 92
   90 DR = COR(LS,N+1) - COR(LS,N  )
      DL = COR(LS,N  ) - COR(LS,N-1)
      CI = DL + 5.0 * DR * (1.0 - DR / DL)
      CJ = 18.0 * (DR + DL) + 5.0 * (DR * DR / DL + DL * DL / DR)
      CK = DR + 5.0 * DL * (1.0 - DL / DR)
      DB = (CI * D(N-1,J) + CJ * D(N,J) + CK * D(N+1,J)) / 48.0
   92 BVEC(J) = BVEC(J) + DB
   94 CONTINUE
      IF(LPAR.EQ.1)GO TO 95
      RETURN
   95 LS = 2
      TH=-CRK * SIN(PS1)
      IF(KND.EQ.4)GO TO 89
      S1(1) = EL
      S2(1) = TH
      S1(2)= TH
      S2(2) =-EL
      L1(1) = ML1
```

```
      L2(1)=NBPT
      L1(2)=1
      L2(2) = ML2
      S1(3)=-ELI
      S2(3)=EL
      L1(3)=MR1
      L2(3)=MR2
      LESP = 3
      GO TO 87
   89 CONTINUE
      TH=-CRK*SIN(PS1)
      S1(1)=EL & L1(1)=ML1
      S2(1)=TH & L2(1)=NBPT
      S1(2)=TH & L1(2)=1
      S2(2)=-ELI & L2(2)=ML2
      S1(3)=WH & L1(3)=MB1
      S2(3)=WW & L2(3)=MB2
      S1(4)=-ELI & L1(4)=MR1
      S2(4)=EL & L2(4)=MR2
      S1(5)=WW & L1(5)=MT1
      S2(5)=WH & L2(5)=MT2
      LESP = 5
   87 DO 106 I=1,LESP
      N1 = L1(I)
      N2 = L2(I)
      DO 96 N=N1,N2
      R = COR(3,N)
      P = COR(5,N)
      RT = SQRT(R)
      DO 96 M=1,N4
      M4 = M * 2
      S = M
      S52 = S - 2.5
      S21 = S - 2.0
      S32 = S - 1.5 - CAY
      S11 = S - 1.0 - CAY
      R32 = S - 1.5 + CAY
      A12 = S + 0.5 + CAY
      A11 = S + 1.0 + CAY
      R11 = S - 1.0 + CAY
      S12 = S - 0.5
      P12 = S + 0.5 - CAY
      P11 = S + 1.0 - CAY
      RI = R ** M
      RR = RI / RT
      SE = -1.0
      IF ((M/2)*2 .EQ. M) SE = 1.0
      SM = - SE
      SS52 = SIN(S52 * P)
      SS21 = SIN(S21 * P)
      SS12 = SIN(S12 * P)
      SS   = SIN(S   * P)
      CS52 = COS(S52 * P)
      CS21 = COS(S21 * P)
      CS12 = COS(S12 * P)
```

```
      CS    = COS(S    * P)
      D(N,M4-1) = SM * RR * ( -(S32*SS12 - S12*SS52) * SPS
     1                        -(R32*CS12 - S12*CS52) * CPS) * BDYLD(1,N)
      D(N,M4   ) = SE * RI * ( -(P11*SS - S*SS21) * SPS
     1                        - (A11*CS - S*CS21) * CPS ) * BDYLD(1,N)
   96 CONTINUE
      DO 106 N=N1,N2
      LS=2
      IF((N1.EQ.MB1.AND.N2.EQ.MB2).OR.(N1.EQ.MT1.AND.N2.EQ.MT2))LS=1
      DO 105 J=1,NTRM
      IF(N1-N)97,99,106
   97 IF(N-N2)103,101,106
   99 X0=S1(I)
      X1 = COR(LS,N1)
      X2 = COR(LS,N1+1)
      C1 = -X0 + (5.0*X1 + 3.0*X2)/8.0 + 0.5*(X1-X0)*(X1-X0)/(X2-X1)
      C2 = 0.125*(X2-X1)-0.5*(X1-X0)*(X1-X0)/(X2-X1)
      DB = C1 * D(N,J) + C2 * D(N+1,J)
      GO TO 105
  101 XN=S2(I)
      XM = COR(LS,N2)
      XL = COR(LS,N2-1)
      CM = XN - (5.0*XM+3.0*XL)/8.0 + 0.5*(XN-XM)*(XN-XM)/(XM-XL)
      CL = 0.125*(XM-XL) - 0.5*(XN-XM)*(XN-XM)/(XM-XL)
      DB = CM * D(N,J) + CL * D(N-1,J)
      GO TO 105
  103 DR = COR(LS,N+1) - COR(LS,N )
      DL = COR(LS,N  ) - COR(LS,N-1)
      CI = DL + 5.0 * DR * (1.0 - DR / DL)
      CJ = 18.0 * (DR + DL) + 5.0 * (DR * DR / DL + DL * DL / DR)
      CK = DR + 5.0 * DL * (1.0 - DL / DR)
      DB = (CI * D(N-1,J) + CJ * D(N,J) + CK * D(N+1,J)) / 48.0
  105 BVEC(J) = BVEC(J) + DB
  106 CONTINUE
      RETURN
C
C 500 FORMAT (4F10.2, 5I5, 1F10.2)
  500 FORMAT(4F10.3, 5I5,1F10.3)
  505 FORMAT (2E20.8)
  600 FORMAT (1H1, /2X39HTHE INPUT DATA WERE READ AS FOLLOWS     18X
     1 4F10.2, 5I5, 1F10.2)
  605 FORMAT (59X 2E20.8, /)
  610 FORMAT (/2X34HTHE PARAMETER NTRM IS CHANGED FROM I4, 3H TO I4,
     1 30H TO CONFORM TO PROGRAM LIMITS. /)
  615 FORMAT (/2X34HTHE PARAMETER NBPT IS CHANGED FROM I4, 3H TO I4,
     1 30H TO CONFORM TO PROGRAM LIMITS. /)
  617 FORMAT (/2X34HTHE PARAMETER NBPT IS CHANGED FROM I4, 3H TO I4,
     1 28H TO ADAPT TO BOUNDARY SHAPE. /)
  619 FORMAT (/2X39HTHE PARAMETER NBPT IS NOW UNACCEPTABLE. /)
  620 FORMAT (/2X34HTHE PARAMETER PS0 IS UNACCEPTABLE. /)
  630 FORMAT (/37X47HBOUNDARY COORDINATES FOR USE IN COMPUTATION ARE
     1 // 2(2X2HNO 7X1HX 9X1HY 9X1HR 7X5HTHETA 6X3HPSI 12X) /)
  640 FORMAT (2(I4, 3F10.3, 2F10.2, 11X))
  650 FORMAT (/1X 8(15H TENSILE LOAD  ) /)
  660 FORMAT (/1X 8(15H PURE BENDING  ) /)
  670 FORMAT (/1X 8(15H COMPACT, CKS  ) /)
  680 FORMAT (1H1)
      END
```

```
      SUBROUTINE MATRIX
      COMMON  COR(5,201), MSID(201), BDYLD(2,201), RA(20,20,10)
      COMMON / CONSTS / EL, HH, WW, PSO, PI, CRK
      COMMON / MATDAT / GMOD, YMOD, PRAT, CAY, F(3,3)
      COMMON / PROBLM /A(20,20),XVEC(20),BVEC(20),NBPT,NTRM,KND
      DIMENSION  C(3,20) , D(3,20) , XR(10) , RX(10) , WX(10)
      DOUBLE PRECISION  A, BVEC
      RX(1) = 0.013046735741414
      RX(2) = 0.067468316655507
      RX(3) = 0.160295215850488
      RX(4) = 0.283302302935376
      RX(5) = 0.425562830509184
      WX(1) = 0.066671344308688
      WX(2) = 0.149451349150581
      WX(3) = 0.219086362515982
      WX(4) = 0.269266719309996
      WX(5) = 0.295524224714753
      DO 05  I = 1,5
      J = 11 - I
      RX(J) = 1.0 - RX(I)
05    WX(J) = WX(I)
      N4 = NTRM / 2
      DO 85  N = 1,NBPT
      REG = COR(3,N)
      PSI = COR(5,N)
      P = PSI
      DO 35  K = 1,10
      R = REG * RX(K)
      RT = SQRT(R)
      DO 10  M = 1,N4
      M4 = M * 2
      S = M
      S72 = S - 3.5
      S31 = S - 3.0
      S32 = S - 1.5
      S11 = S - 1.0
      S12 = S - 0.5
      P12 = S + 0.5
      P11 = S + 1.0
      RI = R ** (M-1)
      IF (M .EQ. 1) RI = 1.0
      SE = -1.0
      RR = RI / RT
      IF((M/2)*2 .EQ. M) SE = 1.0
      SM = - SE
      SS32 = SIN(S32 * P)
      SS11 = SIN(S11 * P)
      SP12 = SIN(P12 * P)
      SS12 = SIN(S12 * P)
```

```
      CS12 = COS(S12 * P)
      CS11 = COS(S11 * P)
      CS32 = COS(S32 * P)
      CP12 = COS(P12 * P)
      SP11 = SIN(P11 * P)
      CP11 = COS(P11 * P)
C FINDS CONTRIBUTION TO STRESSES FOR EACH TERM IN SERIES, IN ORDER
C  A(2N-1), B(2N-1), A(2N), B(2N), FOR N = 1, 2, , , NTRM/4 (= N4)
C
C SIGMA R
      C(1,M4-1) = SM *RR * S12 * (S72 * CS32 - S32 * CP12)
      C(1,M4  ) = SE * RI * S * (S31 * CS11 - P11 * CP11)
C SIGMA PSI
      C(2,M4-1) = -SM * RR * S12 * (P12 * CS32 - S32 * CP12)
      C(2,M4  ) = -SE * RI * S   * (P11 * CS11 - P11 * CP11)
C TAU R-PSI
      C(3,M4-1) = -SM * RR * S12 * (S32 * SS32 - S32 * SP12)
      C(3,M4  ) = -SE * RI * S   * (S11 * SS11 - P11 * SP11)
   10 CONTINUE
  710 FORMAT(1X,7HSIGMA R//5X,6(2F12.5,5X)///)
  720 FORMAT(1X,9HSIGMA PSI//5X,6(2F12.5,5X)///)
  730 FORMAT(1X,9HTAU R-PSI//5X,6(2F12.5,5X)///)
      DO 20  J = 1,NTRM
      DO 20  I = 1,3
      SUM = 0.0
      DO 15  L = 1,3
   15 SUM = SUM + F(I,L) * C(L,J)
   20 D(I,J) = SUM
      DO 30  J = 1,NTRM
      DO 30  I = 1,NTRM
      SUM = 0.0
      DO 25  L = 1,3
   25 SUM = SUM + C(L,I) * D(L,J)
   30 RA(I,J,K) = SUM * R
   35 CONTINUE
      DO 80  J = 1,NTRM
      DO 80  I = 1,NTRM
C RADIAL INTEGRATION (GAUSSIAN, 10 POINTS)
      DO 40  K = 1,10
   40 XR(K) = RA(I,J,K)
      SUM = 0.0
      DO 45  L = 1,10
   45 SUM = SUM + XR(L) * WX(L)
C CIRCUMFERENTIAL INTEGRATION (EQUIVALENT TO TRAPEZOIDAL)
      IF ( 2 - N )  50, 60, 55
   50 IF (N-NBPT+1) 65, 70, 75
C FIRST POINT
   55 DLN = COR(5,1) + PI
      DRN = COR(5,2) - COR(5,1)
      DLP = DRN
```

```
      DRP = COR(5,3) - COR(5,2)
      DP = DLN + 0.375 * DRN + DLN**2 / (2.0*DRN)
     1    + (DLP + 5.0 * DRP * (1.0-DRP/DLP)) / 48.0
      GO TO 80
C SECOND POINT
   60 DLM = COR(5,1) + PI
      DRM = COR(5,2) - COR(5,1)
      DLN = DRM
      DRN = COR(5,3) - COR(5,2)
      DLP = DRN
      DRP = COR(5,4) - COR(5,3)
      DP = DRM / 8.0 - DLM**2 / (2.0*DRM)
     1    + (18.0 * (DRN+DLN) + 5.0 * (DRN**3 + DLN**3) / (DRN*DLN)
     2    + DLP + 5.0 * DRP * (1.0-DRP/DLP)) / 48.0
      GO TO 80
C GENERAL (NTH) POINT
   65 DLM = COR(5,N-1) - COR(5,N-2)
      DRM = COR(5,N  ) - COR(5,N-1)
      DLN = DRM
      DRN = COR(5,N+1) - COR(5,N  )
      DLP = DRN
      DRP = COR(5,N+2) - COR(5,N+1)
      DP = (DRM + 5.0 * DLM * (1.0-DLM/DRM)
     1    + 18.0 * (DRN+DLN) + 5.0 * (DRN**3 + DLN**3) / (DRN*DLN)
     2    + DLP + 5.0 * DRP * (1.0-DRP/DLP)) / 48.0
      GO TO 80
C PENULTIMATE POINT
   70 DLM = COR(5,N-1) - COR(5,N-2)
      DRM = COR (5,N  ) - COR(5,N-1)
      DLN = DRM
      DRN = COR(5,N+1) - COR(5,N  )
      DLP = DRN
      DRP = PI - COR(5,N+1)
      DP = (DRM + 5.0 * DLM * (1.0-DLM/DRM)
     1    + 18.0 * (DRN+DLN) + 5.0 * (DRN**3 + DLN**3) / (DRN*DLN)) / 48.
     2    + DLP / 8.0 - DRP**2 / (2.0*DLP)
      GO TO 80
C LAST POINT
   75 DLM = COR(5,N-1) - COR(5,N-2)
      DRM = COR(5,N  ) - COR(5,N-1)
      DLN = DRM
      DRN = PI - COR(5,N)
      DP = (DRM + 5.0 * DLM * (1.0-DLM/DRM)) / 48.0
     1    + DRN + 0.375 * DLN + DRN**2 / (2.0*DLN)
   80 A(I,J) = A(I,J) + SUM * DP * REG / 2.0
   85 CONTINUE
      RETURN
      END
```

```
      SUBROUTINE SOLVER
      COMMON / PROBLM /A(20,20),XVEC(20),BVEC(20),NBPT,NTRM,KND
      DIMENSION B(20) , NDX(20,2) , PIV(20) , IPV(20)
      DOUBLE PRECISION  A, AX, B, BVEC, PIV
C SOLVES FOR XVEC, USING DOUBLE PRECISION ARITHMETIC
      NS = NTRM
   05 DO 10  I = 1,NS
      B(I) = BVEC(I)
   10 IPV(I) = 0
      DO 55  I = 1,NS
      AX = 0.0D0
      DO 30  J = 1,NS
      IF(IPV(J) .EQ. 1) GO TO 30
      DO 25  K = 1,NS
      IF (IPV(K) - 1) 20, 25, 65
   20 IF (DABS(AX) .GE. DABS(A(J,K))) GO TO 25
      IROW = J
      ICOL = K
      AX = A(J,K)
   25 CONTINUE
   30 CONTINUE
      IPV(ICOL) = IPV(ICOL) + 1
      IF (IROW .EQ. ICOL) GO TO 40
      DO 35  L = 1,NS
      AX = A(IROW,L)
      A(IROW,L) = A(ICOL,L)
   35 A(ICOL,L) = AX
      AX = B(IROW)
      B(IROW) = B(ICOL)
      B(ICOL) = AX
   40 NDX(I,1) = IROW
      NDX(I,2) = ICOL
      PIV(I) = A(ICOL,ICOL)
      A(ICOL,ICOL) = 1.0D0
      DO 45  L = 1,NS
   45 A(ICOL,L) = A(ICOL,L) / PIV(I)
      B(ICOL) = B(ICOL) / PIV(I)
      DO 55  N = 1,NS
      IF (N .EQ. ICOL) GO TO 55
      AX = A(N,ICOL)
      A(N,ICOL) = 0.0D0
      DO 50  L = 1,NS
   50 A(N,L) = A(N,L) - A(ICOL,L) * AX
      B(N) = B(N) - B(ICOL) * AX
   55 CONTINUE
      DO 60  I = 1,NS
   60 XVEC(I) = B(I)
      RETURN
   65 WRITE (6,100)
      RETURN
C
  100 FORMAT (2X 3(21HBOMBED OUT OF SOLVER  ))
      END
```

```
      SUBROUTINE OUTPUT
      COMMON / PROBLM /A(20,20),XVEC(20),BVEC(20),NBPT,NTRM,KND
      COMMON   COR(5,201), MSID(201), BDYLD(2,201), DUM(4000)
      COMMON / CONSTS / EL, HH, WW, PSO, PI, CRK
      DOUBLE PRECISION  A, BVEC
C PREPARES OUTPUT PARAMETERS
      RF = HH - WW
      SP = EL * 2.0
      Y1 = -XVEC(1) * SQRT(2.0 * PI / CRK)
      Y2 =  XVEC(2) * SQRT(2.0 * PI / CRK)
      RA = Y2 / Y1
      NTR2 = NTRM
C PRINTS OUTPUT
      WRITE (6,600) NBPT
      GO TO (10, 20, 30), KND
   10 WRITE (6,610)
      GO TO 40
   20 WRITE (6,620)
      GO TO 40
   30 WRITE (6,630)
   40 WRITE (6,640) SP, CRK, HH, PSO, WW, RF, Y1, RA, Y2
      WRITE(6,660)
  660 FORMAT(  /2X14HSYMMETRIC CASE)
      DO 50  I = 1,NTR2
   50 WRITE(6,550)I,XVEC(I)
  550 FORMAT(8X1HA I2,2H =F13.8)
C     WRITE (7,700) (XVEC(I),  I = 1,NTRM)
      RETURN
C
  600 FORMAT (     /2X70HTHE FOLLOWING PROBLEM HAS BEEN SOLVED FOR COEFF
     1ICIENTS IN THE WILLIAMS /2X70HEIGENVALUE SERIES, FOR A CRACK LYING
     2 AT AN ANGLE TO ITS USUAL POSITION /15X 5HUSING I4, 35H BOUNDARY P
     3OINTS IN THE COMPUTATION )
  610 FORMAT (/4X66HSPECIMEN AND LOAD CONFIGURATION -- SINGLE EDGE NOTCH
     1, PURE TENSION )
  620 FORMAT (/4X66HSPECIMEN AND LOAD CONFIGURATION -- SINGLE EDGE NOTCH
     1, PURE BENDING )
  630 FORMAT (/4X66HSPECIMEN AND LOAD CONFIGURATION -- COMPACT TENSION G
     1EOMETRY, IDEAL )
  640 FORMAT (/8X10HLENGTH   = F6.2, 4H INS 14X14HCRACK LENGTH = F6.2,
     1 4H INS /8X10HWIDTH    = F6.2, 4H INS 14X14HINCLINATION  = F6.2,
     2 4H DEG /8X10HLIGAMENT = F6.2, 4H INS 14X14H(K-I LENGTH) = F6.2,
     3 4H INS //8X5HY-I = F9.6, 6X10HK-II/K-I = F8.5, 5X6HY-II = F9.6,
     4 ///22X30HT H E  C O E F F I C I E N T S /)
C 700 FORMAT (4E20.10)
      END
```

```
      SUBROUTINE LOADING
COMMENT  C=SIG2/SIG1 , BEING  SIG2=STRESS ALONG X
C                             SIG1=STRESS ALONG Y
      COMMON  COR(5,201),MSID(201),BDYLD(2,201),DUM(2000),D(100,20)
      COMMON/CONSTS/ EL, HH, WW, PSO, PI, CRK
      COMMON/MATDAT/ GMOD, YMOD, PRAT, CAY, F(3,3)
      COMMON/LOADS/  ML1, ML2, MB1, MB2, MR1, MR2, MT1, MT2
      COMMON/PROBLM/ A(20,20), XVEC(20),BVEC(20), NBPT, NTRM, KND
      DOUBLE PRECISION A,BVEC
      REAL LOADX,LOADY
      READ(5,50)AA, BB, CB
      C = AA/ BB
      SIG2 = 10.0 * AA
      SIG1 = 10.0 * BB
      SIGB = SIG2 * CB
      SIGMA11=SIG1*EL
      WRITE(6,60)SIG2,SIG1,SIGB
      WRITE(6,63)SIGMA11
   60 FORMAT(1X,* THE LOADING ON THIS CASE IS */
     1           * ----------------------------*//
     1           * STRESS ALONG THE - X - DIRECTION * 1F8.3//
     2           * STRESS ALONG THE - Y - DIRECTION * 1F8.3//
     3           * MAXIMUM BENDING STRESS           * 1F8.3//)
   63 FORMAT(1X,* THE TOTAL OPENING LOAD DUE TO THE SHEAR STRESS APPLIED
     1 ON THE EDGE OF THE PLATE (-Y- DIRECTION) IS*,1F8.3)
      GMD2 = GMOD * 2.0
      DELY = COR(2,MT1) - COR(2,MB1)
      DELX = COR(1,MR1) - COR(1,1)
      XTF = SIG2 * DELY
      YTF = SIG1 * DELX
      LOADX = XTF / FLOAT(MR2 - MR1 + 1 )
      LOADY = YTF / FLOAT(MT2 - MT1 + 1 )
      DO 1 N = 1 , ML2
    1 BDYLD(1,N) = BDYLD(1,N) - LOADX/GMD2
      DO 2 N =   1 , ML2
    2 BDYLD(2,N) = BDYLD(2,N) - LOADY/GMD2
      DO 3 N = MR1 , MR2
    3 BDYLD(1,N) = BDYLD(1,N) - LOADX/GMD2
      DO 4 N = ML1 , NBPT
    4 BDYLD(2,N) = BDYLD(2,N) - LOADY/GMD2
      DO 5 N= ML1, NBPT
    5 BDYLD(1,N) = BDYLD(1,N) - LOADX/GMD2
   50 FORMAT(3F10.2)
      IF(CB.EQ.0.0)GO TO 10
      WRITE(6,61)BDYLD(1,ML1),BDYLD(1,NBPT),BDYLD(1,1),BDYLD(1,ML2)
   61 FORMAT(1X,* THE MAGNITUD OF LOADS ON POINTS ML1, NBPT, 1, ML2
     1            BEFORE APPLICATION OF BENDING STRESS IS RESPECTIVELY*
     2//      12X,4F15.3)
      F1= (SIG2 * CB *EL**2) / (1.5*(COR(2,ML1) - COR(2,NBPT)))
      BDYLD(1,ML1) = BDYLD(1,ML1) + F1/GMD2
      BDYLD(1,NBPT) = BDYLD(1,NBPT) - F1/GMD2
      BDYLD(1,1) = BDYLD(1,1) - F1/GMD2
      BDYLD(1,ML2) = BDYLD(1,ML2) + F1/GMD2
      WRITE(6,62) BDYLD(1,ML1),BDYLD(1,NBPT),BDYLD(1,1),BDYLD(1,ML2)
   62 FORMAT(1X,*ONCE THE BENDING STRESS IS APPLIED, THOSE LOADS BECOME*
     14F15.3/)
   10 RETURN
      END
```

APPENDIX 6a

Stresses at measuring points in the rig.

(a) Opening fingers. Loads to be applied. From Benbow and Roesler (1957)

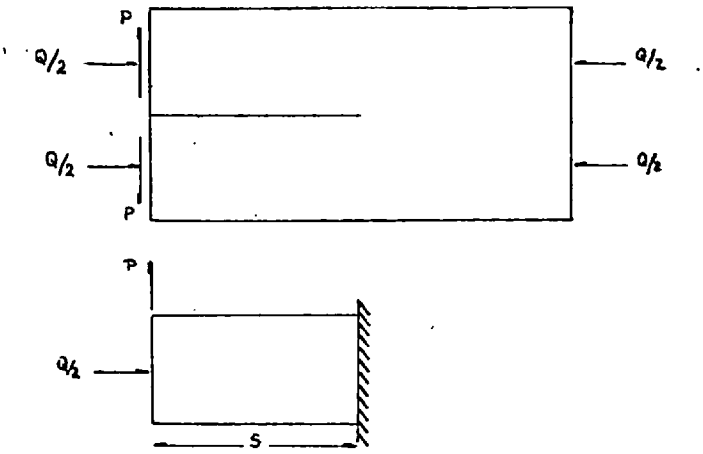

$\sigma = bM/4I$; $M = Ps/2$; $Q = n\ b\ \eta\ \sigma$

$n = 0.25$; $b = 4$; $\eta = 0.2$

P(lb)	S in	M(lb.in)	σ(lb/in^2)	Q(lb)
1180	1.2	708	4240	849
262	2.4	315	1890	378
139	3.6	250	1500	300
91.4	4.8	219	1315	263
67.4	6.0	202	1212	243

The piece for measuring the loads is depicted below

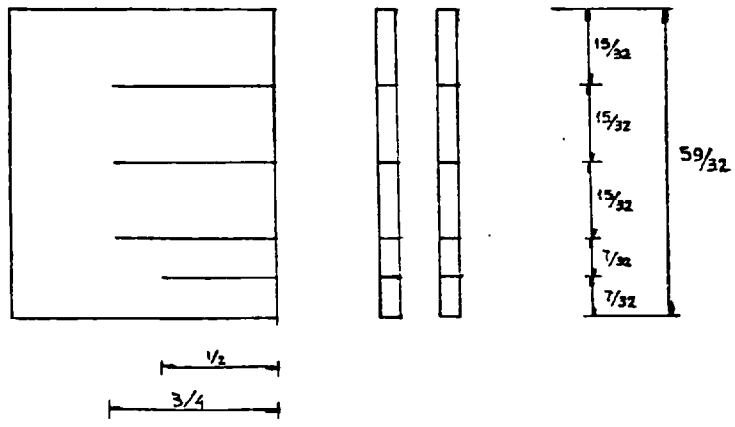

in which each finger is considered as a cantilever beam loaded as shown.

The maximum opening load for a specimen 12 x 4 with a crack 3.6in in length (0.3ℓ) is 1180lb. This load will be applied throughout the eight sections, shown in figure above.

Maximum stress in the beam (opening load)

(i) ℓ = 0.625in (5/8)

y = 0.1093in (7/64)

$I = 2.05 \times 10^{-4} in^4$

P = 75lb

$\sigma = 75 \times 0.625 \times 0.1093/2.05 \times 10^{-4} = 25000$ lb/in^2 O.L.

(ii) ℓ = 0.75in (3/4)

y = 0.2343in (15/64)

$I = 1.068 \times 10^{-3} in^4$

$\sigma = 150 \times 0.75 \times 0.2343/1.068 \times 10^{-3} = 24700$ lb/in^2 O.L.

Stress due to transverse load

$\sigma = 849/1.8437 \times 0.25 = 1150$ lb/in^2 T.L.

The strain (ϵ) is

$\epsilon = \sigma/E$; $E = 10^7$ $\therefore$

$\epsilon = 26150/10^7 = 2615 \times 10^{-6}$

$\epsilon = 2615\ \mu s$

(b) Compressive fingers. Load to be applied.

Each individual finger is to stand a load of 849/8 = 106lb.

The finger to apply transverse load are shown below.

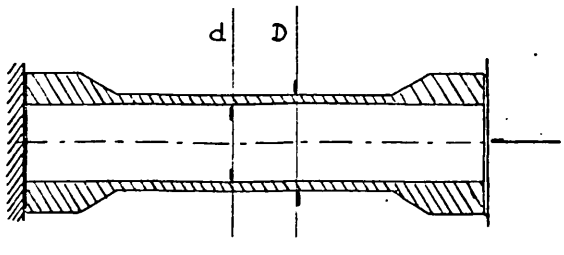

If $D = 0.35in$ and $d = 5/16in$

$A = 0.785\ (D^2 - d^2) = 0.0222\ in^2$

$P = 849/8 = 106lb$ (Eight fingers)

$\sigma = P/A = 106/0.0222 = 5240lb/in^2$

and $E = 10^7 lb/in^2$

$\epsilon = \sigma/E = 5240/10^7 = 524 \times 10^{-6} = 524\ \mu$ strain

Buckling load [p.184 Warnock-Benham Mechs. of solids and strength of materials]

$P = \pi^2\ EI/4l^2$

$I = \pi(D^4 - d^4)/64$

$P = 9.88 \times 10^7 \times 54.8 \times 10^{-4} \times 3.14/64 \times 4 \times 2 \times 2 = 1665lb$

```
      PROGRAM HUNTER (INPUT, OUTPUT, TAPE 5 = INPUT, TAPE 6 = OUTPUT)
      COMMON  G(3,40), COEF(40), EL, HH, WW, BET, PI, ANGLE, CRK,
     1        RADIUS, GMOD, YMOD, PRAT, CAY, DUM(42), NOPT, NTRM,
     2        KNO, ICHOOZ
      PI = 3.14159265358979
      FA = 180.0 / PI
      READ  (5,500) KASE
      DO 90  K = 1, KASE
      READ  (5,505) EL, HH, WW, PSO, NOPT, NTRM, KNO
      READ  (5,510) PRAT, YMOD
      READ  (5,515) (COEF(I),  I = 1,NTRM)
      READ  (5,520) RADIUS
      WRITE (6,600) EL, HH, WW, PSO, NOPT, NTRM, KNO
      WRITE (6,605) PRAT, YMOD
      WRITE (6,610) (COEF(I),  I = 1,NTRM)
      WRITE (6,615) RADIUS
      WH = WW - HH
      PS1 = PSO / FA
      CRK = -WH / COS(PS1)
      BET = 90.0 - PSO
      GMOD = YMOD / 2.0 / (1.0 + PRAT)
C       FOR PLANE SETRESS USE
CC    CAY = (3.0 - PRAT) / (1.0 + PRAT)
CC  FOR PLANE STRAIN, USE
C     CAY = 3.0 - 4.0 * PRAT
      CAY = 3.0 - 4.0 * PRAT
      GO TO (10, 20, 30), KNO
   10 WRITE (6,650)
      GO TO 40
   20 WRITE (6,655)
      GO TO 40


   30 WRITE (6,660)
C A U T I O N - - - ICHOOZ = 3 OPTION NOT FULLY TESTED
   40 DO 90  ICHOOZ = 1,2
      GO TO (50, 60, 70), ICHOOZ
   50 WRITE (6,675)
      GO TO 80
   60 WRITE (6,680)
      GO TO 80
   70 WRITE (6,685)
   80 ANGLE = 0.0
      CALL VALUES (UVAL)
      CALL SEARCH (UVAL)
      SF1 = -COEF(1) * SQRT(2.0*PI)
      SF2 =  COEF(2) * SQRT(2.0*PI)
      RAT = SF2 / SF1
      ANGLE = ANGLE * FA
      IF (ICHOOZ .NE. 2) UVAL = -UVAL
      WRITE (6,695) BET, SF1, SF2, RAT, RADIUS, ANGLE, UVAL
   90 CONTINUE
      STOP
C
  500 FORMAT (I5)
  505 FORMAT (4F10.2, 4I5)
  510 FORMAT (2E20.8)
  515 FORMAT (4E20.10)
  520 FORMAT (F10.5)
  600 FORMAT (1H1, /4X39HTHE INPUT DATA WERE READ AS FOLLOWS
     1    //   4F10.2, 4I5)
  605 FORMAT (2E20.8)
  610 FORMAT (4E20.10)
  615 FORMAT (F10.5, /)
  650 FORMAT (/3X 5(16H TENSILE LOAD    )/)
  655 FORMAT (/3X 5(16H PURE BENDING    )/)
  660 FORMAT (/3X 5(16H COMPACT, CKS    )/)
  675 FORMAT (/3X 3(26H MAXIMUM HOOP STRESS CRIT   ) /)
  680 FORMAT (/3X 2(35H MINIMUM STRAIN ENERGY DENSITY, S CRIT  ) /)
  685 FORMAT (/3X 2(42H MAXIMUM STRAIN ENERGY DENSITY CRIT        ) /)
  695 FORMAT (/4X 33HTHE ANGLE OF CRACK INCLINATION IS F6.2, 37H DEG.  F
     1O. UNIT LOADING, THE K VALUES /13H     ARE K-I = F7.3, 8H, K-II =
     2 F7.3, 40H, BOTH IN LB/IN2 * SQRT(IN).  K-II/K-I = F5.3, // 4X
     3 14HAT A RADIUS OF F7.5, 43H IN, THE ANGLE OF GROWTH IS PREDICTED
     4 TO BE F7.2, 5H DEG. /4X 63HTHE VALUE OF THE CRITICAL PARAMETER, FO
     5R UNIT LOADING, IS EQUAL E13.6, //)
      END
```

```
      SUBROUTINE SEARCH (UVAL)
      COMMON  SPA(164), PI, ANGLE, XTR(6), XP(21), UV(21), IDL(4)
C     IF (SPA(164) .EQ. 90.0) RETURN
      AP =  0.00010
      EP =  0.00010
      PL = -PI + AP
      PR =  PI - AP
      GS = 2.0 / (1.0 + SQRT(5.0))
      GR = (1.0 / GS ** 10 - 1.0) / GS
      XP( 1) = PL
      XP(11) = ANGLE
      XP(21) = PR
      DPL =  (XP(11) - XP( 1)) / GR
      DPR =  (XP(21) - XP(11)) / GR
      DO 65  I = 1,9
      J = 11 + I
      K = 11 - I
      XP(J) = XP(J-1) + DPR
      XP(K) = XP(K+1) - DPL
      WRITE(6,670)K,XP(K),DPL,GS,GR
  670 FORMAT(1X,*K=*,I2,*XP(K)=*,1F10.4,*DPL=*,1F10.4,*GS=*,1F10.4,*GR=*
     1,1F10.4)
      DPR = DPR / GS
   65 DPL = DPL / GS
      UV(11) = UVAL
      IS = 0
      ANGLE = XP(10)
      CALL VALUES (UTMP)
      UV(10) = UTMP
      IF (UTMP - UVAL) 10, 10, 25
   10 DO 15  I = 1,9
      J = 10 - I
      ANGLE = XP(J)
      CALL VALUES (UTMP)
      UV(J) = UTMP
      IF (UTMP - UV(J+1))  15, 15, 20
   15 CONTINUE
      IS = 1
      GO TO 25
   20 IS = -1
      JL =  J
      JM =  J + 1
      JR =  J + 2
      GO TO 60
   25 ANGLE = XP(12)
      CALL VALUES (UTMP)
      UV(12) = UTMP
      IF (UTMP - UVAL) 40, 40, 30
   30 IF (IS)  60, 35, 40
   35 JL = 10
      JM = 11
      JR = 12
      GO TO 60
   40 DO 45  I = 1,9
      J = 12 + I
      ANGLE = XP(J)
      CALL VALUES (UTMP)
      UV(J) = UTMP
      IF (UTMP - UV(J-1))  45, 45, 50
   45 CONTINUE
```

```
      ANGLE = XP(11)
      WRITE (6,600) (XP(I),  I =  1, 7), (UV(I),  I =  1, 7),
     1              (XP(I),  I =  8,14), (UV(I),  I =  8,14),
     2              (XP(I),  I = 15,21), (UV(I),  I = 15,21)
      RETURN
   50 IS =  1
      JL =  J - 2
      JM =  J - 1
      JR =  J
   60 IF (IS)  70, 65, 70
   65 PM = (GS * XP(JR) + (1.0 - GS) * XP(JM) - XP(JL)) * GS
      ANGLE = PM
      CALL VALUES (UM)


      GO TO 75
   70 PM = XP(JM)
      UM = UV(JM)
   75 PL = XP(JL)
      UL = UV(JL)
      PR = XP(JR)
      UR = UV(JR)
      WRITE(6,660)JL,UV(JL),JL,UV(JL),JR,UV(JR)
  660 FORMAT(1X,3(I5,F15.5))
      DO 90  I = 1,40
      K = I
      IF (PL + PR - PM * 2.0)  77, 77, 76
   77 PT = PM - GS * (PR - PM)
      ANGLE = PT
      CALL VALUES (UT)
      WRITE(6,666)ANGLE,UT
  666 FORMAT(1X,2F15.5,8HLEVEL 77)
      IF (UT - UM) 80, 80, 81
   78 PT = PM + GS * (PM - PL)
      ANGLE = PT
      CALL VALUES (UT)
      WRITE(6,667)ANGLE,UT
  667 FORMAT(1X,2F15.5,8HLEVEL 78)
      IF (UT - UM) 83, 83, 84
   80 PL = PM
      UL = UM
      PM = PT
      UM = UT
      GO TO 85
   81 PR = PT
      UR = UT
      GO TO 85
   83 PR = PM
      UR = UM
      PM = PT
      UM = UT
      GO TO 85
   84 PL = PT
      UL = UT
   85 IF (PP - PR + PL) 90, 90, 95
   90 WRITE(6,652)PL,PM,PR,UL,UM,UR,UT,I
C  90 CONTINUE
   95 ANGLE = PT
      UVAL = UT
      WRITE(6,651)UVAL,ANGLE
      WRITE(6,650)(XP(I), I = 1,7),(UV(I), I = 1,7),
     1            (XP(I), I = 8,14), (UV(I), I = 8,14),
     2            (XP(I), I =15,21), (UV(I), I =15,21)
      RETURN
```

```
      SUBROUTINE VALUES (UVAL)
      COMMON   C(3,40), COEF(40), EL, HH, WW, DET, PI, ANGLE, CRK,
     1         RADIUS, GMOD, YMOD, PRAT, CAY, DUM(42), NEPT, NTRM,
     2         KND, ICHOOZ
      P = ANGLE
      R = RADIUS
      RT = SQRT(R)
      N4 = NTRM / 4
      DO 10   M = 1,N4
      M4 = M * 4
      S = M
      S72 = S - 3.5
      S31 = S - 3.0
      S32 = S - 1.5
      S11 = S - 1.0
      S12 = S - 0.5
      P12 = S + 0.5
      P11 = S + 1.0
      RI = R ** (M-1)
      IF (M .EQ. 1) RI = 1.0
      RR = RI / RT
      SE = -1.0
      IF((M/2)*2 .EQ. M) SE = 1.0
      SM = - SE
      SS32 = SIN(S32 * P)

      SS11 = SIN(S11 * P)
      SS12 = SIN(S12 * P)
      SP12 = SIN(P12 * P)
      SP11 = SIN(P11 * P)
      CS32 = COS(S32 * P)
      CS11 = COS(S11 * P)
      CS12 = COS(S12 * P)
      CP12 = COS(P12 * P)
      CP11 = COS(P11 * P)
C FINDS CONTRIBUTION TO STRESSES FOR EACH TERM IN SERIES, IN ORDER
C  A(2N-1), B(2N-1), A(2N), B(2N), FOR N = 1, 2, , , NTRM/4 (= N4)
C
C SIGMA R
      C(1,M4-3) = SM * RR * S12 * (S72 * CS32 - S32 * CP12)
      C(1,M4-2) =-SM * RR * S12 * (S72 * SS32 - P12 * SP12)
      C(1,M4-1) = SE * RI * S   * (S31 * CS11 - P11 * CP11)
      C(1,M4  ) = SE * RI * S   * (S31 * SS11 - S11 * SP11)
C SIGMA PSI
      C(2,M4-3) =-SM * RR * S12 * (P12 * CS32 - S32 * CP12)
      C(2,M4-2) = SM * RR * S12 * (P12 * SS32 - P12 * SP12)
      C(2,M4-1) =-SE * RI * S   * (P11 * CS11 - P11 * CP11)
      C(2,M4  ) =-SE * RI * S   * (P11 * SS11 - S11 * SP11)
C TAU R-PSI
      C(3,M4-3) =-SM * RR * S12 * (S32 * SS32 - S32 * SP12)
      C(3,M4-2) =-SM * RR * S12 * (S32 * CS32 - P12 * CP12)
      C(3,M4-1) =-SE * RI * S   * (S11 * SS11 - P11 * SP11)
      C(3,M4  ) = SE * RI * S   * (S11 * CS11 - S11 * CP11)
   10 CONTINUE
      SGR = 0.0
      SGP = 0.0
      TAU = 0.0
      DO 20   N = 1,NTRM
      SGR = SGR + C(1,N) * COEF(N)
      SGP = SGP + C(2,N) * COEF(N)
   20 TAU = TAU + C(3,N) * COEF(N)
      CALL CHOICE (SGR, SGP, TAU, UVAL)
      RETURN
      END

      SUBROUTINE CHOICE (A, B, C, U)
      COMMON   SPA(168), GMOD, YMOD, PRAT, CAY, DUM(42), IDL(3), ICHOOZ
      GO TO (10, 20, 20), ICHOOZ
C     MAXIMUM HOOP STRESS
   10 U = -C
      RETURN
C     STRAIN ENERGY DENSITY
   20 S = ((CAY+1.0)/8.0*(A+B)*(A+B) + C*C - A*B) / (2.0*GMOD)
      GO TO (10, 30, 40), ICHOOZ
C     MINIMUM STRAIN ENERGY DENSITY
   30 U = -S
      RETURN
C     MAXIMUM STRAIN ENERGY DENSITY
C OPTION - - - ICHOOZ = 3 OPTION NOT FULLY TESTED
   40 U = -S
      RETURN
      END
```

APPENDIX 7

Stress values at the crack tip

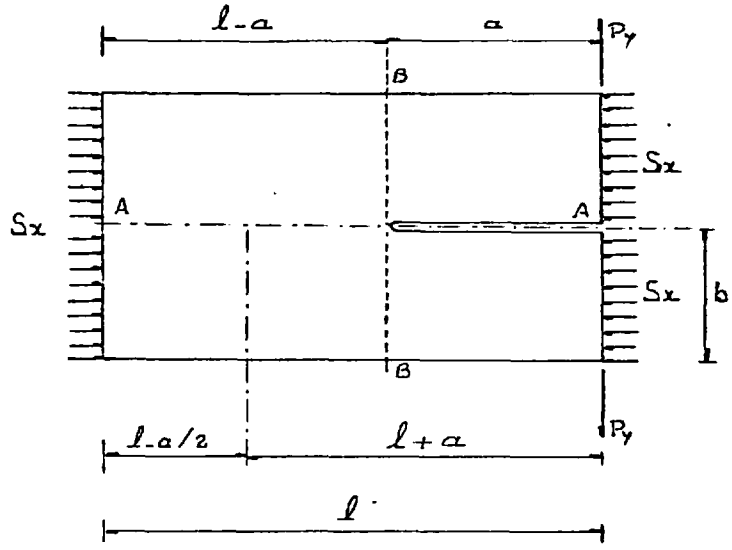

$$S_x = P_x/b$$

Section AA

$$\sigma_{yT} = \sigma_{Py} + \sigma_{Px}$$

$$\sigma_{Py} = \frac{3P_y(\ell + a)}{(\ell - a)^2}$$

$$P_x = S_x \cdot b$$

$$\sigma_{Px} = \frac{3Px\ b}{(\ell - a)^2}$$

$$\sigma_{yT} = \frac{3}{(\ell - a)^2}\ [P_y(\ell + a) + P_x b]$$

Section BB

$$\sigma_{xT} = \frac{6Pya}{b^2} - S_x$$

BIBLIOGRAPHY

Aida, T., Sato, S., Arai, N. Research of Force Fitted Gear. Bulletin of the JSME, Vol.16, No.94, April, 1973

Arad, S. Fracture Mechanics Analysis of Fatigue Crack Growth in Viscoelastic Solids. Ph.D.Thesis, University of London, November 1972

Barenblatt, G.I. On some Basic Ideas of the Theory of Equilibrium Cracks forming during Brittle Fracture. Problems of Continuum Mechs., SIAM, p.21-38, Philadelphia, 1961

Barr, B.I.G. A Study of Crack Propagation. Ph.D.Thesis, University of Wales, 1968

Benbow, T.J. and Roesdler, F.C. Experiments on Controlled Fractures. Proc.Phys.Soc., B70, 201, 1957

Berry, T.P. Some Kinetic Considerations at Constant Deformation. J.Mech.Phys.Solids, Vol.8, p.207-216, 1960

Berry, T.P. The Surface Energy of Polymethylmethocrylate. J.Polymer Sc., Vol.50, p.107-115, 1961

Bueckner, H.F. Propagation of Cracks and the Energy of Elastic Deformation. Trans.Am.Soc.Mech.Eng., 80E, p.1225, August 1958

Chan, S.K., Tuba, I.S., Wilson, W.K. On the Finite Element Method in Linear Fracture Mechanics. Eng.Fract.Mech., 2, p.1-17, 1970

Clausing, D.P. Crack Stability in Linear Elastic Fracture Mechanics. Int.J.Fract., 5, 211-217, 1969

Cotterell, B. On Brittle Fracture Paths. Int.J.Frac.Mech., 1, 96, 1965

Cotterell, B. Notes on the Paths and Stability of Cracks. Int.J.Fract.Mech., Vol.2, p.526-533, 1966

Cotterell, B. On Fracture Path Stability in the Compact Tension Test. Int.J.Fract.Mech., 6, 189-192, 1970

Coughlan, J. and Barr, B.I.G. Future Path Prediction. Int.J.Fract., 10, p.590, 1974

Erdogan, F. and Sih, G.C. On the Crack Extension in Plates under Plane Loading and Transverse Shear. Trans. ASME, J.Basic Engr., 85D, 519, 1963

Finnie I. and Saith, A. A Note on the Angled Crack Problem and the Directional Stability of Cracks. Int.J.Fract., 9, p.484, 1973

Finnie, I. and Weiss, H.D. Some Observations on Sih's Strain Energy Density Approach for Fracture Prediction. Int.J.Fract., 10, p.136, 1974

Forsyth, P.T.E. A Two Stage Process of Fatigue Crack Growth. Proc.Crack Propagation Symp., Cranfield, Vol.1, p.77, The College of Aeronautics, 1961

Griffith, A.A. The Phenomena of Rupture and Flow in Solids. Phi.Proc.Royal Soc., Series A.221, p.163, 1920

Griffith, A.A. The Theory of Rupture. Proc.1st Int.Congr.Appl. Mech., Delft, 1924

Griffith, A.A. and Taylor, G.I. The use of Soap Films in Solving Torsion Problems. Proc.Inst.Mech.Eng., p.755, December 1917

Gross, B. and Srawley, J.E. Stress Intensity Factors by Boundary Collocation for Single-Edge-Notch Specimens subject to Splitting Forces. Theoretical Note D-3295, NASA, February 1966

Gross, B., Srawley, J.E., Brown, W.F. Stress Intensity Factor for a Single-Edge-Notch Tension Specimen by boundary Collocation of a Stress Function. Tech.Note D-2395, NASA, August 1964

Guernsey, R. and Guilmain, J. Photoelastic Study of the Stresses near a Cleavage Crack. Experimental Mech., 1, 8, 50-54, August, 1961

Gurney, C. and Hunt, J. Quasi-Static Crack Propagation. Proc.Royal Soc., London A 299, 502-524, 1967

Hayes, D.J. Some Applications of Elastic Plastic Analysis to Fracture Mechanics. Ph.D.Thesis University of London, October 1970

Hayes, D.J. A Practical Formulation for Determining Stress Intensity Factor for Cracked Bodies. Int.J.Fract.Mech., 8, p.157-165, 1972

Hubbard, R.P. Crack Growth under Cyclic Compression. J.Basic Eng., Vol.91, No.4, p.625, December 1969

Hutchinson, J.W. and Turner, C.E. Private Communication, 1975

Inglis, C.E. Stresses in a Plate due to the Presence of Cracks and Sharp Corners. Trans. of Inst.Naval Arch., London, Vol.60, p.219, 1913

Irwin, G.R. Fracture Dynamics. Fracturing of Metals. Am.Soc. Metals, Cleveland, p.152, 1948

Irwin, G.R. Analysis of Stresses and Strains near the end of a Crack Traversing a Plate. J.Applied Mechs., Trans.ASME, Vol.79, 1957

Irwin, G.R. Fracture Testing of High Strength Materials under conditions Appropriate for Stress Analysis. NRL Report No.5486, July 1960

Jerram, K. and Heller, T.K. Finite Element Techniques in Fracture Mechanics. Proc.Int.Conf.Welding Research related to Power Plant, Southampton, 1972

Kobayashi, A.S., Maiden, D.E., Simon, B.J., Iida, S. Application of Finite Element Analyses Method to Two-Dimensional Problems in Fracture Mechanics. Office of Naval Research, Technical Report, (5), 1968

Larsson, S.G. and Carlsson, A.J. Influence of Non-Singular Stress Terms and Specimen Geometry on Small Scale Yielding at Crack Tips in Elastic Plastic Materials. J.Mech.Phys.Solids, 21, 263-277, 1973

McClintock, F.A. and Irwin, G.R. Plasticity Aspects of Fracture Mechanics. ASTM STP 381, 1964

Mai, Y.W., Atkins, A.G., Cadell, R.M. On the Stability of Cracking in Tapered DCB Test Pieces. Int.J.Fract., 11, 939-953, 1975

Mott, N.F. Fracture of Metals. Theoretical Considerations Engineering, London, 165, p.16-18, January, 1948

Mowbray, D.F. A note on the Finite Element Method in Linear Fracture Mechanics. Eng.Fract.Mech., 2, p.173-176, 1970

Obreimoff, T.W. The Splitting Strength of Mica. Proc.Royal Soc., A127, 805, 290-297, 1930

Oglesby, J.J. and Lomacky, O. An Evaluation of Finite Element Method for the Computation of Elastic Stress Intensity Factors. Nav.Spip.Res. and Dev.Cent.Report 3751, Bethesda, Md., December, 1971

Orowan, E. Notch Brittleness and Strength of Materials. Inst.Engr.s and Ship Bldrs. in Scotland, Vol.80, Pt.3,4, p.165-196, January 1946

Orowan, E. Energy Criteria of Fracture. Welding Journal, Research Supplement, March 1955

Parks, D.M. A Stiffness Derivative Finite Element Technique for Determination of Crack Tip Stress Intensity Factors. Int.J.Fract., 10, 487-502, 1974

Pook, L.P. The Effect of Crack Angle on Fracture Toughness. J.Eng.Fract.,Mech., Vol.3, p.205-218, 1971

Post, D. Photoelastic Stress Analysis for an Edge Crack in a Tensile Field. Naval Res.Lab., Washington, D.C. Proc.Soc. Experimental Stress Analysis, Vol.12, No.1, p.99, 1954

Rice, J.R. A Path Independent Integral and the Approximate Analysis of Strain Concentration by Notches and Cracks. J.Applied Mech., p.379-386, June, 1968

Rice, J.R. and Tracey, D.M. Computational Fracture Mechanics in Numerical and Computer Methods in Structural Mechanics. Academic Press, New York, 585-623 1973

Roberts, J, and Kibler, Y.Y. Mode II Fatigue Crack Propagation. Trans.ASME, J.Basic Eng., (93), 671, 1971

Roberts, D.K. and Wells, A.A. The Velocity of Brittle Fracture. Engineering, Vol.8, p.820-821, 1954

Roesdler, F.C. Brittle Fractures near Equilibrium. Proc.Phys.Soc., Vol.70, 1956

Schijve, J.S. Analysis of Fatigue Phenomenon in Aluminium Alloys. Report and Trans.M.2122, V.29, 63, July 1964 (Nat.Aero. and Astronautical Research Inst.), Amersterdam, Notional Sucht

Sih, G.C. Application of Strain Energy Density Theory to Fundamental Fracture Problems. Tech.Rep.AFOSR-TR-73-1, November 1973

Sumpter, J.D.G. Elastic-Plastic Fracture Analysis and Design using the Finite Element Method. Ph.D.Thesis, Imperial College, 1973/4

Svensson, N.L. Variation of Energy with Temperature. Proc.Phys.Soc., Vol.77, (4-6), 1961

Svensson, N.L. Estimation of Yield Strength Anisotropy due to Preferred Orientation. Met.Soc. of AIME. Trans.Vol.236, No.7, p.1004-1009, July 1966

Swedlow, J.L. Private communication, 1974

Tracey, D.M. Finite Elements for Determination of Crack Tip Elastic Stress Intensity Factors. Eng.Fract.Mech., 3, p.255-265, 1972

Turner, C.E. Fracture Toughness and Specific Fracture Energy. A re-analysis of results. Mats.Sc. and Engr., 11, 275-282, 1973

Urriolagoitia, G. The Analysis of the Stresses in Gear Wheels wi with Novikov Teeth using Photoelastic and Finite Element Method. M.Sc. Thesis, University of Strathclyde, Glasgow, 1970

Valluri, S.R. Fracture under Biaxial Condition in the Presence of a Crack. Proc.1st Int.Conf.Fracture, Sendai, 1727, 1965

Watwood, V.B. The Finite Element Method for Prediction of Crack Behaviour. Nuclear Eng. and Design. 11, 323-332, North Holland Publishing Co., Amsterdam, 1969

Westergaard, H.M. Stresses at a Crack, Size of the Crack and the Bending of Reinforced Concrete. Proc.Am.Concrete Inst., Vol.30, p.93-102, 1934

Westergaard, H.M. Bearing Pressures and Cracks. J.Applied Mech., Trans ASME, Vol.61, p.A-49-53, 1939

Williams, M.L. Stress Singularities resulting from various Boundary Conditions in Angular Corners of Plates in Extension. J.Appl.Mech., p.526-528, December 1952

Williams, M.L. On the Stress Distribution at the Base of a Stationary Crack. J.Applied Mech., 24, p.109, March 1957

Williams, J.G. and Ewing, P.D. Fracture under Complex Stress - the angle crack problem. Int.J.Fract.Mech., 8, 441-446, 1972

Williams, J.G. and Ewing, P.D. Further Observations on the Angled Crack Problem. Int.J.Fract.Mech., 10, 135, 1974

Wilson, W.K. Analytical Determination of Stress Intensity Factors for the Manjoine Brittle Fracture Test Specimen. Rep.No.WERL-0029-3, Westinghouse Research Lab., August 1965

Żener, C. and Holloman, J.H. Plastic Flow and Rupture of Metals. Trans.Am.Soc.Metals, V.33, 162-215, 1944

Zienkiewicz, O.C. The Finite Element Method in Engineering Science. McGraw-Hill, London, 1971